THE UNIVERSITY
of EDINBURGH

The history of the New Caledonia Barrier Reef over the last 1.2Myrs: links with regional palaeoceanography and palaeoclimate

Amanda Gillian Foan

MA(Cantab), MSci, FGS

Thesis submitted for the degree of Doctor of Philosophy
The University of Edinburgh, 2015

Abstract

The timing of glacial-interglacial cycles shows a clear dependence on the periodic variations in the Earth's orbital parameters. However, the Earth's climate is an extremely complex, non-linear system, with many internal feedback mechanisms and there are still features of the climate record for which a definitive explanation remains elusive. Understanding reef history is important due to significant predicted feedbacks between changes in global climate and carbonate production via the carbon cycle; phases of rapid reef growth in shallow water areas being associated with increased release of carbon dioxide to the atmosphere. Previous work on Pleistocene reef history, investigated via reef boreholes, shows a large global expansion of reefs between 800-400ka; approximately concurrent with one of the major unexplained alterations in the climate system, the Mid-Pleistocene Transition (MPT).

Quaternary reef history is usually investigated via reef boreholes, which provide limited spatial information and are subject to dating uncertainties of the order of ±100kyrs. This means that any inferences made about the relationship between reef expansion and specific changes in the climate system are not well constrained. This thesis instead, presents a novel approach to reconstructing reef growth history, using a trial site near the island of New Caledonia, in the south west Pacific. The initiation of carbonate production on shallow shelves is known to produce a signal in the surrounding deeper basins, via sediment shedding. Therefore, this research set out to independently verify the proposed expansion of the New Caledonia Barrier Reef at ~ 400ka (Marine Isotope Stage [MIS] 11) by examining the composition of turbidites deposited in the New Caledonia Trough.

Deep sea sediment core MD06-3019, was collected south west of the New Caledonia Barrier Reef (22^{o}S, 165^{o}E; 3,500m water depth). It is predominantly composed of pelagic carbonate ooze, into which 79 sandy turbidite layers have been deposited.

These layers interrupt, but do not disturb, the background sedimentation and source material from the shallow shelf, which is carried to the deep sea via submarine canyons. A core age model based principally on orbital tuning, yields a core bottom age of 1,260ka, ~MIS38. This chronology has allowed the timing of deposition of the turbidite layers within the core to be assigned to within ±10kyr. Turbidite layers vary in width (1-35cm), grain size (φ=4 to -2) and composition, containing among other shelf derived material, well preserved coral fragments from 1.26Ma through to the present day. Patterns in turbidite timing and frequency, grain size and composition (investigated via point counting, carbonate coulometry and aragonite content) have been analysed, to assess whether there are any temporal changes which may reflect variation in shallow shelf reef extent. This included the development of XRF scanning measurements for [Sr], as a new proxy for the aragonite content of samples. A calibration line with the equation: Aragonite %=0.0011* Sr count +2.64 (R^2 =0.6105, p-value < 0.001) was obtained for turbidite samples from sediment core MD06-3019. The method shows significant promise as a new proxy for quickly establishing the aragonite content of sediment samples.

Corroborating the work of previous investigators, turbidites deposited since MIS11 show an increase in average bulk carbonate and aragonite content, a greater dominance of shallow water bioclasts and a higher occurrence of coral fragments. Additionally, both coarse and fine grained turbidites are present, whereas directly before this period only fine grained turbidites occur. However, there is another significant shift in depositional style further back in the record. Prior to MIS23 both coarse and fine grained turbidites are present, the average carbonate content of turbidite layers is higher and there is a greater dominance of shallow water biota. Coral abundance for turbidites at the base of the core can equal values for turbidites at the top of the core. These results challenge the assumption that the only significant evolution on the western New Caledonia margin over the last 1.2Myrs was the expansion of the barrier reef at MIS11. This suggests that the history of the western New Caledonia margin may be more complicated than initially anticipated.

These temporal variations in turbidite deposition are interpreted as reflecting changes in the level of carbonate production on the shallow shelf over the course of the 1.26Myr record. Shallow water carbonate production having decreased substantially during the period MIS23-MIS11. There are many possible controls on the shallow water carbonate production; such as: sea surface temperature and salinity, sea-level and nutrient availability. However, it is hypothesised that the principal control is glacial-interglacial sea-level change. It is proposed that prior to MIS23 sea-level was high enough during certain interglacial periods for significant carbonate production to occur on the shelf. However, from MIS23 onwards the climate proceeded into a period of 'lukewarm' interglacials which were both cooler and had lower sea-levels. It is hypothesised that during this period sea-level did not rise enough during highstands to flood the shelf sufficiently to allow for significant shallow water carbonate production. The high sea-levels of the long, warm MIS11then allowed for the expansion of the barrier reef (perhaps on substrates provided by former siliciclastic coast lines, deposited between MIS23-11) and its continuation during subsequent interglacial periods until the current day. This pattern of shallow shelf carbonate production is similar to those proposed for the Belize margin and the Gulf of Papua over the last 1.2Myrs.

This thesis provides one of the first detailed investigations of gravity deposits in the New Caledonia Trough, providing information on their composition and timing over an unprecedented 1.26Myr time period. This study demonstrates that deep sea turbidites, sourced from shallow shelf areas, can be used to help reconstruct tropical reef growth histories. The results corroborate the work of previous researchers in the area and provide new insights into the history of reefs along the western New Caledonian margin. The main advantage of this method, compared to traditional borehole techniques, is the 10-fold reduction in the age uncertainty of events, to ±10 kyr. In addition, because turbidite material is sourced from a wide area along the coast, the method is able to provide information on reef history over a larger spatial area than single reef boreholes. This method can now be extended globally to help improve knowledge of the timing and history of tropical reef growth during the

Quaternary. This will enable a better understanding of how reefs have impacted on, and been affected by, changes in climate, linked by feedbacks mechanisms via the global carbon cycle.

Summary for Non-Specialists

Over the last 2.5 million years (the Quaternary period) the Earth's climate has been characterised by recurrent, quasi-regular fluctuations between colder and warmer states, with a concurrent waxing and waning of high latitude ice sheet extent (and thus sea-level height). These so called 'glacial- interglacial' cycles occur on time scales of tens to hundreds of thousands of years. However, despite two hundred years of research on the topic there is no complete global theory of climate. There is a clear strong dependence in the time period of glacial-interglacial cycles on orbital variations (changes in the Earth's orbit around the sun), which cause shifts in the amount of solar radiation the Earth receives. However, there are also internal feedback mechanisms in the Earth system, which create non-linearities in the climate response. Processes associated with large ice-sheets, the carbon-cycle and the ocean circulation system are believed to act to substantially modify the basic climate response to the orbital variations. Two unexplained changes in the climate system are:

1. The 'Mid-Pleistocene Transition', which occurred between 1,200-500ka (ka denotes 'thousand years ago'). This period is characterised by a fundamental shift in the dominant glacial-interglacial time period. What is surprising is that this evolution occurred without any corresponding alteration in the orbital parameters.
2. The increase in amplitude of glacial-interglacial atmospheric carbon dioxide (CO_2) cycles at 400ka. Observations, on various timescales, indicate that periods of warmth are associated with higher atmospheric CO_2 concentrations and vice versa when temperatures were lower. Before 400ka, the average amplitude of change for atmospheric CO_2 over a cycle was ~70ppmv (parts per million by volume); however after 400ka this has increased by 40ppmv to ~110ppmv. This increase is mainly due to higher CO_2 levels during inter-glacial periods.

It has been noted these major unexplained alterations in the Quaternary climate are approximately concurrent with an apparent large, global expansion of tropical coral reefs which occurred between 800-400ka. A possible connection between these two events has been proposed via changes in the global carbon cycle; since phases of rapid reef growth are associated with increased release of carbon dioxide to the atmosphere. This feedback causes amplification of interglacial periods and the associated higher sea-levels, higher temperatures and reduced ice cover.

However, the task of investigating reef history is not necessarily a simple one due to the erosion and alteration of multiple phases of reef growth and large uncertainties associated with dating methods. Reef histories are generally obtained via the examination of sediments from reef boreholes drilled through: a) modern day reef crests or b) uplifted reef structures, that are now above sea-level. The uncertainties on ages provided for coral reef expansion via these methods are of the order of hundreds of thousands of years and thus are not only larger than the length of a glacial-interglacial cycle (~100 or 41 thousand years) but are also significant when compared to the length of the Mid-Pleistocene Transition as a whole. This means that any inferences made about the relationship between reef expansion and specific changes in the climate system are not well constrained.

This thesis, instead, develops a new method for investigating reef history which provides a ten-fold improvement in dating uncertainties. A reconstruction of the history of reef growth around the trial study site of New Caledonia, in the south-west Pacific Ocean, has been obtained via the examination of sediments in a nearby deep marine sediment core that spans the last 1,260,000 years, at around 5,000-10,000 year resolution. Sediments sourced from the shallow water areas surrounding New Caledonia (including reefs, when present) are transported to the deep sea via gravity flows termed ‘turbidites’, a type of underwater sediment landslide. Changes in reef expanse are reflected in variations in the level of reef material observed in these turbidites. The findings of this work were compared and contrasted with previous published results of reef history investigations in the area.

The key findings of this thesis are: firstly, support for the hypothesis of the expansion of the New Caledonia Barrier Reef at ~400ka, as proposed by previous published studies of the area. Secondly, that the history of reefs in the area is probably more complex than previous studies have suggested. There appears to have been a period of more luxuriant reef growth between 1,260-900ka, which has not been identified by previous researchers. Finally, that the principal control on reef growth appears to be due to variations in glacial-interglacial sea-levels. Tropical corals rely on the process of photosynthesis to survive and thus are confined to shallow water areas. Variation in the world-wide expanse of shallow seas is dependent on global sea-level and thus this controls the total amount of coral reef growth around the world.

This new method of investigating reef history shows considerable promise and can now be applied world-wide to investigate the growth history of other tropical coral reefs. This will help reconstruct and constrain the timing of global reef development and thus its place in changes in the global carbon cycle.

Declaration of Own Work

This is to certify that this thesis has been composed by myself and represents entirely my own work. All lab-work and data analysis was undertaken by me, except where this is clearly highlighted in the methods section of each chapter. I acknowledge the contributions of my co-authors in Chapters 5, which is the basis of a paper submitted for publication. I am, however, lead author on this paper and as such wrote the text, composed the figures and developed the arguments presented therein. This work has not been submitted for any other degree or professional qualification.

Amanda Gillian Foan
Edinburgh, October 2015

Word Count

There are 56,560 words in the main body of this thesis and an additional 11,830 words in the references and appendices combined.

Acknowledgements

My first thanks are due to my principle supervisor, Mary Elliot, for all her help and guidance throughout this project; despite the difficulties of being in different countries for the majority of the last four years! I would also like to thank my supervisors in Edinburgh, Sandy Tudhope and Tom Russon, for all their valuable advice, helpful discussions and calming influence. Special thanks are due to Sandy for his concern, understanding and patience during difficult times. Thanks are also due to my co-author, Stephan Jorry.

This work has been funded by the National Environmental Research Council, UK; without which I would have been unable to undertake this PhD. Thanks are due also to the French Zonéco program, IPEV and IRD for contributing to the grants to obtain the cores used in this study. I am grateful to the crew and scientists from cruise AUSFAIR/ZoNéCo12 of the R/V *Marion Dufresne* which allowed the collection of cores MD06-3018, MD06-3019 and MD06-3020.

I am grateful to Stephan Jorry (IFREMER, Brest, France) for extending the invitation to work in Brest to make the XRF measurements used in this thesis. Also to Jean Borgomano (Centre Scientifique et Technique Jean Féger, Pau, France) for the opportunity to trial the use of the DIONISOS model for the western New Caledonia margin. I would also like to thank numerous academic and technical staff for insightful discussions, as well as assistance and advice with experimental work. They are: Jean Borgamano, Nicola Cayzer, Colin Chilcott, Julien Collot, John Craven, Kate Darling, Walter Geibert, Mike Hall, Brandon Harper, Melany McFaddon, Ann Menim, Lucien Montaggioni, Nic Odling, John Reijmer, Angelique Roubi, Pierrick Rouillard, Alex Thomas and Rachel Wood. I am particularly grateful to Ann Menim for our interesting and amusing chats round the coulometer over the last few years, on topics as diverse as opera and ballet to household carpet replacement! Thanks are also due to those who did initial measurements, sampling and research on the core principally used in this study (MD06-3019). These are the three Environmental GeoScience Honours students at the University of Edinburgh: Aidan Farrow,

Rosanna Greenop and Angharad Jenkins; Catherine Kiessel for conducting the magnetic measurements and Tom Russon for sampling of the material for radiocarbon dating and those at Scottish Universities Environmental Research Centre, East Kilbride for the radiocarbon measurements.

Finally, I would like to thank all my many friends from home, Cambridge and those made whilst I have been in Edinburgh for their support and friendship over the past 4 years. Special thanks must go to the community at St. Michael and All Saints, Tollcross; Natalie Read for being my confidant and always taking the time to check on me; Ingrid Berkeley for being my best friend and comfort whilst in the 'North' and Miles Coverdale for making my world a brighter, happier place and always being there for me. Lastly to my parents, for all their unfailing love, help, support and faith in me; I would not be where I am without you.

For my best friend: my Mama

Contents

Figure List

Chapter 1

Chapter 2

Chapter 3

Chapter 4

Chapter 5

Chapter 6

Chapter 7

Appendix

Table List

Chapter 1

Chapter 3

Chapter 4

Chapter 5

Chapter 6

Chapter 7

Appendix

List of abbreviations used in the text

AABW	Antarctic Bottom Water
ACNC	Alis Current of New Caledonia
B-M	Brunhes- Matyuama boundary
BP	Years before present
CCD	Calcite compensation depth
ChRM	Characteristic remnant magnetisation
CM	Cobb Mountain reversal
ENSO	El Niño Southern Oscillation
GBR	Great Barrier Reef
Hol	Holocene
ka/ Ma/ Ga	Thousands/ millions/ billions of years before present
kyr/ Myr	Thousands/ millions of years (duration of time)
LBF	Large benthic foraminifera
LGM	Last glacial maximum
LJ	Lower Jaramillo
LR04	Lisiecki and Raymo 2004 global reference $\delta^{18}O_{benthic}$ curve
MBDI	Mid-Brunhes Dissolution Interval
MIS	Marine isotope stage
MPT	Mid-Pleistocene Transition
NADW	North Atlantic Deep Water
NCBR	New Caledonia Barrier Reef
NCT	New Caledonia Trough
ODV	Ocean Data View
ppm	Parts per million
SEC	Southern Equatorial Current
SPCZ	South Pacific Convergence Zone
[Sr]	Strontium concentration
SSS	Sea surface salinity
SST	Sea surface temperature
UJ	Upper Jaramillo
VPDB	Vienna Pee Dee Belemnite
XRD	X-ray diffraction
XRF	X-ray fluorescence
Φ	Krumbein phi grain size scale
‰	Per mille (parts per thousand)

Chapter 1: General Introduction

1.1 Chapter Overview

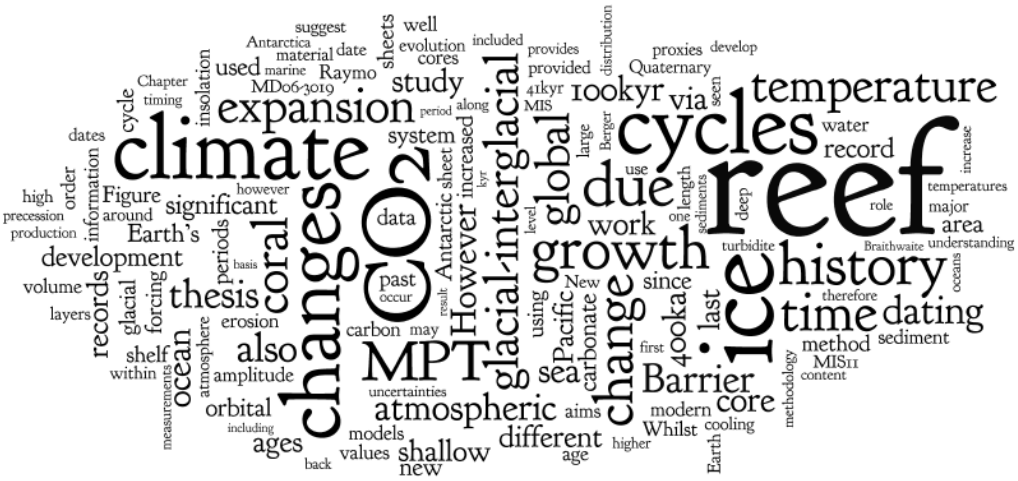

This chapter provides an in-depth review of the wider background and context to this thesis and introduces the aims and purpose of the research. Initially discussed is the evolution of the Earth's climate from the Cenozoic to the present day, a history of our understanding on this topic and the identification of some of the areas that are still not well understood or are a matter of debate. It has been noted that major unexplained alterations in the Quaternary climate are approximately concurrent with large changes in the worldwide distribution of warm water coral reef growth and possible connections between these two events have been proposed. A review of the current knowledge of Quaternary reef growth is therefore provided next, along with a critique of this work. This leads on to the rationale and motivation for this study and the development of a new methodology for investigating reef growth history. Finally, there is a detailed statement of the aims of the study and an outline of the structure of the thesis.

1.2 Plio- Pleistocene Climate Evolution: Into the Glacial World

On million year time scales the mean global temperature of the Earth is thought to be controlled by the carbon cycle, via the balance of degassing from igneous and metamorphic rocks and the weathering of continental silicate rocks [*Berner et al*., 1983]. The general global cooling trend of the Cenozoic has therefore commonly been attributed to the Himalayan orogeny and its subsequent erosion (see *Figure 1.1*) [*Raymo and Ruddiman*, 1992]. However, the climate also shows variations on shorter timescales. After the Early-Eocene climatic optimum, rapid excursions in $\delta^{18}O$ values occur from the Eocene-Oligocene boundary (~34Ma) onwards, due to the glaciations of the Southern Hemisphere. These glaciations were probably a result of either: a) a decrease in atmospheric CO_2 to a threshold level for ice growth in Antarctica [*DeConto and Pollard*, 2003; *Pagani et al.*, 2011; *Goldner et al.*, 2014]; or b) the widening of the seaways between Antarctica and South America and Antarctica and Australia; thus allowing the development of the Antarctic Circumpolar Current which thermally isolated Antarctica [*Kennett*, 1977; *Cramer et al.*, 2009; *Katz et al*., 2011].

There is a general cooling trend seen from 3.5Ma, where late Pliocene and early Pleistocene records suggest gradual deep water cooling but no significant ice expansion [*Sosdian and Rosenthal*, 2009]. The onset of Northern Hemisphere glaciations didn't occur until 2.7-2.5Ma [*Raymo*, 1994]; but must have been significant by 2.5Ma, since ice rafted debris is found in deep ocean sediments [*Shackleton et al*, 1984]. The only tectonic event to occur around this time was the closure of the Panama Seaway between 5-2.7Ma. This would have caused changes in ocean circulation and could have led to a build up warm water around the Caribbean and the development of the Gulf Stream, thus bringing moisture to the North Pole and encouraging ice sheet growth [*Haug et al*., 2001]. Whether the closure of Panama Seaway did act as a catalyst for Northern Hemisphere glaciations however remains a matter of debate [*Molnar*, 2008]. The glacial- interglacial cycles that began in the Pliocene continued into the Pleistocene with a cycle length of ~41kyr until the

Mid-Pleistocene Transition (MPT), when the length changed to 100kyr [*Lambeck*, 2002; *Clark*, 2006].

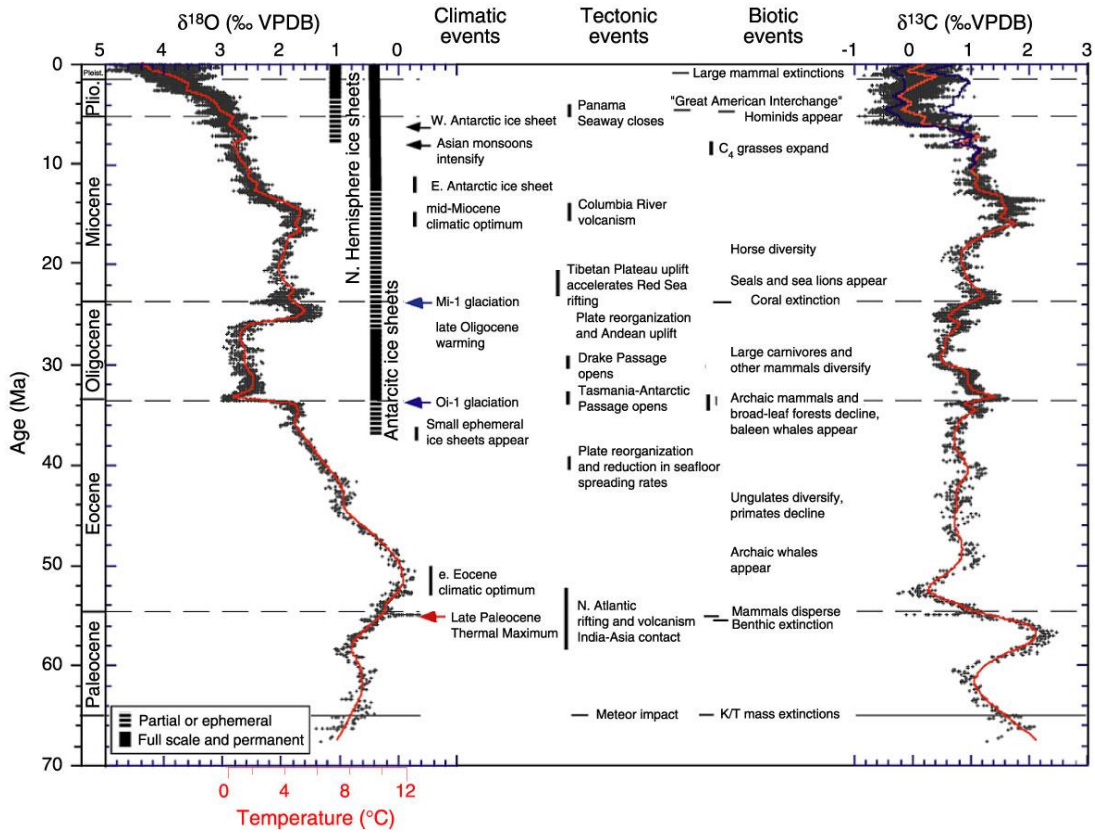

Figure 1.1 The evolution of the Earth's climate since the Cenozoic based on globally distributed $\delta^{18}O_{benthic}$ (left) and $\delta^{13}C_{benthic}$ records for the past 65Ma. (From *Zachos et al*., 2001.)

The Quaternary period (the last 2.5Myr) has been characterised by recurrent glacial-interglacial cycles (see *Figure 1.2*), so called because global ice sheets waxed and waned. However, these cycles were not merely limited to changes in ice sheets; rather they were major climate repercussions which impacted on the biosphere, hydrosphere, cryosphere, atmosphere and lithosphere. Linked via biogeochemical cycles, they participated in an apparently systematic series of interactions, which gave rise to highly patterned changes in global climate. An understanding of this climate variability has been a major goal of palaeoceanographic and palaeoclimatic research since its inception.

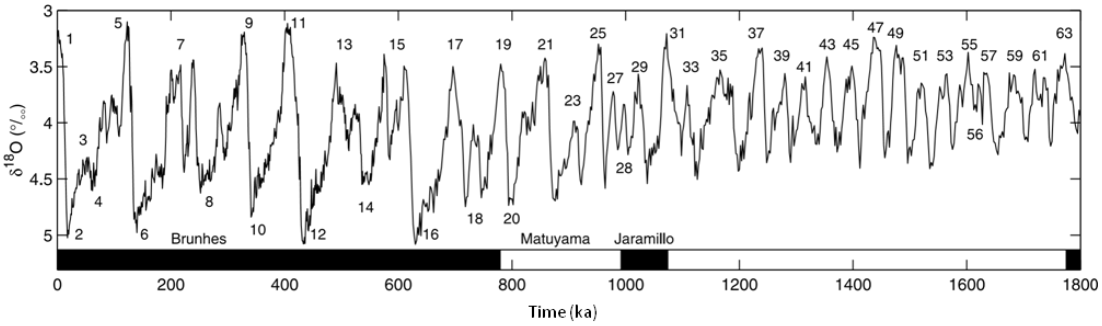

Figure 1.2 The LR04 benthic $\delta^{18}O$ stack constructed by the graphic correlation of 57 globally distributed benthic $\delta^{18}O$ records showing the glacial-interglacial cycles of the last 1.8Ma. (From *Lisiecki and Raymo*, 2005.)

1.3 The Milankovitch Paradigm

The history of the development of orbital theory goes back to the mid-1800s, when scientists realised that changes in climate could have affected the geography of the Earth's surface. *Louis Agassiz* (1838) hypothesised the existence of ice ages due to the presence of erratics, moraines and deeply scratched bedrocks; which were most naturally explained by the expansion and retreat of ice sheets. It was suggested that changes in insolation (the amount of radiation the Earth receives at the top of the atmosphere at a given location/season), which varies on a 10^4-10^5 year timescale due to inconsistencies in the Earth's orbit around the sun, could be enough to force the climate into glacial-interglacial cycles (*Figure 1.3*). Work was continued by those such as *Adhémar* and the first basic astronomical theory of climate change was produced by *Croll* in 1875. This included the importance of changes in the obliquity, precession and eccentricity of the Earth's orbit on insolation, as well as the awareness that internal feedback mechanisms within the Earth's climate system were necessary to explain glacial-interglacial cycles, since the astronomical forcing is only small.

However, it wasn't until over 65 years later, when *Milankovitch's* (1948) discernment and calculations provided an 'orbital solution' and led to an 'orbital theory of climate'. This predicted climatic cyclicity being mainly at 23 kyr due to precession, and 41 kyr because of obliquity changes. A major breakthrough in

understanding in *Milankovitch's* (1948) work came from the realisation that summer insolation also has a key role in ice sheet development, since 'colder summers enable the persistence throughout the year of snowfields in some high latitude regions, leading to a net accumulation of ice and to the building of ice sheets' [*Paillard*, 2001].

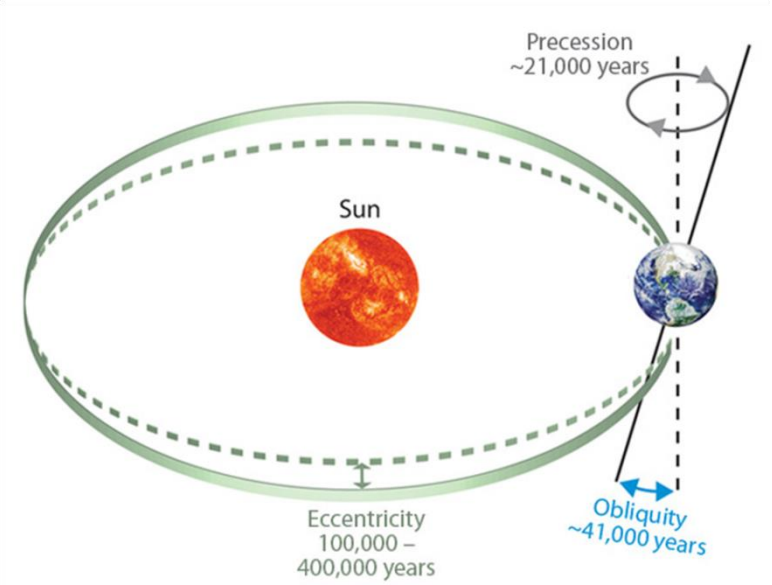

Figure 1.3 Sketch showing the different orbital parameters and their characteristic time-periods. Eccentricity: 100kyr, due to the ellipticity of the Earth's orbit. Obliquity: 41kyr, due to the tilt of the Earth's axis relative to the plane on which it orbits around the sun. Precession: 23kyr, due to the 'wobble' of the Earth's axis. This can also interact with eccentricity to produce the 'precession of the equinoxes' with a 19kyr cycle. (Figure by the Denning Research Group, Colorado State University; http://biocycle.atmos.colostate.edu/shiny/Milankovitch/.)

The first evidence from marine sediment cores, which allowed for evaluation of *Milankovitch's* (1948) hypothesis, came in the 1950s. Those such as *Emiliani* (1955) provided confirmation of cyclicity, using the oxygen isotopic composition of the carbonate shells of foraminifera, attributing the variations to temperature changes. However, *Shackleton* in 1967 suggested that most of the signal seen in *Emiliani's* record was a result of ice volume changes rather than temperature. Fossil coral reefs had been used to demonstrate an 100kyr cyclicity [*Hays et al.*, 1969; *Broecker and van Donk*, 1970], but the main cycles predicted by *Milankovitch's* (1948) work were

at 23 and 41 kyr time periods. It was *Hays, Imbrie and Shackleton's* seminal 1976 paper which provided the first high enough resolution down-core record of variability to give validation to *Milankovitch's* (1948) theory. Spectral analysis of this record identified not only the 100kyr cycle seen before, but also ones at 19, 23 and 41kyrs.

Whilst it is clear that there is a strong dependence on orbital variations in the time period of glacial-interglacial cycles, there are internal feedback mechanisms in the climate and this creates non-linearity in the system. For instance, from orbital calculations a strong precessional forcing would be expected in the data, but this is not seen in ice volume records [*Raymo*, 2006]. This means that conceptual models developed to reproduce glacial-interglacial cycles need to take this non-linearity into account. Conceptual models date back to *Calder* (1974) who used only insolation forcing with a threshold above which ice would grow and below which it would melt. Whilst this captured the main transitions, being a linear model, it didn't replicate the actual glacial-interglacial cycles particularly well. More recent models from *Imbrie and Imbrie* (1980), *Paillard* (1998) and *Paillard and Perrenin* (2004) have improved on this; featuring increasingly complex non-linear systems, which take into account factors such as that ice melts faster than it accumulates and that there is a time lag between variations in insolation and changes in ice volume. These models are now able to replicate the frequency spectrum of cycles reasonably well.

1.4 Non-linearities in the Climate System

Whilst there has been vast progress over the last 200 years in our understanding of the Earth's climate, it is an extremely complex, non-linear system and there are still features for which a definitive explanation remains elusive.

1.4.1 The Mid-Pleistocene Transition

This PhD focuses on the period generally known as the Mid-Pleistocene Transition (MPT), which occurred between 1,200-500ka (as defined by *Head and Gibbard* (2005)) and is characterised by a fundamental shift in the dominant glacial-interglacial time period. During this time the climate shows a change from relatively symmetric, 41kyr obliquity cycles before the MPT to the saw-toothed, higher amplitude, approximately 100kyr eccentricity cycles afterwards (*Figure 1.4*). What is surprising is that this evolution occurred without any corresponding alteration in insolation [*Imbrie et al*., 1993; *Shackleton*, 2000]. Eccentricity variations have a significantly smaller impact on insolation than precession or obliquity and so would be expected to produce the weakest effect. This apparent amplification of the 100kyr cycles compared to the incoming insolation is referred to as the '100kyr problem' and suggests yet to be understood internal feedback processes in the Earth system.

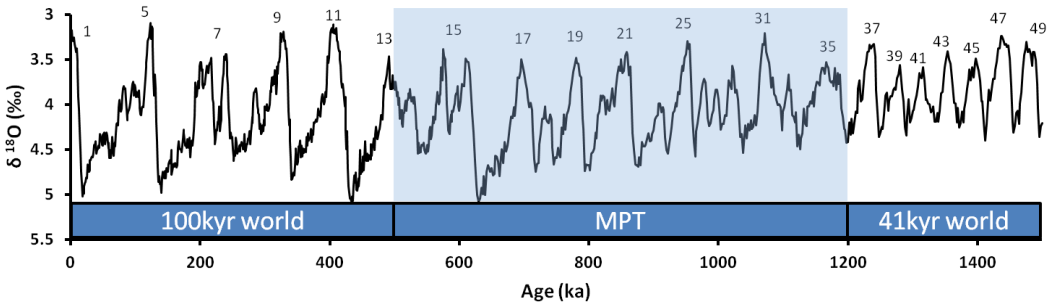

Figure 1.4 The *Lisiecki and Raymo* (2005) global benthic stack with the transition from the '41kyr world' through the 'MPT' (as defined by *Head and Gibbard* (2005)) and into the current '100kyr world'. (Data from *Lisiecki and Raymo*, 2005.)

1.4.2 Possible causes of the Mid-Pleistocene Transition

It is believed that the amplification of the 100kyr signal in the climate record, which occurred during the MPT, must be due to internal feedback mechanisms. However, despite being one of the major focal points in recent palaeoclimate research, there has been no apparent consensus on what these mechanisms were [*Bates et al.*, 2014]. Some authors cite changes in the temperature gradient across the equatorial Pacific

[*de Garidel-Thoron et al.,* 2005; *McClymont and Rosell-Melé,* 2005], others gradually decreasing levels of atmospheric carbon dioxide leading to decreasing sea surface temperatures [*Berger et al.,* 1999; *Raymo et al.,* 1997; *Medina-Elizalde and Lea,* 2005]. Changes in both southern [*Paillard and Parrenin,* 2004; *Raymo et al.,* 2006] and northern [*Clark et al.,* 2006] hemisphere ice sheets have also been suggested. By contrast *Siddall et al.* (2010) and *Bates et al.* (2014) propose that the quasi-100kyr cycles that have occurred since the MPT may not in actuality be due to eccentricity forcing at all, but rather due to missed obliquity cycles. However, it should be noted that researchers' work often (understandably) only focuses on one area, for example: the equatorial Pacific or the Southern Ocean, Northern hemisphere ice sheet dynamics or Southern hemisphere ice sheet dynamics. In reality changes in one part of the climate system will impact on others and feedback processes will occur, thus it is possible to combine many of the proposed causes of the MPT into a more unified single theory that looks at the problem from a global standpoint.

McClymont et al. (2013) bring much of the preceding work together, showing that there is a gradual global cooling in SSTs during glacial periods since 1.2Ma, though interglacial temperatures remain fairly constant [*Berger et al.,* 1999; *Raymo et al.,* 1997; *Medina-Elizalde and Lea,* 2005]. They argue that this pattern is due to climatic feedbacks which operate during glacial periods, via intensified atmospheric circulation, changing patterns of Southern Ocean deep water ventilation and/or dust feedbacks on export production. This may have caused a gradual decrease in pCO_2 and the cooling of upwelling systems and the mid-high latitude oceans could have caused an intensification of both meridional and zonal SST gradients, given the absence of any cooling in the West Pacific Warm Pool [*de Garidel-Thoron et al.,* 2005; *McClymont and Rosell-Melé,* 2005]. The authors argue that these changes led to the development of larger ice-sheets, via the onset and intensification of the modern Walker circulation; which reduced heat flux to the high latitudes but increased moisture transport. This led to modified ice-sheet and climate responses to regular orbital forcing, allowing for the development of 100kyr eccentricity cycles [*Paillard and Parrenin,* 2004; *Raymo et al*., 2006]. These ice-sheets are seen to

develop at ~ 900ka (Marine Isotope Stage 22) [*Elderfield et al.*, 2012] when a large stepwise reduction occurred in both glacial and interglacial temperatures. Explanations for the delay in the formation of these ice sheets at 900ka, after the onset of cooling intensification at 1.2Ma, may include the evolution of basal substrates of the northern hemisphere ice sheets [*Clark et al.*, 2006], unfavourable orbital forcing, temporary restrictions to ice sheet moisture supply by high latitude oceans and a possible threshold decline in glacial pCO_2 values at 900 ka.

The above explanation of the MPT, encompasses ideas from a large body of the research done in the area. It cites an increase in ice volume and reorganisation of the global thermohaline circulation system, which fundamentally combine to produce a new climate regime with an enhanced sensitivity to the 100kyr eccentricity orbital forcing. However, in recent years some authors have challenged the assumption that the solution to the problem of the MPT lies in discovering why the climate shows enhanced sensitivity to eccentricity forcing. By contrast *Siddall et al.* (2010) and *Bates et al.* (2014) suggest that due to the broad nature of the 100kyr spectral peak in the climate record, the quasi-100kyr cycles that have occurred since the MPT may not actually be due to eccentricity forcing at all. Their work shows that glacial Pacific bottom waters approach freezing over the MPT and remain stable for much of the glacial period. It is thought that water mass reorganisation occurred, with a reduction in the transport of heat to the deep ocean via North Atlantic Deep Water (NADW) and an increase in Antarctic Bottom Water (AABW), as a result of the growth of the marine-based East Antarctic ice sheet margin at around 1Ma. These changes are thought to have caused to global cooling and led to such stable conditions in the deep ocean that some obliquity cycles were missed until precessional forcing triggered deglaciation, creating the apparent quasi-100kyr cycles.

Future work on the area needs to resolve the important question as to whether cycles seen in the climate system since ~400ka are due to 100kyr eccentricity forcing or are only quasi-100kyr as a result of precessional cycles and missed obliquity cycles. The

study of sediment cores around Antarctica could be used to test whether glacial deep ocean temperature changes, related to an increase in AABW, were triggered by the configuration of Antarctic ice sheets. Computer modelling studies could also be used to investigate whether the proposed increase in AABW and the cold deep water temperatures it caused, were stable enough to allow obliquity-driven interglacial periods to be missed and quasi-100kyr cycles to be produced due to precessional forcing. Additionally, currently only two high resolution coupled benthic formainifera Mg/Ca and $\delta^{18}O$ records exist for the MPT period, one from the North Atlantic [*Sosdian and Rosenthal.*, 2009] and the other from the South Pacific [*Elderfield et al.*, 2012] and their implications for how ice volume changed during this period do not agree. Both possible explanations of the MPT rely on evidence from the South Pacific record, which appears to show a sudden increase in ice volume at 900ka; however, this increase is not seen in the North Atlantic record. It is therefore important, regardless as to which hypothesis is subscribed to, that more high resolution coupled benthic formainifera Mg/Ca and $\delta^{18}O$ records for the MPT period are produced from cores in various locations, so that changes in global ice volume are accurately known.

1.4.3 Changes in the amplitude of glacial-interglacial CO_2 cycles

Even though there are a variety of possible explanations for this major shift in the mode of operation of our climate system (see § 4.2), most of these theories suggest the existence of a feedback mechanism linking changes in ice volume, ocean temperature, salinity and circulation with the global carbon cycle. Due to the primary influence of the concentration of atmospheric carbon dioxide in regulating the temperature of the Earth, special focus has been placed on obtaining records of palaeo-atmospheric CO_2 levels. High resolution records back to ~800ka have been produced from Antarctic ice cores using the concentration of CO_2 in air pockets trapped in the ice (error of ~ ± 5ppmv). Prior to 800ka atmospheric CO_2 records are not well constrained; though estimates have been made back to the Palaeocene (~60Ma) using methods such as carbon isotopes, boron isotopes, alkenone measurements and stomatal index.

Observations, on various timescales, indicate that periods of warmth are associated with higher atmospheric CO_2 concentrations and vice versa when temperatures were lower [*Petit et al.,* 1999]. This CO_2 - temperature relationship can be clearly seen for the last glacial-interglacial cycles of the last 800kyr in the Antarctic ice core records [*Lüthi et al*., 2008]. The data shows a noticeable change in the amplitude of glacial-interglacial cycles both in the CO_2 and temperature measurements for the last four glacial-interglacial cycles. Before 400ka, Marine Isotope Stage (MIS) 11, the average amplitude of change for CO_2 over a cycle was ~70ppmv (~180-250ppmv). However, since MIS11 this has increased by 40ppmv to ~110ppmv (~180-290ppmv). This increase in amplitude is mainly due to higher CO_2 levels during inter-glacials rather than lower CO_2 concentrations during glacials. The temperature signal shows the same pattern; with a temperature amplitude increase of 2-4^{o}C for glacial-interglacial cycles after 400ka compared to before. Here the increase in amplitude is due to warmer inter-glacials rather than colder glacials, corresponding with the CO_2 record (see *Figure 1.5*).

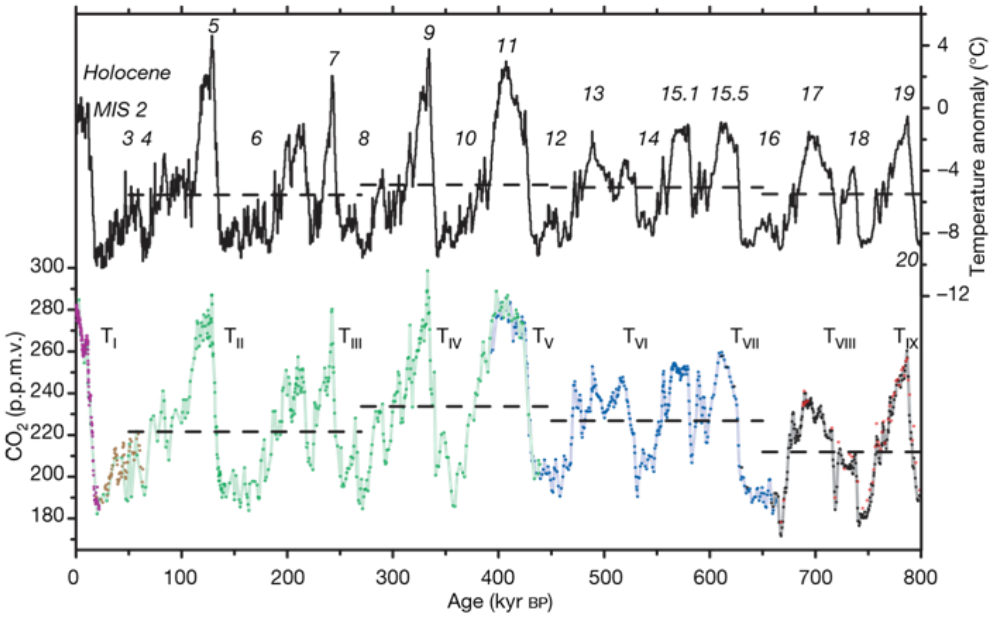

Figure 1.5 Compilation of CO_2 record and EPICA Dome C temperature anomaly (relative to the mean temperature of the last millennium) over the past 800kyr. Horizontal lines are the mean values of temperature and CO_2 for the time periods 799–650, 650–450, 450–270 and 270–50 ka. Glacial terminations are indicated using Roman numerals in subscript; Marine Isotope Stages (MIS) are given in italic Arabic numerals. (From *Lüthi et al*., 2008.)

This sudden shift in the amplitude of glacial-interglacial atmospheric CO_2 change occurs at the end of the MPT and is associated with the onset of full 100kyr climate cycles.

This thesis sets out to investigate the as yet unexplained observation that these major alterations in Quaternary climate are approximately concurrent with a large global expansion in tropical coral reef growth. Possible connections between these two events have been proposed via changes in the global carbon cycle.

1.5 Coral Reef Distribution and History

1.5.1 Worldwide reef history

'Reefs are one of the oldest ecosystems in the world, and coral reefs have had a rich and varied history over hundreds of millions of years.' (See P*andolfi*, 2011 for a review.) The oldest reef-like formations of stromatolites date back to ~3.5 Ga, however these communities were very different to the modern coral reefs we know today and grew under profoundly dissimilar ecological and environmental conditions [*Wood*, 1998; *Allwood* et al., 2006]. Reefs differentiated into open surface and cryptic communities as soon as open frameworks developed in the Proterozoic. After the explosion of metazoans in the early Cambrian (~540Ma), diverse and complex reef-like ecosystems were established on the sea-floor. During the Carboniferous coral reefs were dominated by the now extinct rugosa corals. It wasn't until the Permo-Triassic mass extinction that the modern day scleractinian corals, bivalve molluscs, and encrusting coralline algae reef builders came into dominance [*Wood*, 1998].

Just as the organisms that build reefs have changed over time, so has the global pattern of growth rate, extent and distribution of reefs. Patterns of reef development were highly cyclical during the early-mid Paleozoic time and appear to be related to periods of global warming (reef expansion) or cooling (reef collapse). In periods of major worldwide reef expansion (e.g. Mid-Silurian-Late Devonian), the area covered by equatorial reef is estimated to have exceeded 5 million km^2, nearly ten times that of the modern ocean. However, during times of complete global reef collapse (e.g. Late Devonian) reef complexes were almost completely absent covering no more than 1000 km^2 [*Copper*, 1994].

It was not until the Pliocene that the present day reef distribution was established [*Copper*, 1994]. Modern coral reefs currently cover ~600,000 km^2 [*Kleypas*, 1997], roughly 0.2% of the oceans area; with 91.9% of this area being in the Indo-Pacific

(see *Figure 1.6*) [*Spalding*, 2001]. On average coral reefs produce ~0.9 x10^9 tonnes of carbonate a year, around a fifth of the global production [*Milliman*, 1993].

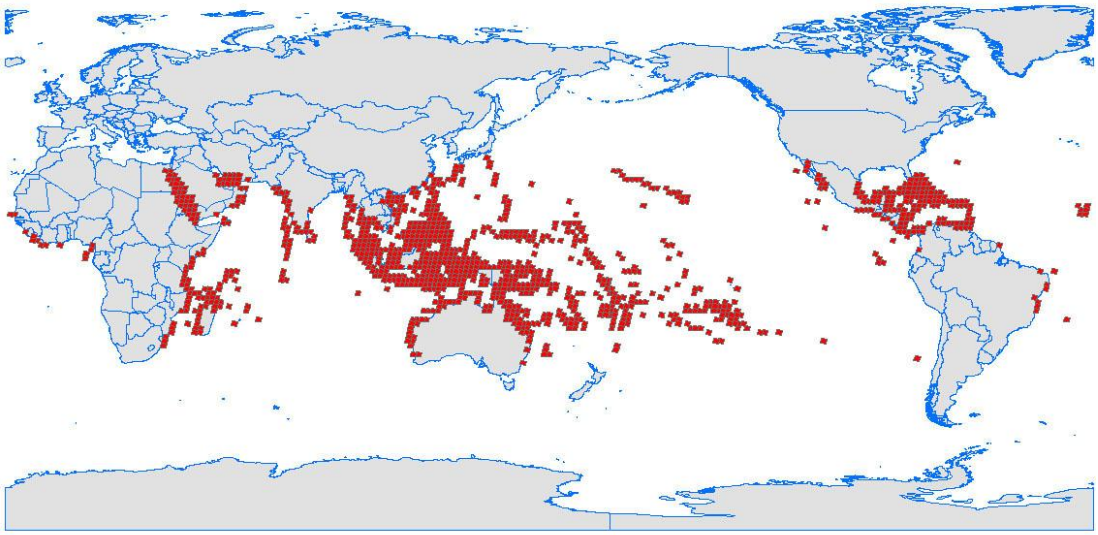

Figure 1.6 Worldwide distribution of modern day reefs. Reefs marked by red squares. (Map from Untamed Science.)

1.5.2 Quaternary reef history

Information on Quaternary changes in reef growth has primarily been obtained via the study of fossilised reef structures [*Alexander et al.*, 2001*; Multer et al.*, 2002*; Braithwaite et al.*, 2004; *Yamamoto et al.*, 2006; *Cabioch et al.*, 2008*; Gischler et al.*, 2010; *Montaggioni et al.*, 2011] and variations in slope and deeper basin sediments [*Dubois et al*., 2008; *Droxler and Jorry*, 2013]. Most observations of fossilised reef structures suggest a rise in shallow water reef production during the last deglacial. Reef growth distribution models such as that used by *Kleypas* (1997) also support this theory; proposing that at the Last Glacial Maximum (LGM), reef area was restricted to 20% of that today and carbonate production to 27%. This reduction in reef production was due primarily to a reduction in available space at the lower sea-level and secondarily to lower sea surface temperatures [*Kleypas*, 1997]. However, information on the timing of growth and extent of coral reefs in previous periods is scarce; this is primarily due to the erosion of past reefs. When available the

information derived from fossilised reefs is hampered by large age uncertainties and only having point records of locations from reef boreholes.

However, studies of coral reef growth appear to show a global acceleration in reef production between 0.8-0.4Ma, including in the South West Pacific where this study is located. Reef history has long been a focus for investigations and thus there is a wealth of data for various locations worldwide including: the Great Barrier Reef (GBR) [*Alexander et al.*, 2001; *Braithwaite et al.*, 2004; *Dubois et al.*, 2008], the New Caledonian Barrier Reef (NCBR) [*Cabioch et al.*, 2008; *Montaggioni et al.*, 2011], the Belize Barrier Reef [*Gischler et al.*, 2010], the Ryukyu Barrier Reef [*Yamamoto et al.*, 2006] and the Florida keys [*Multer et al.*, 2002]. See *Table 1.1* for a summary of estimated reef expansion ages.

Reef Location	Estimated age of expansion	Paper Reference	Method for dating
Great Barrier Reef	600ka ±280ka	*Alexander et al., 2001*	Borehole (Sr/Sr dates)
	560-670ka	*Dubois et al., 2008*	Distal sediments (magnetics, biostratigraphy)
	MIS11 (~400ka)	*Braithwaite et al., 2004*	Borehole (magnetics, radiocarbon, Sr/Sr and U/Th dates,)
New Caledonian Barrier Reef	MIS11 (~400ka)	*Cabioch et al., 2008*	Borehole (U/Th dates, magnetics, biostratigraphy)
	MIS11 (~400ka)	*Montaggioni et al., 2011*	
Belize Barrier Reef	MIS11 (~400ka)	*Gischler et al., 2010*	Borehole (Sr/Sr, biostratigraphy)
Ryukyu Barrier Reef	~800ka	*Yamamoto et al., 2006*	Field exposure (Biostratigraphy)
Florida Keys	MIS 9 (~330ka)	*Multer et al., 2002*	Borehole (U/Th dates)

Table 1.1 A summary of literature values of the ages of expansion obtained for different coral reefs and the dating methods used in each case to establish chronology. For the GBR ages are given in ka, whereas for the NCBR, Belize Barrier Reef and the Florida Keys ages are given in reference to marine isotope stages. The tilde value for the age of the Ryukyu Barrier Reef is how the author records the date, no quantitative uncertainties were given.

1.6 Rationale and Motivation for Thesis

1.6.1 Links between reef expansion and global climate change

There is a possible link between the worldwide expansion of reef growth between 800-400ka and global climate change through modifications in the global carbon cycle. As noted in § 4.3 a clear correlation exists between glacial-interglacial

changes in atmospheric temperature and CO_2 concentrations, as measured from Antarctic ice cores. The warmer temperatures, reduced high latitude ice volume and higher sea-levels of interglacials being associated with greater atmospheric CO_2 levels and vice versa [*Petit et al.,* 1999].

The initial trigger for deglaciations is thought to be insolation, thereafter many different factors contribute to the amplitude of CO_2 shifts seen during glacial-interglacial cycles. For instance, *Parrenin and Paillard* (2012) highlight the importance of initial ice volume on the whether a glacial termination occurs at a given insolation maxima. Decreases in the temperature of glacial oceans allows for the draw-down of CO_2 from the atmosphere, due to the greater solubility of CO_2 in colder waters. However, in contrast, the increase in ocean salinity during glacials (~3%) leads to a concurrent reduction in CO_2 solubility causing an increase in atmospheric CO_2. The reduction in terrestrial biomass during colder more arid glacial conditions causes a decrease in the continental organic carbon reservoir and thus also an increase in atmospheric CO_2 concentrations. However, these factors combined cannot fully explain the CO_2 changes during a deglacial and more complex aspects of the ocean carbon cycle must be explored [*Sigman and Boyle*, 2000].

The 'Coral Reef Hypothesis' was proposed in the 1980s by *Berger*, who argued that changes in the locus of carbonate productivity and preservation is a mechanism for CO_2 transfer between the atmosphere and ocean. During interglacial periods shallow shelf areas are flooded creating greater accommodation space and increased production of shallow water carbonate formations (coral reefs). Phases of rapid reef growth in shallow waters are associated with increased CO_2 emissions to the atmosphere as the carbonate is precipitated (*Equation 1.1*).

Equation 1.1 $2HCO_3^-(aq) + Ca^{2+}(aq) \leftrightarrow CaCO_3 + H_2O + CO_2$

This increased supply of CO_2 to the atmosphere is buffered by dissolution in the deep oceans via *Equation 1.2*; reducing the carbonate ion concentration, alkalinity, of the oceans. This reduction in alkalinity is further compounded by increased sea-levels, which lowers the availability of carbonate deposits for erosion and thus contribution of alkalinity to the ocean via weathering.

Equation 1.2

$$CO_2(g) \leftrightarrow CO_2(aq) \xleftrightarrow{+H_2O} H_2CO_3 \leftrightarrow HCO_3^- \leftrightarrow CO_3^{2-} \updownarrow Ca^{2+} \rightarrow CaCO_3$$

In order to compensate for this reduction in alkalinity the depth of the lysocline shallows, causing increased dissolution of deep sea carbonate sediments (and concurrent reduction in their burial) and thus elevated supply of CO_3^{2-} to the oceans. Eventually a new steady state will be reached and the shoaling of the lysocline will stabilise but at a new, higher atmospheric CO_2 level.

The Coral Reef Hypothesis initially attempted to account for both the triggering of deglaciations and the whole glacial-interglacial CO_2 change [*Berger*, 1982]. However, this hypothesis was rejected for a number of reasons. Firstly, before significant reef growth can occur there must have already been a rise in atmospheric CO_2 and thus temperature, in order to melt high latitude ice sheets and allow for rising sea-level to flood the shallow shelves. Secondly, the observed change in the depth of the lysocline during a deglacial is less than 1km and to explain the complete 80-110ppmv change in atmospheric CO_2 purely via this method requires a theoretical shoaling of lysocline by 3-4.5km, which is not seen. A 25ppmv increase in atmospheric CO_2 being equivalent to a 1km shoaling of the lysocline [*Sigman and Boyle*, 2000].

Sigman and Boyle (2000) support the Southern Ocean Hypothesis that focuses on the idea of greater carbon sequestration in the ocean interior, due to a more efficient biological pump during glacial times; a result of more complete nutrient utilisation at

higher latitudes. Others such as *Vecsei and Berger* (2004), *Opdyke and Walker* (1992) and *Ridgwell et al.* (2003) instead give preference to a more developed version of the coral reef hypothesis first proposed by *Berger* (1982). In reality the explanation behind glacial-interglacial climate change probably lies in a dynamic combination of many factors. Whilst coral reef production in shallow water areas is neither the triggering mechanism for deglaciations, nor entirely responsible for the glacial-interglacial atmospheric CO_2 differences, authors such as *Kleypas* (1997) and *Vecsei and Berger* (2004) note that reefs are still a potentially important factor in explaining glacial- interglacial CO_2 cycles. Modelling of the Last Glacial Maximum (LGM) to present by *Ridgewell et al.* (2003) suggests that corals reefs potentially contributed significantly to CO_2 emissions during the later phases of the deglaciation and may be amplifiers of glacial-interglacial climate change.

It is therefore important to look at the history of coral reef growth and expansion within secure chronological frameworks, so as the temporal relationships between evolution of the climate and ocean systems and changes in reef extent can be properly analysed.

1.6.2 Critique of previous work on coral reef history

There is a large body of work on the Quaternary history of reefs and there appears to a significant synchronous global expansion between 800-400ka which happens concurrently with the climatic changes of the Mid-Pleistocene Transition. However, the task of investigating barrier reef history is not necessarily a simple one due to uncertainties in dating methods and the erosion and alteration of many phases of reef growth. *Droxler and Jorry* (2013) note ‘Because the initial phase of barrier reef evolution is often buried under more recent phases of coralgal growth, the origins of modern barrier reefs have remained elusive’. While *Dubois et al.* (2008) comment ‘Research has been conducted for more than a decade to study and date the onset of the GBR on the Australian continental margin, however, its development remains poorly understood’.

Quaternary reef history is frequently investigated by reef boreholes drilled through the crest of modern day reefs or via field exposures of uplifted reefs. Age-models are developed by radiometric dating of samples, and/or tie points are produced using biostratigraphic markers or magnetostratigraphy. See *Table 1.1* for a summary of literature values for reef expansion and the dating method employed.

However, there are significant problems attached to these dating methods. Firstly, there are frequently only a very limited number of age tie points, even when utilising radiometric dating, biostratigraphy and magnetostratigraphy together. For example, in *Montaggioni et al.'s* 2011 paper which investigates the New Caledonia Barrier Reef, the Ténia 3 borehole which they propose as covering the last 1.2Myr just has nine age-depth tie points, only four of which are absolute ages and these all occur within the last 310kyr (see *Figure 1.7*).

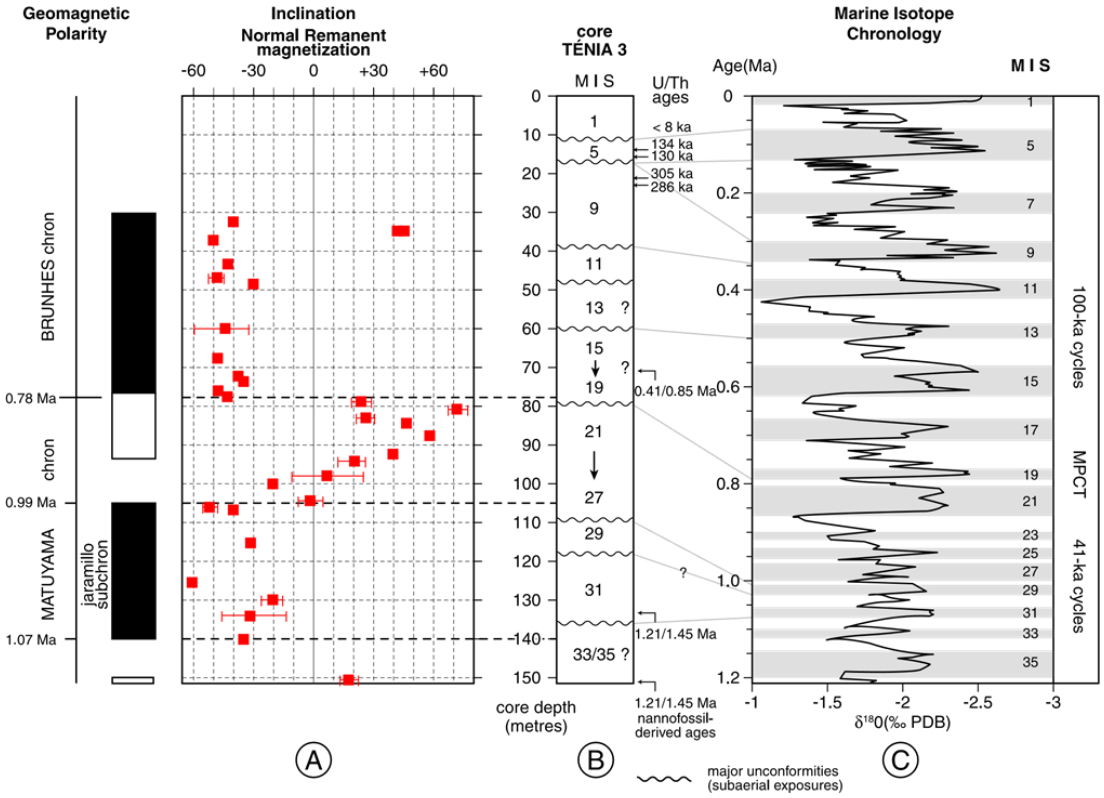

Figure 1.7 Chronostratigraphic model of the Ténia 3 sequence based on **A)** magnetostratigraphy and **B)** uranium-series dating, and nannofossil-biostratigraphy. The successive depositional units identified in the sequence are assigned to interglacial marine isotope stages (MIS) and correlated to the foraminifera-derived oxygen isotope curve (**C**) by *de Garidel-Thoron et al.* (2005). (From *Montaggioni et al.*, 2011.)

This bunching of 'known' ages in the recent past is due to the fact that U-series dating is only able to predict ages back to ~ 400ka due to the open system behaviour of fossil corals and increasing dissolution and recrystalisation with age [*Frank et al.*, 2006]. Whilst it may be entirely coincidental, it is noted that a number of authors such as *Braithwaite et al.*, (2004), *Multer et al.*, (2002), *Cabioch et al.*, (2008). *Montaggioni et al.*, (2011) all of whom use U/Th dating for their age models place the expansion of reefs in their study areas at 400ka, the age limit of the method. It should also be noted that due to erosion, the dated reef fragments very rarely represent closed systems, which is a requirement for radiometric dating. This means

that the errors on the ages are often significant and this can lead to inconsistent and mis-ordered tie-points within an already restricted chronology.

This lack of secure absolute dating often means that chronologies frequently rely on the assignment of stacked depositional units to successive sea-level high stands, even though factors such as erosion and tectonic movements are not well constrained (see *Figure1.7*) [*Multer et al*., 2002; *Cabioch et al.*, 2008; *Gischler et al., 2010; Montaggioni et al.*, 2011].

The uncertainties on ages provided for coral reef expansion (when quantified, which they frequently are not) are of the order of hundreds of kyrs (see *Table1.1*). These uncertainties are therefore not only larger than the length of a glacial-interglacial cycle (100/41kyr) but are also significant when compared to the length of the MPT as a whole. This means that any inferences made about the relationship between reef expansion and specific changes in the climate system are not well constrained.

Also not only do different reefs seem to expand at different times (see *Table1.1*), even within the same reef system (such as the GBR) there are differing ages [*Alexander et al.*, 2001; *Braithwaite et al.*, 2004; *Dubois et al.*, 2008]. Whilst these age differences may be explained by varying morphology of the margins the reefs develop on, there is a significant time difference between a reef established at 880ka (the oldest suggested literature date at the GBR [*Alexander et al.*, 2001]) and one at 330ka (the youngest suggested literature date at the Florida Keys [*Multer et al.*, 2002]). This difference of 550kyr is perhaps large enough, especially in relation to the length of the Quaternary and glacial-interglacial cycles, to be argued not to be synchronous at all.

Though reef borehole studies frequently utilise cores from more than one location along the reef complex [*Gischler et al.*, 2010; *Montaggioni et al.*, 2011], drilling only provides point data and inference must be made for larger spatial scales [*Andréfouët et al.*, 2009] and there is frequently an assumption that reef history will be uniform along a margin. This means that lateral shifts in reef growth, which may occur as a result of progradation, changes in sea-level or tectonic movements, are not picked up on.

In order to further investigate the relationship between coral reef growth and changes in the climate system, such as the MPT, it is necessary to develop a new approach for accurately constraining the dates of changes in reef growth. This study uses the basic premise of those such as *Dubois et al.* (2008) and *Droxler and Jorry* (2013) that patterns in distal sediments can be used to access information on the history of the reef on the shelf.

1.7 Development of a New Methodology for Investigating Reef History

This study presents a trial methodology which attempts to tackle the problem of poor reef history dating, by providing a complementary source of information on reef evolution from a much more secure time framework.

Instead of reef boreholes, which are both destructive to reefs and suffer from inherently poor dating, this study used material sourced from the shallow shelf which has been deposited as sediment gravity desposits, generically known as turbidites, in a deep sea sediment core: MD06-3019 (recovered ~100km off the SW coast of New Caledonia, from a water depth of 3520m; see *Figure 2.5*). The main advantage of this method is the significant reduction in age uncertainty of events. The core (and the turbidites it contains) can be accurately dated using correlation of oxygen isotope curves from the background carbonate ooze (see Chapter 3). Age model uncertainties

for the turbidites dated in sediment core MD06-3019 are of the order of ±10 kyr (see Chapter 3 § 6.2). This is small compared to that of previous methodologies (of the order of 100kyrs, see *Table 1.1*) and relative to both the length of climate cycles [*Lisiecki and Raymo*, 2005] and the MPT [*Head and Gibbard*, 2005]. Palaeoceanographic proxies can be compared directly to reef history, since both data sets are derived from the same sediment core. This allows for comparison of the timing of events which is simply impossible with traditional borehole methods. In addition, because turbidite material is sourced from a wide area along the coast, the method is able to provide information on reef history over a larger spatial area than single reef boreholes.

1.8 Aims and hypotheses

The wider context to this thesis is the need for further investigation into unexplained changes in the climate system that occurred during the MPT and the potential relationship between coral reef growth and changes in climate via the global carbon cycle. These over-arching aims are, of course, far beyond the scope of this project and thus this thesis aims to address only one aspect: that of the poor understanding of the history and timing of tropical coral reef growth over the Quaternary, especially prior to 400ka. A more specific outline of how the thesis aims to achieve this is given below:

I. To trial and develop a new methodology for investigating reef growth history, by using the changes in the properties of turbidites sourced from the shallow shelf and deposited in the deep sea.
II. To compare and contrast the information that this new method is able to provide about shallow shelf history with that of previous published work from borehole dating. Specifically to see if the previously documented expansion of the New Caledonia Barrier Reefs around 400ka (MIS11) is reflected in turbidite deposits in deep sea sediment core MD06-3019.

III. To develop an aragonite proxy using x-ray fluorescence measurements for Sr to investigate the aragonite content (reflecting the dominance of shallow water biota) of turbidite layers.
IV. To interpret the variation in the composition, grain size, timing and volume of turbidite deposits in core MD06-3019 with respect to temporal changes on shallow shelf to provide a history of reef growth in the New Caledonia area over the last 1.26Myr.
V. To discuss the relative importance of the possible controlling mechanisms behind these changes in reef growth and to examine the global significance these interpretations place on the histories of other tropical reef systems.
VI. To aid future research on reef history conducted via examinations of deep sea turbidites by providing an in depth study of sediment shedding to the deep sea on the mixed siliciclastic-carbonate New Caledonia margin over the last 1.26Mayr using the MD06-3019 record.

The completion of these aims allows for the testing of three major hypotheses:

1. The expansion of the western New Caledonia Barrier Reef from an open carbonate ramp into a rimmed shelf has been placed at MIS11, ~400ka, via reef borehole investigations [*Cabioch et al.*, 2008; *Montaggioni et al.*, 2011]. The initiation of carbonate production on shallow shelves is known to produce a signal in the surrounding deep basins, via sediment shedding [*Dubois et al.*, 2008 and *Droxler and Jorry*, 2013]. It is therefore expected that there will be a single change in the composition of turbidites recorded by deep sea sediment core MD06-3019, with those deposited after 400ka showing a significant increase in coral reef material compared to those prior to this period.
2. Many factors impact on the growth of shallow water carbonate producers, including geographic-tectonic, physic-chemical, hydrodynamic and biological variables. Based on the work of *Cabioch*, 2003, *Cabioch et al.*, 2008 and *Montaggioni et al.*, 2011, it is predicted that local sea surface temperatures were the principal control on coral reef growth round New Caledonia over the

last 1.26Myrs. Only after MIS11 did climatic conditions become optimal for luxuriant reef growth during highstand periods.

3. Theories of sediment shedding on siliciclastic and carbonate margins due to changes in sea-level are well established, resulting in the lowstand and highstand hypotheses respectively [*Vail et al.*, 1977 and *Schlager, Reijmer and Droxler*, 1994]. Little work has been conducted on mixed margins such as New Caledonia. However, it is predicted that the record of turbidite deposition in deep sea sediment core MD06-3019 will change at MIS11 (~400ka), due to the expansion of the barrier reef, from a pattern more reflecting lowstand siliciclastic shedding to one reflecting highstand carbonate shedding.

1.9 Thesis Structure

This thesis has been divided into 4 main sections:

Part I: provides a general introduction to the rationale, motivation and aims of the thesis (this chapter).

Part II: Chapter 2 gives an introduction to the marine sediment cores used in the production of this thesis; as well their geographical, geological, climatological and oceanographic setting. A review of current literature on the history of New Caledonia Barrier Reef is also provided here. **Chapter 3** addresses aims I and II, presenting the development and validation of a secure chronology in which to place all subsequent findings. **Chapter 4** covers aims I and II via a thorough description of the physical properties and sedimentology of core MD06-3019; including the classification and description of the content of sandy layer.

Part III: presents the main body of work of the thesis and is dedicated to the interpretation and discussion of the results obtained. **Chapter 5** addresses aim III and

presents the development of strontium concentration, obtained by X-ray fluorescence core scanning, as a proxy for the presence of shallow shelf aragonite using calibration via X-ray diffraction data. **Chapter 6** then focuses on the use of this new proxy, along with analysis of the carbonate content of layers, to provide inferences on reef history in the New Caledonia area, addressing aims IV and V. **Chapter 7** covers aim VI and looks in detail at the relationship between the timing and composition of turbidites with respect to glacial-interglacial sea-level change.

Part IV: Chapter 8 considers the significance of this work in the wider context of the palaeoceanography of the Mid-Pleistocene Transition and coral reef history and provides suggestions for the direction of future work in this area. Finally, overall conclusions are presented.

Six appendices to the thesis are included. **Appendix 1** provides background information on the underlying principles of the experimental methodologies used to obtain the raw data presented in this thesis. **Appendix 2** contains supplementary material on the short gravity core MD06-3020, which was taken close to the main core used in this study, and presents a discussion on variations in apparent sedimentation rates. **Appendix 3** provides a short investigation into dissolution in the New Caledonia Basin**. Appendix 4** provides supplementary information for Chapter 6, including the controls on shallow shelf carbonate production. **Appendix 5** contains the photographs, sedimentary logs and descriptions of cores MD06-3018, MD06-3019 and MD06-3020 core sections. Finally, **Appendix 6** provides descriptions of turbidites present in sediment cores MD06-3019 and MD06-3020 including down-core positions, depositional ages, widths and content. The digital only **Supplementary Data** provides the full down-core data sets obtained during this PhD; as well as the parameters used for, and the results obtained from Monte-Carlo and Mann-Whitney U test analyses.

Chapter 2: Setting and Materials

2.1 Chapter Overview

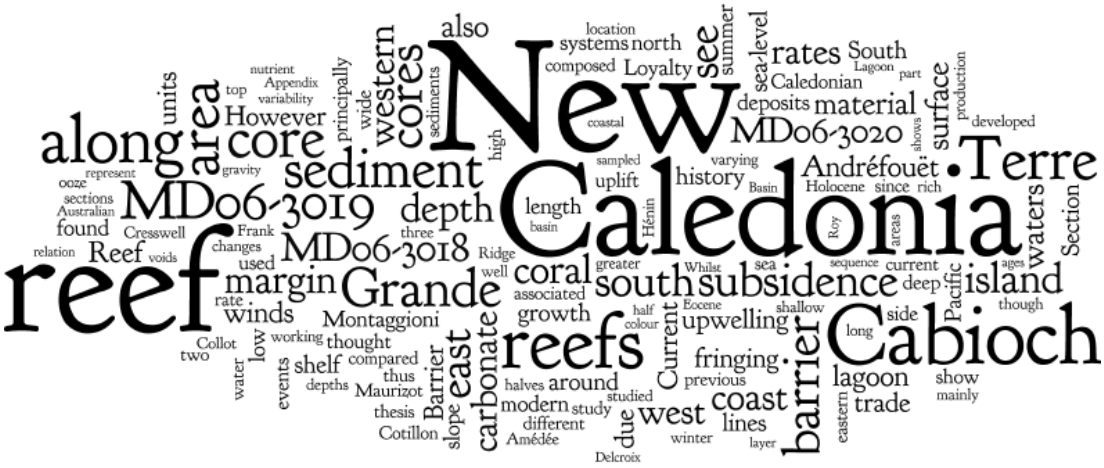

This chapter provides an introduction to the study area and cores (MD06-3018, MD06-3019 and MD06-3020) used in the production of this thesis. Initially, a brief précis of the geology and geography of the area is given, since this thesis examines down-slope deposits sourced from the shallow shelf along the western margin of New Caledonia. This is followed by a description of the current distribution of reefs around New Caledonia; as well as information on subsidence rates and the modern oceanography and climatology of the area which control the distribution of reef growth. A review of work conducted on the history of the New Caledonia Barrier Reef is then provided. Finally, brief descriptions of sediment cores MD06-3018, MD06-3019 and MD06-3020, which were used in the production of this thesis, are given. Whilst MD06-3019 was the sediment core principally used in this work, references are made to the results from nearby cores MD06-3018 and MD06-3020 and thus a brief description of them is given here.

2.2 Regional Setting

2.2.1 Geological setting

The main New Caledonian islands are located on the eastern side of the Coral Sea between 19-23ºS and 163-169ºE, with the Australian continent to the west and the open Pacific Ocean to the east (see *Figure 2.1*). The area is part of a complex zone of oceanic and thinned continental crust, largely submerged continental strips and volcanic ridges or arcs [*Maurizot and Collot*, 2009].

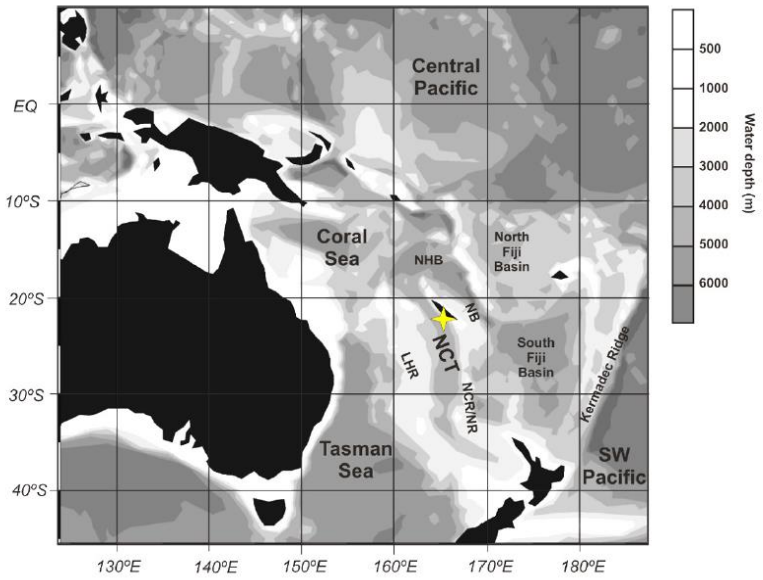

Figure 2.1 Location of the study site (yellow star) and New Caledonia in relation to the regional geography and bathymetry (ODV software [*Schlitzer, R.*, 2007]).

The islands of New Caledonia are situated on two parallel northwest-southeast trending ridges: the Norfolk Ridge (also known as the New Caledonia Ridge) where Grande Terre lies and to the east the volcanic Loyalty Arc, which is the location of the Loyalty Islands (see *Figure 2.2*) The Norfolk Ridge is mainly a submerged continental strip which bares the emergent Grande Terre in the north and in the south connects with New Zealand. The Loyalty Ridge it is thought to be an Eocene arc and the Loyalty Islands, which lie on it, consist of a line of uplifted seamounts capped by Miocene reef formations [*Maurizot and Collot*, 2009].

Immediately to the west of Grande Terre lies the New Caledonia Basin (see *Figure 2.2*), which is composed of thinned intermediate crust [*Klingelhoefer et al.*, 2007]. Close to New Caledonia it is an eastwards dipping foreland basin with sediment cover up to 6km in depth. To the east of Grande Terre lies the South Loyalty Basin, which is believe to be contemporaneous in age with the Tasman Basin [*Cluzel et al.*, 2001]. This is comprised of oceanic crust, with thick sediment cover up to 8km, that rises towards and outcrops on New Caledonia where the root of the basin is exposed in the New Caledonian Ophiolitic Nappe [*Collot et al.,* 1987].

The whole area is on the Australian plate, which is subducting to the east under the Pacific plate, producing the arc trench system of the New Hebrides. This subduction zone, which is in opposition to the overall westward dipping subduction pattern of the west Pacific margin, was established during the Miocene (see *Figure 2.2*). Up until the Cretaceous New Caledonia was part of the eastern margin of Gondawana with Australia and Antarctica. However, since the mid-Cretaceous the basins of this area opened up on the over-riding plate of a westward dipping subduction zone. Cretaceous New Caledonia broke free from Gondwana at ~85Ma and at the end of the Cretaceous (70-65Ma) together with New Zealand it then separated from Australia.

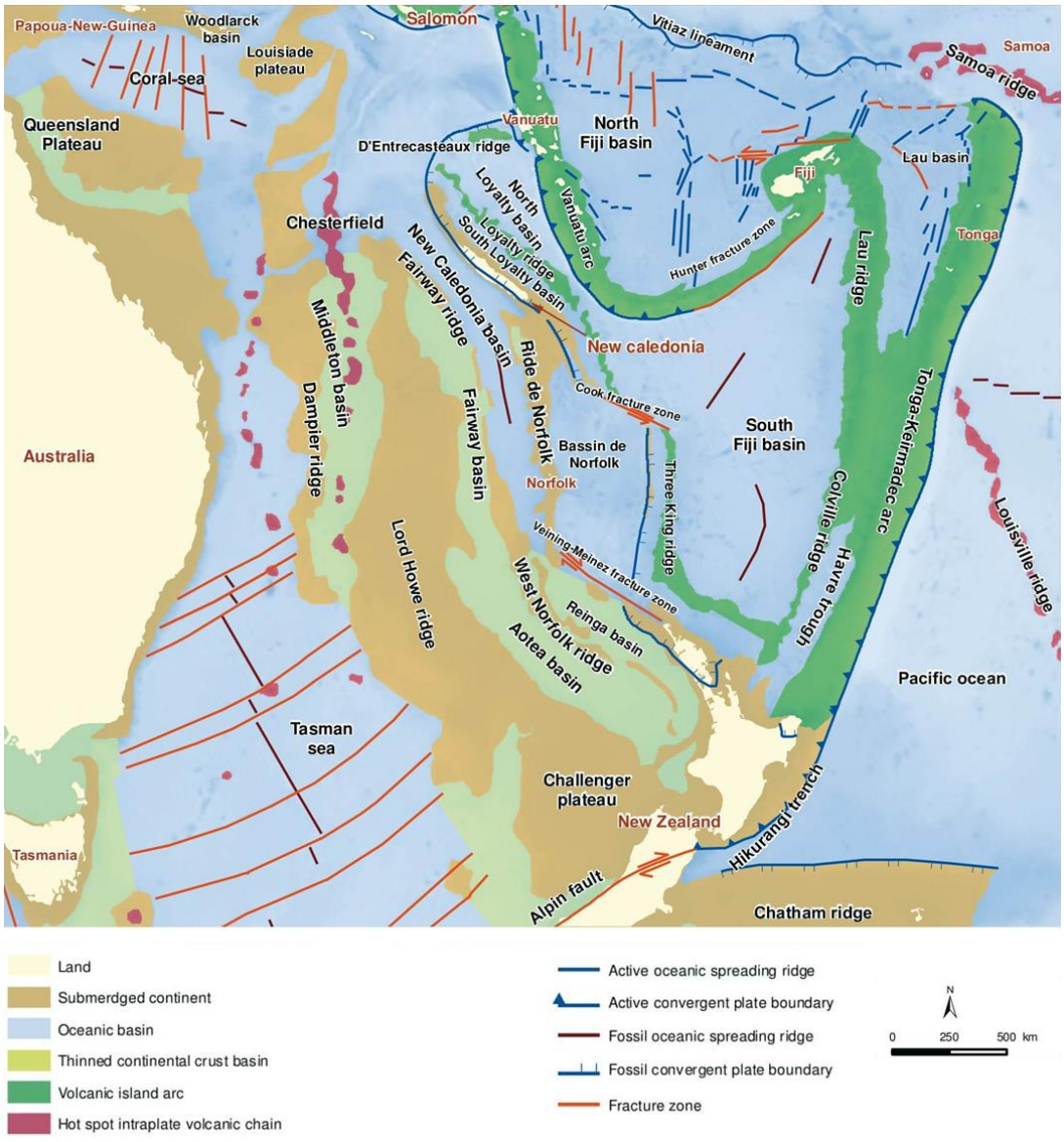

Figure 2.2 Overview of the complex basin-ridge structure of the area surrounding New Caledonia. **(**From *Maurizot and Vendé-Leclerc*, 2009.)

The island of Grande Terre is principally composed of a complex Mesozoic basement of intra-oceanic origin, which is exposed down the centre of the island. These basic igneous rocks are unconformably overlain or overthrust by sediments and, in the south, ophiolite complexes of Late Cretaceous-early Oligocene age. Sediment cover (late Cretaceous-Palaeocene) reflects a rift environment on the Eastern Gondwana margin. This was followed in the late Eocene by a change to convergent tectonics which resulted in the emplacement of the ophiolitic sequence in the south and the exhumation of the deeply buried metamorphic complex in the north [*Maurizot and Collot*, 2009]. The Eocene Flysch reflects the gradual progression of the Norfolk Ridge into the convergence zone [*Maurizot and Collot*, 2009]. The peridotite nappe covers approximately a third of Grande Terre and dominates the island's geology [*Pelletier*, 2006, *Maurizot and Collot*, 2009]. The ultrabasic rocks are mainly composed of harzburgite-dunite mantle sequences and are of economic importance, being mined for their mineral deposits. Basalt on the west coast is also spatially associated with the ultrabasics being remnants of the oceanic floor overthrust before the ophiolite. The high pressure-low temperature metamorphic complex in the north of island is one of the largest and best preserved in the world [*Maurizot and Collot*, 2009]. These blueschist-greenschist units underwent peak metamorphism between the Early –Middle Eocene [*Spandler et al*, 2005] and have cooling ages dated to the Middle-Late Eocene [*Ghent et al.*, 1994; *Rawling,*, 1998; *Baldwin et al.*, 2007].

During the Oligocene and Miocene New Caledonia was dominated by uplift and erosion. On Grande-Terre, this is reflected in extensional fault movements [*Lagabrielle et al.*, 2005; *Chardon et al.*, 2008] that led to collapse of ridge margins and exposure of the Mesozoic basement with variable deformation and faulting along the topographic axis. Sedimentary formations consist of fluvial and deltaic deposits [*Chardon & Chevillotte*, 2006]. Perched palaeosurfaces with lateritic weathering profiles and iron caps represent remnants of former basins that have since been uplifted. This weak extensional tectonics setting has persisted, resulting in the

accumulation of sediments in the New Caledonia Trough from the Miocene to the present. (See *Figure 2.3* for a geological map of the New Caledonia area.)

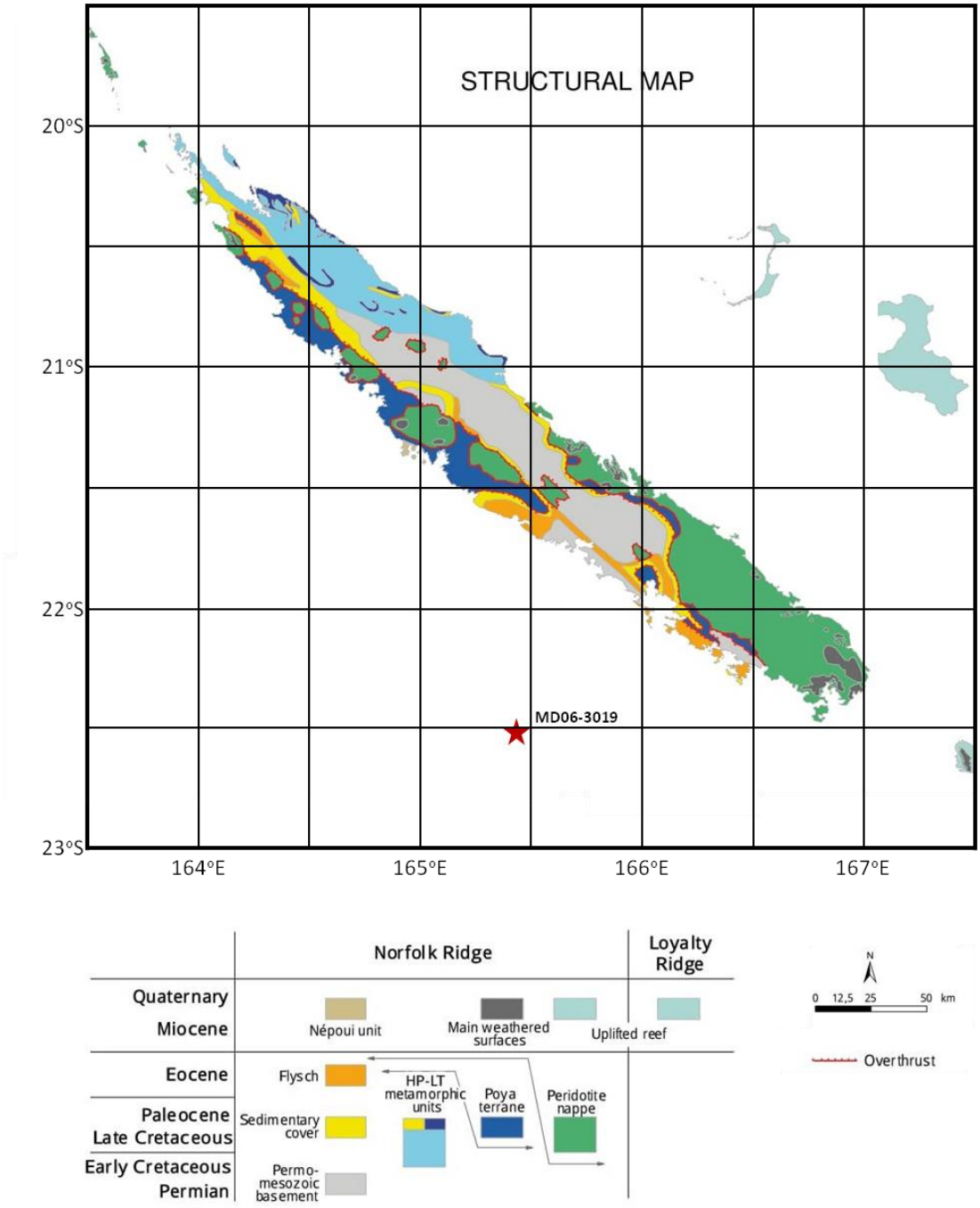

Figure 2.3 Simplified geological map of Grande Terre highlighting the main geological units. Location of core deep sea sediment MD06-3019, which is used in this PhD, show by a red star. **(**From *Maurizot and Vendé-Leclerc*, 2009.)

2.2.2 New Caledonia Basin canyon systems: sediment production, supply and shedding

Currently carbonate sediment is produced along the western New Caledonia margin in large volumes on the shallow shelf by the New Caledonia Barrier Reef, as well as by fringing reefs and other carbonate producers in the lagoon. Carbonate debris found in the lagoon is mainly composed of forams and molluscs but also calcareous algae and coral, which while never dominant is significant close to reefs and in inlets and the back reef slope [*Ouillon et al.*, 2010]. Terrigenous sediment from New Caledonia is delivered to the lagoons by the island's rivers and is largely trapped near the coast in mangroves and small deltas (see *Figure 2.4A*) [*Clavier et al.*, 1995]. Only a minute part of the terrigenous sediment supplied by rivers reaches the lagoon and that which does is rarely >63µm in size [*Clavier et al.*, 1995]. Sediment supply by rivers is heavily dependent on rainfall induced erosion in the area and thus varies seasonally, due to movement of the Inter Tropical Convergence Zone (ITCZ) between the wet (Jan-March) and dry seasons; as well as annually, depending on ENSO (20-50% increase in rainfall during La Nina periods). Sediment discharge per year can vary by a factor of 100 depending on annual rainfall differences [*Ouillon et al.*, 2010]. Generally sediment supply is very low during dry periods, since rivers deliver infiltrated waters and draining ground waters which do not favour suspended particulate transport [*Ouillon et al.*, 2010]. However, during periods of heavy rainfall (e.g. cyclones and storms) intense erosion can occur with high volumes of suspended sediment being transported into the lagoon via fluvial plumes which reach out into the bays, though not across the entire lagoon, with heightened turbidity lasting for around a week [*Ouillon et al.*, 2010]. Sediments deposited in the lagoon are resuspended not only with each tidal cycle but also during high energy events and are then redistributed through the lagoon by currents. After a storm or cyclone event there is approximately a four day lag between reducing particle flux in the inner lagoon and canyons on the barrier reef [*Magand*, 1999].

By contrast, during Last Glacial Maximum sea-level dropped by around 120m, to below the shelf edge and sediment supply along the western New Caldonian margin

would have been very different. Carbonate production on the barrier reef was suspended and would have been limited to a narrow band on the steep slope. Terrigenous supply would also have changed with rivers running out, perpendicular to the reef, across the subaerially exposed shelf, allowing terrigenous sediment to be transported directly to the outer shelf/ upper slope area (see *Figure 2.4 B, C and D*).

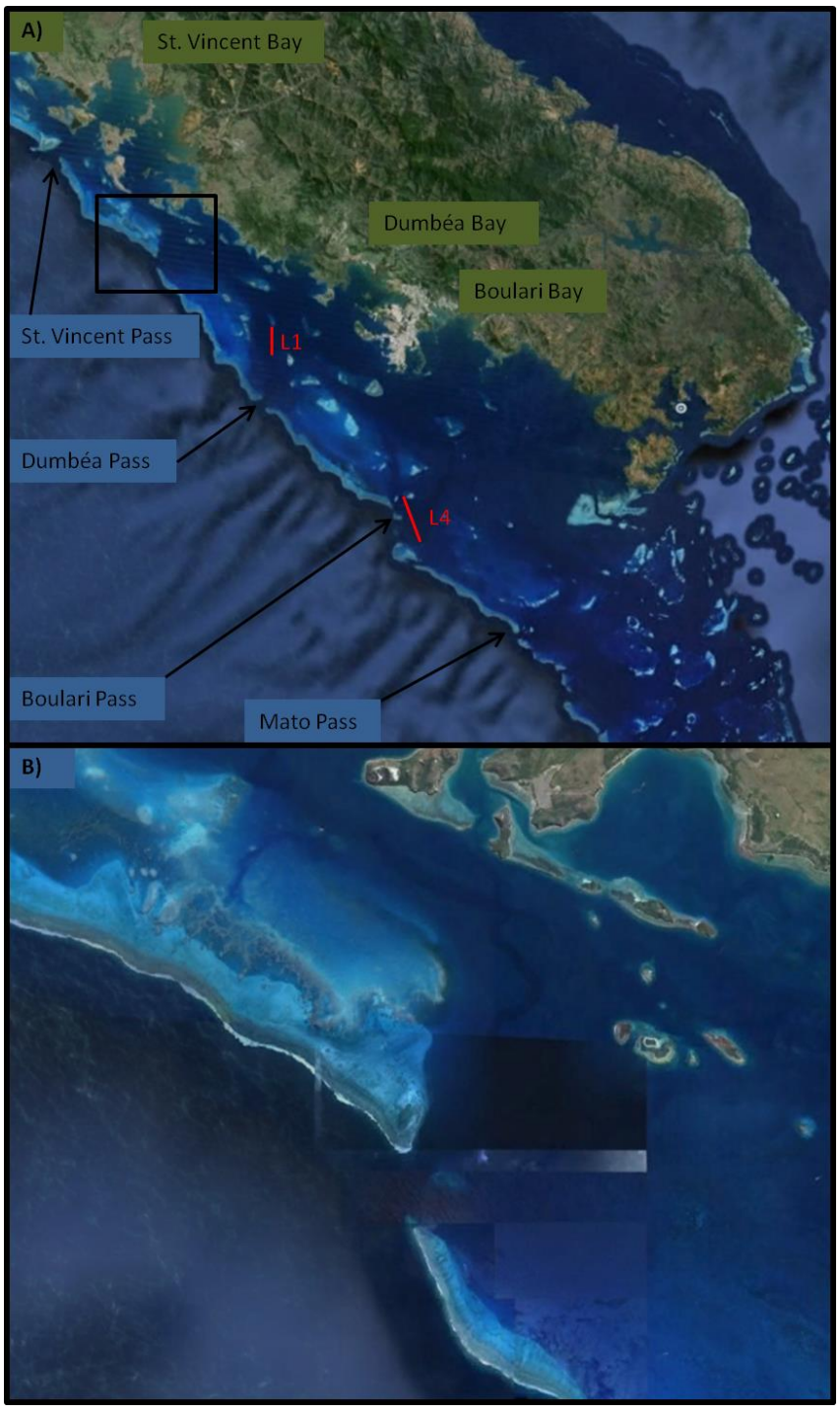

Figure 2.4 A) Satellite image of the southern half of western New Caledonian margin showing the occurrence of deltas along the coast, where rivers entering the lagoon deposit terrigenous material and the slope canyon systems. The black box highlights the close up in panel B, red lines show the position of seismic lines in panels C and D. **B)** Close up satellite image of the area of St. Vincent's Bay, showing a darker blue colour for past river channels due to their greater depth.

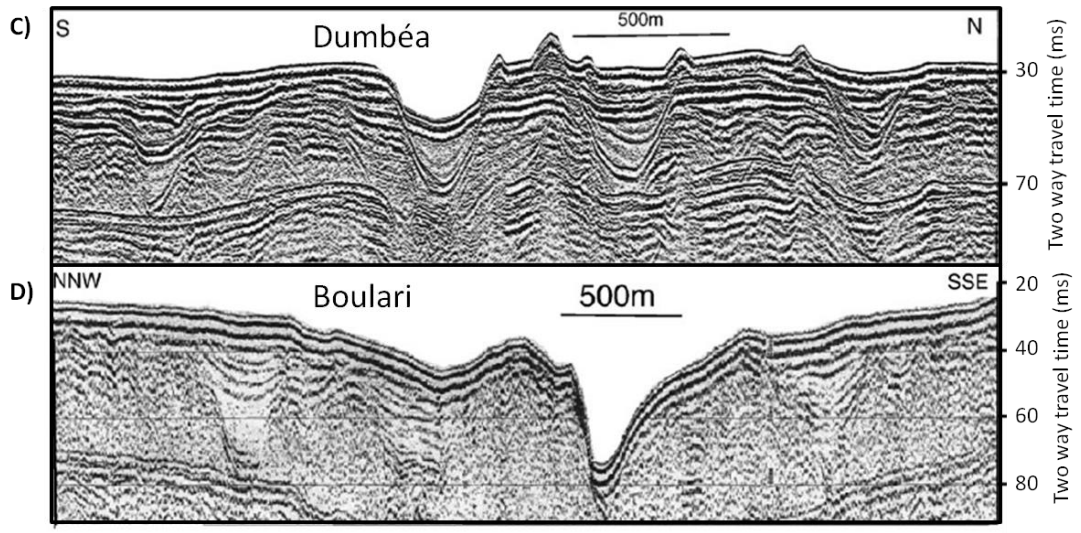

Figure 2.4 Seismic lines L1 and L4, as highlighted in panel B, showing the presence of deeply incised palaeoriver channels formed during previous lowstands, located in **C)** the Dumbéa system and **D)** the Boulari system respectively. (From *Le Roy et al.*, 2008.)

The southwest margin of New Caledonia is characterised by a very shallow rimmed continental shelf and a very steep slope (~10^{o}); corresponding to the 'escarpment margin' type, using the carbonate platform classifications of *Emery* (1996). Erosion predominates along the slopes, where there is generally only a thin coating of hemipelagic sediments, demonstrating that gravity induced movement of sediments is relatively frequent. The slopes around New Caledonia are incised along on all or part of their length by numerous submarine canyons up to 25km long, 1-3km wide and 100-500m deep [*Cotillon et al.*, 1989b]. The most spectacular are to be seen in the south-west of New Caledonia, where the canyons are well developed and stretch out well into the deep basin (see *Figure 2.5*). Generally, the canyons are parallel to the lines of greatest slope. The greater the slope the more it is cut into by wide, cross-sectionally concave canyons, separated by narrow spurs. This gives a morphology dominated by gravity erosion, determined by large shifts in mass. The canyons seem to ensure an almost direct transport of material from the external platform to deep/middle depths via gravity flows [*Cotillon et al.*, 1989b]. Evidence of these events are found in the two deeper cores used in this study, MD06-3019 and MD06-

3020. However, the shallower MD06-3018 site is situated on a topographic high and therefore does not receive material from these flows.

Research during the late 1980s by *Cotillon et al.*, based on samples and bathymetry data collected during the 1987 BIOCAL cruise, provides limited information about the content of these gravity deposits. The work largely focuses on sediments deposited during the last glacial-interglacial cycle to the East of New Caledonia; in the Loyalty Basin, along a transect between Thio (on Grande Terre) and Lifou (on the Loyalty Ridge). However, broadly similar depositional regimes could be expected on both sides of the island.

In the area studied by *Cotillon et al.*, 1989b the basin is supplied with turbidites (frequently with an erosive base) from the New Caledonian margin which travel over 50km. The sediments are comprised of a mixture of peri-platform carbonate debris and clays from the continent, mixed to a greater or lesser extent with remobilised hemipelagic ooze from the slope [*Cotillon et al.*, 1989b]. The material found in turbidites recovered during the BIOCAL cruise are very similar in composition to those found in core MD06-3019 and comes from 5 sources [*Cotillon et al.*, 1989a; *Cotillon et al.*, 1989b, *Cotillon et al*., 1990]:

1. Terrigenous material from New Caledonia: 5-40% (mainly clay minerals, quartz, iron oxides and heavy minerals).
2. Bioclastic silts and sands derived from the reefs and lagoons around New Caledonia: 15-25%.
3. Mixed bioclasts: 1-20% (furnished by benthic species which colonise the slopes and the basin).
4. Plankton debris: 30-75% (forams, pteropods and nannofossils)
5. Volcanics:- 0.5-10% (glass and pumice)

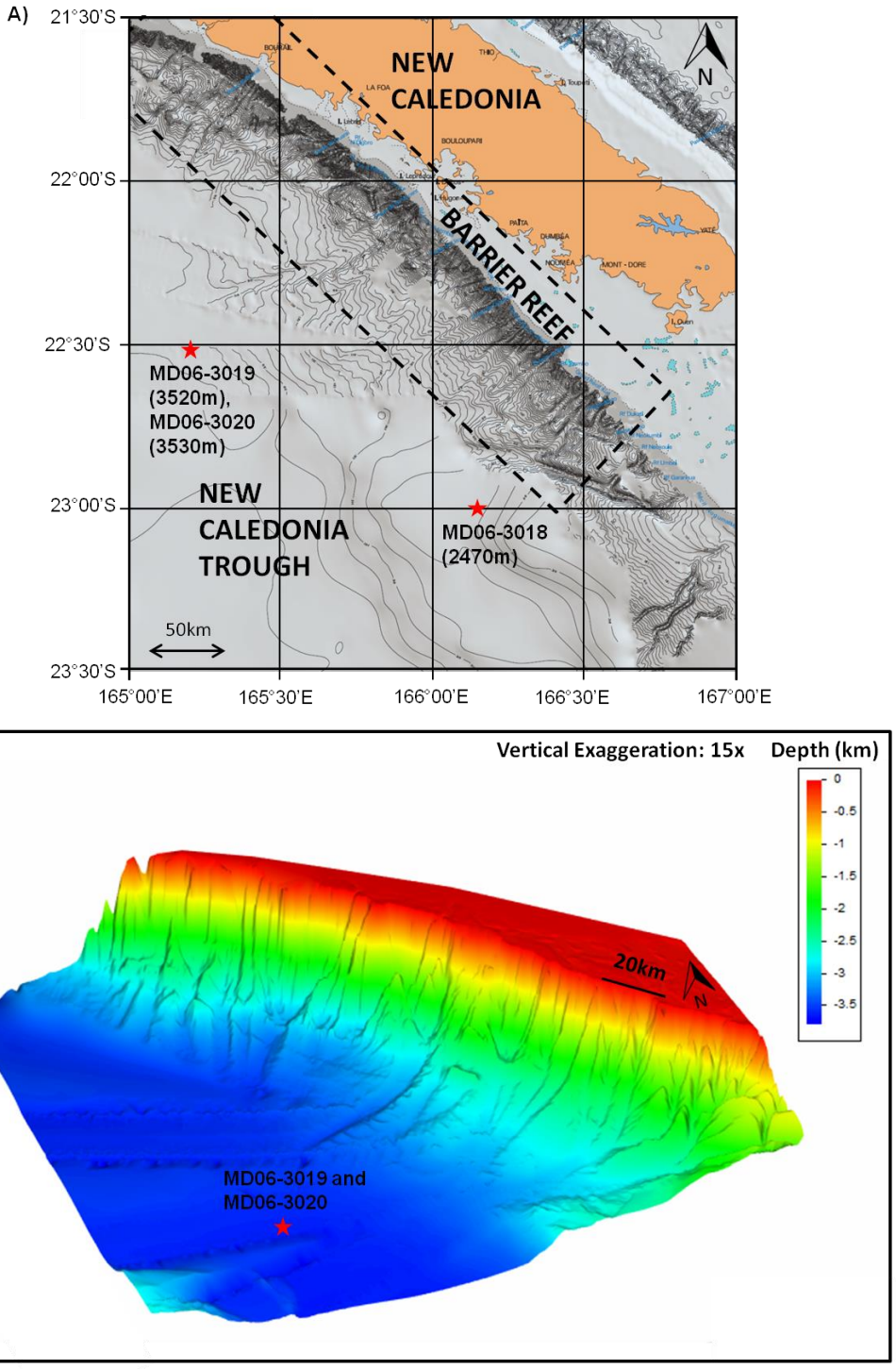

Figure 2.5 A) Detailed bathymetric map of the eastern New Caledonia Trough showing the exact positions of the cores used in this study, in relation to the island of Grande Terre, western New Caledonia Barrier Reef and underwater canyon systems in the area (dashed box). (Bathymetry from the ZoNéCo program [*Foucher et al.*, 2006].) **B)** 3D view of the canyon systems on the Western New Caledonia margin (dashed box in A) viewed from the south-west. (Bathymetry from the ZoNéCo program [*Foucher et al.*, 2006].)

2.2.3 The modern day New Caledonia Barrier Reef

The New Caledonia Barrier Reef (NCBR) is one of the largest continuous coral reef systems in the world, reaching over 1000 km in length and enclosing lagoons of 23,400km^2 [*Cabioch et al.*, 1999]. Located on the South-Eastern side of the 'Coral Sea' the reefs show great diversity of types and occur on both sides of the island of Grand Terre, as well as atolls round the nearby Loyalty Islands (see *Figure 2.6*) [*Andréfouët et al.*, 2009]. The width of the lagoons varies from hundreds of metres to up to 60km and the reef tracts extend past the ends of the island creating the vast lagoons to the north and south: the 'Great North Lagoon' and 'South West Lagoon of Nouméa' [*Cabioch et al.*, 2008]. The depth of the lagoon varies between an average 17.5m for areas bordering the coast and 35m for the South West Lagoon; but deeper meandering channels, believed to be palaeorivers, are found linked to passes of greater than 70m depth out on the barrier reefs. During the low sea-levels of glacial periods, rivers discharge closer to the shelf edge; crossing the current day lagoon and reef area that is currently submerged [*Le Roy et al.*, 2008].

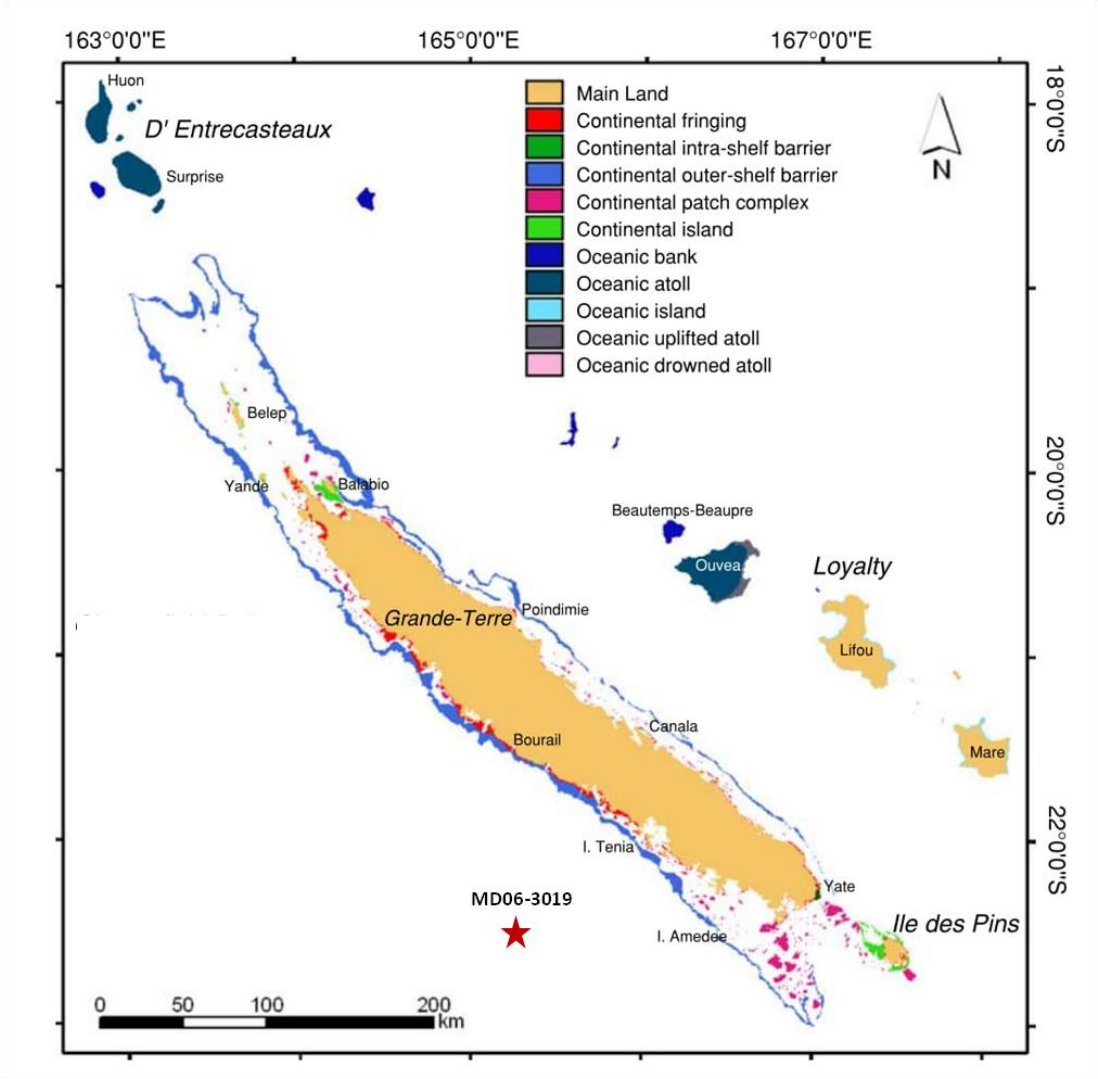

Figure 2.6 Reef geomorphology map of New Caledonia according to the Millennium Mapping Project typology proposed by *Andréfouët et al.* (2006). Location of deep sea sediment core MD06-3019, which is used in this PhD, is shown by a red star. (From *Andréfouët et al.*, 2009.)

Fringing reefs are common in near shore areas where hard substrates are present, especially along the eastern coast [*Cabioch et al.*, 1999]. They can be differentiated into two types as a function of wave energy. Firstly, 'high energy' reefs along the south east coasts (Poindimié, Thio and Mamié-Ounia), which are subjected to strong swells, genrated by trade winds and are not protected by barrier reefs. Secondly, 'low energy' reefs along the west coast (Poum and Ricaudy) which are protected by the well developed barrier reef tract [*Cabioch et al.*, 1995] (see *Figure 2.7*).

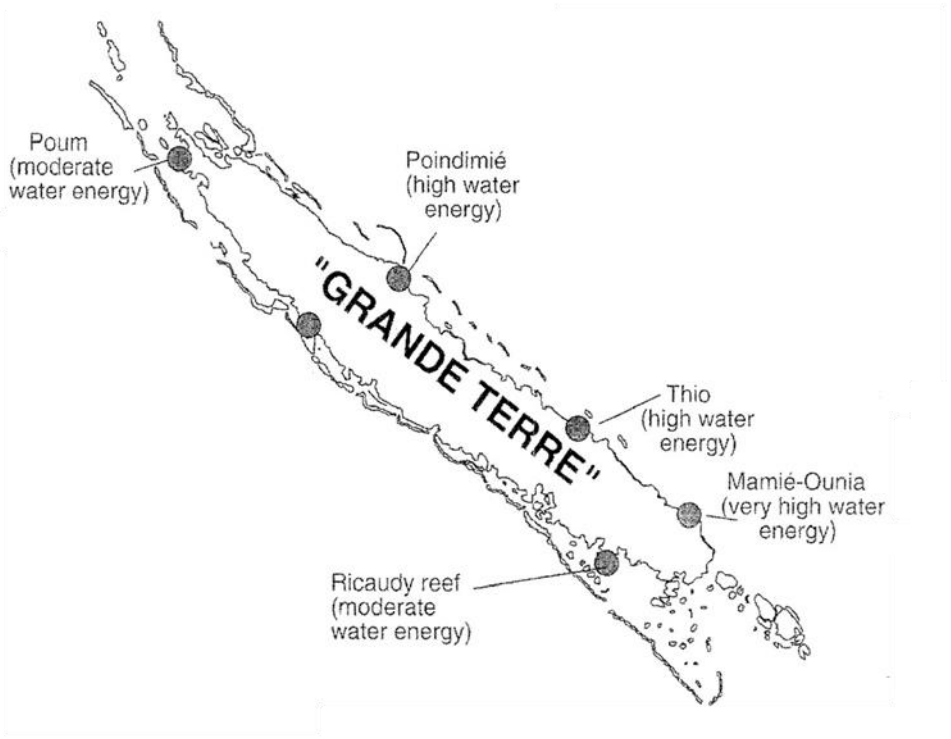

Figure 2.7 Map detailing the locations of high and medium energy fringing reefs round the island of Grande Terre, New Caledonia. (From *Cabioch et al.,* 1999.)

Inner reefs and coral islets are found throughout lagoon areas and along the west coast are orientated parallel to the shoreline [*Cabioch et al.*, 1995; *Frank et al.*, 2006]. The wide South West Lagoon (including the Ile des Pins) has a very complex morphology, with many fringing and patch reef systems orientated in a variety of directions and living in varied hydrodynamic contexts. When the tide is low connecting paths between the reefs can be seen on wide common foundations and rims [*Andréfouët et al.*, 2009]. This is thought to result from subaerial exposure forming an antecedent karst platform topography during the last glacial, which was suitable for colonization and growth of reefs during the Holocene [*Purdy and Bertram,* 1993].

Locally the barrier reef develops as double, or even triple reef tracts and is interrupted by passes every 25-30km, thought to be eroded by the island's river systems during low-stands [*Cabioch et al.,* 2008]. The western New Caledonia

margin is an escarpment margin and bounded by very steep slopes; thus horizontal progradation of the barrier reef is restricted, favouring its vertical development and the broad extension of the lagoonal deposits [*Le Roy et al.*, 2008]. The west coast of Grande Terre is characterised by a succession of morphological features [*Le Roy et al.*, 2008]:

1. A narrow barrier reef a few km wide, emergent at low tide with an outer reef slope made of spurs and grooves.
2. 5-10m shallow back reef area.
3. Outer reef lagoon enclosing several coral islets at depths of 10-30m on N140^{o} trending ridges, which run parallel to the barrier reef and coastline.
4. Inner reef lagoon characterised by coastal bays and fringing reefs.
5. Coastal plains and mangroves are typical features in some areas in the vicinity of bays (settling over the prograding deltas) but in the most part the lagoon is bounded by steep continental hills reaching several 100m in elevation.

Multibeam bathymetric data shows several drowned terraces have developed along the edge of the barrier reefs. These terraces are tens of metres wide and can be found between depths of 120-20m below sea-level. They are believed to have developed during the late Quaternary highstands since MIS15 [*Flamand*, 2006].

2.2.4 Controls on Barrier Reef Growth

The modern day NCBR is one of the largest continuous coral reef systems in the world and a hot spot of reef diversity [*Cabioch et al.*, 1999; *Andréfouët et al.*, 2006] There are many factors which control the location, extent and geometry of tropical reef growth; these may be split into a number broad groups. Geographic-tectonic factors include: antecedent topography, tectonics- subsidence and uplift rates and sea-level changes. Physico-chemical factors include: temperature, salinity, nutrients, dust input, light availability and aragonite saturation state. Hydrodynamic factors include: waves, currents and storm frequency. Biological variables include: larval sources, dispersion, diversity and disease.

This section examines the modern conditions (vertical tectonic movements, oceanography and climatology) around New Caledonia, which have proven so suitable for reef growth.

2.2.4.1 Vertical Tectonic Movements

Variations in subsidence and uplift rate are important factors in determining coral reef growth history and can explain much of the modern reef and lagoon morphology in the New Caledonia area [*Andréfouët et al.,* 2009]. Generally, subsidence dominates round Grande Terre but rates show significant spatial variability and some areas, especially in the south east, have been subjected to uplift [*Andréfouët et al.*, 2009]. The New Caledonia Ridge is thought to display a double longitudinal and lateral warping. This is believed to be in part due to the still active post-obduction isostatic readjustments after the emplacement and continuing erosion of the peridotite nappe in the south of the island during the upper Eocene [*Le Roy et al*., 2008]. Another prominent dynamic regional feature is the subduction zone to the east of the Loyalty Islands where the Australian plate subducts under the Vanuatu arc-North Fiji Basin micro plates and the Pacific Plate at a rate of 12cm/yr. This causes a lithospheric bulge and explains the uplifted reefs of the Loyalty Islands, Ile Des Pins and south east Grande Terre (Yate) [*Dubois et al.*, 1974].

Subsidence rates calculated for over the last 125kyr show variation along the western New Caledonian margin. High rates of subsidence (>0.1m/kyr) are found in the North around the Great North Lagoon, before decreasing mid-way down the island, where at Ilot Vert (Bourail) the subsidence rate is 0.03m/kyr [*Andréfouët et al.,* 2009]. However, greater subsidence returns in the South of the island with a subsidence rate of 0.16m/kyr on the barrier reef at Amédée (Nouméa) [*Cabioch et al.*, 1995; *Frank et al.,* 2006]. By contrast, the Ile Des Pins in the south lagoon has an uplift rate of ~0.12m/kyr [*Le Roy et al.,* 2008]. (See *Figure 2.8* for locations.). The greater subsidence rates (>0.1m/kyr) explain the presence of the wide (15-30km) north and south west lagoons [*Andréfouët et al.,* 2009] and the much narrower lagoon (<5km) along the middle of the SW coast, for instance at Bourail, which is associated with a much lower subsidence rate (0.03m/kyr) [*Andréfouët et al.,* 2009]. In addition to this subsidence rates are also seen to vary across the lagoon. Closer to the shore, where Holocene fringing reef units are not as thick as their barrier reef counterparts, subsidence rates are also lower: 0.07m/kyr at the Ricaudy Reef close to Nouméa compared to 0.16m/kyr at Amédée on the barrier reef [*Cabioch et al.*, 1995; *Frank et al.,* 2006].

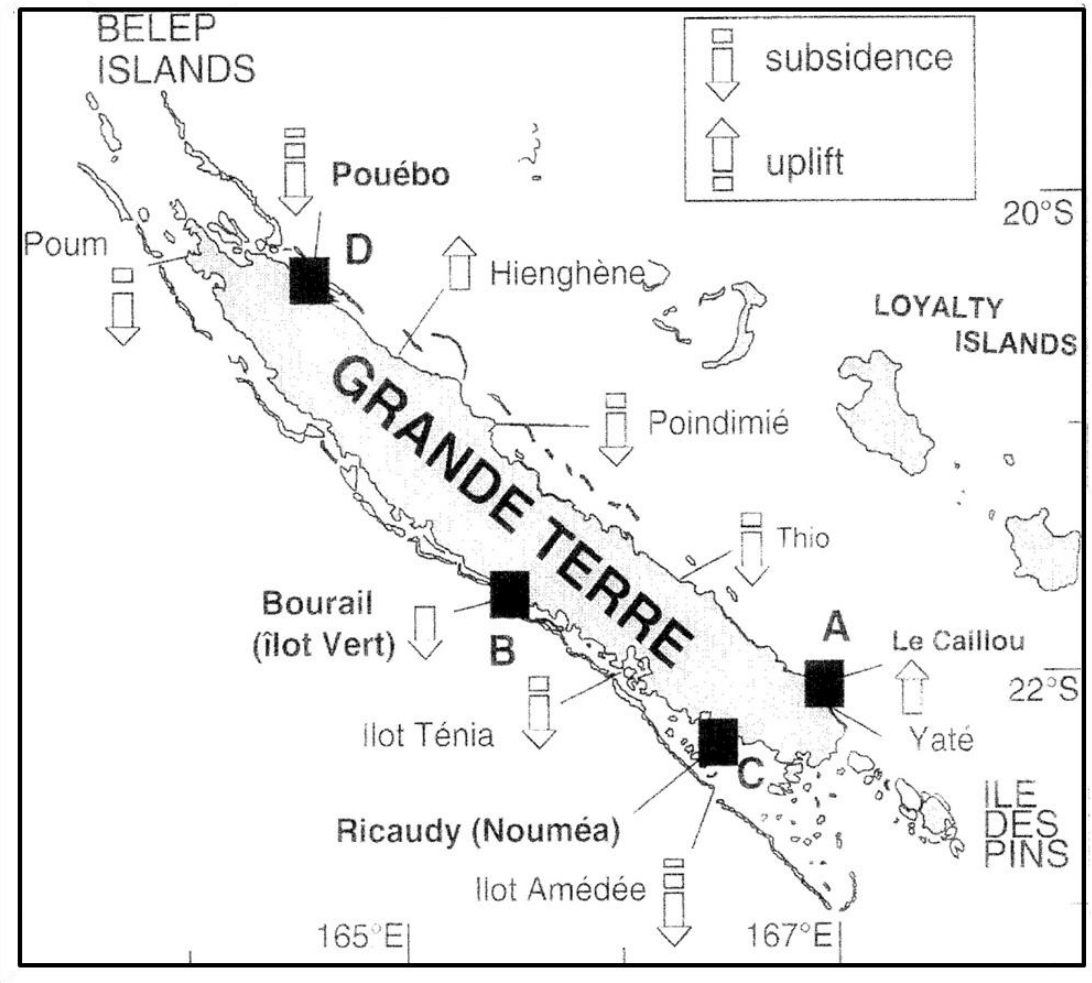

Figure 2.8 Neotectonic behaviour along the margins of New Caledonia. (From *Cabioch et al.*,1999.)

Varying levels of subsidence and uplift affect where reefs are able to grow during sea-level highstands and their spatial relationship to previous reef units. If subsidence is sufficient new reefs can grow directly on top of the previous highstand reefs, as is seen along the western New Caledonia Barrier Reef (see §2.3). However, if subsidence is too great compared to sea-level rise and the topographic highs provided by old reef units are too deep to be utilised by new colonising reefs, the reef location will shift to a new more suitable depth substrate. By contrast, if subsidence is low (or uplift occurs) and the previous reef deposits are still entirely or partially emergent, reefs are unable to develop directly on top and either grow in a completely new

location or are juxtaposed with the older unit [*Cabioch et al.*, 1995]. (For examples see *Figure 2.9.*)

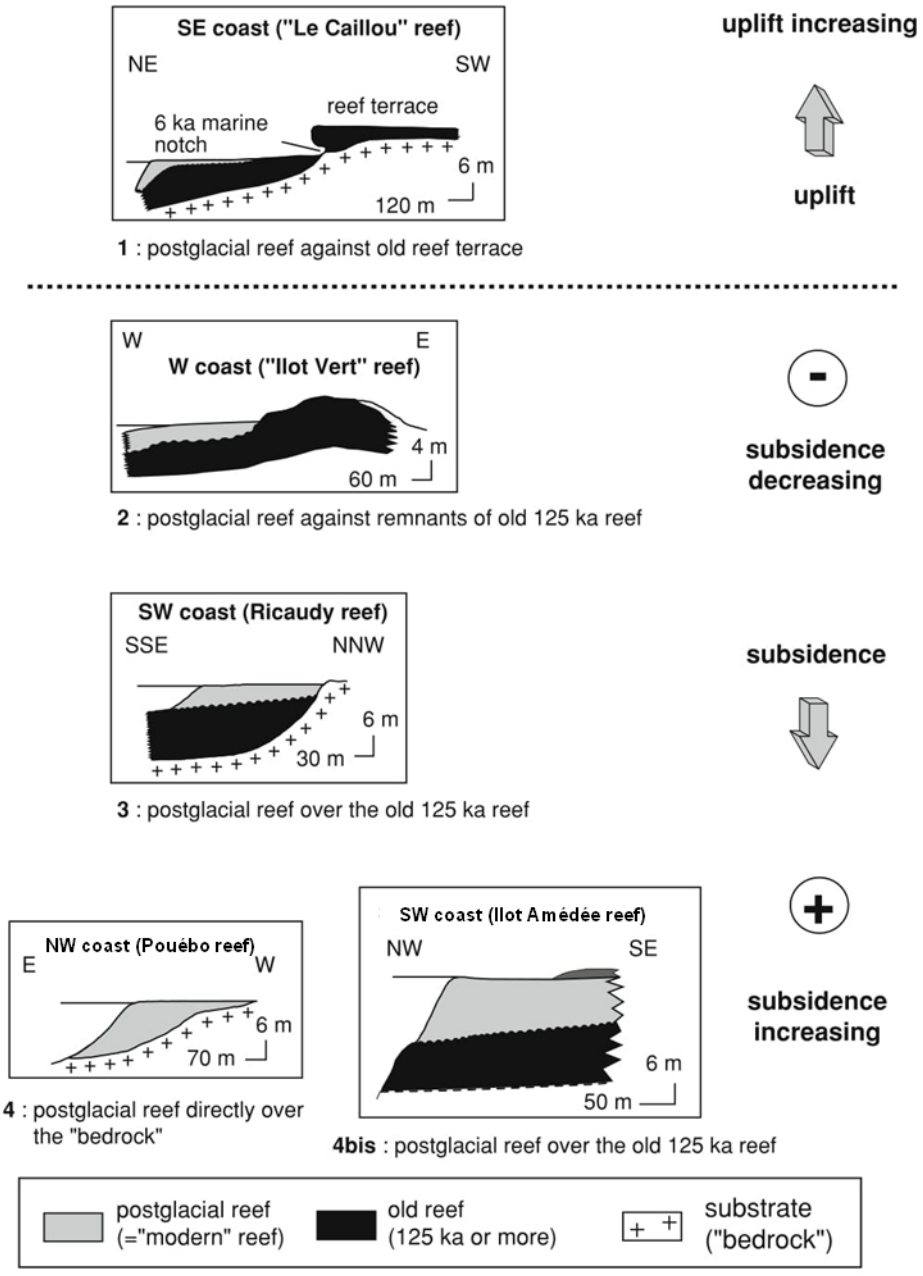

Figure 2.9 Holocene reef morphology in relation to subsidence and uplift rates. (From *Cabioch et al.*, 1995 and *Cabioch*, 2003.)

2.2.4.2 Modern oceanography

The surface flow around New Caledonia is predominantly westward due to the Southern Equatorial Current (SEC), advecting subtropical thermocline waters westwards from the Southeast Pacific to the Coral Sea [*Kessler and Cravatte*, 2013a]. This flow, which is a result of the south east trade winds in the area, occurs between the equator and 20°S and splits into northern and southern branches (North and South Caledonian Jets) when it reaches the island of Grande Terre which acts as an obstacle to its progression [*Cravatte et al.*, 2015] (see *Figure 2.10A*).

Locally the SEC bifurcates against New Caledonia's east coast into a north-westward boundary current (the East Caledonian Current) and into a weak south-eastward current (Vauban Current) (see *Figure 2.10B*). The Vauban Current extends down to 500m and carries warm, low salinity waters from Vanuatu, against the prevailing trade winds, along the east coast of Grande Terre. It is however, highly variable at intra-seasonal timescales, often reversing its flow, due to incoming mesoscale eddies from the east and south of New Caledonia [*Cravatte et al.*, 2015]. Along the west side of the island there is also a flow of warm water to the south east, the Alis Current of New Caledonia (ACNC) (see *Figure 2.10B*). The ACNC flows along the reef slope down to a depth of 150m and overlays a weaker north-westward current, creating an unusual coastal circulation. The ACNC is a persistent feature of the observations, though like the Vauban Current, it is strongly modulated by the presence of offshore eddies and can be significantly affected by the south east trade winds [*Hénin and Cresswell*, 2005; *Cravatte et al.*, 2015].

In the modern day the influence of the East Australian Current, which transports warm water from the west equatorial Pacific southwards towards the Tasman front at 32°S, is mainly restricted to the Australian margin and western side of the Coral Sea. (See *Figure 2.10A*)

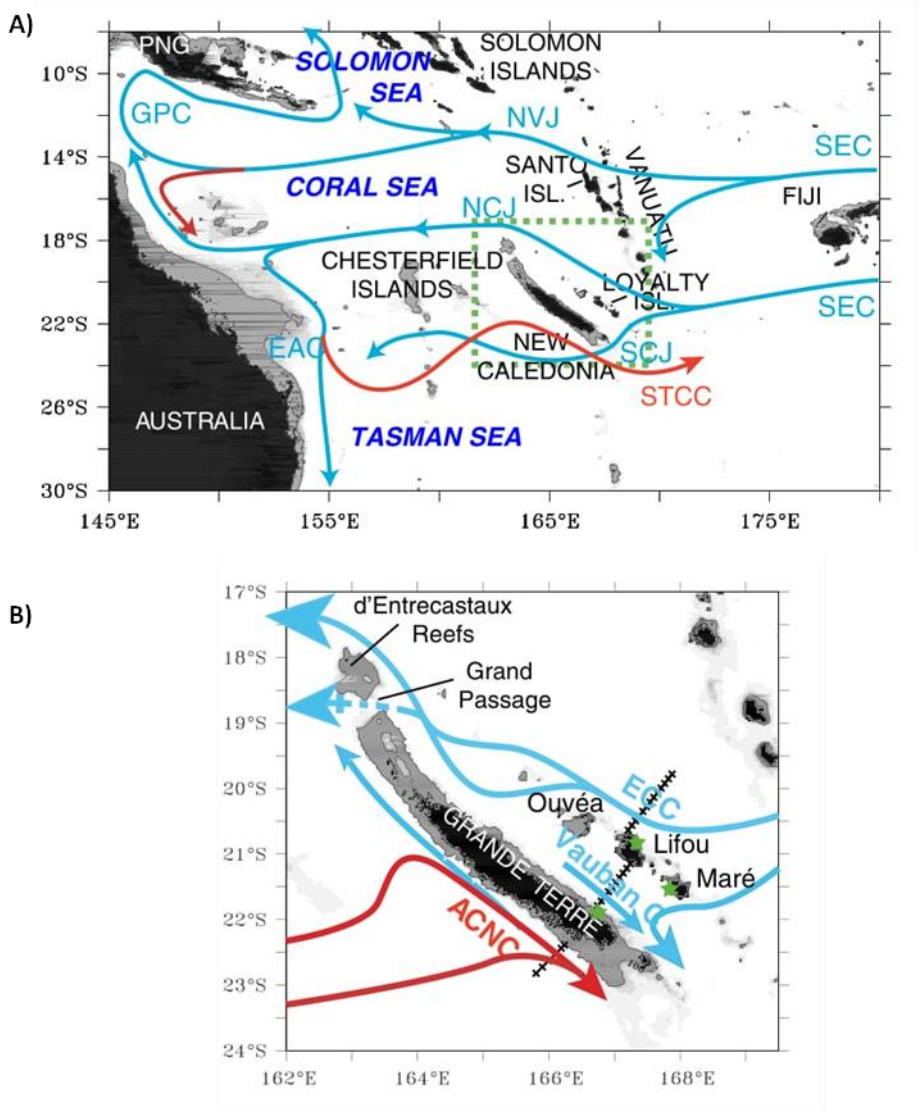

Figure 2.10 A) Map of the regional Southwest Pacific showing the thermocline circulation (blue lines) and surface circulation (red lines) when different from thermocline circulation. **B)** Zoom of green dashed area in panel A. Map of the New Caledonia area and local surface currents. Abbreviations are as follows: PNG- Papua New Guinea, GPC- Gulf of Papua Current, EAC- East Australian Current, NVC- North Vanuatu Current, NCJ and SCJ- North and South Caledonian Jets, SEC- South Equatorial Current, ECC- East Caledonian Current and ANC- Alis current of New Caledonia. (From *Cravatte et al.*, 2015; green stars and dashed black lines relate to the study sites used in the paper and are not related to this thesis.)

The mixed layer depth in the New Caledonia Trough is ~75m but in coastal regions varies with season: 20-50m during the austral summer and 100-150m during the winter [*Alory et al.*, 2006].

Whilst there is no permanent eastern boundary current along Grande Terre, its northwest-southeast orientation presents a favourable configuration for upwelling along its western coast. This is due to alignment with the south east trade, winds which blow parallel to the axis of the land. Upwelling is more frequent in the summer months, when the trade winds are stronger, and occurs as narrow band (~10km wide) along the reef front, extending for several hundred kilometres. Generally, upwelling occurs along the southern half of the west NCBR but occasionally spreads further north [*Hénin and Cresswell*, 2005]. These events take around five days to fully develop and then around the same amount of time to decay again. A succession of closely spaced or prolonged wind events can cause upwelling to occur for up to a month. Colder (<23ºC), more saline and nutrient rich waters from ~100m depth cause cool sea surface temperature (SST) anomalies of up to 5 ºC in the summer (1ºC in the winter) and positive salinity anomalies of 0.1 near the reef front [*Hénin and Cresswell*, 2005 and *Alory et al.*, 2006]. Upwelling is associated with higher salinities due to the subsurface salinity maximum at 160m, which is characteristic of South Pacific tropical waters [*Delcroix and Lenormand*, 1997].

Upwelling acts on a daily timescale but is strongly modulated by seasonal changes in subsurface stratification. The strongest cooling events are seen during the summer months when not only are the surface waters warmer than in the winter but the mixed layer is thin and thus cool waters are easier to bring to the surface. In the winter the mixed surface layer, of 23ºC or colder, extends down to ~100m, thus the upwelling waters are not much colder than surface ones [*Hénin and Cresswell*, 2005]. In the absence of coastal upwelling chlorophyll-a concentration is very low immediately off shore from the barrier reef towards the open ocean. During summer cooling events coastal chlorophyll-a concentrations increase by 0.1- 0.4mgm^{-3}, a factor of 10

compared to the open ocean. This increase has been attributed to upwelling of nutrient rich waters [*Alory et al*., 2006]. The waters around New Caledonia are oligotrophic and nutrient enrichment has been proposed as a limiting factor for reef growth in the area on geological time periods [*Montaggioni*, 2006]. The biological impact is, however probably modulated by strong seasonality in the subsurface nutrient availability.

Inter-annual variations in upwelling are linked to large scale climate variability dominated by El Niño Southern Oscillation (ENSO) variations. There are slight decreases in SSTs and a clockwise rotation of wind direction during El Niño events (the opposite in La Niña periods) which affects the frequency and magnitude of upwelling events *[Delcroix and Lenormand*, 1997].

2.2.4.3 Modern climatology

The island of New Caledonia lies across the Tropic of Capricorn between 20-23ºS. Its general climate and hydrological features are considered to be moderately tropical in nature [*Rougerie*, 1986]. The humid austral summer (November - April) is tempered by the prevailing south east trade winds, associated with the South Pacific Convergence Zone (SPCZ). During the cooler, drier winter (May-October) the SPCZ moves north of the equator and the weaker trade winds are disturbed by westerlies (generated by polar air masses) which are associated with cyclones [*Cabioch et al.*, 1995, *Flamand et al.*, 2008]. The trade winds represent about 75% of the total winds, while westerlies (associated with low pressure systems, including cyclones) represent less than 15% [*Alory et al*., 2006].

The area is affected by the Australasian Monsoon system which causes more intense precipitation in the austral summer (>140mm/month) than the winter (~50mm/month) and leads to some typhoon activity during the later part of the season [*Delcroix and Lenormand*, 1997]. ENSO related phenomenon can cause

significant inter-annual variability in the hydrological cycle. Inter-annual differences in long-term annual means can be 50% and these are highly significant against the seasonal precipitation cycle. El Niños (La Niñas) are characterised by dry (wet) conditions [*Nicet and Delcroix*, 2000].

SSTs show a seasonal variability of 5-7ºC with average summer temperatures of 26-28ºC and 21-23ºC in the winter along both coasts [*Cabioch et al.*, 1995]. SST variability due to ENSO is of a relatively low amplitude (<1ºC) when compared to seasonal variations; though El Niños (La Niñas) correspond to regionally cooler (warmer) surface waters [*Gouriou and Delcroix*, 2002]. Sea surface salinity (SSS) normally varies from 35.2 to 35.8, generally driven by precipitation changes; though it shows high local variability in the South West Lagoon. The waters surrounding New Caledonia are oligotrophic, with dissolved nutrient concentrations of: phosphate: 0.3-0.5mmol.m^{-3}, nitrate: 0.2-0.6mmol.m^{-3}, silicate: 2-3mmol.m^{-3} and chlorophyll-a: 0.1-0.3mg.m^{-3}. The dissolved oxygen concentration is also relatively low in surface waters at 4.5-5ml/l [*Cabioch et al.*, 1995].

As noted in §2.4.2 whilst there is no permanent eastern boundary current along the west coast of Grand Terre, upwelling events can have a significant and sudden effect on the surface waters over time periods of a few days to a month [*Hénin and Cresswell*, 2005; *Alory et al.*, 2006]. Upwelling is more common in the summer months, when the trade winds that drive the events are more prevalent. The 2005 study by *Hénin and Cresswell* found < 10% of days had upwelling between May and September compared to 75% between January and March. Colder (ΔT= -1 to -5ºC), more saline (ΔS= +0.1 to +0.2), nutrient enriched waters upwell from a depth of ~100m, in a band ~10km wide and up to 400km long along the western barrier reef [*Hénin and Cresswell*, 2005 and *Alory et al.*, 2006]. These changes are superimposed on the seasonal record and are not only more frequent, but also stronger (ΔT= 5-6ºC compared to 1ºC), during the summer. During El Nino conditions the south east trade

winds are more closely aligned to the barrier reef and so this favours greater upwelling [*Delcroix and Lenormand,* 1997].

The hydrologic regime of New Caledonia's coasts is principally due to the dominant trade winds in the area. The main island of Grande Terre is orientated northwest-southeast and thus a southeast swell (2-4m) is perceptible in all coastal areas. Tides are unequal and semi-diurnal ranging between 1.5 (spring) to 0.3m (neap) [*Cabioch et al.*, 1995].

2.3 The history of the western New Caledonia Barrier Reef

History of reefs in the New Caledonia area has mainly been investigated via numerous boreholes drilled through fringing and barrier reef areas (see *Figure 2.11* and *Figure 2.12*) [*Coudray*, 1976; *Cabioch et al.*, 1995 *Cacbioch et al.* 1999; *Cabioch*, 2003; *Frank et al.*, 2006; *Cabioch et al.*, 2008 and *Montaggioni et al.*, 2011]. One investigation by *Andréfouët et al.* (2009) instead utilised remote sensing methods such as satellite photographs, high resolution bathymetry maps and seismic lines. However, this only investigated the coral reef history back to 125ka and provided no information on the internal structure and sequence of reef deposits laid down during previous successive highstands beneath the modern day barrier reef line. Others such as *Flamand* (2006) and *Chardon et al.* (2008) used seismics lines, shot from the shoreline out to sea past the barrier reefs, to comment on the history of carbonate production in the area and noted the presence of submerged submarine terraces. Much less is known about the history of the barrier reef along the eastern side of the Grande Terre than the west, principally due to a lack of borehole studies. This thesis examines deep sea sediment cores which are situated offshore from the southern half of the western New Caledonia Barrier Reef (fortuitously the best studied area in the region) and thus here only the history of the barrier reef along the western side of the island will be considered. Whilst there are almost certainly many similarities between history of reefs along the east and west coasts of New

Caledonia, differences will have occurred. The barrier reefs on the western side of the island tend to be better developed than those on the east and provide protection for the fringing reefs along their coast lines [*Cabioch et al.,* 1995]. Subsidence (uplift) rates are known to vary geographically between the coast lines over at least the last 125ka and quite possibly prior to that. The east coast shelf is also narrower than that of the west, restricting potential production area at highstands.

The fringing reefs round New Caledonia began growing during the previous interglacial, with Holocene sequences either occurring on top of the MIS5 fringing reefs or on terrigenous bed rock depending on subsidence rates [*Cabioch et al*., 1995]. There appears to be a variety of ages for the initiation of the Holocene fringing reefs round Grande Terre, with those in the south (Ricaudy, Mamié-Ounia and Tara) dating back to ~7ka compared to younger ages in the north (Thio, Pouébo and Poum) at ~4.2 ka [*Cabioch et al.,* 1995; *Cabioch et al.,* 1999]. (See *Figure 2.11* for locations.)

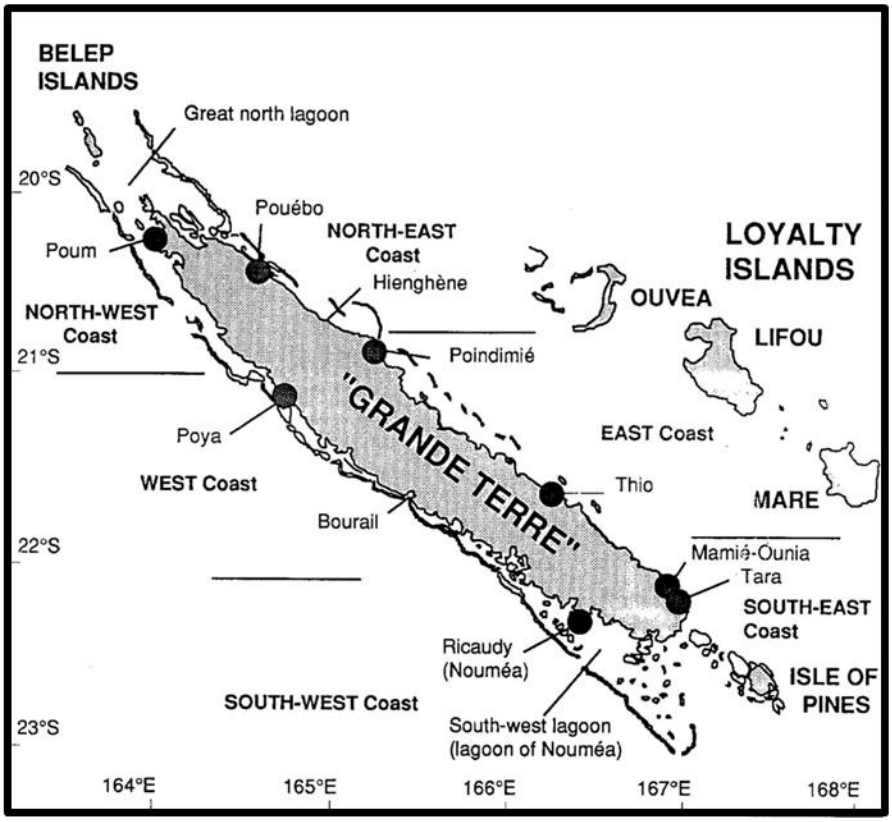

Figure 2.11 Locations of fringing reefs around Grande Terre, New Caledonia. (From *Cabioch et al.*, 1995.)

There are many possible controls on reef development, such as: water depth, temperature, water turbidity and upwelling. However, it is thought this spectrum of ages is probably a result of the different types of substrate being colonised in the north and south of the island. The early settled reefs grew on a karstified limestone foundations and generally non-carbonate bedrock was colonised later. It is believed that the roughness of the karstic surfaces may have facilitated recruitment and attachment of coral larvae and successfully catalysed coral growth [*Cabioch et al.*, 1995]. By contrast smooth metasedimentary and terrigenous outcrops may be less suitable for rapid coral colonisation [*Cabioch et al.*, 1995]. Generally the fringing reefs reached the surface somewhere between 5-2.5kyr after the stabilisation of sea-level and thus are all classified as catch up reefs [*Cabioch et al.*, 1995].

The first comprehensive study dedicated to the internal structure and growth of the New Caledonia Barrier Reef was conducted by *Coudray* in the late 1970s. A 226m long core drilled from Ténia Islet (see *Figure 2.12*) was studied. He concluded that reef building began on the western margin of Grande Terre during the Plio-Pleistocene transition and produced four superimposed units in relation to successive sea-level changes. Since then cores have also been drilled at Kendec Islet in the north, Amédée Islet in the south and a second core at Ténia, the closest site to the the deep sea sediment cores studied in this thesis (see *Figure 2.12*). These reef boreholes have been studied by *Cacbioch et al.* (1999), *Frank et al.* (2006), *Cabioch et al.* (2008), *Andréfouët et al.* (2009) and *Montaggioni et al.* (2011). A summary of their findings follows.

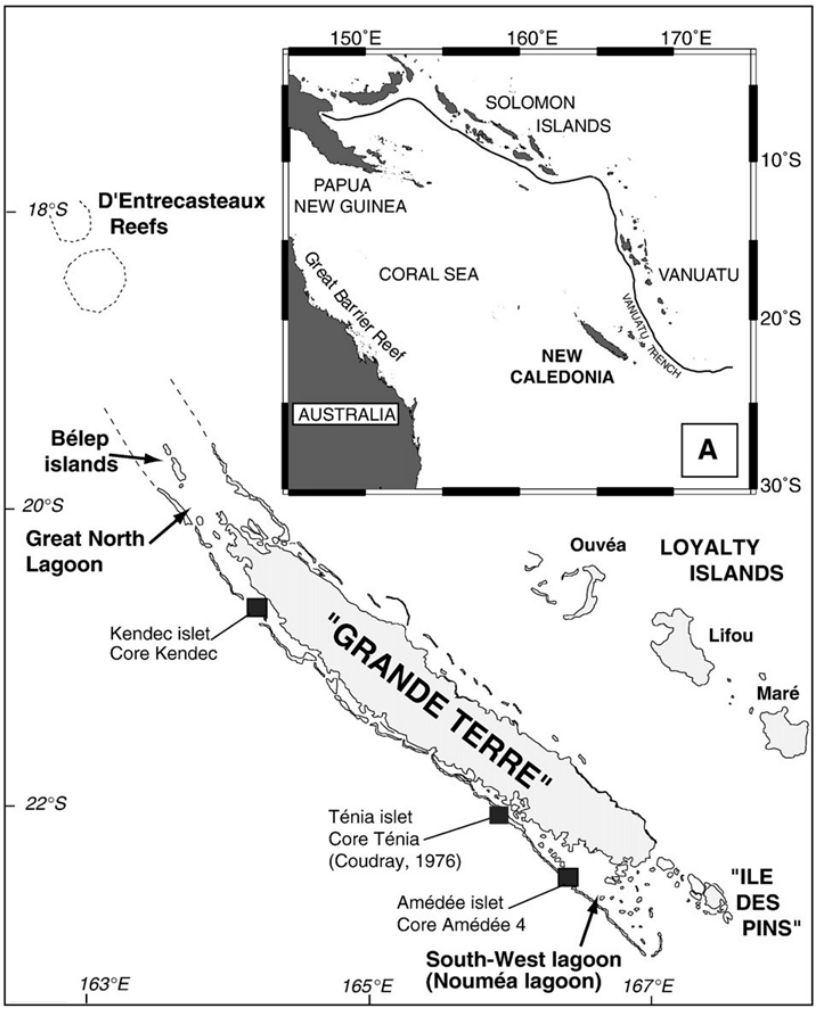

Figure 2.12 Location map of New Caledonia and drilling sites studied along the west coast of Grande Terre. (From *Cabioch et al.*, 2008.)

The cores taken at Kendec, Ténia and Amédée are formed of a succession of stacked sedimentary carbonate units, separated by unconformities which show evidence of erosion, dissolution, calcareous crusts and palaeosoil formation. These units are thought to have been deposited during successive Quaternary highstands, with erosional and diagenetic features forming during lowstand exposure periods [*Cabioch et al.*, 2008]. The cores show a common succession of units with a variety of detrital facies predominating at the base of the core, before giving way to a coralgal framework at the top [*Montaggioni et al.*, 2011]. Cores taken at Amédée and Ténia both drilled peridotite bed-rock and can be considered to represent the full carbonate sequence deposited at that location.

Chronological frameworks have been derived based on lithostratigraphy, magnetostratigraphy, U-series dating and nannofossil biostratigraphy. The Holocene sequences do not seem to initiate before 8.5ka and it is postulated that prior to this time sea surface temperatures were too cold for there to be significant reef development [*Cabioch et al.*, 1999]. It is estimated that before 8.5ka temperatures would have been similar those currently experienced at 30^{o}S, which is the limit of modern reef development [*Andréfouët et al.*, 2009]. Lower units become progressively more heavily altered and as a result of this U-series dating becomes increasingly unreliable, due to differing degrees of U-series open system behaviour and calcite remineralisation. However, *Frank et al.* (2006) were able to obtain ages to confirm that in the Amédée core the two units underneath the Holocene sequence were from MIS5 and MIS7. Below this point though accurate dating is not possible and chronologies are based almost entirely on the lithostratigraphy with sparse magnetostratigraphic tie points [*Montaggioni et al.*, 2011].

Comparison of cores from all three sites shows that the coral communities are dominated by massive forms (mainly poritids). Given the striking compositional similarities between the fossil and modern coral fauna, the coral species pool is postulated to have survived over a longer period than 1Ma through habitat stability

[*Montaggioni et al.,* 2011]. But there is a question over the ecological significance of these communities [*Montaggioni et al.,* 2011]. All the cores studied on the western margin show that the Pleistocene record is composed of two distinct sequences:

1. The lower sequence (base to ~50m core depth), thought to be deposited up until MIS13, which is characterised by a dominance of detrital material such as grainstones- wackestones rich in coralline algae, free living and encrusting forams, molluscs and corals. The corals are mainly massive forms: poritids and faviids. In-situ coral colonies are occasionally found but are not found at a high enough density to be thought to represent a true reef framework.
2. The upper sequence (~50m core depth to core top), deposited since MIS11, which predominantly contains coralgal frameworks, giving evidence for true coral reef tracts for the last 400kyrs.

There are a number of possible explanations of this change in depositional style. It is possible that the coral bearing detritus of the lower units are indicative of the settlements typical of outer-shelf reef rims. Settlement of early typical barrier reef tracts occurred landward or seaward of modern barrier reef line, so that the cores penetrate the inner/outer, detritus dominated zones. An alternative explanation is that the climate prior to 400ka was not optimal for reef growth and this resulted in the development of sub-tropical, non-reefal coral communities including scattered patch reefs [*Cabioch et al.*, 2008].

Whilst the role of climate is not certain due to conflicting records from the tropical Pacific, the authors postulate that the later climate limiting hypothesis is the most probable explanation [*Montagioni et al.*, 2011]. The history of the western New Caledonia Barrier Reef is therefore interpreted as beginning with carbonate deposition initiated during interglacial high stands prior to 1.2Ma on an open, shallow water margin, i.e. a ramp or non-rimmed shelf margin [*Cabioch et al.*, 2008 and *Montaggioni et al.*, 2011]. The carbonate platform is thought to have acted as a ramp until about 500-480ka (MIS13) since the depositional pattern seems to have

remained stable over this whole time period, reflected in the composition and texture of detrital material and the nature of the coral fauna. The ramp is likely to have developed into a rimmed platform with coral reef tracts during the long, warm highstand of MIS11. From this point typical coral-algal framework developed, being predominantly made of massive poritids and arborescent acroporids, at least in inner reef flat settings [*Cabioch et al.*, 2008 and *Montaggioni et al.*, 2011].

The reef history along the western margin has been generally similar, with local differences controlled by the interaction of sea-level change and varying vertical tectonic movements. Recent subsidence rates, since 125ka, have been calculated for Amédée (0.16±0.04m/kyr) and Kendec (0.1m/kyr) with lower rates at Ténia (0.08m/kyr) [*Frank et al.*, 2006; *Cabioch et al.*, 2008; *Montaggioni et al.*, 2011]. However, these rates must have changed in the past since applying them further down-core does not produce magnetic reversal ages at the depths that they actually appear in the cores. As noted in §2.4.1 varying subsidence rates can alter the location and thickness of reefal deposits and it is important to consider subsidence in relation to rates of sea-level change in order to gain a full understanding reef morphology. Whilst substrate needs to be flooded before carbonate production can begin, the rate of relative sea-level rise/fall also matters and different communities that have colonised an area will react differently under the same rate of sea-level rise. This produces different reef growth strategies: keep-up, catch-up or give-up and this can lead to different reef morphologies on very similar antecedent topography [*Neumann and MacIntyre*, 1985].

The influence of different controlling factors on the growth history of the New Caledonia Barrier reef is examined in detail in Chapter 6.

2.4 Core Descriptions

Deep sea sediment cores MD06-3018, MD06-3019 and MD06-3020 were taken on the eastern side of the New Caledonia Trough (NCT) during the 2006 AUSFAIR/ZoNéCo12 cruise of the Marion Dufresne. Core MD06-3018 was recovered from 23º00'S, 166º09'E and water depth of 2470m, ~60km offshore from the main island of New Caledonia, Grande Terre. Core MD06-3019 was collected from 22 º31'S, 165 º 12'E and water depth of 3520m, ~110km offshore from Grande Terre. Core MD06-3020 was taken from 22 º 31'S, 165 º 12'E and a water depth of 3530m, ~110km offshore from Grande Terre (see *Figure 2.5A*).

Deep marine sediment core MD06-3018 is a 24.5m long giant piston core, which is composed of foraminifera rich pelagic ooze. The core is divided into 18 sections of 150cm (I-XVIII), though four of these are not the complete length of the tube. The carbonate ooze is a homogenous pale fawn-cream colour with few distinguishing details down-core. The carbonate content shows little variation and is almost always in excess of 60 weight. (wt.) % (see Appendix 3).

Deep marine sediment core MD06-3019 is 36.25m long giant piston core, which is principally composed of foraminifera rich pelagic ooze. The core is divided into 25 sections (I-XXV), these are generally of 150cm though two sections are not the complete length of the tube and sections XXIV and XXV are only 100cm and 75cm in length respectively. The core shows more variation in colour than MD06-3018, with carbonate ooze varying from a pale fawn-cream to a rich olive-green/ brown. This colour variation is due to fluctuating levels of carbonate content in the sediments, varying between 20-85 wt.% (see Appendix 3 and Appendix 5). However, the principal contrast to MD06-3018 is that the MD06-3019 also contains 79 mixed siliciclastic-carbonate sandy layers of varying widths (1-35cm), with a total accumulation of 4.4m. These layers differ in grain size from very fine sand (grain size principally $2 \leq \varphi \geq 4$) to coarse sand/gravel (grain size principally $-3 \leq \varphi \geq 1$) and are mainly composed of shallow shelf bioclasts and terrigeneous grains; though some

have a significant pelagic foraminiferal component. These layers are sediment gravity deposits, generically known as turbidites, which source eroded material from the shallow shelf and upper slope near Grand Terre and transported it to the deep basin via the canyon systems that incise the slope.

Deep marine sediment core MD06-3020 is a 2.14m long gravity core, which is principally composed of foraminifera rich pelagic ooze. The core is divided into two sections (I-II) of 150cm and 64cm. Like MD06-3019 it shows changes in the carbonate content of the pelagic ooze, which is reflected in the changing colour of the sediment. In a similar fashion to MD06-3019 it also contains 6 sandy layers of varying widths and grain sizes, with a total accumulation of 0.25m.

2.5 Corrected Core Depth Scale

All three sediment cores contain internal voids of varying lengths, which are included in the original 'raw' depth scale obtained by location of sediment with respect to the core section tubes.

MD06-3018 has three voids of: 15cm (Section VII: 855-870cm), 10cm (Section IX: 1,060-1,070cm) and 3cm (Section XI: 1,383-1386cm); additionally 4 sections were shorter than the 150cm tube length: Section I (20 cm in length), Section II (130cm in length), Section VIII (142cm in length) and Section XIII (145cm in length). MD06-3019 has three voids of: 81cm (Section VI and VII: 835-916cm), 30cm (Section X: 1320-1350cm) and 6cm (Section XV: 1950-1956cm). MD06-3020 contains only one void of 5cm (Section I: 29-34cm).

In MD06-3020 the void occurs within a sandy layer where sediment cohesion is less than for mud, making voids more likely. For MD06-3019 two of the three voids are associated with a boundary between different sediment grainsizes (one at the base of a sandy layer and the other at the top), where the change in sediment cohesion makes the core more susceptible to splitting during extraction by the piston corer. Whilst these voids may represent unconformities, there is a good match between stable

isotope measurements on either side; therefore the gaps are ‘closed up’ to create a ‘corrected’ depth scale.

Any data plotted with respect to depth in the results or discussion chapters of this thesis is done in relation to the ‘corrected’ depths below core top. However, depths given in the data tables of the appendices are ‘raw’ depths.

2.6 Experimental Measurement Procedures- Initial Sampling

The working halves of cores MD06-3018, MD06-3019 and MD06-3020 were sampled at the School of GeoSciences, University of Edinburgh. The working halves of cores MD06-3019 and MD06-3020 and are currently stored at the School of GeoSciences, University of Edinburgh. The working half of MD06-3018 and the archive half of MD06-3020 are stored at the Institut de Recherche pour le Développement (IRD), Bondy-CEDEX, Paris. The archive halves of cores MD06-3018 and MD06-3019 are stored at Institut Français de Recherche pour l'Exploitation de la Mer (IFREMER), Brest.

During this study work was performed on the working halves of sediment cores MD06-3018, MD06-3019 and MD06-3020, as well as the archive halves of MD06-3018 and MD06-3019. Prior to the main sampling, the working halves of sediment cores MD06-3018 and MD06-3019 had material removed by u-channel in order to conduct magnetic measurements. The working halves of MD06-3018, MD06-3019 and MD06-3020 were then examined and visual observations recorded. In cores MD06-3019 and MD06-3020 sandy layer positions, widths and type were identified via eye and observed changes in the texture of sampled material.

Digital photographs and core logs are presented in Appendix 5. The photographs were not taken in a controlled light setting and thus there are colour discrepancies between different sections and when compared to the true hue of the sediments.

However, they serve to convey a general impression. Further detail on turbidite deposits is given in Chapter 4, Appendix 5 and Appendix 6.

The cores were sampled every centimetre, with a precision of better than ±0.5cm. Since enough material for analysis is obtained by using only half of the available working material, the remainder was left in the plastic casing for use at a later date if needed. MD06-3018 was sampled in a previous PhD project by Thomas Russon at the University of Edinburgh [*Russon et al.,* 2009; *Russon et al.,* 2010]. MD06-3019 was sampled by four people including three previous Environmental Geoscience students at the University of Edinburgh. Sections I-IV by Aidan Farrow, V-VII by Rosanna Greenop, IX-XII by Angharad Jenkins and XIII-XXV during this project by the author. MD06-3020 was also sampled by author during this project. Sampled material was transferred to sealed plastic bags and all material stored in a cold room before further analysis.

All samples that were prepared for stable isotope or point counting analysis were wet sieved at 150µm and oven dried. Those samples prepared by the author were also sieved at 63µm and the initial total dry sample weight recorded.

All core data sets obtained during this PhD are available in the digital only Supplementary Material associated with this thesis.

Chapter 3: Chronology

3.1 Chapter Overview

A robust chronology for deep sea sediment core MD06-3019, which is utilised throughout the rest of this PhD, is developed in this chapter. The age model for MD06-3019 was principally obtained by tuning its $\delta^{18}O_{planktic}$ record to that of the local, independently dated, MD06-3018 core [*Russon et al.*, 2009]. Additional radiocarbon and magnetostratigraphic measurements allowed for further refinement of the age model. The base of the core is placed at 1.26Ma, covering marine isotope stages (MIS) back to MIS38. This chronology has allowed the timing of deposition of the 79 sediment gravity deposits, generically known as turbidites, within the core to be assigned to within ±10kyrs and thus places subsequent observations of their changing nature within a chronological framework with an accuracy of thousands of years.

3.2 Introduction

Age models, which relate depth and age variables to one another, are required so that comparisons of temporal environmental change can be made between different locations with varying sedimentation rates. Age models can be constructed by using independent dating methods such as radiometric dating, biostratigraphy or magnetostratigraphy to create 'tie points' between specific depths down-core and reference ages. Alternatively, as is principally used in this thesis, isotope stratigraphy can be employed, which is based on the orbital tuning method. The Earth's orbital configuration can be calculated to a high degree of accuracy for the past tens of millions of years [*Laskar et al.*, 2004]. The orbital tuning method relies on the assumption that certain environmental variables vary (and are recorded in the composition of sediments) in a way that is highly correlated to changes in orbital parameters for the Earth: an 'orbital theory of climate' [*Hays et al.*, 1976; *Imbrie et al.*, 1984; *Martinson et al.*, 1987; *Lisiecki and Raymo*, 2005; *Huybers and Aharonson*, 2010]. Continuous down-core proxy measurements for an environmental variable, such as temperature or ice volume, (generally $\delta^{18}O$ as obtained from benthic foraminifera) are correlated ('tuned') to a reference record for that variable, which in turn has been correlated to a computed theoretical orbital solution for the Earth for that variable. The potential of this method had been recognised as far back as the late 1800s [*McGee*, 1892; *Gilbert*, 1900], but it wasn't until the unambiguous identification of orbital period variability in marine sediment core records was made by *Hays et al.* (1976) that orbital tuning become standard practice [*Huybers and Aharonson*, 2010].

Orbital tuning can be a powerful tool, having the advantage of significantly increasing the number of age-depth tie points that can be used in the age model when compared to independent dating methods. This reduces age model interpolation uncertainty, which arises when uniform sedimentation rates have to be assumed between widely spaced tie-points. Whilst there are still uncertainties that stem from limitations of sedimentation rates, sediment preservation, the choice of tie-point positioning and the correlation of records from specific locations to global stacked

reference curves, orbital tuning can provide age models with uncertainties of the order of 5-10 kyrs [*Martinson et al.*, 1987].

This chapter uses the orbital tuning method, along with additional radiocarbon and magnetostratigraphic tie points, in order to obtain an age model for deep sea sediment core MD06-3019. This chronology is then used to provide the depositional ages of the 79 sediment gravity deposits, generically known as turbidites, contained within the core and thus place subsequent observations of their changing nature within a chronological framework.

3.3 Experimental Methods

3.3.1 Planktonic foraminifera stable isotope measurements

Samples for stable isotope analysis were selected from the background pelagic carbonate ooze at approximately 10cm intervals along the length of the core, avoiding sandy layers. However, certain areas were sampled at a higher 5cm resolution and additional samples taken adjacent to the top and base of sandy layer intervals and voids to check for possible unconformities which could affect the age model.

There was a concern, given the depth of recovery of MD06-3019 (3520m) and its known varying carbonate content, that it was possible that dissolution and recrystalisation may have led to a lack of suitable quality material for stable isotope analysis. Whilst there were not enough *Cibicides wuellerstorfi* to produce a benthic record and there were sometimes limited good quality planktic specimens available, a single species stable isotope record, using *Globigerinoides ruber* (white) foraminifera, has been obtained.

Measurements of the stable isotopes, $\delta^{18}O$ and $\delta^{13}C$, were made on cleaned planktonic *Globigerinoides ruber* (white) foraminifera. 8<n<15 individuals, from the >315μm size fraction were used per sample. The aim was to pick only well formed *G. ruber sensu stricto,* to reduce isotope shifts caused by different morphotypes [*Löwmark et al.*, 2005]; however, when these were not present the second (*G. ruber sensu lato*) and third morphotypes had to be used. The foraminifera were picked under a binocular microscope and then cleaned in distilled water and ultrasonicated for between 10seconds to 4 minutes. The cleaning time depending on initial cleanliness of the sample and aimed to break up tests but not cause complete disintegration to a powder.

Samples were then analysed on a Thermo Electron Delta+ Mass Spectrometer with Kiel Preparation Device in the School of GeoSciences, University of Edinburgh. All $\delta^{18}O_{calcite}$ measurements presented in this thesis are given relative to the Vienna Pee Dee Belemnite (VPDB) unless otherwise stated. (From this point onwards $\delta^{18}O$ will be used as an abbreviation for $\delta^{18}O_{calcite}$ unless otherwise stated.) The analytical uncertainty, calculated with respect to an internal calibrated standard, was $2\sigma_a$=0.18‰ for $\delta^{18}O$ and $2\sigma_a$=0.16‰ $\delta^{13}C$. Repeat analyses were done at 6 depths down-core ($3 \leq n \leq 5$), reproducibility uncertainty was calculated as $2\sigma_r$= 0.15‰ for $\delta^{18}O$ and $2\sigma_r$= 0.18‰ for $\delta^{13}C$.

Around half of the stable isotope measurements for MD06-3019 were completed by Environmental Geoscience honours students (Aidan Farrow, Rosanna Greenop and Angharad Jenkins) who had worked on the core prior to this PhD.

3.3.2 Magnetic measurements

Measurements of natural remnant magnetisation were made on u-channels taken from the middle of the working half of core MD06-3019. The analyses and post-processing were conducted by Catherine Kissel at the Laboratoire des Sciences du Climat et de l'Environnement (LSCE), Gif-sur Yvette, France, in a shielded room using a 2G-pass-through cryogenic magnetometer equipped with high resolution coils. Measurements were taken every 2cm, though data from the outer 3cm at the top and bottom of each core section is not presented due to edge-effects. The natural remnant magnetisation was stepwise demagnetized at 5, 10, 15, 20, 25, 30, 35, 40, 45, 50, 60 and 80 mT. The Characteristic Remnant magnetisation (ChRM) record was then determined using principal component analysis [*Mazaud*, 2005]. Nine out of thirteen steps were taken into account to define the ChRM, with mean angular deviations normally ranging between 5-10^{o} (a few horizons reach 20^{o}).

3.3.3 Radio carbon dating

Five radiocarbon dates were obtained from MD06-3019 using 500mg of *Globigerinoides sacculifer* foraminifera, taken the >315µm fraction, for each sample (material sampled by Tom Russon). Analyses were conducted via AMS radiocarbon dating at the Scottish Universities Environmental Research Centre, East Kilbride. A foraminifera specific background correction was used to adjust the ^{14}C measurements. Radiocarbon ages were converted to calendar dates using the Calib 6.0 software (developed by *M. Stuiver, P.J. Reimer, and R.W. Reimer* at the Quaternary Isotope Lab, University of Washington) using the Marine09 ^{14}C curve and an open-ocean 400 year marine reservoir correction [*Stuiver and Braziunas*, 1993; *Reimer et al.*, 2009].

3.4 Results

3.4.1 Planktic foraminifera stable isotope results

The $\delta^{18}O$ planktic foraminifera record (*Figure 3.1A*) values vary between -1.59 to +0.81 ‰ and show a succession of well-defined cycles which vary in length between 20-500cm. These cycles have an average amplitude of 1.80‰ between 0- ~1800cm, 1.11‰ between ~1800-2700cm and 0.76‰ below ~2700cm.

The $\delta^{13}C$ planktic foraminifera record (*Figure 3.1B*) varies between -0.59 to +1.73‰, but shows less well defined cycles. There appears to be a background cyclicity to mean values throughout the whole core at 500-800cm scale, which is overlain by a shorter period oscillation at the 100cm scale, but the record is noisy and neither of these periodicities seems be clearly related to the cycles seen in the $\delta^{18}O$ data.

3.4.2 Magnetic measurement results

The ChRM Inclination record (*Figure 3.1C*) shows a series of reversals between normal (negative polarity) and reversed (positive polarity) inclination. These changes in magnetic inclination have been identified using the chronology of *Cande and Kent* (1995), which is based on the South Atlantic magnetic anomaly sequence and dated using radiometric dating. This is the currently accepted timescale and most widespread in use [*Ocean Bottom Magnetometry Laboratory, Woods Hole Oceanographic Institution*, 2011], as well as being the magnetic chronology used for the creation in the MD06-3018 age model [*Russon et al.*, 2009]. From the top down to ~2530cm the core has an almost entirely consistent negative inclination, which corresponds to the Bruhnes Chron [*Cande and Kent*, 1995]. This is followed by a period of overall positive inclination corresponding to the Matuyama Chron. Within the Matuyama there are two negative excursions identified, those of the Jaramillo (~2900cm to ~3110cm) and the shorter Cobb Mountain reversal (~3320cm) [*Cande and Kent*, 1995].

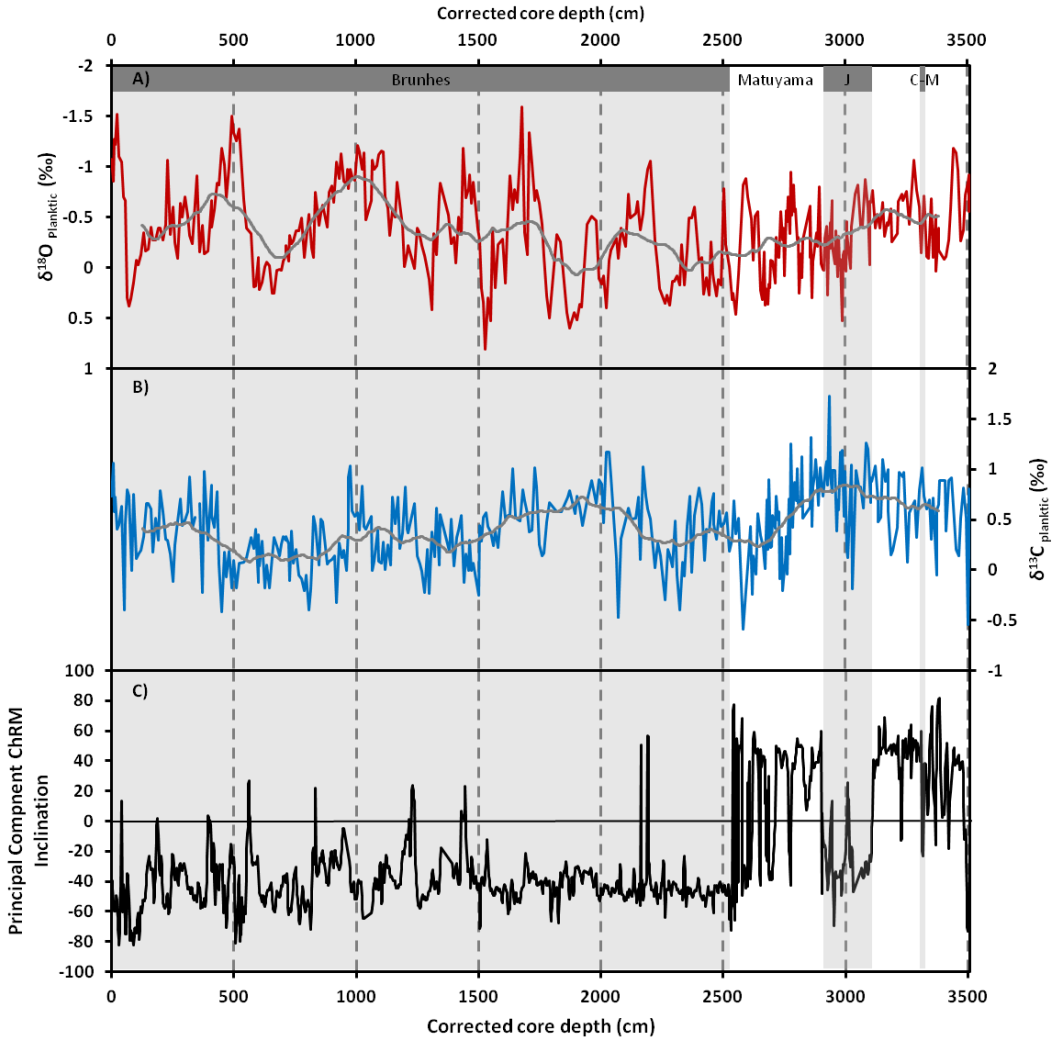

Figure 3.1 A) MD06-3019 $\delta^{18}O_{planktic}$ with respect to depth (grey line is 250cm linear smoothed mean value); **B)** MD06-3019 $\delta^{13}C_{planktic}$ record with respect to depth (grey line is 250cm linear smoothed mean value) and **C)** Principal Component of ChRM Inclination from MD06-3019 with respect to depth. The position of identified magnetic reversals and events are highlighted with light grey boxes representing periods of normal polarity. Abbreviations used for geomagnetic periods stand for- J: Jaramillo and C-M: Cobb Mountain.

3.4.3 Radiocarbon results

Five radiocarbon measurements were made on *Globigerinoides sacculifer* foraminifera, taken the >315μm fraction (see *Table 3.1*). These show increasing age with depth down-core and no age inversions, though for the deepest sample no estimated age was obtainable since it was indistinguishable from the background.

Depth (cm)	**14C age (BP)**	**Median Age (BP)**	**Age Range (BP)**	**Estimated Calendar Age (BP)**
0	3,700	3,586	3,450 - 3,707	Modern
40	6,500	6,955	6,825 - 7,122	7,000 ± 200
80	17,100	19,835	19,556 – 20,149	20,000 ± 450
120	27,000	31,159	30,970 - 31,337	31,000 ± 250
210	Indistinguishable from background			

Table 3.1 Radiocarbon dates of 5 foraminifera samples from MD06-3019. Radiocarbon ages were converted to calendar dates using the Calib 6.0 software and the Marine09 ^{14}C curve, using an open-ocean 400 year reservoir ($\Delta R=0$) reservoir correction.

3.5 MD06-3019 Age Model

As was noted in §3.1 due to a lack of *Cibicides wuellerstorfi* it was not possible to obtain a $\delta^{18}O_{benthic}$ record for sediment core MD06-3019 to tune to the global LR04 benthic stack. [*Lisiecki and Raymo*, 2005] Unlike benthic $\delta^{18}O$ records, which largely represent the changes in ice volume, planktic $\delta^{18}O$ measurements also contain a large component of local surface temperature variations. Therefore, given the close proximity of MD06-3018 to MD06-3019 (~110km) the MD06-3019 age model was principally developed via tuning of the $\delta^{18}O_{planktic}$ curve to the local MD06-3018 $\delta^{18}O_{planktic}$ record using Analyseries software [*Palliard et al.*, 1996]. The MD06-3018 core was previously tuned to the LR04 benthic stack [*Lisiecki and Raymo*, 2005] using its $\delta^{18}O_{benthic}$ record by *Russon et al.* (2009).

In the development of the MD06-3019 age model three radiocarbon dates were used as additional tie-points at the top of the core and the magnetic stratigraphy to check the chronology at the base (see *Figure 3.2*). The magnetic tie points are particularly useful in adding confidence to the age model, since they cover a period of the record (3230-2850cm; 980-1,140ka) where orbital tuning is more difficult due to the increased noise of $\delta^{18}O$ data with respect to glacial- interglacial cycles.

The tuned core age model covers the period from 1.26Ma to the present day and the $\delta^{18}O_{planktic}$ record allows the identification of Marine Isotope Stages (MIS) back to MIS38 (see *Figure 3.3*). The running mean value (using a 250cm linear smoothing box-car method) of the MD06-3019 $\delta^{18}O_{planktic}$ is -0.35± 0.21‰ compared to -0.44± 0.10‰ for MD06-3018. The amplitude of glacial-interglacial cycles in the two records is broadly similar throughout the entire core, though slightly greater for MD06-3019. This can probably be attributed to the higher sedimentation rate and thus sampling resolution of the core.

The age model yields apparent average sedimentation rates of 3.7cm/kyr between 0-1830cm and 2.0cm/kyr between 1830cm to base (see *Figure 3.2B*). It has been noted that the sediments of Calypso drilled cores (particularly in the upper 10-15m) can be affected by significant extension, being 1.5-3 times longer than the same sequences recovered by conventional piston cores from the same site. Therefore the ratio of thickness to time does not necessarily accurately represent the real sedimentation rate [*Thouveny et al.,* 2000; *Skinner and McCave,* 2003; *Rothwell et al.,* 2006]. Evidence of the expansion of sediments in the upper parts of core MD06-3019 (a Calypso piston core) has been observed by comparison to the apparent sedimentation rates obtained for nearby core MD06- 3020 (gravity core), see Appendix 2. Therefore the sedimentation rates obtained for MD06-3019 should not be taken as absolute values, particularly in the upper 15m. It is to be emphasised however, that stratigraphic order is preserved and structural deformation is limited to the edge of the cores [*Thouveny et al.,* 2000].

The planktic stable isotope sampling resolution, based on the core model, is approximately 2.7- 5.1kyr, therefore a 1cm thick sample of pelagic ooze represents an averaging of 270-510 years of sediment.

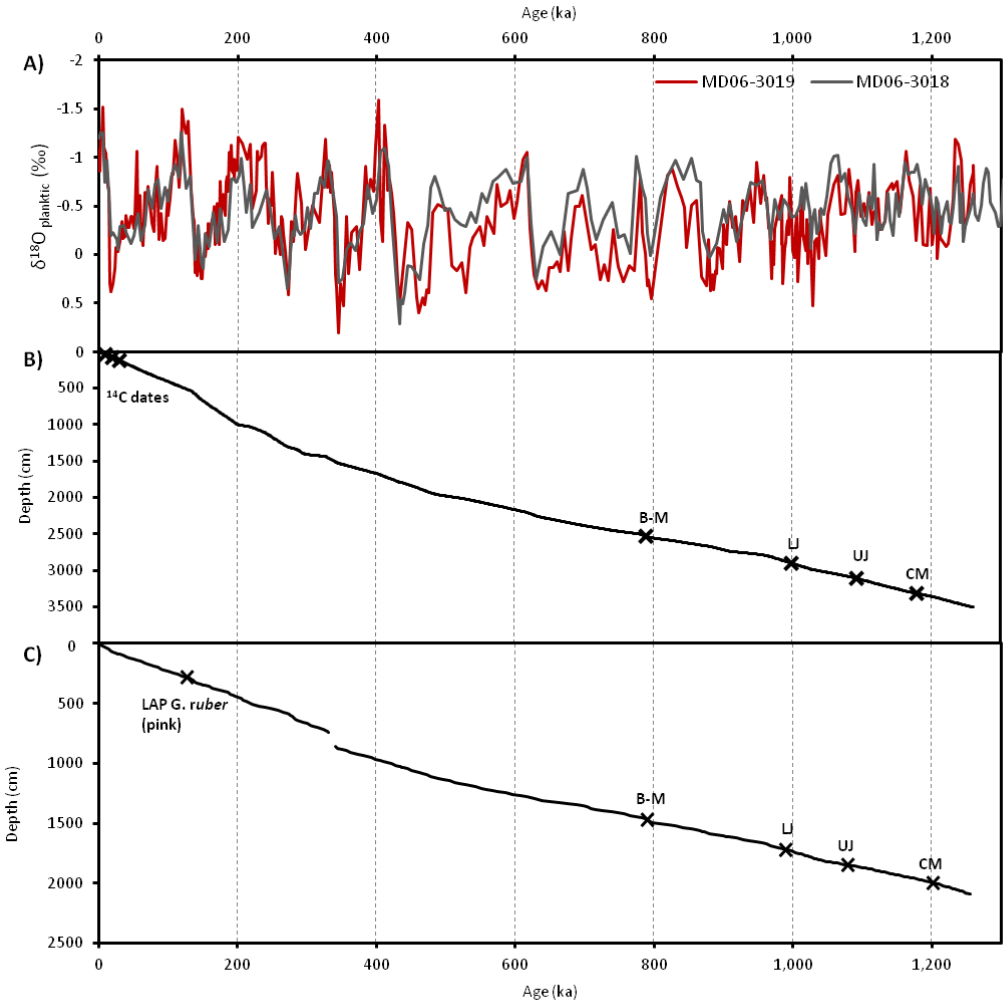

Figure 3.2 A) Comparison between the $\delta^{18}O_{planktic}$ records of the tuned MD06-3019 and the reference MD06-3018 [*Russon et al.*, 2010]. **B)** Line showing the MD06-3019 age model as derived from MD06-3018. Crosses mark the position of the radiocarbon dates and the four magnetic reversals: B-M = Bruhnes-Matuyama, UJ = Upper Jaramillo, LJ = Lower Jaramillo and CM = mid-point of the Cobb Mountain. **C)** Line showing the MD06-3018 age model [*Russon et al.*, 2010] as derived from the LR04 record [*Lisiecki and Raymo*, 2005]. Crosses mark the position of the four magnetic reversals B-M = Bruhnes-Matuyama, UJ = Upper Jaramillo, LJ = Lower Jaramillo and CM = mid-point of the Cobb Mountain and the Last Appearance (LAP) of G. *ruber* (pink). Gap in the age-model arises from the interval of disturbed sedimentation at 740-855cm.

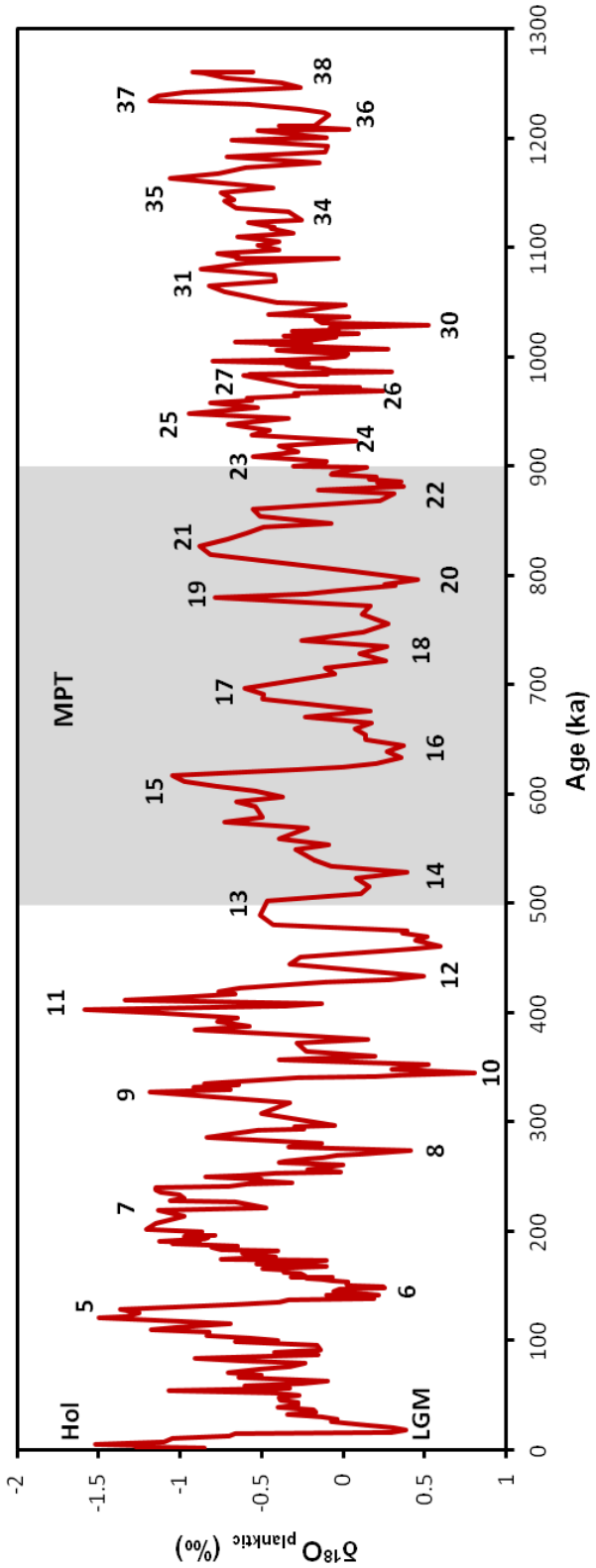

Figure 3.3 MD06-3019 *G. ruber* $\delta^{18}O_{planktic}$ record plotted with respect to the core age model. The Mid-Pleistocene Transition (MPT) period (as defined by *Head and Gibbard*, 2005) is highlighted in grey. Numbers are the assigned marine isotope stages (MIS), LGM= Last Glacial Maximum (MIS2), Hol= Holocene (MIS1).

3.6 Discussion

3.6.1 Reliability of the MD06-3019 age model

The location of the core MD06-3019, means that the record may contain significant unconformities, due to the inherent erosive nature of the base of turbidity currents. This has the potential to cause severe limitations on dating, especially when the age model is not created using independent dating mechanisms. The age model for MD06-3019 was developed by matching the planktic oxygen isotope curve to an independently dated curve, MD06-3018 [*Russon et al.*, 2009]; however there are no absolute ages obtained for the pelagic material either above or below sandy layers in MD06-3019. The method relies on the assumption that little to no material is missing due to erosion at the base of turbidites and that it is therefore acceptable to close up the gaps once sandy layer depths have been removed. In the case of MD06-3019 this seems a reasonable assumption, given the distal location of the core where the erosive power of the turbidite would be significantly reduced [*Puga-Bernabéu et al.*, 2014]. Most turbidite layers are relatively thin (of the order of a few centimetres) and composed of fine grained sand, probably representing the low-energy 'tails' of turbidite flows, with low erosive ability. Even the coarsest and thickest deposits in MD06-3019 would not have had the potential to remove significant amounts of material, such that there could be the concern that a whole glacial- interglacial cycle could have been lost. Isotope values on either side of large sandy layers were analysed to check for large excursions that could highlight an unconformity problem; none were found.

Additionally, radiocarbon measurements provide extra tie points for the last 20kyr and further back in time and the ages associated with the magnetic reversals of the Brunhes- Matuyama (780ka), Upper Jaramillo (990ka) and Lower Jaramillo (1,070ka) (using the ages of *Cande and Kent*, 1995) have been used to check the accuracy of the age model. Nor are all cycles alike and tuning using the distinctive features associated with different marine isotope stages of a local record can also provide a powerful tool.

Comparisons of the $\delta^{18}O$ records for MD06-3019 and MD06-3018 and the global LR04 stack (*Figure 3.4C*) show there is a good match between MD06-3019 $\delta^{18}O_{planktic}$ and MD06-3018 $\delta^{18}O_{planktic}$, both in terms of absolute values, amplitude and regional features such as the double peak seen between MIS13 and MIS12. The difference in both the absolute values and amplitude of cycles between the planktic record of MD06-3019 and benthic curves of MD06-3018 and LR04 is to be expected due to the differing height in the water column that measured samples are recording. There is, however, still a good correlation between records.

This high fidelity between records meant that 'wiggle matching' the MD06-3019 record was relatively simple. There was only one area where noise in the stable isotope record, between 3230-2850cm (see *Figure 3.1*), made this particularly difficult. Though the resolution of measurements was increased to every 5cm over this interval, this did not significantly aid the ease of tuning. Hence during the period MIS31-27 (1060 - 980 ka), and to a lesser extent MIS35-31 (1140 -106 ka), the accuracy of dating less is secure. This is reflected in the differences of ages obtained for magnetic reversals between MD06-3019 and literature values (*Table 3.2*).

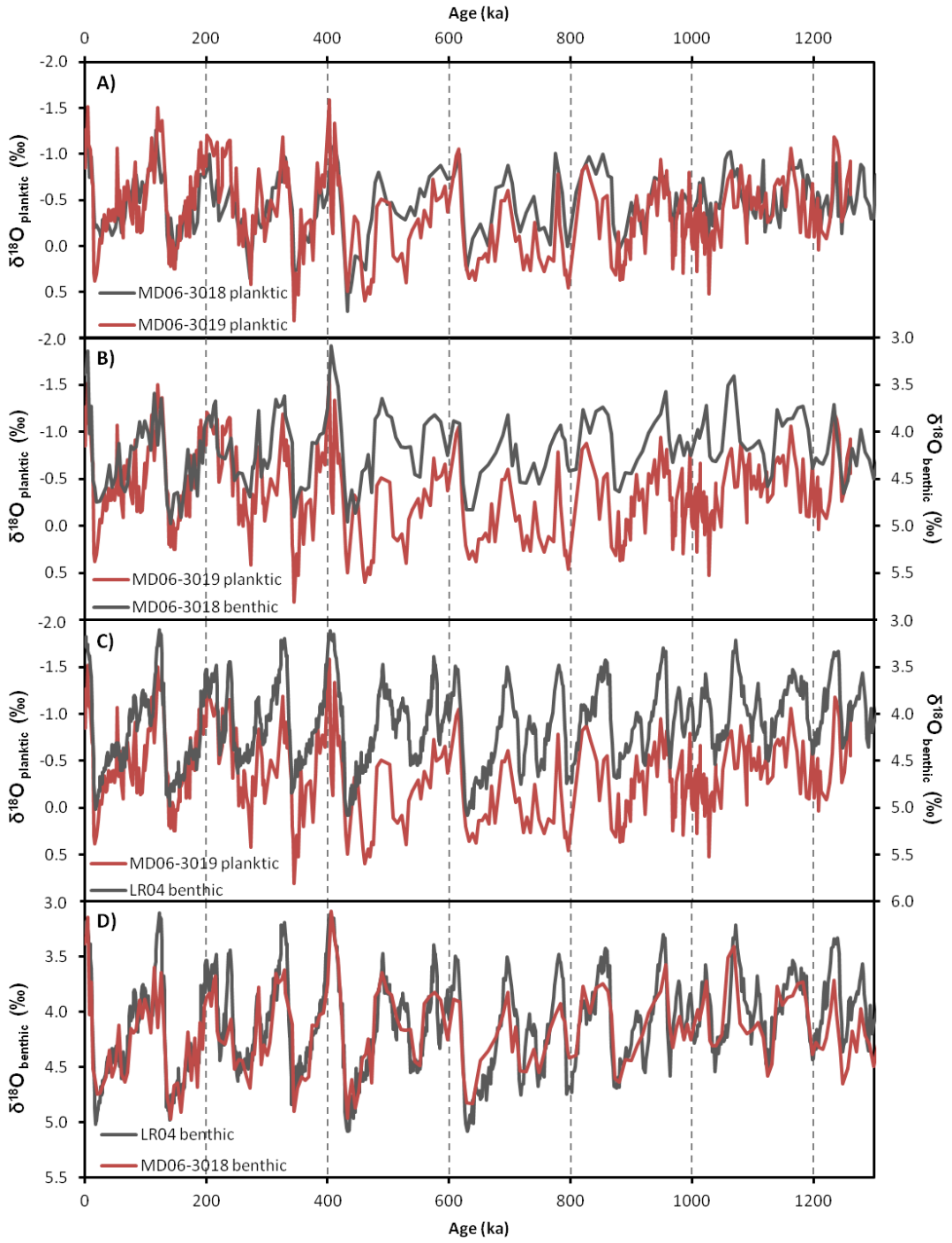

Figure 3.4 A) Comparison between the $\delta^{18}O_{planktic}$ records of the tuned MD06-3019 and the reference MD06-3018. **B)** Comparison between the $\delta^{18}O_{planktic}$ record of the tuned MD06-3019 and the $\delta^{18}O_{benthic}$ from MD06-3018 [*Russon et al.*, 2009]. **C)** Comparison between the $\delta^{18}O_{planktic}$ record of the tuned MD06-3019 and the $\delta^{18}O_{benthic}$ from the LR04 stack [*Lisiecki and Raymo*, 2005]. **D)** Comparison between the MD06-3018 $\delta^{18}O_{bethic}$ record [*Russon et al., 2009*] and the LR04 benthic stack [*Lisiecki and Raymo*, 2005].

To check for accuracy, the dates yielded for magnetic reversals were compared to both literature values of *Cande and Kent* (1995) and those for MD06-3018 (see *Table 3.2*). The age obtained for the Brunhes-Matuyama (B-M) transition is exactly the same for MD06-3019 and MD06-3018 (789ka) and 9kyr older than the literature value (780ka). For the Upper Jaramillo (UJ) the MD06-3019 date is once again 9kyr before the *Cande and Kent* value and 11kyr prior to that obtained from MD06-3018. Values diverge more at the Lower Jaramillo (LJ) where the core age model becomes less well constrained; here there is a difference of 22kyr between MD06-3019 and the published age and 14kyrs when compared to the MD06-3018 result. However, by the Cobb Mountain (CM) when the age model has once again improved and there is a difference of 11kyr between the literature age and MD06-3019.

Magnetic Reversal	**Corrected Core Depth MD06-3019 (cm)**	**Published age (ka) [*Cande and Kent*, 1995]**	**MD06-3019 (ka)**	**MD06-3018 (ka)**
B-M	2533	780	789	789
UJ	2903	990	999	988
LJ	3108	1070	1092	1078
CM	3316	1190	1179	1200

Table 3.2 Comparison of the ages predicted for magnetic reversals by the MD06-3019 age model with those of MD06-3018 and literature values as given by *Cande and Kent* (1995). Acronyms are as follows: Brunhes-Matuyama (B-M), Upper Jaramillo (UJ), Lower Jaramillo (LJ) and Cobb Mountain event (CM).

3.6.2 Age model uncertainty

Overall, the stable oxygen isotope results for MD06-3019 have allowed the construction of a reliable age model for the core, with for the most part an expected 'pelagic depth scale' uncertainty of the order of ±5kyr. [*Martinson et al.*, 1987] This uncertainty is greater (of the order of ±15yr) in the interval between MIS35-27 (1140-980ka) due to the increased noise of the MD06-3019 $\delta^{18}O$ record (a feature

that is also seen in both the MD06-3018 and LR04 records as well) where MIS assignment become less certain.

An additional uncertainty which affects the whole record is due to the fact turbidite layers were left in during the production of the chronology. Since turbidites can be treated as essentially instantaneous events, ideally all sandy layer depths should be removed and the gaps closed up to produce a 'pelagic depth scale', before tuning the record. In reality turbidite layers were left in during the production of the final chronology for a number of reasons. Firstly, it is necessary to leave the depths of sandy layers in to later be able to plot continuous data sets, such as x-ray fluorescence element concentrations, against age. If turbidite layers are represented as instantaneous events, with a single age for their whole width, all data for that layer would plot in one place. By contrast, if a small age difference between the top and bottom of the layer is permitted, one is able to see data for that layer properly since it is spread out over a small range of dates.

Secondly 80% turbidite layers are small (≤6cm) and are equivalent to no more than a 3kyr period (applying lowest average pelagic ooze sedimentation rates) and frequently less. They do not, therefore, constitute a significant bias to dating. Larger sandy layers (>6cm) could potentially produce greater uncertainties because, being wider, a greater amount time is allocated to them (maximum of 18kyr for the widest layer applying lowest average pelagic ooze sedimentation rates) when in reality they are instantaneous events. However, when the sedimentation rate for the core, with sandy layers left in, is examined we see spikes in apparent sedimentation rate associated with turbidite layers (see *Figure 3.5*). This means that less time is allocated across the sandy layer than would be if the background sedimentation rate was used. These spikes in apparent sedimentation rate mean even wide sandy layers represent no more than a ±5kyr uncertainty in the age model because the increased sedimentation rate 'corrects' for the greater width of the sandy layer. This is supported by trials using a depth scale with large sandy layers removed, showing that

the chronology developed leaving sandy layer depths in produced very similar ages for equivalent pelagic ooze depths.

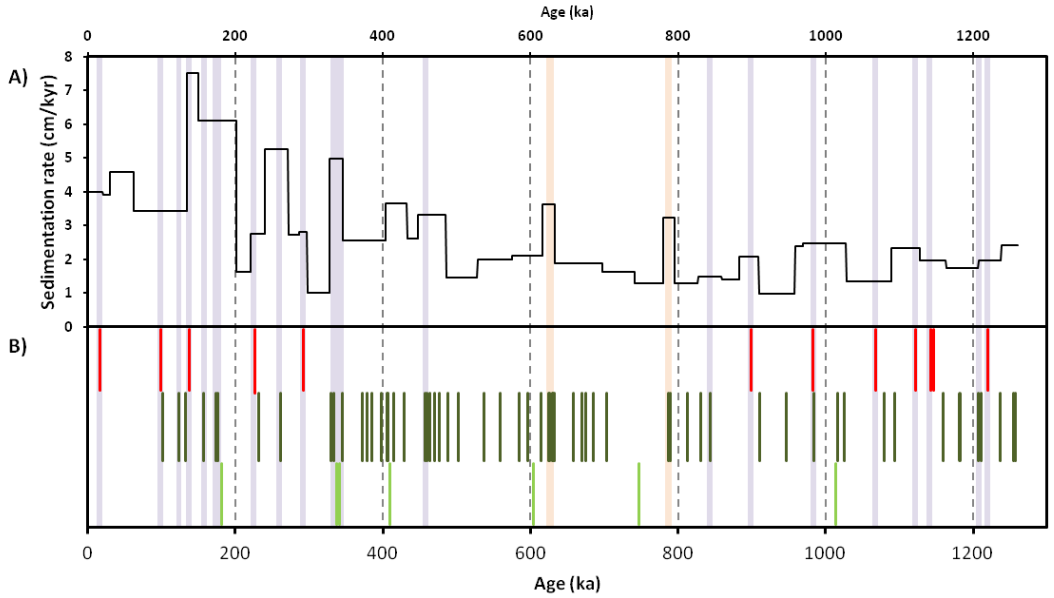

Figure 3.5 A) MD06-3019 sedimentation rate with respect to age, **B)** positions of MD06-3019 turbidite layers plotted with respect to age. The lines indicate the depth of turbidite layers, there is no component indicating the thickness of the deposit. Red- coarse grained (grain size principally $-3 \leq \varphi \geq 1$), dark green- dark fine grained and light green- light fine grained (grain size principally $2 \leq \varphi \geq 4$). Lilac lines highlight turbidite layers >6cm- most of these correspond to peaks in sedimentation rate and pale orange lines highlight a succession of closely spaced turbidites linked to a spike in sedimentation rate.

Overall the combined uncertainty of the age model is of the order of ±10kyr, with the exception of the period between MIS35-27 where this uncertainty increases to ±20kyr. Given an average model uncertainty of ±10kyr (±20kyr between MIS35-27), the ages obtained for the magnetic reversals observed in MD06-3019, are consistent with both the published ages of *Cande and Kent* (1995) and MD06-3018. This chronology therefore provides a secure framework within which turbidite layers can be accurately dated.

3.6.3 Defining the age of turbidite deposits

For the recent past, where it is possible to obtain ages on material via radiocarbon or U/Th dating, there are three main approaches to dating turbidite depositional events. All of these are subject to some uncertainty in providing the actual date of sedimentation (see *Owen et al.*, 2007 for a review). Firstly, pelagic sediments from directly above a turbidite can be dated, this provides the youngest possible age for emplacement. However, it can be difficult to differentiate between the finer grained 'tails' of turbidites and the overlying pelagic mud, especially if bioturbation has occurred, which can lead to mixed ages. Alternatively, material within a turbidite layer can be dated, but this gives the age of the material and not the timing of turbidite emplacement and will generally be biased towards older ages. Finally, pelagic sediments from directly underneath the turbidite layer can be dated, providing the oldest possible age of deposition. This approach has the advantage that it is generally easy to distinguish where a turbidite layer begins, however, there is the possibility of bias towards older dates if sediment has been removed by the erosive base of the turbidite. This third approach is generally considered superior due to the greater ease in distinguishing the pelagic mud from the turbidite sequence [*Goldfinger et al.*, 2007].

Core MD06-3019 is located in a distal position removed from the canyon axis and as a result erosion due to passing turbidity currents is believed to be minimal. This is also observed in the work of *Puga-Bernabéu et al.* (2014). Therefore, in this thesis the third methodology has been utilised; all dates presented for turbidite deposition in sediment core MD06-3019 have been obtained from using the depth at the base of the respective layers (see *Figure 3.6*). This method should allow us to date the deposition ages of turbidite layers at the same resolution as the isotope chronology, that is to within ± 10 kyrs. (Ages for individual turbidite layers can be found in Appendix 6.)

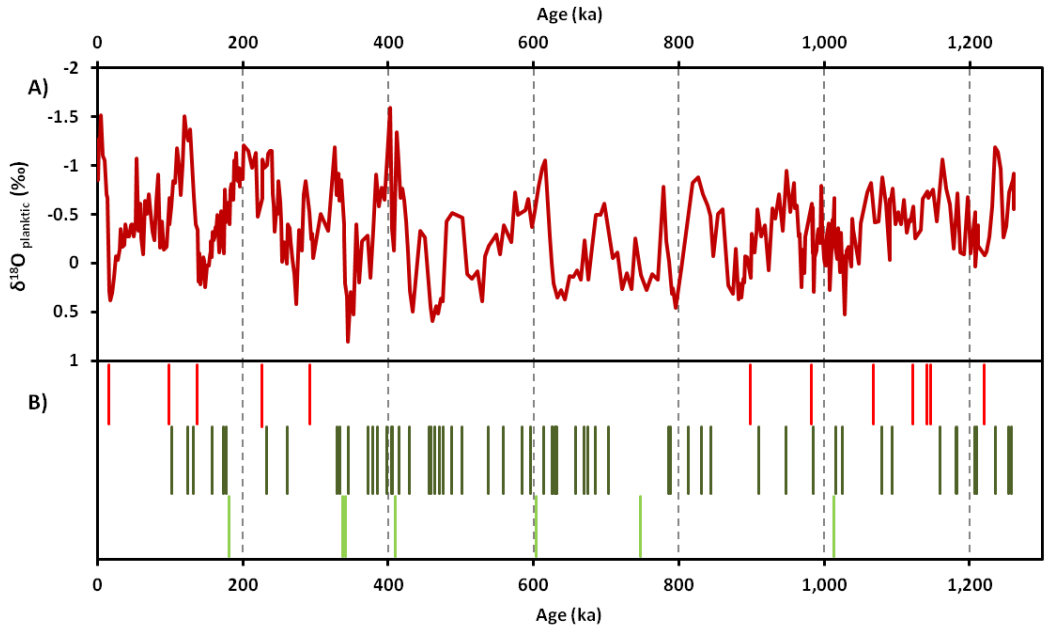

Figure 3.6 A) MD06-3019 $\delta^{18}O_{planktic}$ record with respect to age and **B)** The positions of turbidite layers plotted with respect to the core age model. The lines indicating the position of turbidite layers show their assigned age, there is no component indicating the thickness of the deposit. The differing colours of lines indicating turbidite positions represent designation of sandy layers into one of three categories: red- coarse grained (grain size principally $-3 \leq \varphi \geq 1$), dark green- dark fine grained and light green- light fine grained (grain size principally $2 \leq \varphi \geq 4$).

3.7 Conclusions

The age model for sediment core MD06-3019 was developed by tuning its $\delta^{18}O_{planktic}$ record to that of the local, independently dated, MD06-3018 core. There were initial concerns that possible deep sea dissolution and erosion from turbidites may prevent the acquisition of high quality isotope data and thus preclude the development of a core age model. However, this proved not to be the case and a robust continuous chronology, which is utilised throughout the rest of this PhD, has been developed. The base of the core is placed at 1.26Ma covering marine isotope stages back to MIS38. Apart from a less well constrained area between 1064ka and 982 ka (MIS31–MIS27) the chronology matches in detail with both the local (MD06-3018) and global (LR04) stable isotope records and the magnetic stratigraphy. For the majority of the length of the core the uncertainty in the age model is ±10kyr, except for the interval between MIS35-27 (1140-980ka) where this rises to ±20kyr.

This chronology has allowed the 79 turbidite layers in deep sea sediment core MD06-3019 to be dated. These depositional ages will be used in the following chapters to place observations of the changing nature and content of turbidites within a time framework (Chapter 4, 5 and 6) and to allow for analysis of the timing of deposition of turbidites with respect to glacial-interglacial cycles (Chapter 7).

Chapter 4: Initial investigations into the implications of changes in turbidite composition in sediment core MD06-3019

4.1 Chapter Overview

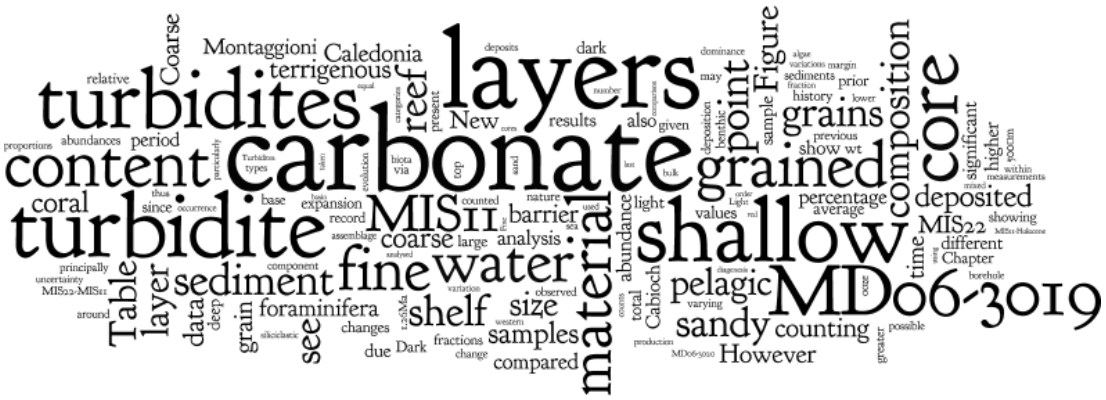

Investigations into Quaternary reef history show an expansion of the New Caledonia Barrier Reef around marine isotope stage (MIS) 11 (~400ka), from an open carbonate ramp into a rimmed shelf [*Cabioch et al.*, 2008; *Montaggioni et al.*, 2011]. The initiation of carbonate production on shallow shelves is known to produce a signal in the surrounding deeper basins, via sediment shedding [*Dubois et al.*, 2008 and *Droxler and Jorry*, 2013]. Therefore, this research set out to verify that the proposed establishment of a barrier reef at MIS11 [*Cabioch et al.*, 2008; *Montaggioni et al.*, 2011] is reflected in changes of the composition of the shallow shelf sourced turbidites deposited in the New Caledonia Trough.

The nature and content of turbidite layers deposited over the last 1.26Myr in sediment core MD06-3019, taken from the New Caledonia Trough, have been

analysed via grain size analysis, point counting and total carbonate content measurements. These results were compared with reef borehole records to assess whether the hypothesised changes in turbidite composition are observed.

There are strong similarities between the shallow water carbonate biota observed in sediment core MD06-3019 turbidite deposits (this work) and reef boreholes [*Cabioch et al.*, 2008; *Montaggioni et al.*, 2011]. As predicted, turbidites deposited since MIS11 show an increase in average bulk carbonate content, a greater dominance of shallow water bioclasts and a higher occurrence of coral fragments. Additionally, since MIS9 (~340ka) both coarse and fine grained turbidites are present, compared to only fine grained during the MIS22-11 (900-400ka) period. These results appear to corroborate the work of previous investigators, such as *Montaggioni et al*. (2011) and *Cabioch et al*. (2008). However, there are significant differences in the record prior to MIS22. Before MIS22 both coarse and fine grained turbidites are present, the average carbonate content of turbidite layers is higher, there is a greater dominance of shallow water biota and coral occurrence in turbidites is higher. Coral abundance for turbidites at the base of the core can equal or exceed values for turbidites at the top of the core. These results challenge the assumption that the only significant evolution on the western New Caledonia margin over the last 1.2Myr was the expansion of the barrier reef at MIS11. If this were the case, it would be predicted that the sediment core MD06-3019 turbidite record prior to MIS11 should be relatively consistent. Instead there is an apparent shift in the nature of turbidite deposition around MIS22. This suggests that the history of the western New Caledonia margin may be more complicated than initially anticipated (see Chapter 6 for further discussion).

There is a scarcity of point counting data for core MD06-3019. This is due to turbidite layers with low point counts being excluded from analysis, as a result of the large uncertainties in their relative assemblage percentages. This means that whilst point counting is useful for gaining an overall impression of the turbidites, it is not

sufficient on its own to accurately characterise the temporal changes in turbidite content in sediment core MD06-3019. This is a particular problem between MIS22-MIS9; which is a critical time period for investigation, given the proposed expansion of the barrier reef in New Caledonia at ~MIS11. In order to further investigate the composition of the turbidite deposits an alternative method for assessing the presence of shallow water carbonate material in samples was needed. Chapter 5 develops the use of X-ray fluorescence measurements for the strontium concentration of sediments as a proxy to assess the shallow water aragonite content of turbidite layers.

4.2 Introduction

Investigations into Quaternary reef history appear to show a significant worldwide expansion of tropical coral reefs at around marine isotope stage (MIS) 11 (400ka), including the establishment of the New Caledonia Barrier Reef [*Alexander et al.*, 2001; *Multer et al.*, 2002; *Braithwaite et al.*, 2004; *Yamamoto et al.*, 2006; *Dubois et al.*, 2008; *Cabioch et al.*, 2008; *Gischler et al.*, 2010; *Montaggioni et al.*, 2011]. It is believed from reef borehole studies that around this time the western New Caledonia margin developed from an open carbonate ramp with localised patch reefs, into a rimmed shelf with a barrier reef [*Cabioch et al*., 2008 and Monta*ggioni et al.*, 2011]. (See Chapter 2 § 3.)

The initiation of carbonate production on shallow shelves is known to produce a signal in the surrounding deeper basins, via sediment shedding [*Dubois et al.*, 2008 and *Droxler and Jorry*, 2013]. Therefore, this research project set out to verify that the significant evolution in ecosystem caused by the establishment of the barrier reef, is reflected in a simultaneous change in the composition of turbidites sourced from the shallow shelf and deposited in the New Caledonia Trough. In this chapter the nature and content of turbidite layers deposited in sediment core MD06-3019 are analysed via grain size analysis, point counting and total carbonate measurements, to assess whether their composition can be used to help reconstruct the carbonate production history of the shallow shelf. A significant limitation on previous borehole studies is the lack of accurate dating (as discussed in Chapter 1 § 6.2) leading to errors of the order of 100kyr for proposed dates for the expansion of tropical reefs. Using the chronology, based on stable isotope stratigraphy, developed in the previous chapter it is possible to date turbidite layer emplacement in sediment core MD06-3019 to an accuracy of ±10kyr. This allows for the comparison of point counting results from sediment core MD06-3019 with reef borehole records, to assess whether the predicted changes in turbidite composition are observed. It also has the future potential to greatly improve not only the accuracy of the ages given for events in reef history but also to increase the time period over which accurately dated information on reef evolution can be obtained.

According to the current literature it is predicted that the composition of turbidites deposited prior to the expansion of the barrier reef would be comparatively uniform from 1.2Ma (the base of the core) until MIS11, with relatively low carbonate content and coral dominance [*Cabioch et al*., 2008 and Monta*ggioni et al.*, 2011]. However, after MIS11 when the barrier reef is believed to have been established, it is hypothesised that there would not only be an increase in the carbonate content of turbidites deposited, but also a general change in the shallow water biota composition, including higher proportions of coral. The overall percentage carbonate content may be expected to rise not only due to increased carbonate production on the shelf but also due to the trapping of siliciclastic material behind the newly formed barrier reef, blocking its transit to the deeper basin [*Dubois et al.*, 2008].

This chapter begins with a description of the procedures used to investigate the content of turbidite layers in deep sea sediment core MD06-3019. Detailed descriptions of the core follow, along with carbonate content and point counting data for the turbidite layers. The possible implications of these results are discussed within the chronological framework developed in the previous chapter and in relation to current knowledge of reef history along the New Caledonia margin as obtained via reef boreholes [*Cabioch et al.*, 1999; *Cabioch et al.*, 2008 and *Montaggioni et al.*, 2011]. The limitations of the point counting data collected is assessed and the need for further work and alternative additional methods for investigating turbidite content acknowledged, before being developed in the subsequent chapters.

4.3 Experimental Methods

4.3.1 Grain size analysis

All sandy layer samples (1cm) that were point counted were wet sieved at 150µm and oven dried. Those samples prepared by the author were also wet sieved at 63µm and the initial total dry sample, 63-150µm and >150µm fraction weights recorded[1]. However, previous researchers did not take notes of sample weights and this has led to an incomplete data set of grain size analyses for MD06-3019, particularly for sediments younger than MIS11. Numerous sandy layer samples were also sieved at varying smaller size fractions ($150<x\leq250$µm, $250<x\leq315$µm, $315<x\leq500$µm, $500<x\leq1000$µm and >1000µm) to investigate the variation in grain size within a sandy layer.

4.3.2 Bulk carbonate measurements

Bulk weight% $CaCO_3$ was measured using a UIC Inc CM5012 CO_2 coulometer with a CM5130 acidification module at the School of Geosciences, University of Edinburgh. Analyses were made on 201 background carbonate pelagic ooze samples (including 19 made by previous Environmental Geoscience students during their 4th year honours project) and 150 individual sandy layer samples from MD06-3019. Bulk samples were oven dried and then ground to a powder using a pestle and mortar. Around 10-15µg of material was used for the analysis of background carbonate ooze samples and 15-20µg for measurements on sandy layer samples, where carbonate content is generally lower. Samples were reacted with 8ml of 2N perchloric acid, heated to 60^{o}C and analysed for 10 minutes. Measurements of a carbonate reference material made during runs indicates an analytical uncertainty of better than $2\sigma_a$= 0.32% weight (wt.) %. Repeat analyses were done at seven depths down-core (n=3), reproducibility was found to be $2\sigma_r$= 0.4 wt.%.

[1] MD06-3019 sections I-XII were sampled by Aidan Farrow, Rosanna Greenop and Angharad Jenkins during previous Environmental GeoScience honours projects at the University of Edinburgh. Sections XIII-XXV were sampled by the author at the University of Edinburgh.

Further information on the coulometry methodology may be found in Appendix 1.

4.3.3 Magnetic susceptibility measurements

Measurements of magnetic susceptibility were made on u-channels taken from the middle of the working halves of cores MD06-3018 and MD06-3019. The measurements were conducted in a shielded room using a 2G-pass-through cryogenic magnetometer equipped with a susceptibility meter. Measurements were taken every 2cm, though data from end 3cm of each core section is not presented due to edge-effects. The palaeomagnetic lab-work and post processing were undertaken by Catherine Kissel and Thomas Russon at the Laboratoire des Sciences du Climat et de l'Environnement (LSCE), Gif sur Yvette, France.

4.3.4 Point counting

For sediment core MD06-3019 samples from depth intervals corresponding to sandy layers were selected and wet sieved at 63 and 150μm; the 63-150μm and >150μm fractions were kept. For some samples the >150μm portion was then dry sieved into a further five size fractions: $150<x\leq250$μm, $250<x\leq315$μm, $315<x\leq500$μm, $500<x\leq1000$μm and >1000μm. These size fractions were weighed and the amount of material in the <63μm fraction estimated from this based on the initial weight of the whole dried sample.

Point counting was conducted on the 500-1000μm and >1000μm fractions of samples using a number of categories and sub-categories (see *Table 4.1*). Once point counting had been completed, data from multiple samples in the same turbidite layer were combined to produce an overall assemblage count for the deposit as a whole. This approach should even out intra-turbidite assemblage variation caused by grain size sorting that occurs during turbidite deposition. A general impression of the preservation and the degree of rounding was also recorded for each sample. Finally, the combined data for all sandy layers was then analysed for trends in content variation through time.

Broad Category	Sub-categories	
Pelagic	Planktic foraminifera	Foraminifera unknown
	Benthic foraminifera	Pteropod
Terrigenous	Terrigenous siliciclastic	Organic (wood)
Shallow shelf carbonate	Coral	Bryozoan
	Halimeda	Large benthic foraminifera (LBF)
	Bivalve	Gastropod
	Bivalve/ gastropod	Calcareous red algae
	Echinoderm spine	Echinoderm plate
	Carbonate mud	Diagenetic carbonate
	Shallow water carbonate unidentified	
Miscellaneous	Pteropod/ bivalve/ gastropod	
	Fish tooth	
	Miscellaneous	

Table 4.1 Point counting categories for assemblage determination of the >500µm fractions of sandy layer samples. The 'bivalve/gastropod' category was used for grains that were thought to be fragments of a bivalve or gastropod, but it was not certain which. Similarly the 'Pteropod/ bivalve/gastropod' category was used for grains that were thought to be fragments of a pteropod, bivalve or gastropod, but it was not certain which. 'Carbonate mud' grains are interpreted as weakly cemented shallow water intraclasts, which differ from the surrounding mud matrix. They are made of fine grained, weakly cemented, carbonate mud into which sand sized grains, of generally terrigenous origin, are attached; the grains are frequently flat on one side. 'Diagenetic carbonate' grains are those which have clearly undergone diagenesis, showing evidence recrystalisation and cementation. This alteration is presumed to have occurred during subaerial exposure on the upper shelf during sea-level lowstands.

Despite an abundance of material, point counting for size fractions <500µm was not conducted. 12 trial samples across all three categories of turbidite layer and over the complete length of the core were point counted in the $150<x\leq250$µm, $250<x\leq315$µm and $315<x\leq500$µm size fractions. However, reliable identification of small grains proved difficult beyond the broadest classification of pelagic, terrigenous, shallow water carbonate or miscellaneous. Even using this most basic of systems, percentages of grains designated as miscellaneous could reach 25% and even greater proportions using the more detailed classification scheme. Results such as these are unable to

contribute any meaningful data to the investigation and thus point counting was restricted to size fractions >500μm.

4.3.5 Reliability of point counting data

One obvious question was whether diagenesis of turbidite material in the deep basin environment, subsequent to deposition, could have occurred to such an extent that it would limit interpretation on the original composition and origin of the turbidite material. The preservation of turbidite sediments is not always good and there is evidence of erosion, dissolution and recrystalisation of individual grains. However, these processes are believed to have occurred whilst the material was still in the shallow shelf environment. Many layers are exceptionally well preserved with grains exhibiting little evidence of diagenesis. In other cases whilst the pelagic fraction appears well preserved the shallow shelf material is less so, suggesting diagenesis on the shallow shelf. These observations suggest that the instantaneous deposition of turbidites allows good preservation of material in the deep sea, though the sediments may have suffered prior diagenesis in the shallow water realm before this stage.

In total 244 sandy layer samples (representing 76 turbidite layers) were point counted for the composition of their >500μm fraction. Relative percentage abundance values obtained from layers with low point counts are subject to large proportional uncertainties. It is recommended to point count 300 grains when individual categories comprise 10% of the sample, 500-1,000 grains when an individual category comprises 5% of the sample and several thousand counts when a category that makes up 1% of the sample [*Patterson and Fishbein*, 1989]. Given the composition and nature of samples in this study, a lower limit of 300 point counted grains per turbidite was set. Below this cut off the uncertainty errors on the relative percentage abundances of different sediment components rises steeply [*Pye*, 2007]. With a point count of ≥300 grains per turbidite layer, the percentage abundance maximum 2σ uncertainty for any component is 6% [*van der Plas and Tobi*, 1965; *Patterson and Fishbein*, 1989]. (2σ varies from 2-6% depending on the relative percentage of the component in the sample.)

Due to paucity of material it was frequently not possible to point count more than 300 grains per turbidite, even when all grains >500µm in a sample were counted. Of the 76 turbidite layers analysed 30 (39%) contained fewer than 300 grains in the >500µm size fraction, these were all dark fine-grained layers. Over 50% of dark fine layers contained fewer than 300 grains in the >500µm size fraction (see *Table 4.2*).

Percentage of layers with <300 grains >500µm		
Whole core		39% (30/76)
MIS11-Holocene		24% (6/25)
MIS22-MIS11		63% (19/30)
1.26Ma-MIS22		24% (5/21)
1.26Ma- MIS11		47% (24/51)
Coarse grained		0% (0/12)
Fine grained	**Dark**	52% (30/58)
	Light	0% (0/6)

Table 4.2 Percentage of layers for different time periods and turbidite types (coarse grained, dark fine grained and light fine grained) for which the number of grains available for point counting was <300.

Therefore data from turbidites with fewer than 300 grains point counted were excluded from the following analysis. The removal of the most unreliable data and thus extreme percentage abundance values, aimed to give more realistic average values for turbidite composition with time. However, the removal of data from turbidites with low point counts, significantly reduces the number of layers used in the analysis, particularly in the MIS22-11period.

In addition to the temporal analysis of the varying proportions of the broad categories of pelagic, terrigenous and shallow water carbonate grains, an analysis of the variations in the abundances of different shallow water carbonate organisms has also been conducted. Given the relative percentage abundances of species are frequently in the 1-5% range, point counts of several thousand grains are required to obtain acceptable uncertainty levels [*Patterson and Fishbein*, 1989]. However, due to the

lack of material, the requirement of shallow water grain point counts to be in the thousands would only allow analysis of the content of a few turbidite layers. Instead a lower limit of 300 shallow water grains has been imposed, allowing the shallow water content of 18 out of the 76 turbidites (24% of layers) to be analysed. The 2σ uncertainty around the percentage abundances of these shallow water carbonate organisms is between 2-6% and thus of the same order of the percentages of the species themselves.

4.4 Results

4.4.1 MD06-3019 sandy layer descriptions

Deep marine sediment core MD06-3019 is principally composed of foraminifera rich pelagic ooze. The carbonate ooze shows significant colour variation from a pale fawn-cream to rich olive-green/ brown. These changes in colour relate to differences in the total carbonate content of the pelagic ooze, which varies between 18-85 wt.%., in phase with glacial-interglacial climate change (see Appendix 3). The core also contains 79 mixed siliciclastic-carbonate sandy layers. These are believed to be gravity deposits, which source eroded material from the shallow shelf area near Grand Terre and transported it to the deep basin via the canyon systems that incise the slope.

Turbidite layers were identified based on visual observations of the core. They vary in: width from 1-35cm (with a total accumulation of 4.4m), grain size from fine sand (φ=4) to coarse sand/gravel (φ=-3) and composition, with varying levels of shallow shelf bioclasts, terrigenous grains and pelagic components. The presence of sandy layers can also be identified in grain size analysis and via the magnetic susceptibility record for the core (see Appendix 5 for photographs and sedimentary logs of core MD06-3019). Full details of sandy layers positions, ages (as assigned in Chapter 3), widths, classifications, short descriptions and grain size allocations are given in Appendix 6.

Sandy layers were classified based on their grain size (see *Figure 4.1* and *Figure 4.2*) as either:

- **Fine grained**: when principally composed of very fine to fine grained sand ($-3 \leq \varphi \geq 1$) and containing little/no coarse grained fragments. These layers can be further split into dark fine grained (principally terrigenous sediment derived silt/mud component) and light fine grained (principally carbonate sediment derived silt/mud component), based on the varying carbonate content of the silt/mud contained in them. The assemblage composition of their sand sized components tends to be similar regardless of the silt/mud

composition. Whilst generally found individually as either dark or light layers, on one occasion (3058-3063cm) a light fine layer grades into a dark fine layer.

- **Coarse grained**: composed of significant amounts of coarse, very coarse or granule sized grains (grain size principally $2 \leq \varphi \geq 4$), with varying mud to fine sand content. Some coarse layers do however show a pronounced fining up sequence and become fine grained at their top.

Figure 4.1 shows core photographs with examples of all three sandy layer types within the surrounding pelagic ooze. *Figure 4.2* provides examples to show the varying grain size compositions of different sandy layer types.

Whilst fine sandy layers are found throughout the core, coarse sandy layers are only present between the 1.26Ma - MIS22 (base and 2820cm) and MIS9 - Holocene (1490cm to core top).

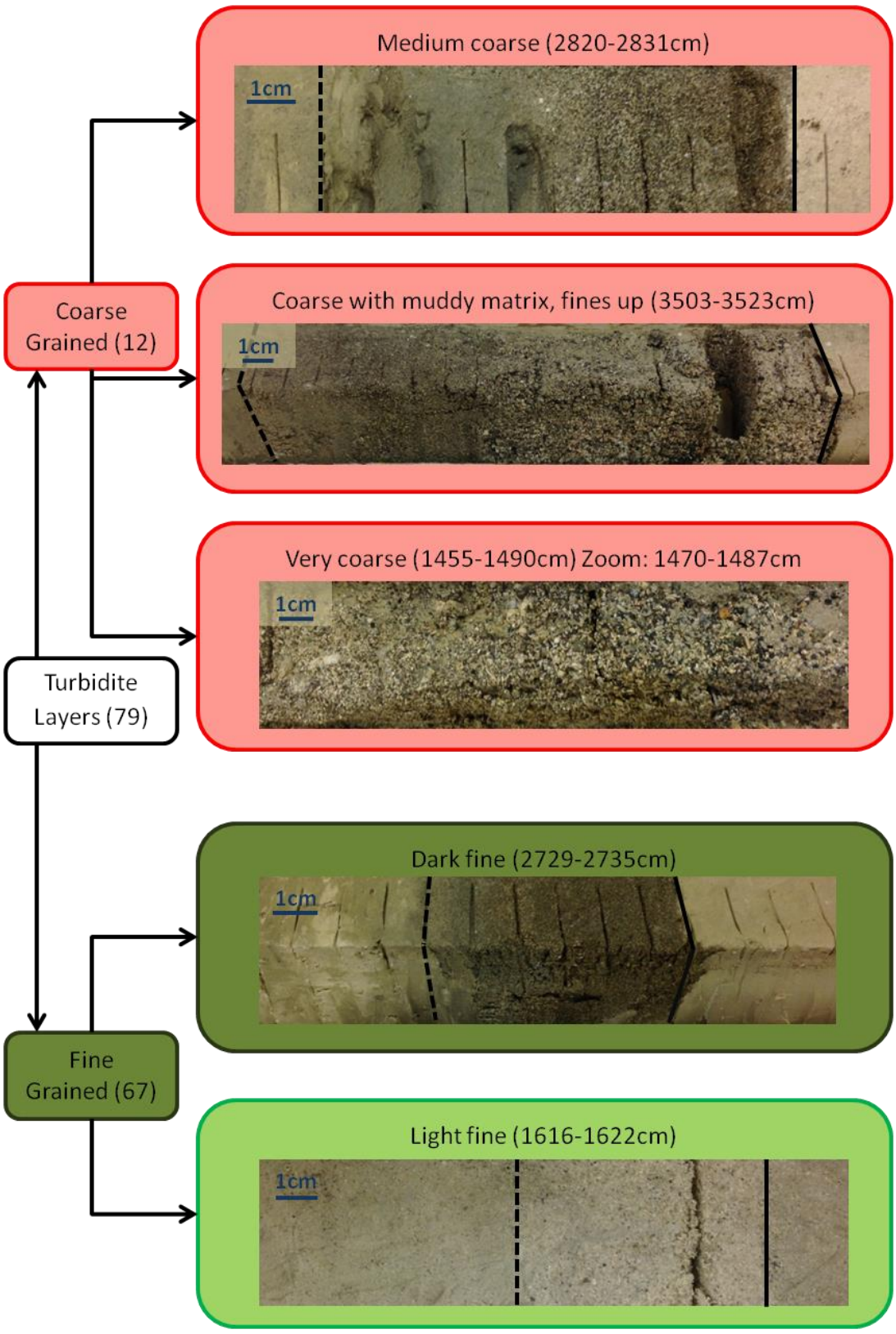

Figure 4.1 Photographs of example turbidite layers of different grain sizes and compositions within the surrounding pelagic ooze. Where the complete length of the

turbidite is shown the base is indicated by a solid line and the top with a dotted line. The top of a photographed section is always on the left hand side of the picture.

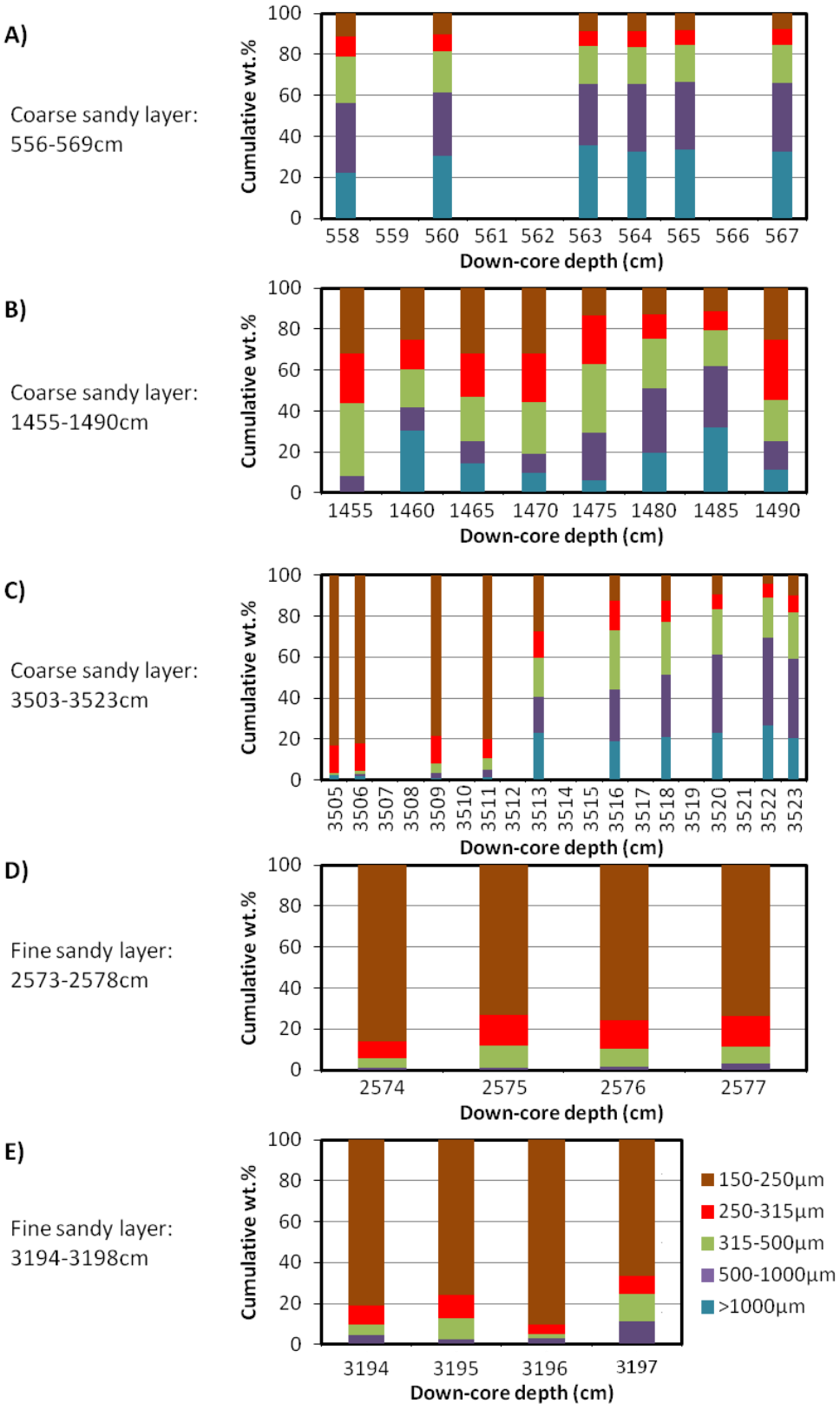

Figure 4.2 Showing the grain size distribution of different layer types. **A)** coarse grained-consistent grain size distribution and **B)** coarse grained- variable grain size distribution, **C)** coarse grained- showing fining up sequence, **D)** and **E)** fine grained.

4.4.2 MD06-3019 bulk carbonate results

The total weight % bulk carbonate content of turbidites in core MD06-3019 is presented in the bottom panel of *Figure 4.3*. Their carbonate content varies between 4-71 wt. %, showing the mixed carbonate-siliciclastic nature of the area. Turbidites were assigned as being either calciturbidites (>60 % carbonate), mixed (40-60% carbonate) or siliciclastic turbidites (<40% carbonate) depending on their composition, as per the definitions of *Puga-Bernabéu et al.* (2014). There is a clear relationship between layer type and total carbonate content (see *Table 4.3* and *Table 4.4*). Dark fine grained layers, as would be expected, have a lower carbonate content and are principally classed as siliciclastic turbidites and with no instances of calciturbidites. By contrast, light fine and coarse grained layers are mainly 'mixed' turbidites. Coarse layers vary in carbonate content significantly and can be siliciclastic, mixed or calciturbidites; whereas light fine layers, as would expected from their colour, have a higher carbonate content and none are classified as siliciclastic turbidites.

Subdivision of MD06-3019 Turbidites Based on Carbonate Content				
Turbidite Type	**Coarse**	**Dark fine**	**Light fine**	**All**
Calciturbidite (n=3)	9%	0%	29%	4%
Mixed turbidite (n=27)	55%	27%	71%	35%
Siliciclastic turbidite (n=48)	36%	73%	0%	62%
Carbonate Content of MD06-3019 Turbidites				
Turbidite Type	**Coarse**	**Dark fine**	**Light fine**	**All**
Carbonate wt.% range	33-66%	4-59%	41-71%	4-71%
Median carbonate wt.%	48%	29%	52%	34%

Table 4.3 Percentages of each turbidite type (coarse grained, dark fine grained or light fine grained) in MD06-3019 that are classed as either carbonate (n=3), mixed (n=27) or siliciclastic (n=48) turbidites. The median carbonate wt.% content for each turbidite type (coarse grained, dark fine grained or light fine grained) is also provided.

There is a significant reduction in the overall total carbonate content of turbidite layers in the middle section of the core (MIS22-11: 900-400ka) compared to the base (MIS~38-22: 1,260-900ka) and the top (MIS11-Holocene: 400ka-Holocene) (see *Figure 4.3* and *Table 4.4*.) There is no obvious consistent relationship between the bulk carbonate content of turbidites and glacial-interglacial cycles (see *Figure 4.3*). For a more in depth analysis of the relationship between the carbonate content of turbidites and depositional age with respect to glacial-interglacial cycles see Chapter 7.

Weight % bulk carbonate content of MD06-3019 turbidite layers				
	Coarse (n=11)	**Dark fine (n=60)**	**Light fine (n=7)**	**All turbidites (n=78)**
Complete record	48%	29%	52%	34%
MIS11- Holocene	48%	36%	53%	41%
MIS22-MIS11	-	23%	57%	24%
1.26Ma-MIS22	45%	34%	41%	36%
1.26Ma- MIS11	45%	27%	44%	29%

Table 4.4 Median total carbonate content of turbidite layers in different sections of the core.

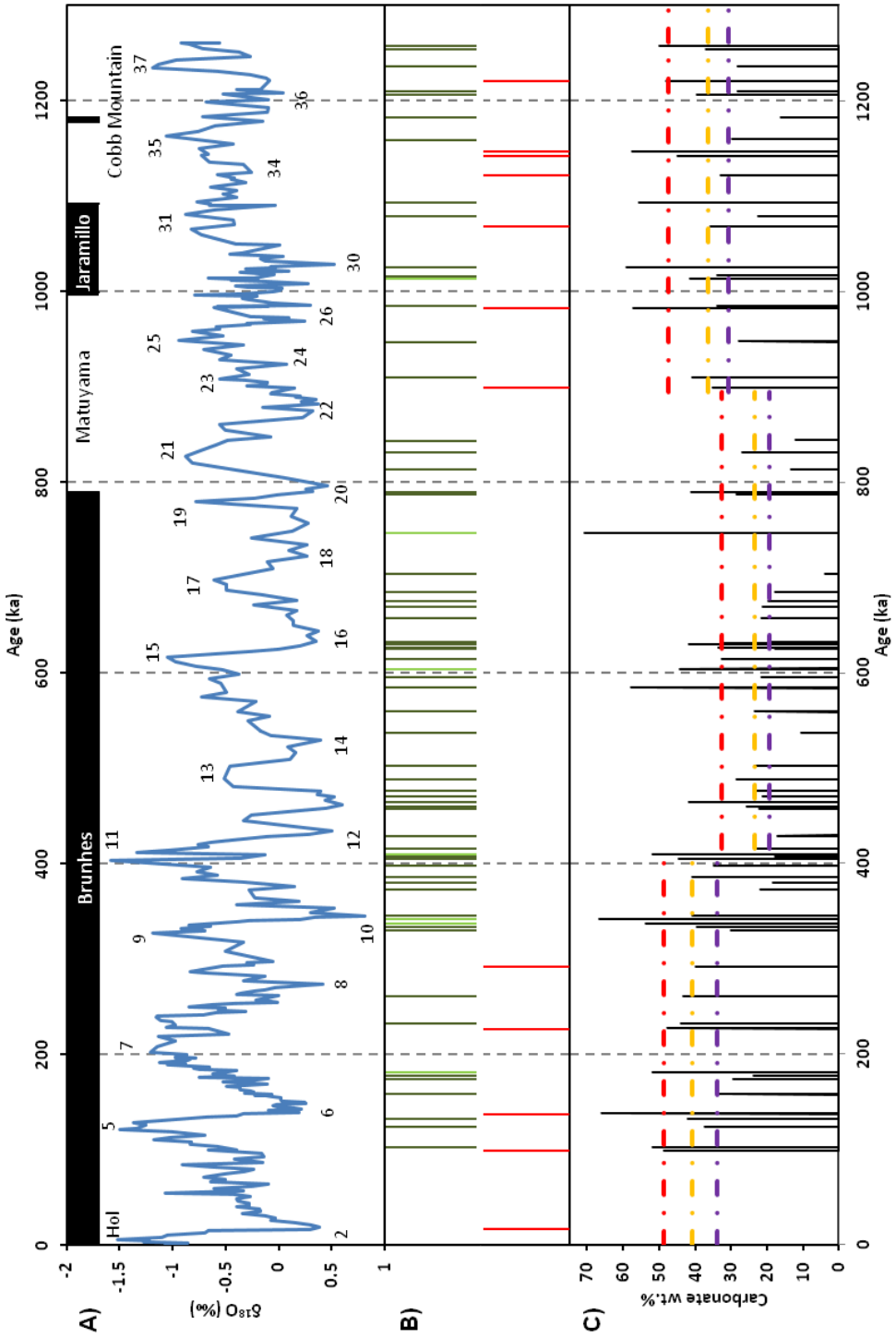

Figure 4.3 A) MD06-3019 $\delta^{18}O$ record obtained from G. *ruber* foraminifera. **B)** Positions of sandy layers. Red: coarse; dark green: dark fine layers; pale green: light fine layers. **C)** Sandy layer carbonate wt. %. Upper quartile (red), median (yellow) and lower quartile (purple) for sections representing: 1.26Ma- MIS22, MIS22-MIS11, MIS11- Holocene.

4.4.3 MD06-3019 point counting results

Sandy layers present in core MD06-3019 contain a wide variety of pelagic, terrigenous and shallow water carbonate grains (see *Figure 4.4.1 and Figure 4.4.2*) and show varying composition with time. Whilst there are intra-layer variations in the composition of turbidite layers, the general profile of the assemblage tends to remain fairly consistent between samples from the same layer. Intra-layer differences are assumed to be due to the turbulent nature of the turbidity current. (Full point counting data is presented in the digital only Supplementary Data spreadsheet.)

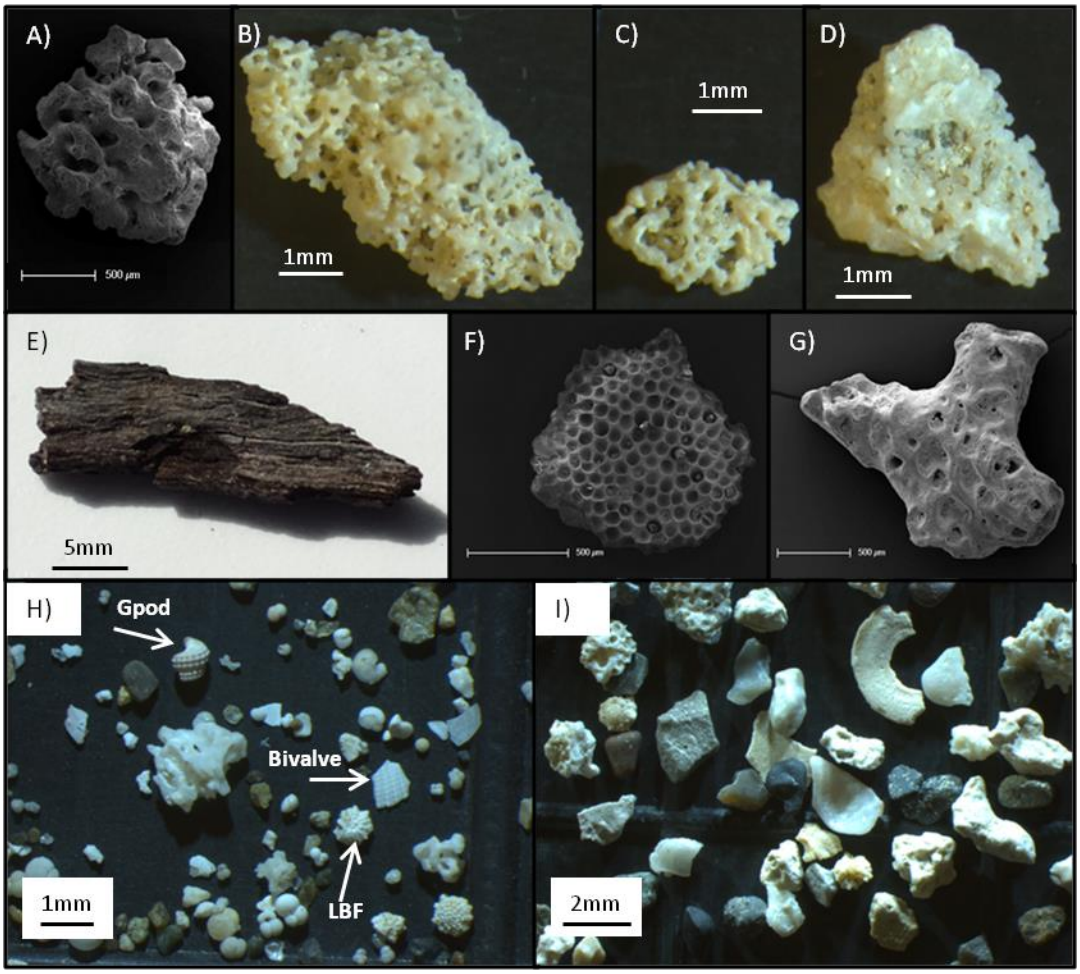

Figure 4.4.1 Photographs of loose sediment, thin sections and SEMs showing examples of sandy layer content. **A-D)** 1458cm: coral, **E)** 3506cm: wood, **F)** 418cm: halimeda, **G)** 404cm: bryozoans, **H)** 1460cm: Gpod= gastropod, bivalve, LBF= large benthic foraminifera (calcrinid) and **I)** 560cm: general view of sample including large benthic foraminifera (sortid), terrigenous material, coral and bivalves.

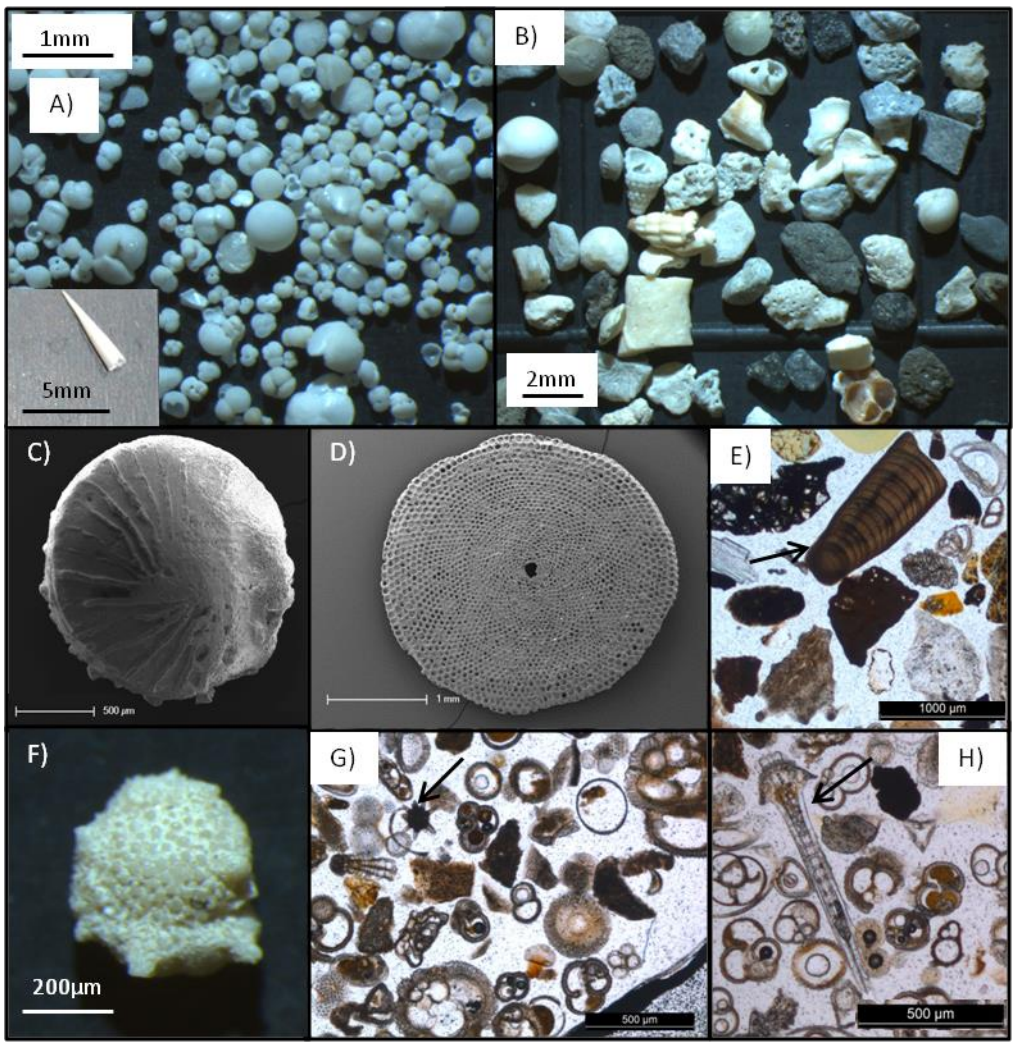

Figure 4.4.2 Photographs of loose sediment and thin sections and SEMs showing examples of sandy layer content. **A)** 765cm: photograph of a loose sediment planktic and benthic foraminifera assemblage, inset: pteropod (59cm), **B)** 3250cm: photograph of a general view of a loose sediment sample showing terrigenous and carbonate material, **C)** 2825cm: SEM large benthic foraminifera (amphistiginid), **D)** 560cm: SEM large benthic foraminifera (sortid), **E)** 3522cm: thin section photograph showing articulated coralline algae, **F)**1460cm: SEM of large benthic foraminifera (calcrinid- incomplete), **G)** 2366cm: thin section photograph showing large benthic foraminifera (calcrinid) and **H)** 3194cm: thin section photography showing echinoderm spine.

The content of turbidite layers can be allocated into three broad categories: pelagic organisms, terrigenous sediment (including woody material) and shallow water carbonate material. *Figure 4.5*, *Figure 4.6* and *Table 4.5* show the range of compositions for sandy layers. There is a wide spread of results throughout the core with terrigenous plus shallow water grain compositions normally varying between 0-60% and pelagic material varying from 0-100%.

Fine grained layers, regardless of classification as a 'light' or 'dark' layer, show similar compositions for the >500μm fractions; this supports the belief that the difference in colour and carbonate content is principally due to variations in the composition of the finer grained material within the layers. Comparison between fine and coarse grained layers show a greater dominance of pelagic material for fine grained turbidites and a higher percentage of shallow water carbonate and terrigenous material in coarse grained samples.

Median composition of MD06-3019 turbidite layers				
		Pelagic (%)	**Terrigenous (%)**	**Shallow water carbonate (%)**
Whole core		67	8	20
MIS11-Holocene		40	32	33
MIS22-MIS11		96	0	2
1.26Ma-MIS22		78	6	11
1.26Ma- MIS11		93	2	6
Coarse grained		45	19	30
Fine grained	**Dark**	80	5	7
	Light	90	6	5

Table 4.5 The median composition of the >500μm fraction of sandy layers in different sections and layer types within the core according to the broad classifications of pelagic, terrigenous and shallow water carbonate material. (Totals for each time period do not sum to 100% due to the fact the values given are medians and the miscellaneous category data is not shown here.)

All turbidites, when averaged over 400-500kyr time periods, show a fairly equal split between terrigenous and shallow water carbonate derived grains (see *Table 4.6*). However, the dominance of pelagic material changes more dramatically through time. Turbidites deposited from MIS11 to present on average contain far less pelagic material than those deposited prior to MIS11 (~40% compared to ~90%) and thus have greater proportional terrigenous and shallow water carbonate content. There is, however, a change in the spread of the importance of the pelagic component in turbidites deposited before MIS11. Prior to MIS22 there is greater variation in the abundance of pelagic material when compared to those layers deposited between MIS22 and MIS11. Overall, there is no clear evolution or clustering of the composition of turbidite layers with age; turbidites of highly varied compositions can be found at all depths down-core (see *Figure 4.5* and *Figure 4.6*).

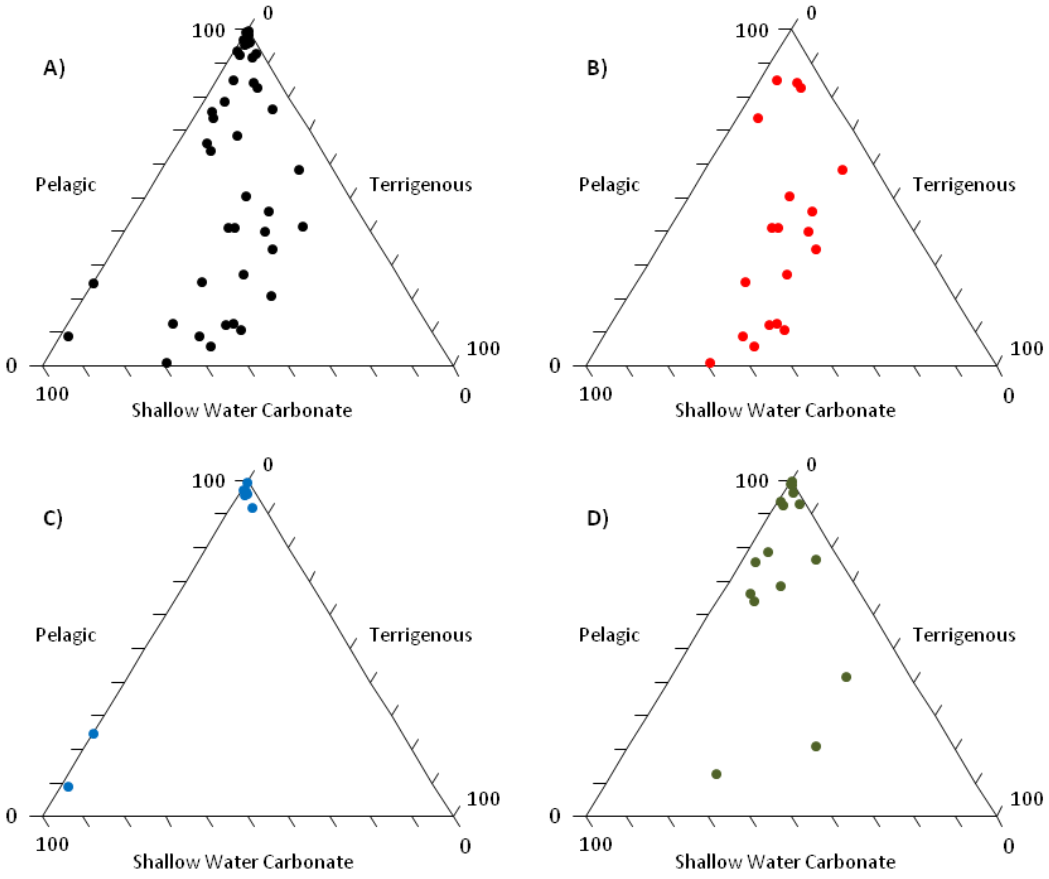

Figure 4.5 Ternary diagrams for the composition of sandy layers**: A)** all sandy layers, **B)** sandy layers between MIS11-Holocene, **C)** sandy layers between MIS22-MIS11, **D)** sandy layers between 1.26Ma-MIS22.

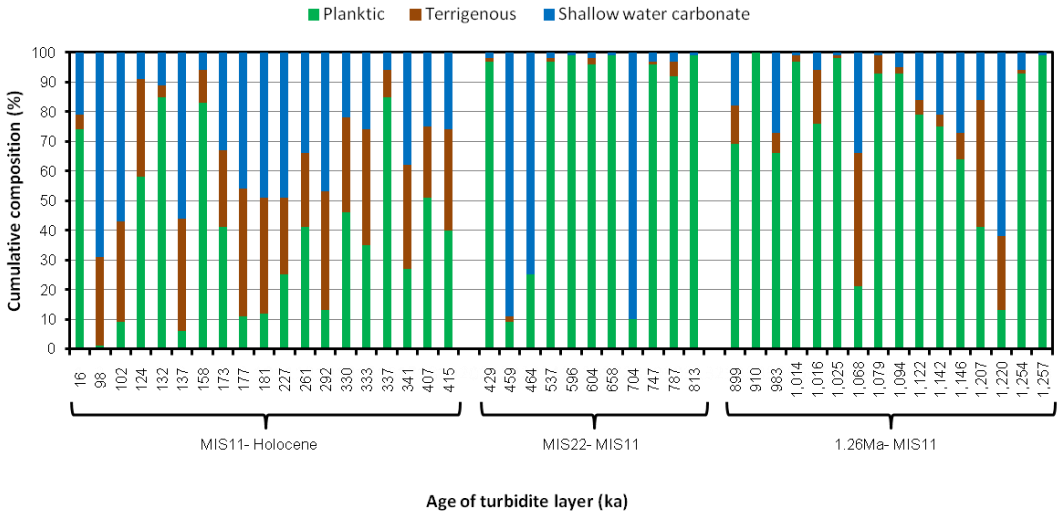

Figure 4.6 Histogram showing the variation in composition of MD06-3019 turbidite layers over the last 1.26Myrs.

On the shallow shelf deposition of pelagic foraminifera and pteropods only tends to represent 1-2% of the total sediment [*Montaggioni et al.*, 2011]. The high proportions of pelagic material seen in many turbidites may reflect an entrainment signal, as turbidites erode pelagic ooze during their turbulent downhill flow to the deep basin. Alternatively, high proportions of pelagic material could represent changing compositions/locations of the sediment destabilised during gravity flows. Variations in the pelagic component of turbidites is not thought to accurately reflect temporal changes in shallow shelf ecology or morphology. Therefore, to examine the changing nature of sediment supply from the shallow shelf to the deep ocean via turbidites the pelagic component of turbidite layers was removed and only the ratio between terrigenous and shallow shelf carbonate was considered.

Coarse grained turbidites on average contain a greater proportion of shallow shelf carbonate (~70%) than terrigenous material (~30%). By contrast, both light and dark fine grained layers show roughly equal amounts of both terrigenous and shallow water carbonate grains (see *Table 4.6*). When averaged over 400-500kyr periods there is no apparent change in the ratio of terrigenous to shallow water carbonates, remaining constant at ~ 45%: 55% throughout the whole time period (see *Table 4.6*).

Average relative proportions of terrigenous and shallow water carbonate material in MD06-3019 turbidites			
		Terrigenous (%)	**Shallow Shelf Carbonate (%)**
Whole core		46	54
MIS11-Holocene		47	53
MIS22-MIS11		43	57
1.26Ma-MIS22		48	52
1.26Ma- MIS11		45	55
Coarse grained		32	68
Fine grained	**Dark**	49	51
	Light	48	52

Table 4.6 Average relative proportions of terrigenous and shallow water carbonate material for sandy layers in different sections and layer types of core MD06-3019.

The coral content of turbidite layers varies down-core, generally representing 0-5% of the shallow water carbonate material present (see *Table 4.7* and *Figure 4.7).*On average turbidites deposited since MIS11 have a slightly higher coral content than those deposited before (see *Table 4.7* and *Figure 4.7)*. However, given the percentage uncertainties and the small number of layers available for analysis this is not a significant difference. Coral content percentages at the base of the core at 1.26Ma can equal, or exceed the coral content of turbidites deposited since MIS11. By contrast, since MIS11 there is a greater consistency in the number of turbidite layers with some coral present, particularly since MIS9. Prior to this there were far lower numbers of layers recorded as being coral bearing, 25% compared to 77%, the values being particularly low between MIS22-11 (20%) and slightly higher between 1.26Ma at the base of the core and MIS22 (33%) (see *Table 4.7*).

Coral content of MD06-3019 turbidite layers			
		Percentage of coral bearing turbidites	**Average coral content (% of shallow shelf carbonate material)**
Whole core		41% (32/79)	3 (n= 18)
MIS11-Holocene		77% (20/26)	4 (n= 10)
MIS22-MIS11		20% (6/30)	0 (n= 3)
1.26Ma-MIS22		33% (7/21)	3 (n= 5)
1.26Ma- MIS11		25% (13/51)	1 (n= 8)
Coarse grained		100% (12/12)	3 (n= 10)
Fine grained	**Dark**	29% (17/58)	3 (n= 7)
	Light	71% (5/7)	6 (n= 1)

Table 4.7 The percentage of coral bearing turbidite layers and the relative average abundance of coral with respect to shallow shelf carbonate material for layers with >300 shallow water grains at different time periods and for different layer types.

Proportions of other shallow water carbonate material (Halimeda, bryozoans, large benthic foraminifera, bivalves, gastropods, echinoderms- spines and plates, carbonate mud and lithic carbonate grains) also vary in turbidite layers through time (s*ee Figure 4.7*). The proportions of calcareous red algae have not been included, since identification under a binocular microscope was difficult. Fragments frequently resembled other eroded carbonate material and were classified as 'carbonate unidentified'. Thus the percentage abundances for calcareous red algae are thought to be unreliable.

In general, relative percentage abundances for shallow water carbonate species varies between 0-15%, with a maximum 2σ uncertainty of 6%. For most of the shallow water carbonate species categories there are no apparent significant trends through time in their abundance in turbidites. The gap in presence of shallow water material between ~MIS22-MIS11 is due to a lack of results over that period, not a pattern in

abundance change in its own right. The abundance of different organisms varies but values at the base of the core are comparable to those at the top

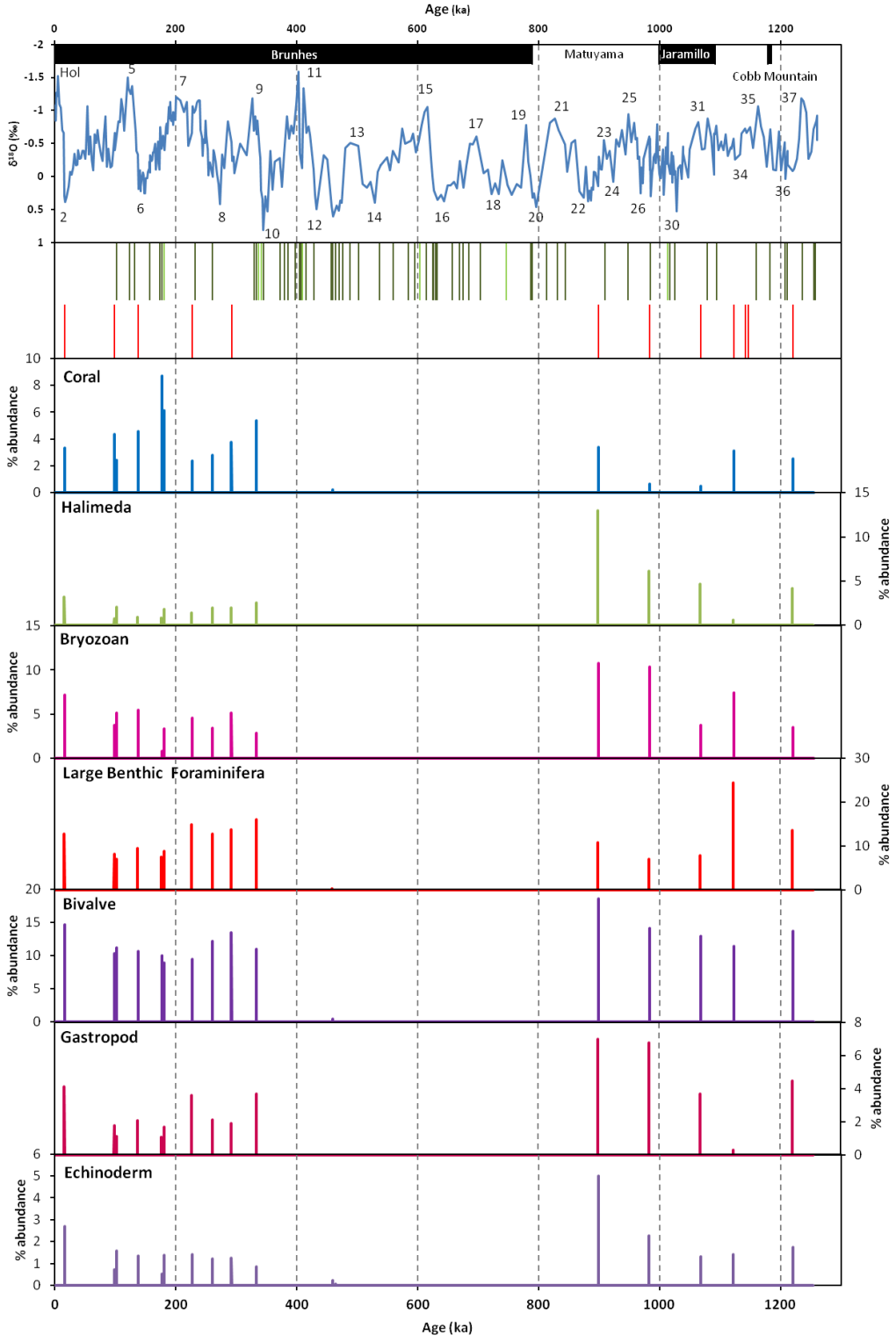

Figure 4.7 The variations in the shallow water carbonate biota composition of turbidites in MD06-3019 with >300 shallow water grains point counted. Top panel: MD06-3019 $\delta^{18}O$ record obtained from G. *ruber* foraminifera and below the position of the turbidite layers (red-coarse grained, dark green-dark fine grained and light green- light fine grained). There then follows the percentage abundance variations of each component with respect to the total shallow water carbonate content.

The significant quantities of pelagic and terrigenous material present in sediment core MD06-3019 turbidites mean their total assemblages are not directly comparable with those seen in reef boreholes taken from the western New Caledonia Barrier Reef (Amédée, Ténia and Kendec) [*Cabioch et al.*,1999; *Cabioch et al.*, 2008; *Montaggioni et al.* 2011]. However, the shallow water carbonate composition of sandy layers can be compared. Both the deep sea and barrier reef records show the presence of corals, bryozoans, molluscs, echinoids, large benthic foraminifera and coralline algae. The deep sea record from sediment core MD06-3019 also includes moderate amounts of halimeda (up to 20%, more akin to shallow shelf sediment compositions), which were not seen in the shallow shelf records (<0.5%); where this absence was attributed to the poor preservation due to later freshwater diagenesis [*Montaggioni et al.,* 2011]. In this study it was generally only possible to identify carbonate biota at family level and thus a comparison with previous published data on the genus and species of the biota present is not possible. However, higher level identification was normally possible for foraminifera and strong similarities can been seen between turbidite deposits and borehole data. Both deposit types contain free living hyaline (amphistiginids, nummulitids and calcrinids), porcelaneous (sortids, alveolinids and miliolids) and agglutinated (textulariids) forms. Encrusting foraminifera are quite common in the reef borehole detritus (5-20%) [*Montaggioni et al.*, 2011] but though sometimes observed in MD06-3019 turbidites there presence is far less common.

Ideally it would be possible to make direct comparisons between the shallow water assemblages observed in sediment core MD06-3019 and compare these and their evolution to the facies identified in the Ténia reef borehole (closed geographical study to MD06-3019) [*Montaggioni et al.,* 2011]. However, this is difficult for a number of reasons. Firstly, for the last 400kyr the boreholes sampled a barrier reef framework and percentage abundances are not given for the different biota, so no comparison is possible. Prior to this period the composition of the detrital facies sampled is given. However, these sediments only sample one area of the shelf and

may not necessarily be regionally representative, particularly if they were taken from an open shelf environment with patch reefs, which by nature would be inhomogeneous. Additionally, point counting abundance values for MD06-3019 turbidites have large uncertainty values due to small sample sizes, as well as problems in identification of calcareous red algae (calcareous red algae is a major component of borehole samples). Therefore only the qualitative comparison given above has been attempted.

Overall, whilst there is variation in turbidites through time, the nature of the samples observed at the base and top of the core both in terms of content, rounding and preservation appear remarkably similar.

4.4.4 Comparison between turbidite deposits in cores MD06-3019 and MD06-3020

Ideally, any study aiming to reconstruct barrier reef history from deep sea turbidites would be able to compare and contrast sediments from a number of cores in different locations along the barrier reef. This helps to resolve the issue that temporal changes in turbidite deposits may reflect evolution in the shallow shelf ecosystems and/or variations in transport processes.

It was possible to compare sediments from core MD06-3019, with those taken from the nearby (~100m apart) short gravity core MD06-3020 which also contained six turbidites (see Chapter 2, *Figure 2.5*). Unfortunately, this core does not cover the whole Quaternary period, only back to MIS5 (~120ka), and is located very close to MD06-3019. However, comparison of these sediment cores allows some assessment of the reproducibility of sedimentary records.

There are many similarities observed between sediment cores MD06-3019 and MD06-3020, which supports the use of the MD06-3019 core record in reconstructing

barrier reef history. Both record turbidites, which within error, appear to have been deposited at the same time; with the turbidite type (fine versus coarse) being consistent for five out of the seven layers (see *Table 4.8*). (For more information on the turbidites contained in MD06-3020 see Appendix 6.)

MD06-3019				**MD06-3020**		
Raw layer depth (cm)	**Age (ka)**	**Layer type**		**Raw layer depth (cm)**	**Age (ka)**	**Layer type**
40-42	11	Coarse		19-21	11	Coarse
58-64	16	Coarse		27-39	20	Coarse
398-406	98	Coarse		171-174	113	Coarse
416-420	102	Dark fine		180-182	119	Dark fine
498-506	124	Dark fine		186-187	122	Coarse
522-536	132	Dark fine		204-207	133	Coarse
556-569	137	Coarse		210-214	134	Coarse

Table 4.8 Comparison between the age of deposition and grain size of turbidites deposited in deep sea sediment cores MD06-3019 and MD06-3020. In core MD06-3019 a small amount of sand was observed at 40-42cm at the edge of the core, by the casing. This was not recorded as a sandy layer, since it was not certain if the sand was merely due to distortion and smearing of sediments along the edge of the core casing during extraction with the piston corer. In comparison with turbidites in MD06-3020 however, it seems likely that the sand present at 40-42cm is associated with a separate turbidite event.

4.5 Discussion

4.5.1 Implications of MD06-3019 turbidite content analysis

Results obtained via examination of the turbidites in deep sea sediment core MD06-3019 help to support the hypothesis that the expansion of the New Caledonia Barrier Reef, at MIS11, was associated with a change in the composition of shallow shelf sediment supplied to the New Caledonia Trough.

Firstly, there are strong similarities between the shallow water composition of turbidites in MD06-3019 and the organisms observed in reef bore hole deposits studied on the shallow shelf [*Cabioch et al.*, 2008; *Montaggioni et al.*, 2011]. Secondly, there is a marked change in the pattern of turbidite sedimentation in core MD06-3019 after MIS11. Turbidites deposited since MIS11 show an increase in average bulk carbonate content (41 wt.%) compared to those deposited just before (24 wt.%) (see *Figure 4.3* and *Table 4.4*) suggestive of increased production (and later export to the deep sea) of carbonate material on the shallow shelf. Similarly sandy layers emplaced since MIS11 show a greater dominance of shallow water bioclasts in their assemblages (on average 33 ± 6% abundance), compared to prior (on average 6 ± 6% abundance) when layers tend to be more heavily dominated by pelagic material (see *Table 4.5*). This increase in shallow water carbonate material may reflect increased production on the shelf. As would be predicted given the establishment of a barrier reef on a previously open shelf, there is a higher occurrence of coral bearing turbidites deposited after MIS11 than just prior, 77% versus 20% (see *Table 4.7*). The change in grain size at MIS9 with the reappearance of coarse grained turbidite layers could be interpreted as showing that carbonate production increased later at ~MIS9 as opposed to MIS11. However, a more plausible explanation of this delay between barrier reef establishment at MIS11 and the deposition of coarse grained, coral rich turbidites at MIS9 is, that time is needed to establish the barrier reef before subsequent erosion, deposition on the upper slope, remobilisation and export can occur.

The results from this thesis thus appear to corroborate the work of previous investigators who proposed a significant expansion and establishment of a barrier around MIS11 [*Cabioch et al*., 2008; *Montaggioni et al*., 2011]. However, if this were to have been the only significant evolution on the shallow shelf over the last 1.26Myr, one would expect the record prior to MIS11 to be relatively constant. Instead, there is an apparent shift in the nature of turbidite deposition in core MD06-3019 around MIS22.

Prior to MIS22 there are coarse and fine grained turbidites, compared to just fine grained between MIS11 and MIS22. When compared to turbidites deposited between MIS22-MIS11, those occurring before MIS22 have a higher average carbonate content (36 wt.% compared to 24 wt. %) there is a reduction in pelagic material (78 ± 6% compared to 96 ± 6%) (see *Figure 4.3*, *Table 4.4* and *Table 4.5*). There is a slight reduction in shallow water carbonate material in turbidite layers deposited between MIS22-11 (6 ± 6%) compared to before MIS22 (11 ± 6%); however, within error these values are the same (see *Table 4.5*). Finally coral occurrence is higher for layers deposited prior to MIS22 than between MIS22 and MIS11: 33% of layers compared to 20% (see *Table 4.7*). Coral abundance for individual turbidites at the base of the core can equal values for turbidites at the top of the core. However, the occurrence of coral bearing layers is lower prior to MIS22 (33%) compared to after MIS11 (77%) (see *Table 4.7*).

These results challenge the work of previous investigators who state that prior to the expansion of the barrier reef at MIS11 carbonate deposition in the area had occurred since its inception, around 1.2Ma, as principally non-reefal communities along an open shelf margin (i.e. a ramp/ non-rimmed platform), with only occasional patch reefs [*Cabioch et al.*, 2008; *Montaggioni et al.*, 2011]. However, the results presented here suggest that the history of the western New Caledonia margin may be more complicated than this simple single step model.

4.5.2 Requirement for further study

Close examination of turbidite sediments is a useful exercise. It provides an overall impression of the sediments and their variations and yields information on the presence/absence of particular sediment grains and their relative abundances on a broad scale. However, for 30 out of the 76 turbidite layers point counted (39% of turbidites), due to a paucity of material, point counting was unable to provide relative abundances with acceptable uncertainty levels and thus this data was excluded from further analysis (see §3.5). This is particularly a problem for turbidites deposited between MIS22- MIS11, which are all fine grained, where during this period over 60% of sandy layers had to be removed from the working data set. Similarly only data 18 out of the 76 layers point counted (24% of layers) could be used to analyse changes in shallow water carbonate material, in particular coral content. Uncertainties on these values are of the same order as the percentage abundances themselves. Overall, this scarcity of data means that point counting is not sufficient on its own to accurately characterise the temporal changes in turbidite content in sediment core MD06-3019. This is a particular problem in the period MIS22-MIS9; which is a critical time period for investigation, given the proposed expansion of the barrier reef around New Caledonia at ~MIS11.

Rather additional study is needed in order to further quantify and constrain the changes in shelf material being transported to the deeper basin, particularly during the period MIS22-11 (where only fine grained turbidites are present and data is sparse). This led to the development of X-ray fluorescence measurements for strontium, as a proxy for aragonite, and thus the amount of shallow water carbonate biota in turbidite samples. Advantages of this method are that it allows both fine and coarse grained turbidites to be studied equally and provides an estimation of the aragonite content for the whole sample, not just certain size fractions. The development of this proxy is the presented in Chapter 5 and its utilisation in further investigating the history of the New Caledonia Barrier Reef is the subject of Chapter 6.

4.6 Conclusions

Deep marine sediment core MD06-3019 is principally composed of foraminifera rich pelagic ooze. It also contains 79 mixed siliciclastic-carbonate turbidite layers, which source material from the shallow shelf near Grand Terre and transported it to the deep basin via the slope canyon systems. These layers vary in width, grain size and composition.

Turbidites deposited since MIS11 show an increase in average bulk carbonate content, a greater dominance of shallow water bioclasts in their assemblages and a higher occurrence of coral bearing turbidites. These results appear to corroborate the work of previous investigators such as *Montaggioni et al*. (2011) and *Cabioch et al*. (2008). However, there are significant differences in the record prior to MIS22 compared to the period MIS22-MIS11. The average carbonate content of turbidite layers is higher, there is a lower dominance of pelagic material in assemblages and coral occurrence in turbidites is higher. Coral abundance for turbidites at the base of the core can equal or exceed values for turbidites at the top of the core. These results challenge assumption that the only significant evolution on the western New Caledonia margin over the last 1.2Myr was the expansion of the barrier reef at 400ka and suggests that the history of the western New Caledonia margin may be more complicated than initially anticipated.

There is a scarcity of point counting data for core MD06-3019. This is due to turbidite layers with low point counts being excluded from analysis, as a result of large uncertainties in their relative assemblage percentages. This is a particular problem in the period MIS22-MIS9; which is a critical time period for investigation, given the proposed expansion of the New Caledonia Barrier Reef at ~MIS11. In order to further investigate the composition of the turbidite deposits an alternative method for assessing the presence of shallow water carbonate material in samples is presented in Chapter 5.

Chapter 5: Development of X-ray fluorescence measurements of strontium concentration as a proxy for aragonite content

5.1 Chapter Abstract

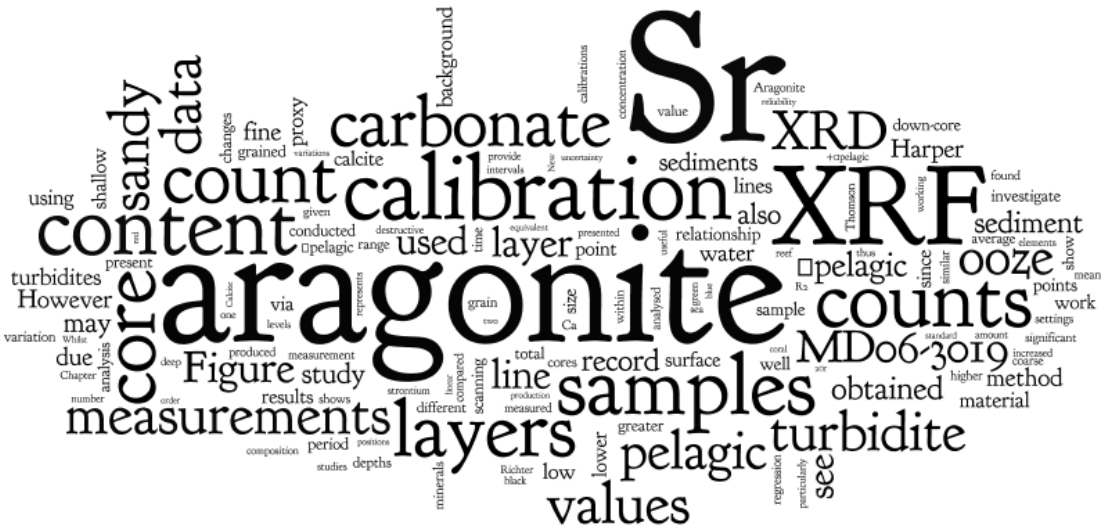

Measurements of the aragonite content of periplatform and deep sea sediments are used to reconstruct past changes in tropical shallow shelf carbonate production, which has a high aragonite abundance, and the shedding of this material to the deep sea. Direct quantification of the aragonite content of sediment by conventional X-ray diffraction (XRD) methods is not only destructive but also time consuming (due to extensive sample preparation) and comparatively expensive. By contrast X-ray fluorescence (XRF) core scanning measurements, for a variety of elements, is quick, inexpensive and non-destructive.

Strontium (Sr) is found as a trace element in a number of minerals, but its concentration in aragonite is significantly higher than that of other common Sr bearing minerals. Therefore, XRF measurements for strontium concentration ([Sr]) can be used as a proxy for the amount of aragonite present in sediment cores. This chapter provides one of the first calibration lines for the relationship between [Sr], measured via XRF, and aragonite percentage, measured via XRD. A calibration line with the equation:

Equation 5.1 Aragonite %=0.0011 x Sr count + 2.64

(R^2 =0.6105, p-value < 0.001, valid between 10,500-26,000 counts)

has been produced for turbidite samples from deep sea core MD06-3019. Whilst further work will be needed to refine the calibration line and test its universal applicability, it shows significant promise as a new proxy for quickly establishing the aragonite content of sediment samples. The XRF scan results are easily calibrated via relatively few XRD measurements and the method may be used in its own right to investigate aragonite content when material for destructive analysis is limited. Alternatively, it can be used as a way to rapidly assess aragonite changes down-core before deciding whether to pursue further study.

5.2 Introduction

5.2.1 The requirement for an aragonite content proxy

Recent literature on the western New Caledonia Barrier Reef places its expansion into a barrier reef, from patch reefs on an open carbonate platform, at MIS11 [*Cabioch et al.*, 2008; *Montaggioni et al.*, 2011]. It was therefore predicted that there would be a single noticeable increase in reef derived material in turbidites deposited in MD06-3019 since 400ka. There is an increase in the abundance of shallow water carbonate material and a higher occurrence of coral bearing turbidites post MIS11 (see Chapter 4 §4.3). However, the record of turbidite deposition is not consistent for the whole time period prior to 400ka; instead, there is another observed change at MIS22 (~900ka). The MIS22-11 period is characterised by only fine grained turbidites which are dominated by pelagic content and low shallow water carbonate and coral levels. However, prior to MIS22 both coarse and fine grained turbidites are present, the average carbonate content of turbidite layers is higher, there is a greater dominance of shallow water biota and coral occurrence in turbidites is higher. Turbidites at the base of the core, from some million years ago, can show a similar dominance of reef fragments within their assemblages to those deposited since MIS11 (see Chapter 4 § 4.3). These results suggest that there may have been multiple phases of reef evolution on the western New Caledonian margin over the last 1.2Myrs.

The reliability of point counting results are often severely compromised for layers with low grain counts in the analysed size fraction. This is particularly a problem for fine grained turbidites where large fragments >500µm are rare [*Van Der Plas and Tobi*, 1965; *Pye*, 2007]. The absence of coarse grained turbidites between MIS22-9 thus significantly reduces the reliability of results over this period. However, this is a critical period for investigation, given the proposed expansion of the New Caledonia Barrier Reef occurred during this time (see Chapter 4 §5.2). In order to further investigate the composition of the turbidite deposits and fill in the record between

MIS22-9 (900-300ka) an alternative method for assessing the presence of reef material, particularly in fine grained samples, is needed.

5.2.2 Use of [Sr] as an aragonite proxy

Carbonate production on tropical reefs, such as the New Caledonia Barrier Reef, is characterised by high aragonite abundance due to the presence of corals, molluscs and calcareous green algae (Halimeda). In such settings the aragonite content of sediments in periplatform and deep sea settings have frequently been used to investigate the history of shallow shelf carbonate production and the shedding of this material to the surrounding slopes and deep sea [*Droxler and Schlager*, 1985; *Reijmer et al.*, 1988; *Paul et al.*, 2012; *Droxler and Jorry*, 2013; *Harper*, 2015]. Given that coral is one of the three principal sources of aragonite in tropical shallow water biota (calcareous green algae, coral, molluscs), the aragonite content of samples should give a clue as to reef development at the time (see *Table 5.1*). Thus measurements of the aragonite content of the turbidite deposits of MD06-3019 can give us an indication as to their shallow water carbonate biota content, in the absence of point counting data.

The aragonite content of sediment samples is usually ascertained via XRD measurements. However, these analyses are both comparatively expensive, destructive and time consuming; since samples must be ground to a fine powder, homogenised and loaded into samples holders. Generally, only a limited number of samples from a sediment core are analysed by this technique and therefore the aragonite record is non-continuous. An alternative technique for establishing the aragonite content of samples has been developed; this method instead uses XRF core-scanning measurements of strontium concentration [*Thomson et al.*, 2004; *Harper et al.*, 2015]. XRF measurements, when conducted via a core scanner, have the advantages of providing high resolution (mm-cm scale) elemental concentration data on sediments. They are also quick (due to the limited sample preparation

required), relatively inexpensive and non-destructive [*Rothwell et al*., 2006; *Richter et al.*, 2006].

Strontium (Sr) is a metallic lithophile and found as a trace element in a number of minerals, such as: plagioclase, orthoclase and gypsum at low levels (300-1000ppm), calcite and dolomite at intermediary levels (~1000ppm) and aragonite at much higher levels (2,000-8,000ppm) [*Mielke*, 1979]. The size of the Sr^{2+} cation (118 pm) is similar to that of Ca^{2+} (100 pm) and thus it is easily substituted into the carbonate lattice. Sr^{2+} is preferentially substituted for Ca^{2+} in orthorhombic aragonite, whereas the smaller Mg^{2+} (72pm) is favoured as a replacement in trigonal calcite [*Shannon*, 1976; *Boardman and Neumann*, 1984]. The preferential incorporation of Sr within aragonite makes the strontium concentration ([Sr]) of sediments a useful proxy for the amount of neritic aragonite in sediments, especially where aragonite is the dominant Sr bearing mineral in the sample [*Boardman and Neumann*, 1984; *Dunbar and Dickens*, 2003; *Rothwell et al.*, 2006] (see *Table 5.1*). Calibrated XRF measurements for [Sr], as a proxy for aragonite in sediments, have the potential to be useful for those researching platform margin settings. Such measurements can be applied to work aiming to reconstruct the degree and timing of carbonate production and shedding from the shallow shelf, but also the effects of dissolution. The method may be used in its own right to investigate aragonite content when material for destructive analysis is limited but also as a way to rapidly assess aragonite changes down-core before deciding whether to pursue further study or to inform sample selection for further analysis [*Richter et al.*, 2006].

Carbonate Biota	Composition	[Sr] mg/kg
Coral	Aragonite	>7,500
Molluscs	Aragonite	<3,500
Halimeda	Aragonite	>8,500
Bryozoan	Low Magnesian Calcite (rare aragonite)	<2,000
Calcareous Red Algae	High Magnesian Calcite	<2,000
Echinoderm	High Magnesian Calcite	<2,000
Pteropod	Aragonite	<2,000
Foraminifera	Low Magnesian Calcite	<1,500
Coccolithophores	Low Magnesian Calcite	<1,500

Table 5.1 Showing the carbonate composition of different carbonate biota that are found in core MD06-3019. [Sr] values from *Boardmann and Neumann* (1984) and *Pilkey and Goodell* (1963).

5.2.3 Development of a methodology for using XRF [Sr] as an aragonite proxy

Whilst XRF measurements for Sr have been used previously as an aragonite proxy [*Rothwell et al.*, 2006; *Richter et al.*, 2006; *Thomson et al.*, 2006], there are few studies which have attempted to calibrate this data to provide a quantitative estimate of aragonite % for samples [*Harper et al.*, 2015; *Thomson et al.*, 2004].

This study aims to develop the use of [Sr], as measured via XRF core scanning, as a quantitative proxy for the amount of aragonite present in sediment deposits. XRF core scanning measurements were obtained along the length of sediment core MD06-3019, as well as complimentary XRD composition measurements from 54 individual depths. The down-core XRF [Sr] record for MD06-3019 is presented and the data calibrated via XRD measurements to give an equivalent aragonite % for samples. The calibration obtained is then compared to a previous calibration of XRF [Sr] measurements [*Harper et al.*, 2015] and an assessment made of the reliability of calibration proposed here. The calibration is then applied to core MD06-3019 to

provide an inferred aragonite % record for turbidites. Finally proposals for future work are suggested.

5.3 Experimental Methods

5.3.1 XRF measurements

XRF analysis for 13 elements was conducted on the archive half of core MD06-3019 (and MD06-3018), using an Avaatech XRF core scanner at IFREMER, Brest, France. Core sections were prepared by using a glass slide to create a fresh, clean, flat level surface. A thin (4μm) ultralene film was laid down the middle where analysis would take place, this reduces surface roughness and prevents contamination of the prism unit with sediment. The core was analysed at 1cm intervals throughout with a 10 second count time at 10kV (scanning for aluminium, silicon, phosphorus, sulphur, chlorine, potassium, calcium, iron and rhodium) and 30kV (scanning for iron, nickel, bromine and strontium). Post-processing was conducted by Angelique Roubi at IFREMER, Brest, France.

Areas with either slumped or missing material or an especially raised surface were excluded from measurement. For a lowered surface the head of the machine does not contact the core surface directly and records anomalously low results. For a raised surface the head sinks into the sediment, also producing unreliable results. In total this led to the non-measurement of 233cm (7% of the core length) of the MD06-3019 core and the removal of 127cm (4% of the core length) of anomalous measured points (see digital only Supplementary Data). The problem of a lowered core surface was a particular issue in this study, since the height of sediments was most frequently reduced over sandy layers, which are the periods of greatest interest. The increased grain size, particularly in coarse grained turbidites (φ>-2), causes changes in the cohesion of the sediments and frequently leads to uneven surfaces when the core is cut into working and archive halves. Data points from outer 2cm at the top and bottom of each core section are generally not presented due to edge distortion effects.

Anomalous data from a few centimetres either side of a slumped area or from areas of uneven surfaces are also removed from the working data set. Results are quoted to the nearest 100 counts and the reproducibility uncertainty of the method is $2\sigma_r$= 200 counts for strontium counts based on 149 repeat measurements (for reference, count values for the whole core vary between 3,200-26,000 counts with a mean of 10,100 counts).

More information on the principles of the XRF methodology may be found in Appendix 1.

5.3.2 XRD measurements

XRD measurements were conducted on 8 pelagic ooze and 46 sandy layer samples from core MD06-3019 using a Bruker D8 Advance with Sol-X Energy Dispersive detector at the School of GeoSciences, University of Edinburgh. Sandy layer samples for XRD analysis were selected to cover the majority of the range of Sr count values obtained for sandy layers (5000-26,000). Background samples were selected at 8 intervals covering the total length of the core from positions with varying total carbonate content. Samples were oven dried and ground to a fine powder using a pestle and mortar, before being loaded into sample holders and a flat surface prepared. Samples were then analysed for their carbonate content using a standard frequency scan. Post processing of raw peak data to obtain mineral percentages was conducted by Nic Odling. The analytical uncertainty of the method, calculated with respect to known standards is $2\sigma_a$= 1.5%. Repeat analyses conducted on five depths down-core (n=3) yield a reproducibility uncertainty of $2\sigma_r$= 2.3 %.

More detailed information on the XRD methodology may be found in Appendix 1.

5.3.3 Choice of XRF variable

Ideally, XRF data should always be presented as ratios of elements, such as Sr/Ca (to investigate aragonite: calcite ratios) and Sr/Al or Sr/K (to investigate changes in aragonite: terrigenous ratios). This reduces the effect of element interaction problems, removes the dilution effect and circumnavigates the issue of the constant sum constraint [*Rothwell et al.,* 2006; *Thomson et al.,* 2006; *Weltje and Tjallingii*, 2008]. Reporting the data as a Sr/Ca ratio would also reduce the background pelagic carbonate noise level and make turbidite peaks in the record easier to "see", since their Sr content is principally controlled by their aragonite content and not the calcite content. Previous authors have used Sr/Ca XRF ratios to investigate changing aragonite: calcite levels in sediments [*Rothwell et al*., 2006; *Richter et al.*, 2006; *Thomson et al.,* 2006] and a calibration between aragonite % and XRF Sr/Ca values has been previously published [*Thomson et al.,* 2004].

In order to assess whether Ca counts accurately reflect the carbonate content of samples, bulk carbonate content values were obtained via carbonate coulometry. Bulk weight% $CaCO_3$ was measured using a UIC Inc CM5012 CO_2 coulometer with a CM5130 acidification module at the School of Geosciences, University of Edinburgh. Analyses were made on 201 background carbonate pelagic ooze samples (including 19 made by a previous Environmental Geoscience student during their 4th year honours project) and 150 individual sandy layer samples from MD06-3019. Samples were oven dried and then ground to a powder using a pestle and mortar. Around 10-15μg of material was used for the analysis of background carbonate ooze samples and 15-20μg for measurements on sandy layer samples, where carbonate content is generally lower. Samples were reacted with 8ml of 2N perchloric acid, heated to 60^{o}C and analysed for 10 minutes. Measurements of a carbonate reference material during the runs indicate an analytical uncertainty of less than 0.3 wt.% ($2\sigma_a$). Repeat analyses were conducted at seven depths down-core (n=3), reproducibility was found to be $2\sigma_r$= 0.4 wt.%.

Further information on the coulometry methodology may be found in Appendix 1.

For core MD06-3019, whilst the Ca counts for the pelagic ooze correlate well with the total carbonate content of samples measured via coulometry (R^2=0.70), this is not the case for turbidite layers where the Ca count is much less well correlated to the total carbonate content (R^2=0.34) (see *Figure 5.1*). The lack of relationship between the total wt. % carbonate and Ca counts for turbidite layers may be due to the increased inhomogeneity of samples as a result of the larger grain size of sandy layers [*Richter et al.,* 2006]. Additionally, turbidite layers, due to being less well sorted and composed of a larger grain size, show both an increased and more varied porosity compared to pelagic ooze. This leads to changing water content and surface roughness between samples. Pore water dilutes the solid phase, but also absorbs the X-ray radiation of the sample resulting in lower intensities of the target elements, as well as lower measurement precision and accuracy [*Hennekam and de Lange*, 2012]. Changes in surface roughness can lead to differences in the pore water film, which *Hennekam and de Lange* (2012) note can lead to large deviations in results from XRF core scanning compared to conventional dry XRF measurements. They attribute these differences to variations in thickness of the pore-water film, which forms directly below a protective film covering the core surface. This causes significant apparent variability in all elements from Al to Fe, which includes Ca and K but not Sr. These changes in pore water between samples are often unpredictable and thus not easily corrected for.

Therefore, it is concluded that the Sr/Ca ratio cannot be used for the calibration of turbidite layers, since it does not accurately represent the aragonite to total carbonate ratio (see *Figure 5.1*) and cannot be easily corrected. Thus a calibration using only Sr count values has been developed to provide the equivalent inferred aragonite % of samples.

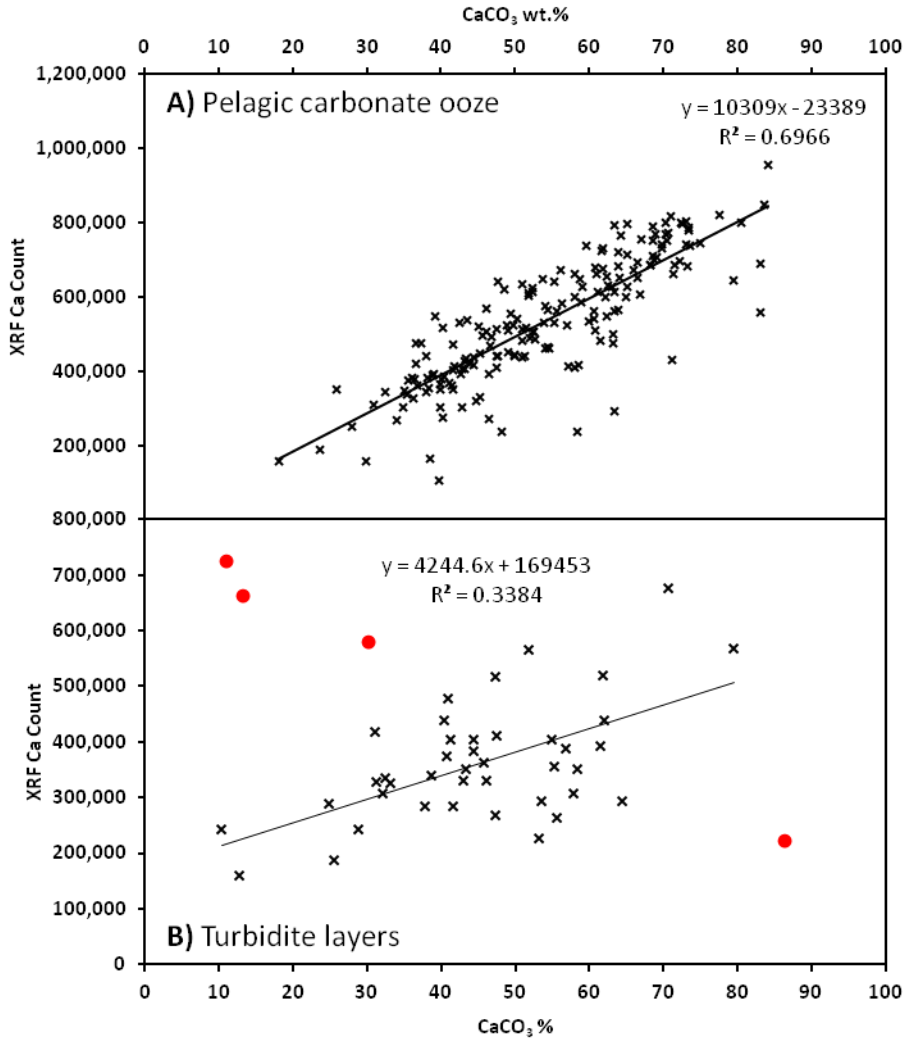

Figure 5.1 A) Cross plot of XRF Ca counts against $CaCO_3$ wt.% for MD06-3019 pelagic ooze samples. **B)** Cross plot of XRF Ca counts against $CaCO_3$ wt.% for MD06-3019 turbidite layer samples. Calculated linear regression lines are plotted for both cross-plots. 4 outlier points (highlighted in red) have been removed (86.5, 222100) due to carbonate content measurement error and (13.3, 661200), (30.2, 577500) and (11.1, 724600) due XRF measurement mis-match errors.

5.4 Results

5.4.1 Down-core XRF [Sr] record

XRF Sr values for sediment core MD06-3019 as a whole vary between ~ 3,200-26,000 counts, with a mean and standard deviation of 10,100 ± 2,600 counts (see *Figure 5.2*). The Sr mean and standard deviation for the pelagic carbonate ooze ($\mu_{pelagic}$) is 9,200 ± 1,300.

The distinctive feature of the record are a number of prominent peaks (~20) with values >13,200 counts ($\mu_{pelagic}+3\sigma_{pelagic}$). These excursions are strongly associated with sandy layer depths, out of 265 data points with XRF Sr values greater than 13,2000 counts 61% are associated with sandy layer depths (See *Figure 5.3*). Additionally, the width of the peaks generally corresponds accurately to the widths of the sandy layers present in the core, to within ±2cm. Differences between the recorded sandy layer positions and widths and those delineated by the XRF data generally occur due to the XRF scanning being conducted on the archive half of the core and the positions of sandy layers being determined from the working half.

There is considerable variation in the Sr count values of the background pelagic carbonate ooze, with the standard deviation representing 14% of the mean. It is thought that this background pelagic ooze Sr variation is largely attributable to glacial-interglacial controlled dissolution changes in the deep sea. (For a fuller discussion on this topic see Appendix 3.) It is also noted that many of the lowest Sr count values, especially between 800-500ka, correspond with sandy layer depths (see *Figure 5.2*).

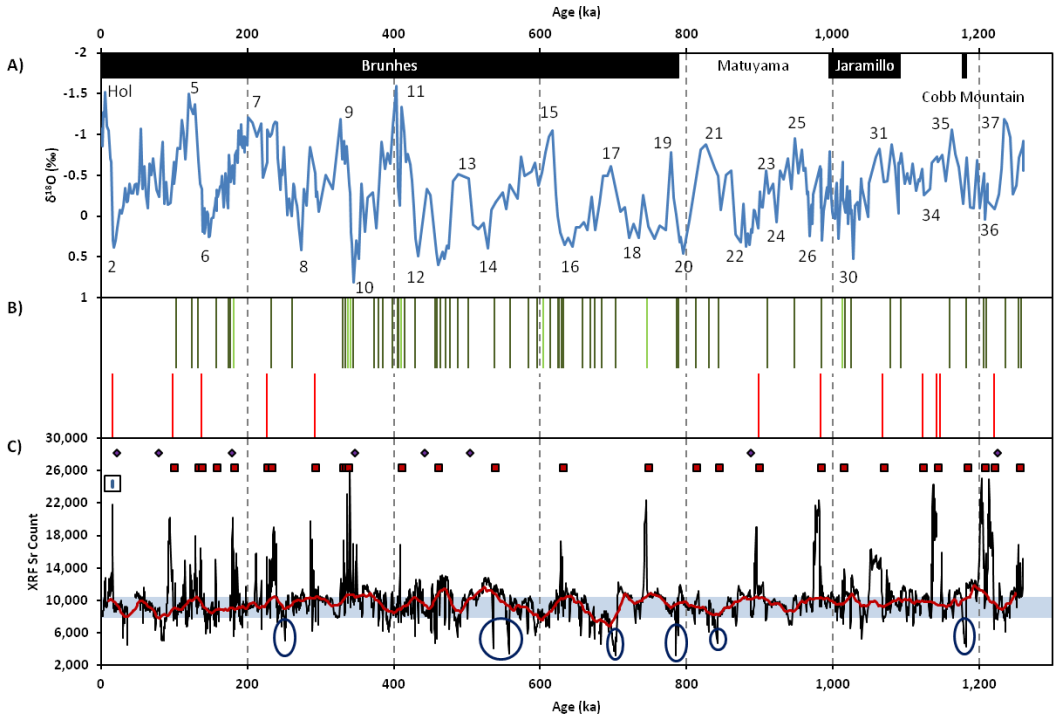

Figure 5.2 A) MD06-3019 $\delta^{18}O$ record obtained from G. *ruber* foraminifera. **B)** Positions of sandy layers. Red: coarse, dark green: dark fine layers, pale green: light fine layers. **C)** Upper section: XRD sample positions- purple diamonds represent background ooze samples and red squares, sandy layer samples. Lower section: XRF Sr count record for the core (black) and XRF Sr pelagic ooze 20kyr running mean (red); the blue shaded area represents $\mu_{pelagic} \pm \sigma_{pelagic}$ and the reproducibility uncertainty for Sr values is shown in the blue bar on the top left. Blue circles highlight Sr lows in the record associated with sandy layers.

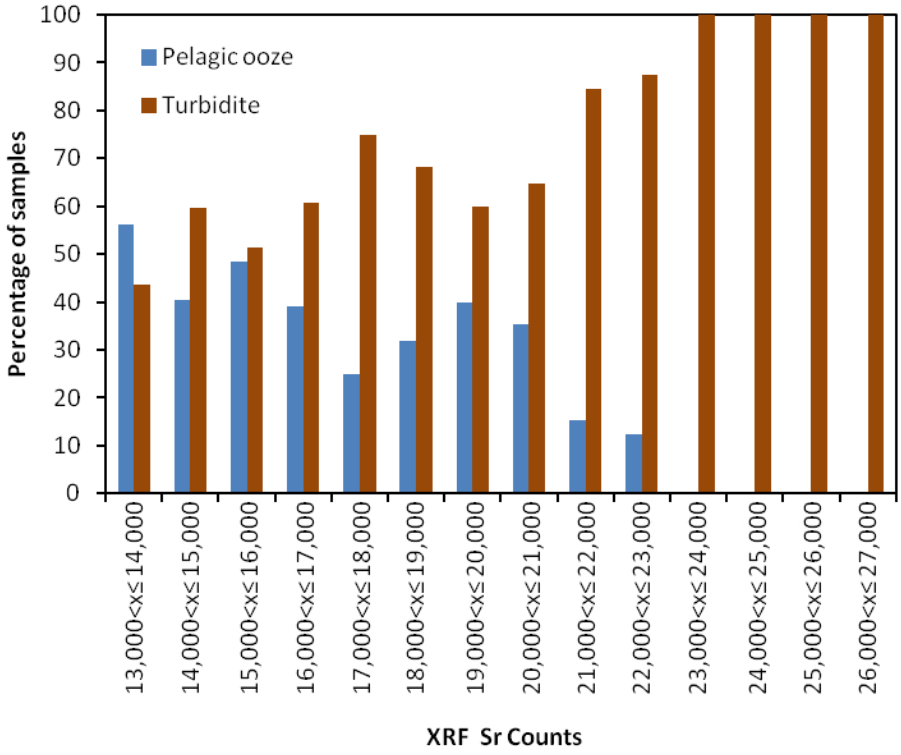

Figure 5.3 Percentage of data points in different XRF Sr ranges that are associated with pelagic ooze or turbidite depths. Of a total of 276 data points analysed 110 (40%) were associated pelagic ooze samples and 166 (60%) with turbidite layers.

5.4.2 Comparison of XRF and XRD measurement pairs

XRF-XRD measurement pairs were obtained for 28 sandy layers (see *Figure 5.4*). Eight layers were analysed at multiple depths within the same layer ($2<n<4$) and since variation in these measurements is small (μ_{layer} ±4%), average XRD-XRF values are used for these layers. The background carbonate XRF-XRD value was obtained by an average of the measurements from 8 pelagic ooze samples. One data sandy layer point has been removed from the working data set (see *Figure 5.4*), due to an anomalously low aragonite value for its recorded Sr count and known shallow water carbonate content. This is suspected to be an XRD measurement error.

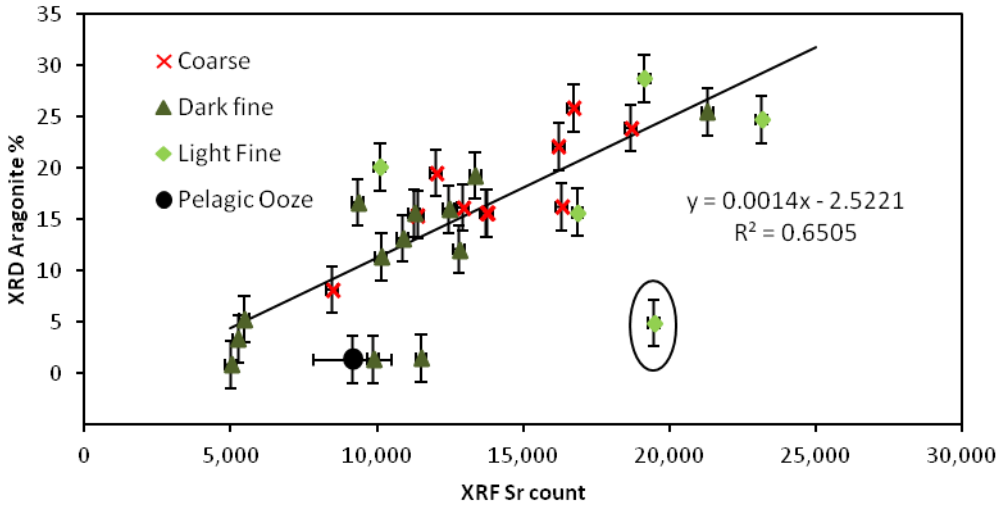

Figure 5.4 Averaged turbidite layer aragonite % values, from XRD measurements, plotted against averaged XRF Sr count measurements for 28 independent turbidite layers. Error bars show $2\sigma_r$ for XRD measurements. Horizontal XRF $2\sigma_r$ error bars are of the order of the size of the plotted point. The position of the average pelagic ooze sample is also plotted. The circled point shows the anomalous result removed from the working data set.

The data for the sandy layer samples show a clear positive correlation between XRD aragonite % and Sr XRF count and there does not appear to be separate trend lines for the different layer types (see *Figure 5.4*).

5.5 Discussion

5.5.1 Calibration of the XRF data using XRD measurements

As seen in the previous section there is a clear positive correlation between XRF [Sr] counts and XRD measurements of aragonite % (see *Figure 5.4*). This relationship is particularly well constrained for XRF Sr counts greater than ~10,500 counts. However, there is an increased scatter of points at lower Sr count and aragonite values. As noted previously there are large variations in the Sr counts recorded for the background pelagic ooze. As a result turbidite layers (particularly ones that are only a few cms in width) with low aragonite content (<10%), and thus low corresponding XRF Sr count values, can be difficult to distinguish from the background pelagic ooze. Additionally, for turbidite layers with a low aragonite content, the Sr count value increasingly becomes affected by the contribution of Sr from other minerals, such as calcite and feldspars. Therefore there is an increased likelihood of inaccurate XRF values being used in the calibration.

The precise form of the relationship between Sr count and aragonite % for core sediments is not well constrained from either theory or existing empirical evidence. The Sr count for the average pelagic ooze composition does not lie on the trend line defined by turbidite layer samples (see *Figure 5.4*). However, it is not necessarily expected that the pelagic carbonate ooze would represent an end member point for the observed turbidite relationship, given the contrasting sources and depositional mechanisms for the two. Additionally, even for samples completely devoid of aragonite Sr will still be present in other minerals. As a result it is not predicted that the calibration line between XRD aragonite content and XRF Sr count would continue to the origin, or necessarily even be linear at low aragonite values. However, it is to be expected that samples from turbidite layers, where aragonite is no longer the primary Sr bearing mineral, would show increased scatter at low aragonite values, due to variations in pelagic and terrigenous content.

In the face of this limitation, the present study adopts the approach of developing a calibration only over the range for which a linear regression model describes the presented data well. An objective approach to determining the cut-off point, above which a quasi linear relationship holds, is given by Sr count values that exceed the pelagic carbonate ooze mean by one or more standard deviations ($>\mu_{pelagic} + \sigma_{pelagic}$). All data points with a Sr count lower than $\mu_{pelagic} + \sigma_{pelagic}$ (10,500 counts) were deemed as either indistinguishable from the carbonate ooze or unreliable and so were not used in the calibration. The more stringent criteria of only using samples with a Sr count value greater than $\mu_{pelagic} + 2\sigma_{pelagic}$ was not employed because, due to the wide spread of carbonate ooze values, this would compromise the reliability of the calibration by the significant reduction of the amount of data points available for use (27 to 15). One point (11513, 1.5) was above the $\mu_{pelagic} + \sigma_{pelagic}$ cut off but was not used in the calculation of the regression line, since it is believed to represent the scatter seen at low aragonite values (see *Figure 5.5*).

The calibration line for sandy layers in core MD06-3019 with Sr values greater than $\mu_{pelagic} + \sigma_{pelagic}$ was calculated as:

Equation 5.1 Aragonite %=0.0011 x Sr count +2.64

$R^2 = 0.6105$, p-value < 0.001 (see *Figure 5.5*)

The 5-95% confidence interval on the slope coefficient is [0.0006-0.0015]. (By comparison the regression line for the complete data set, with no lower cut off limit is: Aragonite % = 0.0014*Sr count - 2.5221 ($R^2 = 0.6505$, p-value < 0.001). This lies within the 5-95% confidence interval for the calibration presented here.) This calibration is valid between $\mu_{pelagic} + \sigma_{pelagic}$ (10,500 counts) and the highest XRF value for a turbidite layer (26,000 counts), any application beyond this upper bound represents an extrapolation outside the constraining data.

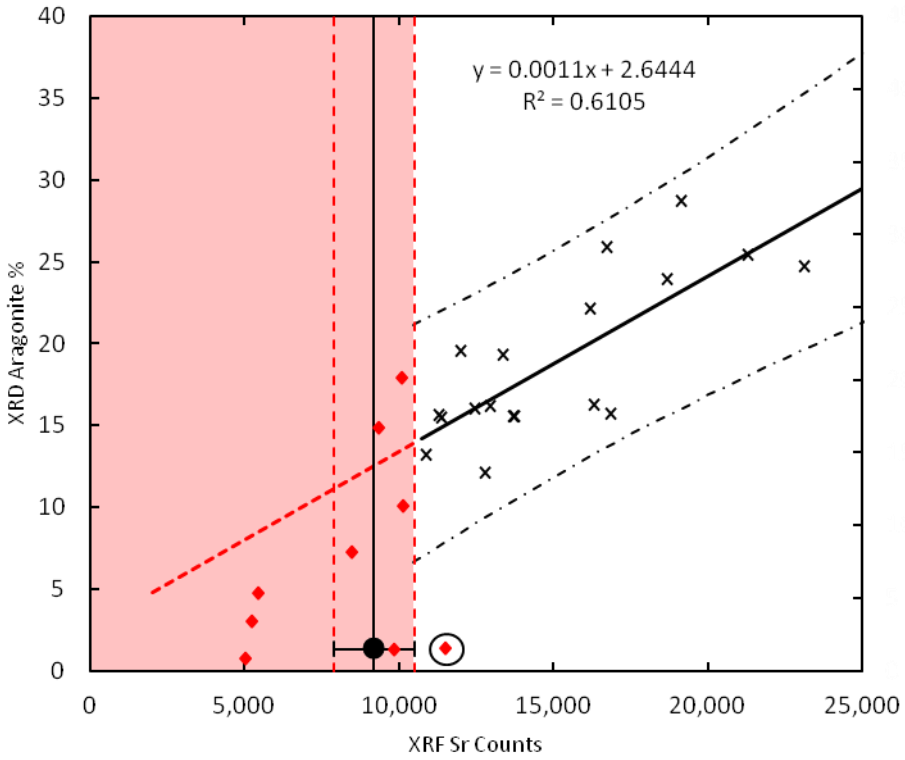

Figure 5.5 Calibration line (black) between XRD aragonite % and the XRF Sr count for turbidite layer samples above the pelagic ooze noise level, as well as the ±2σ confidence intervals. The black circle represents the average background pelagic carbonate ooze; lines representing the pelagic mean (black) ±σ (red) are shown. Red points are sandy layer samples not included in the calibration (circled point has an Sr count >10,500 but was not used in the calibration) and the red dotted line extends relationship to lower Sr count values where it is not certain that the relationship is reliable (shaded area).

5.5.2 Assessing the reliability of the proposed calibration

The data for the sandy layer samples show a clear positive correlation between XRD aragonite % and Sr XRF count and there does not appear to be separate trend lines for the different layer types, suggesting the calibration is applicable to all sandy layer types in core MD06-3019. A calibration line has been produced for MD06-3019 turbidite samples with a Sr count greater than $\mu_{pelagic} + \sigma_{pelagic}$, this calibration may also be applicable at lower Sr counts but this is not certain with the data presented here. This means that for those turbidite layers with an Sr count < $\mu_{pelagic} + \sigma_{pelagic}$ only a maximum equivalent aragonite % can be given. However, changes in the proportion of sandy layers registering with Sr counts greater $\mu_{pelagic} + \sigma_{pelagic}$ over a given time period can be a useful tool in investigating aragonite content.

In core MD06-3019 the pelagic ooze record shows considerable variation in XRF Sr count values (from 4,100-13,000 counts), which can make it difficult to identify turbidite layers with a low aragonite content in the Sr record. This is particularly the case for layers which are relatively thin (1-3cm). This highlights the problem of the sensitivity of the method to 'seeing' sandy layers in cores. This problem may arise when the pelagic ooze has an aragonite content similar to that of the turbidites. For instance, in shallow-water cores which do not suffer from significant aragonite dissolution. Or alternatively, when sufficient Sr is present in other minerals, such as calcite and feldspars, that low-aragonite turbidites are difficult to distinguish from the background sediment counts.

5.5.3 Comparisons to other calibrations

A previous study by *Harper et al.* (2015) attempted to calibrate XRF Sr counts with XRD data to provide an estimated aragonite % for samples.

Harper et al. (2015) produced a similar Sr count-aragonite % calibration based on sediments from IODP Expedition 325 Hole 58A. Hole 58A is located on the upper

forereef slope of the north- central portion of the Great Barrier Reef, by Noggin Passage (17°6'S, 146°35'E, 170m water depth). The sediments mainly varied from silt to fine sand, though some intervals reached medium or coarse sand. The fine fraction (< 63 μm) of the core varies between 0% to 94% of the total sediment. The bulk carbonate content (aragonite, low-magnesian calcite and high-magnesian calcite) varies between 28-76%; with the quartz, feldspars and clay minerals representing the main siliciclastic minerals. Bulk aragonite varied from 9-41%, high-magnesian calcite from 0-30% and low-magnesian calcite from 5-24%. The coarse fraction (>63μm) is almost completely composed of carbonate grains, which are dominated by pelagic skeletal components with varying levels of neritic material. Sr counts (measurements conducted on an Avaatech core scanner) varied from 2,000-11,000 and aragonite content from 10-45%. A calibration line was obtained, with an equation of:

Equation 5.2 Sr count = 128.75 x aragonite % +3594.2

$R^2 = 0.82$, $p < 0.001$

The results obtained both by *Harper et al.* (2015) and in this study show a positive correlation between XRF Sr counts and XRD aragonite % measurements. However, there are significant differences in the range of Sr counts and aragonite percentages obtained and the slopes of the calibration lines produced by the different studies (*Figure 5.6*). It should be noted that *Harper et al.* (2015) used XRD aragonite % as the independent variable, following the work of *Dunbar and Dickens* (2003) and *Boardman et al.* (1986) who attempted similar calibrations comparing the Sr content of sediments (in μg/g) with aragonite %. By contrast this thesis uses XRF Sr counts as the independent variable, since the purpose of the calibration is to be able to infer sample aragonite % from Sr counts. In order to make an accurate comparison between two calibration lines it is necessary that the same axis arrangement is used for both and that the regression lines are calculated from the original data in this format. A simple inversion of one of the linear calibration equations is not sufficient, since this will not produce the same equation as a regression line calculated from the

original data with reversed axes. Therefore, the regression line and ±2σ confidence intervals for *Harper et al.* (2015) have been recalculated from the original data, but with XRF Sr counts as the independent variable and XRD aragonite % as the dependent variable (see *Figure 5.6*).

Whilst both studies show a lower limit of ~2,000 Sr counts, this study had a much wider range of counts, up to ~26,000 compared to 11,000 for *Harper et al*. (2015). The aragonite % values obtained also vary between the studies, 0-45% for *Harper et al*. (2015) and 0-30% in this work. This variation in ranges ultimately yields different gradients for the calibration lines obtained. The *Harper et al.* (2015) data set lie over a range of Sr count values which this work has been unable to calibrate over (since these Sr values are too close to the pelagic ooze Sr count range). The gradient of the line obtained by *Harper et al*. (2015) does not appear to fall within error of that obtained by this study. However, the calibration has a higher R^2 value and significantly less scatter compared to results obtained in this thesis (*Figure 5.6*). Both studies used the same model of Avaatech XRF core scanner, therefore variations in calibration lines are probably due to the differing geographical settings of the cores, which leads to variation in grain size and composition of sediments at the different sites. The XRF integrals (count values) produced for elements do not have a constant relationship with element concentration over changing sediment types due to variations in mineralogy, grain size and water content [*Thomson et al.*, 2006]. Caution is therefore advised in generalising any single XRF [Sr]- XRD aragonite % calibration models to other cores. However, these studies do suggest that robust core-specific calibrations can be obtained. The development of other such calibrations may also allow for future progress towards regional scale calibrations.

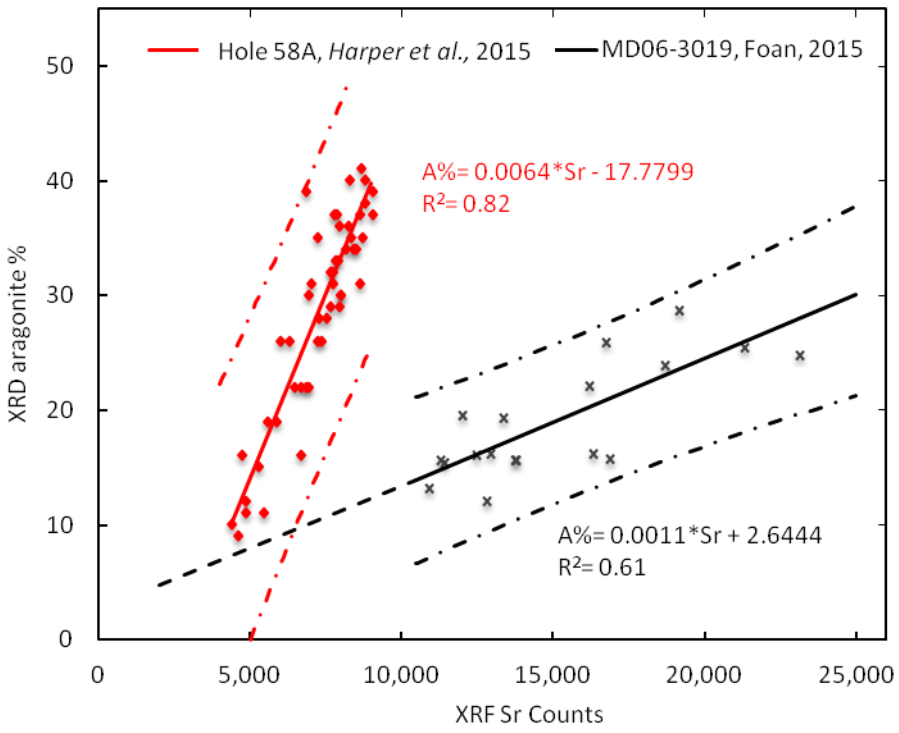

Figure 5.6 Comparison between the data and XRF-XRD calibration lines obtained in this study (New Caledonia) and by *Harper et al.* (2015) (Great Barrier Reef). The black dashed line represents Sr counts for which the calibration obtained in this work may not hold. The dotted lines represent the ±2σ confidence intervals for each calibration line. Equations are given for each line, A: aragonite %, Sr: Sr count value.

5.5.4 Application of the calibration

The calibration line produced in §5.1 can be applied to the down-core Sr record for MD06-3019 in order to provide inferred aragonite %s for sandy layers (see *Figure 5.7*). The prominent peaks that dominate the record between 1,200-900ka and 400-present along with two during the middle period are able to be converted to equivalent aragonite values. However, overall during this middle period there is a reduction in the number of sandy layers with Sr count values greater than $\mu_{pelagic} + \sigma_{pelagic}$ and thus the method can only provide a maximum possible aragonite % for layers with a Sr count lower than $\mu_{pelagic} + \sigma_{pelagic}$. Due to the poor quality scanning samples compared to traditional fused beads or powder samples, XRF core scanning results can only be considered as semi-quantitative. However, the relative down-core elemental concentrations are faithfully recorded [*Richter et al.*, 2006]. Thus while the decrease in aragonite during the 900-400ka period cannot be accurately quantified, the reduction in the proportion of layers with Sr counts above the threshold for calibration can. There is a clear change in the Sr record for MD06-3019 between 900-400ka (see *Figure 5.7*) with a reduction in the number of high aragonite peaks during this period.

This calibration is used in Chapter 6 to investigate the variation in the amount of shallow water derived aragonite present in the sandy turbidite layers in core MD06-3019, including those layers where the grain size is too fine for point counting.

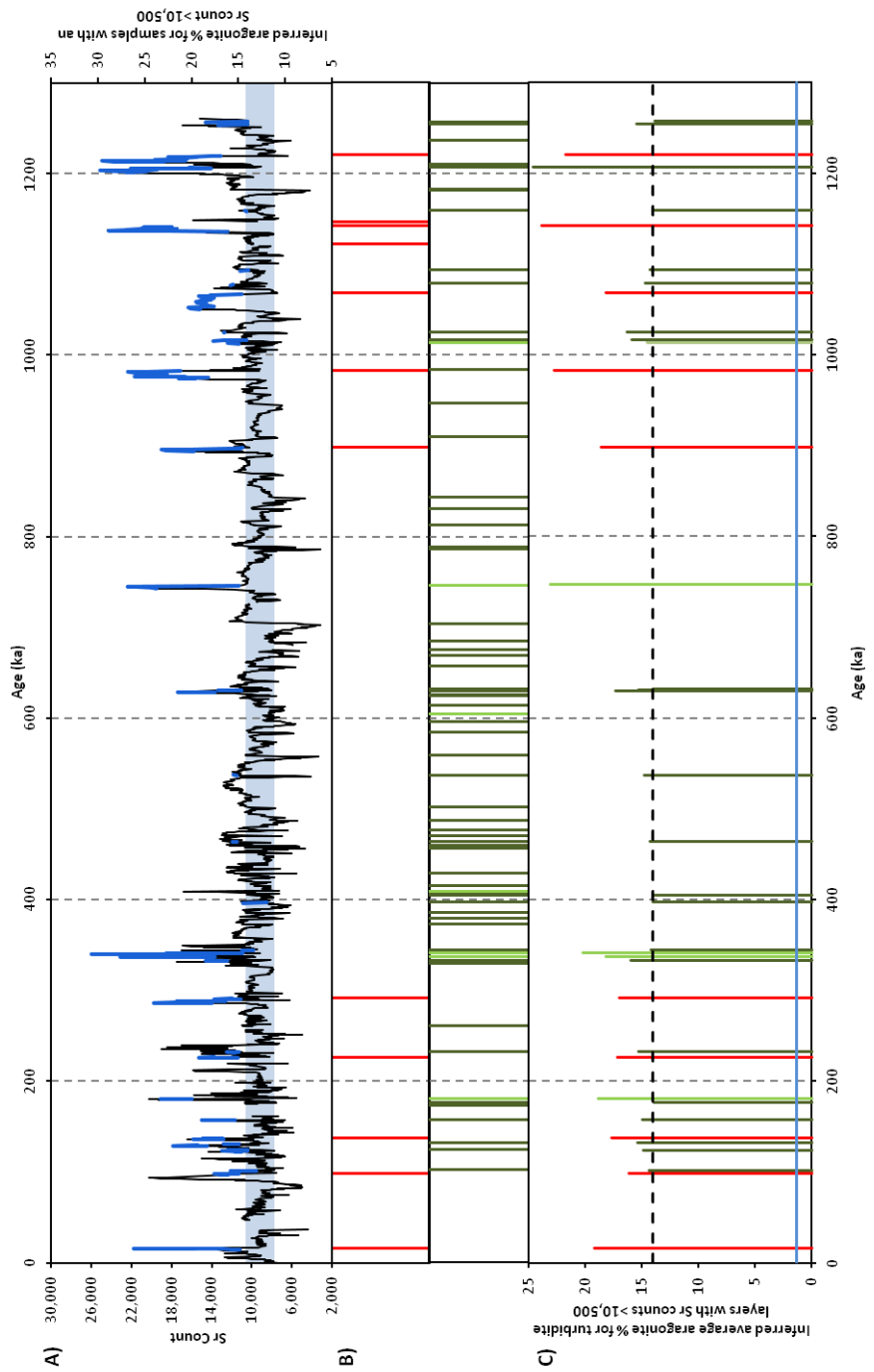

Figure 5.7 A) XRF Sr counts as a proxy for aragonite. LHS axis: Sr counts. RHS axis: for blue coloured portions of the record- inferred aragonite content of sandy layers with a count value >10,500 ($\mu_{pelagic} + \sigma_{pelagic}$) calibrated using XRD. The blue shaded area represents $\mu_{pelagic} \pm \sigma_{pelagic}$, $\mu_{pelagic}$ equivalent to ~1.3% aragonite. **B)** Positions of sandy layers. Red: coarse, dark green: dark fine layers, pale green: light fine layers. C) Inferred average aragonite % for turbidite layers with Sr counts $>\mu_{pelagic} + \sigma_{pelagic}$. The dashed black line shows the maximum possible aragonite content for turbidite layers with Sr counts $<\mu_{pelagic} + \sigma_{pelagic}$ (~13.9%). The blue line shows the average pelagic ooze aragonite % content (~1.3%).

5.5.5 Suggested improvements and developments to the method and future work

This study provides one calibration for XRF Sr counts and sediment aragonite %. Further work will be required to fully understand the effects of differing mineral content, heterogeneity and grain size on the calibration line. However, the overall positive trend of the calibration is believed to hold for all settings, and thus XRF scans can be used for initial, quick qualitative core investigations. Individual calibrations would be needed for different cores though to allow for accurate conversion from Sr counts to aragonite content. A method, by which to make this study more readily comparable with others, would be to produce a calibration line for MD06-3019 which shows the relationship between XRF Sr count and absolute Sr concentrations. However, there are significant limitations to the quality of such calibrations, see §3.3.

For those who would aim to produce a similar calibration for turbidite deposits, which have been deposited in background carbonate ooze, the following suggestions are made. Whilst not always practicable it would be advisable to scan the working half of the core before sampling for destructive analysis is begun. This means that any uncertainties caused by the inhomogeneity of sandy layer widths, positions and content between the two core halves is reduced. Whilst the selection of samples to be measured via XRD should cover the full range of Sr counts for the turbidites, ideally samples for calibration should come from the middle of wide sandy layers where it reasonably certain that the Sr count is representative of that sample. By nature, cores containing both fine grained carbonate ooze and coarser grained turbidites show significant variation in their sediment properties down-core. Since the parameters used to extract the ‘count’ data vary depending on the sedimentology of the core, it may be useful to run two extractions: one for the core as a whole and another just for turbidite layers which is more suited to their composition. It may also be useful, though more time consuming, to conduct repeat scans on sandy layers so as to help reduce the errors caused by inhomogeneity inherent within coarser grained samples.

Whilst being able to reconstruct general shallow shelf carbonate productivity using XRF Sr counts as a proxy for the aragonite content of turbidites is useful, a proxy specifically for coral reef productivity would be the ideal. It would therefore be useful to know what percentage of shallow shelf aragonite is comprised from coral and how much from calcareous green algae. Future work could include a survey of sediment samples taken from the lagoon, various areas of the reef complex and the upper slope, to obtain their average carbonate biota composition. These results could then be used to provide and estimate as to how much of the aragonite present in turbidite samples came from coral reefs. Though whether these modern day compositions are representative of communities growing during highstand periods on the western New Caledonian margin throughout the past million years is uncertain.

5.6 Conclusions

In conclusion, a calibration line has been produced for sediment core MD06-3019 turbidite samples with Sr counts greater than $\mu_{pelagic} + \sigma_{pelagic}$. This calibration may also be applicable at lower Sr counts though this is not yet certain. In comparison to the previous published study, this work provides a calibration over a wider and higher range of Sr count values.

The method shows significant promise as a new proxy for quickly establishing the aragonite content of sediment samples. Advantages are the high resolution, speed, reduced cost and non-destructive nature of the method when compared to traditional XRD measurements or point counting. XRF scan results may be easily calibrated via relatively few XRD measurements. The method may be used in its own right to investigate aragonite content when material for destructive analysis is limited and also as a way to make rapid qualitative assessments of changes in down-core aragonite content before deciding on whether to pursue further study.

This method could be useful for those researching platform margin settings, when attempting to reconstruct the amount and timing of carbonate production and shedding from the shallow shelf, as well as dissolution effects. The present study demonstrates that robust calibrations can be developed for specific cores, but comparison with similar a study suggests that further work is required to understand the extent to which any given calibration can be generalised to other settings.

Chapter 6: Inferences on the history of the New Caledonia Barrier Reef from deep sea turbidite deposition.

6.1 Chapter Abstract

This chapter examines the history of carbonate production on the western New Caledonia shallow shelf over the past 1.26Myr. Previous investigations into Quaternary reef history, mainly based on reef borehole studies, appear to show an expansion of the New Caledonia Barrier Reef around marine isotope stage (MIS) 11(~400ka), from an open carbonate ramp into a rimmed shelf [*Cabioch et al.*, 2008; *Montaggioni et al.*, 2011]. This chapter aims to independently verify the timing of this expansion, by using changes in the nature of shallow shelf derived turbidites, which are deposited in deep sea core MD06-3019. The hypothesis being that such a large expansion of reef ecosystem should be reflected in temporal changes in shelf derived deposits. Analysis of the variations in grain size, frequency, accumulation rate, total carbonate content and aragonite content (obtained via the X-ray

fluorescence strontium concentration proxy developed in Chapter 5) of turbidites has been conducted.

The results of these analyses show that there is indeed a change in the nature of turbidite deposits after MIS11 (~400ka). However, there is also another noticeable change in turbidite deposits at MIS22 (~900ka). These variations effectively split the record into 3 sections: Section I: MIS11-Holocene, Section II: MIS22- MIS11 and Section III: 1.26Ma- MIS22. Compared to the periods 1.26Ma- MIS22 and MIS11-Holocene the middle period contains no coarse grained turbidites, only fine grained; there is an increased frequency of turbidite deposition but an overall reduction in turbidite accumulation rate and a significant reduction in total carbonate and aragonite content. However, patterns of turbidite deposition are largely indistinguishable between Section I and III: both contain coarse and fine grained turbidites and there is no significant difference in the median carbonate or aragonite content of turbidites deposited in the two different time periods.

There are three main possible causes which may explain these temporal variations in turbidite deposition: dissolution, changes in transport processes and variations in shallow water carbonate production. This work concludes that, while the first two options cannot be ruled out, variations in the nature of turbidite deposition in sediment core MD06-3019 most probably reflect changes in carbonate production on the shallow shelf over the course of the 1.26Myr record. This suggests a more complex history of shallow water carbonate production on the western New Caledonian margin than a simple one-step increase at MIS11, when the initiation of the modern day barrier reef system occurred. Rather shallow water carbonate production is believed to have decreased substantially between MIS23-MIS11, compared to the periods 1.26Ma-MIS23 and MIS11-present, where carbonate production is believed to be similar in nature. Possible controls on reef growth are explored within the regional and global palaeoceanographic context, with glacial-

interglacial changes in sea-level being proposed as the most likely principal control on these variations in carbonate production.

6.2 Introduction

Investigations into Quaternary reef history, mainly via reef borehole studies, appear to show a worldwide expansion of reefs around marine isotope stage (MIS)11(~400ka) [*Alexander et al.*, 2001; *Multer et al.*, 2002; *Braithwaite et al.*, 2004; *Yamamoto et al.*, 2006; *Dubois et al.*, 2008; *Cabioch et al.*, 2008; *Gischler et al.*, 2010; *Montaggioni et al.*, 2011]. This includes the New Caledonia Barrier Reef (NCBR) which is believed to have evolved from an open carbonate ramp with patch reefs into a rimmed shelf at around this time [*Cabioch et al.*, 2008; *Montaggioni et al.*, 2011].

The initiation of carbonate production on shallow shelves is known to alter the nature and timing of turbidite deposition in the surrounding deep basins [*Dubois et al.*, 2008; *Droxler and Jorry*, 2013; *Puga-Bernabéu et al.*, 2014]. Therefore, it is hypothesised that the establishment of a barrier reef would be reflected in the composition of the shallow shelf sourced turbidites deposited in the New Caledonia Trough. It was predicted that there would be a noticeable increase in reef derived material in turbidites deposited in sediment core MD06-3019 after this period.

6.2.1 Summary of point counting results for core MD06-3019 and the requirement for a further study

Point counting results from Chapter 4 demonstrated that turbidites deposited since MIS11 show a greater dominance of shallow water bioclasts and a higher occurrence of coral fragments compared to the immediately preceding interval. These results appear to corroborate the work of previous investigators such as *Montaggioni et al*. (2011) and *Cabioch et al*. (2008). However, there are significant differences in the record prior to MIS22. Before MIS22 there is a greater dominance of shallow water biota and coral occurrence in turbidites is higher. Coral abundance for turbidites at the base of the core can equal or exceed values for turbidites at the top of the core. These results challenge a simple model in which the only significant evolution on the

western New Caledonia margin over the last 1.2Myr was the expansion of the barrier reef at MIS11; rather suggesting that the history of the western New Caledonia margin may be more complicated than initially anticipated.

Due to turbidite layers with low point counts being excluded from analysis, as a result of large uncertainties in their relative assemblage percentages, there is a scarcity of point counting data for core MD06-3019. This means that whilst point counting is useful for gaining an overall impression of the turbidites, it is not sufficient on its own to accurately characterise the temporal changes in turbidite content in sediment core MD06-3019. This is a particular problem between MIS22-MIS9 (~900-300ka) due to an absence of coarse grained layers; which is a critical time period for investigation, given the proposed expansion of the New Caledonia Barrier Reef occurred at ~MIS11 (~400ka). In order to further investigate the composition of the turbidite deposits an alternative method for assessing the presence of shallow water carbonate material in samples was needed. Chapter 5 developed the use of X-ray fluorescence core scanning measurements for the strontium content of sediments as a new proxy to assess the shallow water aragonite content of turbidite layers. The strontium concentration of sediments was calibrated via X-ray diffraction measurements to give an inferred aragonite % for turbidite layers in the core. The source of this aragonite is principally shallow shelf biota: corals, calcareous green algae (halimeda) and molluscs. The development of this proxy allows us to explore the aragonite composition of turbidite layers, including for fine grained turbidites, and therefore to make inferences about the evolution of the shallow shelf and associated reef system through time.

6.2.2 Controls on shallow water carbonate production

Numerous factors impact on the growth of shallow shelf carbonate producers, with different organisms requiring different conditions and have varying tolerance limits to deviations from these ideal hydrographic and physical settings. Geographic-tectonic factors include: latitude, antecedent topography, substrate and relative sea-

level change (controlled by the interplay between subsidence/ uplift rates and eustatic sea-level). Physico-chemical factors include: sea surface temperature (SST), sea surface salinity (SSS), nutrient availability, dust input, sediment input, light availability and aragonite saturation state. Hydrodynamic factors include: waves, currents and storm frequency. Biological factors include: larval sources and dispersion, diversity, disease and predation [*Cabioch et al.,* 1999; *Kleypas et al.,* 1999, *Cabioch et al.,* 2008; *Montaggioni and Braithwaite,* 2009; *Montaggioni et al.,* 2011]. See Appendix 4 for a detailed literature review of the various conditions required for tropical coral reef growth. "Where these factors fall within the range conducive to the production of biogenic carbonate…, a vigorous carbonate factory can result" [*Handford and Loucks,* 1993].

There are a number of large scale processes which combine together to influence these controlling geographic-tectonic, physico-chemical and hydrodynamic variables on varying timescales (see *Table 6.1*). For example, the availability of suitable substrate is influenced by relative sea-level, which in turn is dependent on rates of tectonic subsidence/ uplift (acting on 10s-100s kyr timescales) combined with glacial-interglacial changes in sea-level. SSS is controlled both by glacial-interglacial changes in salinity (on 10s-100s kyr timescales) but also the movement of the South Pacific Convergence Zone (SPCZ) (on 100s-1000s year time scales). Movement of the SPCZ not only changes the degree of precipitation in the New Caledonia area by variations in the intensity of *El Niño Southern Oscillation (ENSO), but a*lso alters the direction of wind stress in the area and thus degree of upwelling along the western New Caledonia margin (see Chapter 2 §2.4.2).

Tectonics Timescale:10s-100skyrs	**Glacial-Interglacial climate change** Timescale: 40-100kyrs	**Movement of the South Pacific Convergence Zone** Timescale: seasonal- kyrs
Latitude		
Subsidence/ uplift (accommodation space)		
Antecedent topography		
Coastal morphology		
Relative sea-level change (including rate of change)		
	Aragonite saturation state	
	Sea surface temperature	
	Sea surface salinity	
	Nutrients	
	Dust input	
	Waves	
	Currents	
	Storm frequency	
Sediment input		

Table 6.1 Proposed summary of the influence of large scale processes on conditions affecting tropical coral reef growth in the New Caledonia area.

The modern day tectonics, oceanography and hydrology along the western margin of New Caledonia (see Chapter 2 §2.4) are clearly conducive to luxuriant coral reef growth. However, these conditions will have changed over the last 1.26Myrs, as seen, for example, in local SST reconstructions [*Russon et al.*, 2010] and these climatic variations will have affected shallow water carbonate production. There remains a question as to which factors have been the principal controls on changes in coral reef growth along the western margin of New Caledonia since 1.26Ma.

6.2.3 Aims of this study on the history of the New Caledonia Barrier Reef

This chapter aims to independently verify the timing of reef expansion along the western New Caledonia margin, provide new insights into the history of the New Caledonia Barrier Reef and make inferences on the possible controls on this evolution. In order to investigate the history of reef growth along the western New Caledonia margin this chapter utilises the new aragonite proxy (developed in Chapter 5), as well as measurements for total carbonate content to assess the content of turbidites present in core MD06-3019. This is combined with an analysis of the timing, frequency, grain size and accumulation rate of turbidite sediments. Temporal changes in these features may provide clues as to the history of the western New Caledonia Barrier Reef over the last 1.26Myr. The pattern of evolution in MD06-3019 turbidites is then compared to reconstructions of possible variables which influence shallow water carbonate production: local SST [*Russon et al.*, 2010] and global eustatic sea-level [*Miller et al.*, 2005]. This enables an assessment of whether variations in these factors have been a significant controlling influence on carbonate production on the New Caledonia margin over the last 1.26Myr.

6.3 Analytical Methodology

6.3.1 Timing and frequency of turbidite deposits

Turbidites were initially analysed to examine the timing and frequency of deposits, temporal changes in grain size and overall flux of shallow shelf sediments to the core site. Previous work has highlighted that the presence or absence of a barrier reef has an effect on the sediments grain size, flux and timing of sediments reaching the deep sea [*Handford and Loucks*, 1993; *Dunbar et al.*, 2000; *Francis et al.*, 2007; *Webster et al.* 2012, *Droxler and Jorry*, 2013; *Puga-Bernabéu et al.*, 2014]. (See Chapter 7 for more detail.)

The timing of all turbidite events over the complete 1.26Myr record (as assigned using the sediment core age model developed in Chapter 3) was tested for significance via Monte Carlo analysis. Initially an entirely stochastic system was assumed and the frequency of deposition of all layers over the whole time period was analysed. A Monte-Carlo simulation, of 5,000 repeats, was set up to generate 79 randomly distributed layers across a 1.26Myr time period. The number of layers present in 400, 200 and 100kyr moving windows was then calculated and the distribution of results with time for these simulated layers compared to the actual distribution of turbidites in the MD06-3019 record. Layers that were clustered close to each other (±4kyrs), and conceivably related to a single 'trigger' event, were then combined into single points and the distribution re-assessed.

The significance of the gap in coarse layer deposition between 899-292ka was then examined. A Monte-Carlo simulation, of 5,000 repeats, was set up to generate 12 randomly distributed layers (corresponding to the 12 coarse layers in the MD06-3019 record) across a 1.26Myr time period. The number of layers present in 600, 400, 200 and 100kyr moving windows was then calculated and the distribution of results for these simulated layers compared to the actual distribution of coarse grained turbidites in the MD06-3019 record. If any aspect of the pattern of actual turbidite deposition

lay outside the 5-95% confidence interval of what would be expected from a random distribution, then it is said to be a significant feature and thought likely to have some controlling mechanism behind its occurrence, rather than being a purely stochastic feature.

6.3.2 Bulk carbonate measurements

Periods of high carbonate production on the shallow shelf can cause an increase in carbonate material shed to the deep basin. Therefore an increase in the overall carbonate content of turbidite sediments can be indicative of greater carbonate production on the shelf. The average total carbonate weight percentage of each turbidite layer was obtained by coulometry measurements (see Chapter 4§3.2). As per the definitions of *Puga-Bernabéu et al.* (2014) these layers were then assigned as being either calciturbidites (>60 % carbonate), mixed (40-60% carbonate) or siliciclastic turbidites (<40% carbonate) depending on their composition. An analysis was then made as to the relationships between: turbidite carbonate content and a) layer type (coarse, dark fine, light fine) and b) time period of deposition.

6.3.3 Inferred aragonite content

Similarly periods of high carbonate production on the shelf are also associated with increased aragonite flux to the deep sea, since corals and halimeda are primary producers of aragonite. Therefore an increase in the aragonite content of turbidite sediments is likely indicative of greater carbonate production on the shelf, in particular reef development. The aragonite content of the sandy layers was assessed by XRF core scanning for [Sr] and where possible converted to an inferred aragonite % by use of the calibration developed in Chapter 5 §5.1. Temporal changes in turbidite aragonite content and the overall flux of aragonite delivery to core site MD06-3019 was then analysed.

6.3.4 Statistical treatment of results

Temporal evolution in the total carbonate and aragonite content of the turbidites was assessed via the non-parametric Mann-Whitney U test to see if certain time periods have significantly higher carbonate or aragonite content than others. The non-parametric Mann-Whitney U test is required since the distributions being considered are strongly non-normal. For a two-tailed test, an alpha value of 0.05 was set for rejection of the null-hypothesis (that the median carbonate or aragonite content of the two sample groups are equal). The turbidite record was split into 3 sections: 1.26Ma-MIS22 (~1.26Ma-900ka), MIS22-MIS11 (~900-400ka) and MIS11-Holocene (~400ka- present). The division of the record at MIS11 was chosen so as to be able to compare the results of this study with the borehole work of *Cabioch et al.* (2008) and *Montaggioni et al.* (2011) who propose and expansion of the New Caledonia Barrier Reef at this time. The division at MIS22 was based on the change in turbidite content and grain size as observed via the point counting results presented in the previous chapter. However, sensitivity tests were also conducted for all analyses presented using section boundaries defined by changes in sedimentation in the core, i.e. the presence/ absence of coarse turbidites (boundaries at 898 and 292ka) and changes in the climate system, i.e. the occurrence of the 'lukewarm interglacials' (boundaries at MIS23 and MIS11) [*Masson-Delmotte et al.*, 2010; *Jaccard et al.*, 2013].

6.4 Results

6.4.1 Timing of turbidite emplacement over the complete 1.26Myr MD06-3019 record

Over the complete MD06-3019 record, back to 1.26Ma, 79 sandy turbidite layers were deposited (see *Figure 6.1B*). These vary in grain size from very fine sand (φ=4) to coarse sand with small pebbles (φ=-2), width (1-35cm), content (see Chapter 4) and frequency of deposition.

There are a number of features of this turbidite record that immediately strike as noticeable:

i. The 600kyr absence of coarse grained turbidites between 899-292ka (see *Figure 6.1B*), which is a statistically significant result when tested via Monte Carlo simulations (see Chapter 7).
ii. The increase in frequency of turbidite events, of any type, in the middle period of the record (see *Figure 6.1C*).
iii. The reduction in turbidite sediment accumulation rate in the period MIS22-MIS11: 0.18cm/kyr compared to 0.50cm/kyr for MIS11- Holocene and 0.43cm/kyr 1.26Ma- MIS22. This is due to generally thinner turbidite layers being deposited between MIS22-11: average sandy layer width between MIS22-MIS11 being 3cm, compared to 8cm for MIS11- Holocene and 7cm for 1.26Ma-MIS22. (See *Figure 6.1 D*)
iv. The repeated occurrence of clusters of a number of turbidite layers within a few kyrs of each other (see *Figure 6.1B*), this is a statistically significant result when tested via Monte Carlo simulations (see Chapter 7.).

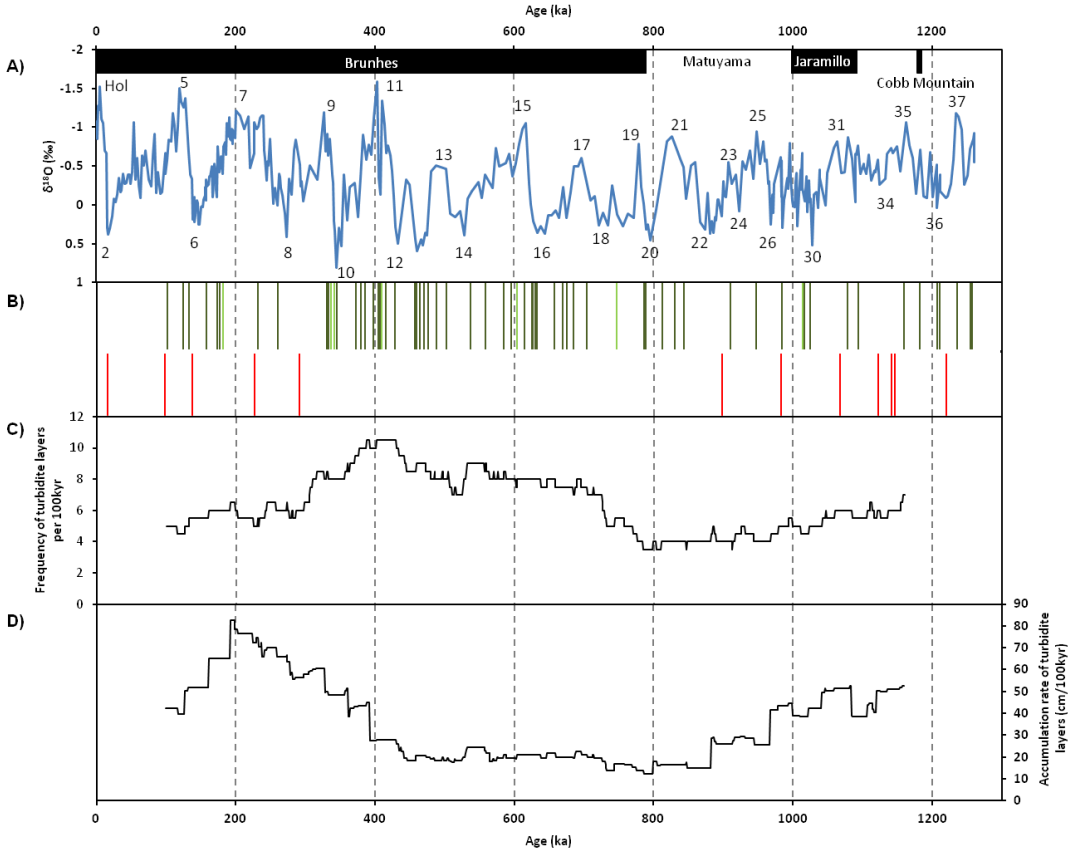

Figure 6.1 A) $\delta^{18}O$ record for MD06-3019, **B)** Positions of turbidite layers. Red: coarse, dark green: dark fine, pale green: light fine. **C)** Turbidite frequency, of any type, per 100kyr using a 200kyr moving window. **D)** Turbidite accumulation rate using a 200kyr moving window.

6.4.2 Evolution in the carbonate and aragonite content of turbidites over the last 1.26Myr in the MD06-3019 record

The total weight % (wt.%) carbonate content of turbidites in core MD06-3019 varies between 4-71%, showing that the area is a mixed carbonate-siliciclastic margin. As per the definitions of *Puga-Bernabéu et al*. (2014) turbidites were assigned as being either calciturbidites (>60 % carbonate), mixed (40-60% carbonate) or siliciclastic turbidites (<40% carbonate) depending on their composition. There is a clear relationship between layer type and total carbonate content (see *Table 6.2*). Dark fine grained layers, as would be expected, have a lower carbonate content and are principally classed as siliciclastic turbidites, with no instances of calciturbidites. By contrast light fine and coarse grained layers are mainly mixed turbidites. Coarse layers vary in carbonate content significantly and can be siliciclastic, mixed or calciturbidites; whereas light fine layers, as would be expected from their colour, have a higher carbonate content and none are classified as siliciclastic turbidites.

Percentage of each turbidite type in MD06-3019 that is classified as a calci-, mixed- or siliciclastic turbidite				
Turbidite Type	**Coarse n=11**	**Dark fine n=60**	**Light fine n=7**	**All n=78**
Calciturbidite (n=3)	9% (1/11)	0% (0/60)	29% (2/7)	4% (3/78)
Mixed turbidite (n=27)	55% (6/11)	27% (16/60)	71% (5/7)	35% (27/78)
Siliciclastic turbidite (n=48)	36% (4/11)	73% (44/60)	0% (0/7)	62% (48/78)
Median carbonate wt.%	48%	29%	52%	34%

Table 6.2 Percentages of each turbidite type (coarse grained, dark fine grained or light fine grained) in MD06-3019 that are classed as either calciturbidites (n=3), mixed turbidites (n=27) or siliciclastic (n=48) turbidites. The median carbonate wt.% content for each turbidite type (coarse grained, dark fine grained or light fine grained) is also included.

There is also a statistically significant reduction in the overall total carbonate content of turbidite layers between MIS22-11compared to the 1.26Ma- MIS22 and MIS11-Holocene periods (see *Table 6.3* and *Table 6.4* and *Figure 6.2*).

Weight % bulk carbonate content of MD06-3019 turbidite layers				
	Coarse (n=11)	**Dark fine (n=60)**	**Light fine (n=7)**	**All turbidites (n=78)**
Complete record	48%	29%	52%	34%
MIS11- Holocene	48%	36%	53%	41%
MIS22-MIS11	-	23%	57%	24%
1.26Ma-MIS22	45%	34%	41%	36%

Table 6.3 Median total carbonate content of turbidite layers in different sections of the core.

Mann-Whitney U test for temporal variations in MD06-3019 turbidite $CaCO_3$ wt.% content			
Group 1	**Group 2**	**Mann-Whitney U Value**	**Two-tailed P value**
MIS11-Holocene n= 26 Median= 41 wt.%	MIS22-MIS11 n= 30 Median= 24 wt.%	602	0.005 (Reject null-hypothesis)
MIS22-MIS11 n= 30 Median= 24 wt.%	1.26Ma-MIS22 n= 22 Median= 36 wt.%	509	0.001 (Reject null-hypothesis)
MIS11-Holocene n= 26 Median= 41 wt.%	1.26Ma-MIS22 n= 22 Median= 36 wt.%	262	0.624 (Cannot reject null hypothesis)

Table 6.4 Comparison of the total wt. carbonate content of turbidites deposited in different time periods using a Mann-Whitney U test. α=0.05 for rejection of the null hypothesis (that the median turbidite carbonate content is the same in the two time periods).

Similarly the average aragonite content of sandy layers is also seen to vary with layer type and timing of deposition. Coarse and light fine sandy layers have a higher aragonite content than dark fine sandy layers (see *Table 6.5*). There is a statistically significant reduction in the measured XRF Sr count value, as a proxy for aragonite, of turbidite layers in the middle section of the core between MIS22-MIS11 compared to the base and top (see *Table 6.5* and *Table 6.6* and *Figure 6.2*).

XRF [Sr] count (and inferred aragonite %) of MD06-3019 turbidite layers				
	Coarse n=11	**Dark fine n= 58**	**Light fine n=7**	**All turbidites n= 76**
Complete record	14,500 (18.2%)	9,400 (13.9%)	13,900 (17.5%)	9,700 (13.9%)
Section I (MIS11-Holocene)	13,500 (17.2%)	9,800 (13.9%)	14,000 (17.7%)	10,300 (13.9%)
Section II (MIS22-MIS11)	-	7,000 (13.9%)	13,600 (17.3%)	7,000 (13.9%)
Section III (1.26Ma-MIS22)	16,200 (20.0%)	10,500 (13.9%)	9,700 (13.9%)	10,600 (14.1%)

Table 6.5 Median XRF Sr count and equivalent maximum aragonite content for turbidite layers in different sections of the core. For those layers with a Sr count below the cut off for the XRF-XRD calibration a maximum aragonite value of 13.9% (the equivalent aragonite value for the lowest Sr count value in the calibration) is given.

Mann-Whitney U test for temporal variations in MD06-3019 turbidite XRF Sr counts			
Group 1	**Group 2**	**Mann-Whitney U Value**	**Two-tailed P value**
MIS11-Holocene n= 26 Median= 10,300	MIS22-MIS11 n= 29 Median= 7,000	625	<.0001 (Reject null hypothesis)
MIS22-MIS11 n= 29 Median= 7,000	1.26Ma-MIS22 n= 21 Median= 10,600	498	0.0002 (Reject null hypothesis)
MIS11-Holocene n= 26 Median= 10,300	1.26Ma-MIS22 n= 21 Median= 10,600	298	0.6031 (Cannot reject null hypothesis)

Table 6.6 Comparison of XRF Sr count values for turbidites deposited in different time periods using a Mann-Whitney U test. α=0.05 for rejection of the null hypothesis (that the median turbidite XRF Sr count values are the same in the two time periods).

The Sr count value of turbidite layers was used in the above analysis rather than inferred aragonite %. This is because many of the turbidites, especially in the middle section of the core, are below the cut off for accurate conversion to an aragonite % (the pelagic carbonate mean Sr count plus one standard deviation: $\mu_{pelagic} + \sigma_{pelagic}$ =10,500 counts). (See Chapter 5 §5.1 for more detail.) Therefore, only maximum possible aragonite values can be given for these layers (the equivalent aragonite value for the lowest Sr count value used in the calibration), which is unlikely to be an accurate representation of their aragonite content. However, it is possible to examine the trend in the aragonite % of samples by looking at the variation in the number of layers through time which have Sr counts greater than the calibration cut off limit (see *Table 6.7*). There is a clear reduction in the number of layers with a Sr count greater than the calibration cut off limit in the period MIS22-MIS11.

MD06-3019 turbidite layers with an XRF Sr count > $\mu_{pelagic} + \sigma$				
	Coarse	**Dark fine**	**Light fine**	**All turbidites**
Complete record	91% (10/11)	40% (23/58)	71% (5/7)	50% (38/66)
Section I (MIS11-Holocene)	100% (5/5)	59% (10/17)	75% (3/4)	69% (18/26)
Section II (MIS22-MIS11)	-	19% (5/27)	50% (1/2)	21% (6/29)
Section III (1.26Ma-MIS22)	83% (5/6)	57% (8/14)	100% (1/1)	67% (14/21)

Table 6.7 The amount of layers (expressed as a percentage and as absolute numbers of layers for each category- numbers in brackets) which register with an XRF Sr count greater than the calibration cut off limit ($\mu_{pelagic} + \sigma_{pelagic}$ =10,460 counts) for different layer types and time periods.

The reduction in total average carbonate and aragonite content of turbidite layers between MIS22-MIS11 is not merely due to the lack of coarse grained layers in this period. As can be seen from *Table 6.3*, *Table 6.5* and *Table 6.7* there a reduction in the average carbonate content, XRF Sr count and number of layers registering with an Sr count greater than $\mu_{pelagic} + \sigma_{pelagic}$ for all layer types combined in Section II. Additionally, an important observation is that the same trends can be observed when examining the composition of only dark fine grained layers, which are present in significant numbers throughout the entire core (see *Table 6.8*). This shows that the reduction in average carbonate and aragonite content it is not just due to the presence of coarse layers in the periods 1.26Ma-MIS22 and MIS11-Holocene.

Varying composition of dark fine grained MD06-3019 turbidites			
	MIS11-Holocene	**MIS22-MIS11**	**1.26Ma-MIS22**
wt.% $CaCO_3$	36%	23%	34%
Sr count	9,800	7,000	10,500
% of layers registering with XRF Sr count > $\mu_{pelagic} + \sigma_{pelagic}$	59% (10/17)	19% (5/27)	57% (8/14)

Table 6.8 Temporal variation in the total carbonate and aragonite content of dark fine grained turbidites from MD06-3019.

An assessment of the sensitivity of the above Mann-Whitney results (that there is a significant reduction in aragonite and calcite content of turbidites deposited between MIS22 and MIS11, ~900-400ka) to the position of section boundaries has been conducted. The analysis was repeated using boundaries defined by the presence/ absence of coarse turbidite layers (~900ka and 300ka) and by changes in the climate system, i.e. the reduction in the height of interglacial sea-level in the period MIS23-MIS13 (~915-480ka) [*Miller et al.*, 2005]. Results of these sensitivity tests show that the significance of the reduction of carbonate and aragonite content of turbidite layers in the middle period is not sensitive to small changes (of the order of 20-100kyr) in the section boundaries.

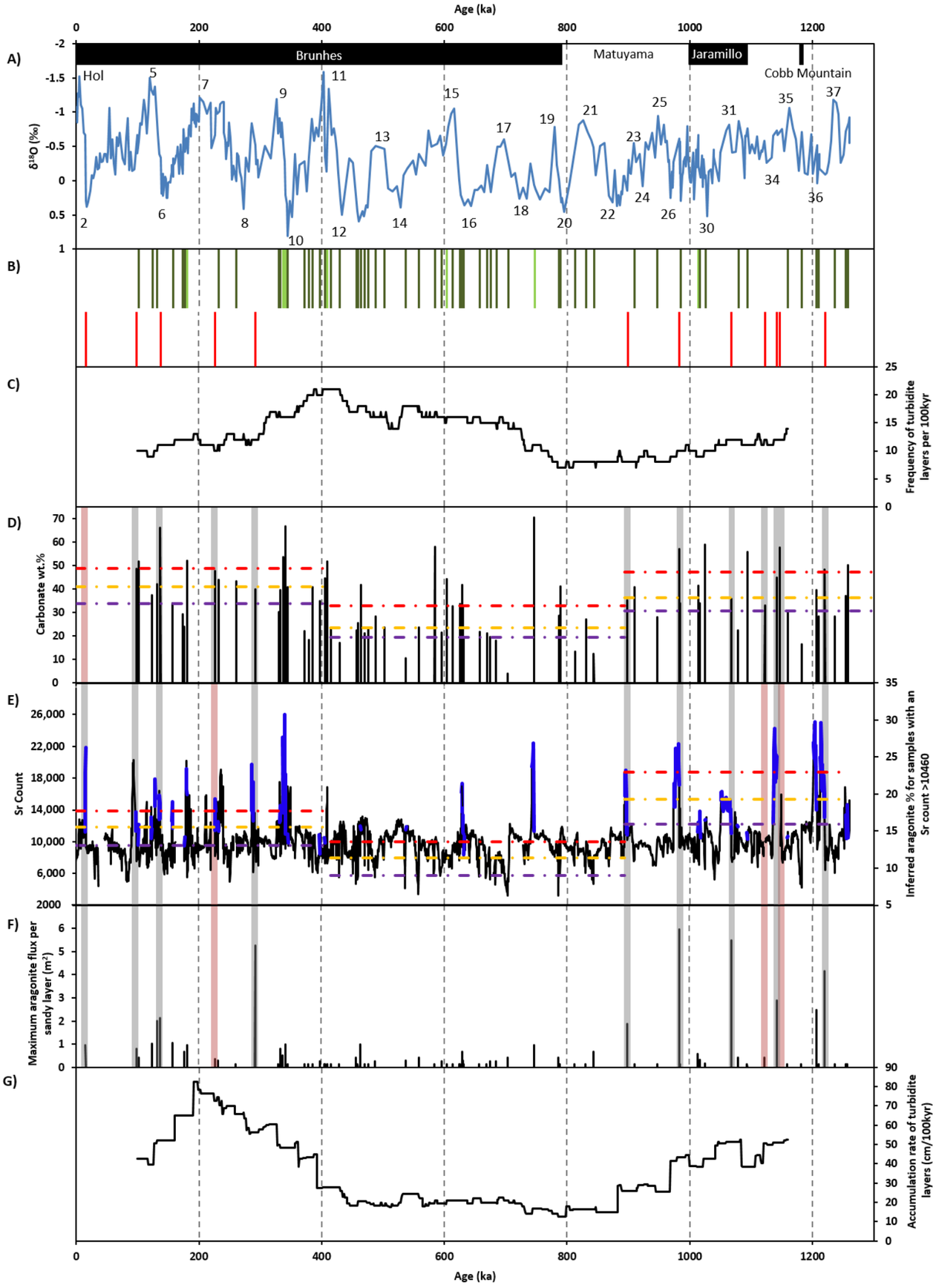

Figure 6.2 A) $\delta^{18}O$ record for MD06-3019 obtained from G. *ruber* foraminifera.
B) Positions of sandy layers. Red: coarse, dark green: dark fine layers, pale green: light fine layers.
C) Turbidite frequency per 100kyr using a 200kyr moving window.
D) Carbonate wt. % values for sandy layers with upper quartile (red), median (yellow) and lower quartile (purple) shown for each section. Shaded grey areas show coarse layer positions (red when data missing)
E) XRF Sr counts as a proxy for aragonite. LHS axis: Sr counts. RHS axis: for blue coloured portions of the record- inferred aragonite content of sandy layers with a count value > $\mu_{carbonate\ ooze} + \sigma_{carbonate\ ooze}$ calibrated using XRD. Background aragonite values ~1.3%. Upper quartile, median and lower quartile for Sr counts shown for each section.
F) Estimated flux of aragonite delivered via turbidite layers through time.
G) Turbidite sediment supply in cm/100kyr using a 200kyr moving window.

6.5 Discussion

6.5.1 Changes in turbidite deposition in core MD06-3019: dissolution, source or transport signal?

As has been described in the previous section and Chapter 4 §4 there are a number of distinctive features in the record of turbidite deposition in core MD06-3019. A summary of these variations is given in *Table 6.9*.

There are three main possible causes for the observed temporal variations in the nature of turbidites deposited in sediment core MD06-3019:

1. changes in the depth of the lysocline (the depth in the ocean below which the rate of dissolution of calcite increases dramatically) and aragonite compensation depth, i.e. changes deep sea carbonate **dissolution**,
2. modifications in the **transport** processes (e.g. turbidite flow direction, size and flow rate) which supply the core site with turbidites,
3. evolution of the **source** area which supplies the material for turbidites (i.e. changes in the extent and nature of shallow shelf carbonate production on the western New Caledonian margin)

This section discusses the merits of each of these hypotheses in detail, in order to ascertain the most likely controls on turbidite deposition at core site MD06-3019; as these will directly inform the extent to which it is possible to make inferences on reef history in the area from the turbidites deposited in core MD06-3019.

Section I (MIS11-Holocene)	**Section II (MIS22-MIS11ka)**	**Section III (1.26Ma-MIS22)**
Coarse and fine layers	Fine layers only	Coarse and fine layers
Thicker layers: Average= 8cm	Thinner layers: Average= 3cm	Thick layers: Average= 7cm
Higher average turbidite accumulation rate: 0.50cm/kyr	Lower average turbidite accumulation rate: 0.18cm/kyr	Higher average turbidite accumulation rate: 0.43cm/kyr
Higher carbonate content (41%)	Lower carbonate content (24%)	Higher carbonate content (36%)
Distribution of turbidite types: C- calciturbidites, M- mixed carbonate-siliciclastic turbidite, S-siliciclastic turbidite		
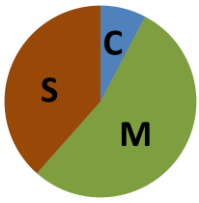	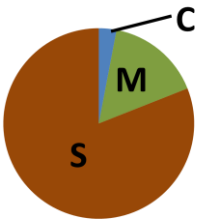	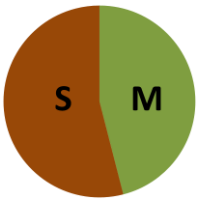
Point counting results		
Higher relative shallow water biota content (33%) Higher occurrence of coral bearing layers (77%) Higher average relative coral abundance (4%)	Lower shallow water biota (2%) Lower occurrence of coral bearing layers (20%) Lower average relative coral abundance (0%)	Higher shallow water biota (11%) Higher occurrence of coral bearing layers (33%) Higher average relative coral abundance (3%)
Higher inferred aragonite based on Sr count: 10,300	Lower inferred aragonite based on Sr count: 7,000	Higher inferred aragonite based on Sr Count 10,600
Sandy layers registering with an Sr count value > $\mu_{pelagic}+\sigma_{pelagic}$ = 69%	Sandy layers registering with an Sr count value > $\mu_{pelagic}+\sigma_{pelagic}$ = 21%	Sandy layers registering with an Sr count value > $\mu_{pelagic}+\sigma_{pelagic}$ = 67%

Table 6.9 Summary table of the different characteristics and compositions of turbidites deposited in the three time periods allocated down-core.

6.5.2 Dissolution signal

Firstly, the observed decrease in the aragonite and carbonate content of turbidites presented in core MD06-3019 during in the middle period, MIS22-11, may be a result of deep sea dissolution of the carbonate content of turbidites. Only fine-grained turbidites are present between MIS22-11 and these layers tend to be relatively thin (of the order of a few cm). Thus they are likely to be more susceptible to bioturbation and dissolution than wider, coarser grained turbidites. As a result they may have an artificially lower carbonate and aragonite content due to post depositional alteration. It is possible that this dissolution may be related to the Mid-Brunhes Dissolution Interval (MBDI), which is a period of global carbonate dissolution centred around MIS11 and lasting several hundred thousand years (600-200ka) [*Barker et al*., 2006].

It is noted, however, that the timing of lower carbonate and aragonite content in MD06-3019 turbidites occurs between MIS22- MIS11 (900-400ka) and not 600-200ka, as for the MBDI [*Barker et al.*, 2006]. Nor indeed is there any evidence of the expression of the MBDI in core MD06-3019 from measurements of the carbonate content of the pelagic ooze. Dissolution levels experienced by the MD06-3019 core site appear to have varied in sync with glacial-interglacial cycles (see Appendix 3); however, there is no apparent relationship between turbidite carbonate or aragonite content and the timing of its deposition within the climate cycle (see Chapter 7). This, along with the exceptional preservation of shallow water carbonate material in turbidites (see Chapter 4 §4.3), suggests that, due to instantaneous deposition, turbidites are not subject to particularly high dissolution in the deep sea. Additionally, the MBDI cannot explain the changes in grain size, frequency and flux of turbidite material during this period.

Dissolution is not, therefore, thought to be the primary cause of the patterns of turbidite sedimentation change seen in sediment core MD06-3019 between MIS22-MIS11.

6.5.3 Transport Signal

The second hypothesis is that the observed pattern of turbidite deposition in sediment core MD06-3019 is due to a transport signal; this could occur in two ways. Firstly that, due to the migration of channels on the basin floor, which supply turbidite material to the core site, sediment core MD06-3019 no longer receives material from a source area that contained significant amounts shallow water carbonate production during the MIS22-11. However, from around MIS11 onwards and prior to MIS22 turbidites must have been sourced from a region with at least periodically significant reef development. Alternatively it is possible that throughout the whole time period covered by the core there has been a consistent level of shallow water carbonate production on the western New Caledonia margin. However, due to transport processes, such as reduced flow intensity, shallow shelf carbonate material is not transported to the core site. Therefore, deep sea turbidite content at the MD06-3019 core location no longer accurately records the carbonate production shallow shelf and the signal of reef presence is not seen in core MD06-3019 site between MIS22-11.

All turbidites deposited in sediment core MD06-3019 will be sourced from somewhere along the western New Caledonia margin, the nearest alternative source of mixed siliciclastic-carbonate material being the east Australian margin, on the other side of the Coral Sea (see *Figure 2.1*). However, there is relatively little known about the turbidite deposition system in the New Caledonia Trough. Though research during the late 1980s, based on samples and bathymetry data collected during the 1987 BIOCAL cruise, provides some limited information. This work largely focuses on sediments deposited to the East of New Caledonia, in the Loyalty Basin, along a transect between Thio (on Grande Terre) and Lifou (on the Loyalty Ridge). However, broadly similar depositional regimes could be expected on both sides of the island.

Erosion predominates along the slopes of New Caledonia, where there is generally only a thin coating of hemipelagic sediments, demonstrating that gravity induced

movement of sediments is relatively frequent. The slopes around New Caledonia are carved on all or part of their length by submarine canyons up to 25km long, 1-3km wide and 100-500m deep [*Cotillon et al.*, 1989b]. The most spectacular are to be seen in the south-west of New Caledonia (see *Figure 6.3*). Generally the canyons are parallel to the lines of greatest slope. The greater the slope the more it is cut into by wide, cross-sectionally concave canyons, separated by narrow spurs. This gives a morphology dominated by gravity erosion, determined by large shifts in mass. The canyons seem to ensure an almost direct transport of material from the external platform to deep/middle depths [*Cotillon et al.*, 1989b]. This material is always mixed with greater or lesser quantities of elements from the slope. In the area studied by *Cotillon et al.* (1989a, 1989b, 1990) the basin is supplied with turbidites (frequently with an erosive base) from the New Caledonian margin which travel over 50km. The sediments are comprised of a mixture of peri-platform carbonate debris, clays from the continent and remobilised hemipelagic ooze [*Cotillon et al.*, 1989b]. The material found in turbidites recovered during the BIOCAL cruise are very similar in composition to those found in core MD06-3019 and come from 5 sources [*Cotillon et al.*, 1989a; *Cotillon et al.*, 1989b, *Cotillon et al*., 1990]:

1. Terrigenous material from New Caledonia: 5-40% (mainly clay minerals, quartz, iron oxides and heavy minerals).
2. Bioclastic silts and sands derived from the reefs and lagoon around New Caledonia: 15-25%.
3. Mixed bioclasts: 1-20% (furnished by benthic species which colonise the slopes and the basin).
4. Plankton debris: 30-75% (forams, pteropods and nannofossils)
5. Volcanics: 0.5-10% (glass and pumice)

6.5.3.1 Channel migration

The first option to explain the reduction in the carbonate and aragonite content of turbidites between MIS22-MIS11 is channel migration. The following discussion is illustrated in *Figure 6.3*. It is possible that due to the migration of the channels which feed turbidites to the core site, MD06-3019 no longer received material from a proximal area with high carbonate production between MIS22-MIS11. Whilst the submarine canyon systems on the slope seem well established, once the gravity flows have reached the flatter deep basin and moved out of deep channels into either: shallow meandering distributary channels or sheet flows of the middle or outer fan, their trajectories would not be so predictable. It is possible that there would be significant irregularity in deposits due to local bathymetry. The absence of coarse grained turbidites between MIS22-MIS11 could suggest that there had been the loss of locally sourced material (the St. Vincent Bay area, see *Figure 6.3*) and a switch to only a source(s) further afield. (Finer grains being transported greater distances before sedimenting out of the gravity flow than coarse grains, since finer grains require less energy to be transported.) For a time period proximal, coarse grained deposits may have been diverted off due to channels meandering and only fine grained turbidites from more distal margin locations reached the core site via sheet flow (see *Figure 6.3*). Material may have been sourced from further north (around Bourail) or south (towards Amédée) along the island from an area of lower shallow shelf carbonate production (see *Figure 6.3*). However, a significant supply of material from either a northern source from near Bourail (arrow A in *Figure 6.3*) or slightly more southerly source (arrow B on *Figure 6.3*) do not seem particularly likely given the direction of canyons is not towards the MD06-3019 core site. The lateral extent of the turbidites' lobes in the deep basin would need to be of the order of 50km from the canyon axis in order to reach the core site, suggesting large initial volumes of material were mobilised at each event and at a time of increased frequency of turbidite deposition. Canyons from south east of Amédée (arrow C on *Figure 6.3*) are directed towards the core site; however, they are significantly further away (~150km from the MD06-3019 core site) and would once again require large

initial flows for material to reach MD06-3019. By comparison turbidites deposited in the Loyalty Basin only cover a distance of around 50km [*Cotillon et al.*, 1989b].

A consistent 600kyr break in proximally sourced coarse grained deposits due to channel migration seems somewhat unlikely; especially given the consistent supply and nature of fine grained material throughout the core. If there had been a switch in supply area of turbidites recorded in core MD06-3019, it would be expected that there would be a concurrent change in the terrigenous content of turbidites deposited during this time, reflecting the geology of the different locations. As seen from Chapter 2 §2.1 the south of the island (Amédée) is dominated by the obducted ophiolite complex. Slightly further north (Bay of St Vincent) rivers drain areas of mixed terrain- ophiolite, flysch, Permo-mesozoic basement and the Poya Terrane (overlapping slices of oceanic crust). Further north still (Bourail) the area is almost entirely comprised of Permo-mesozoic basement (see *Figure 6.3*).

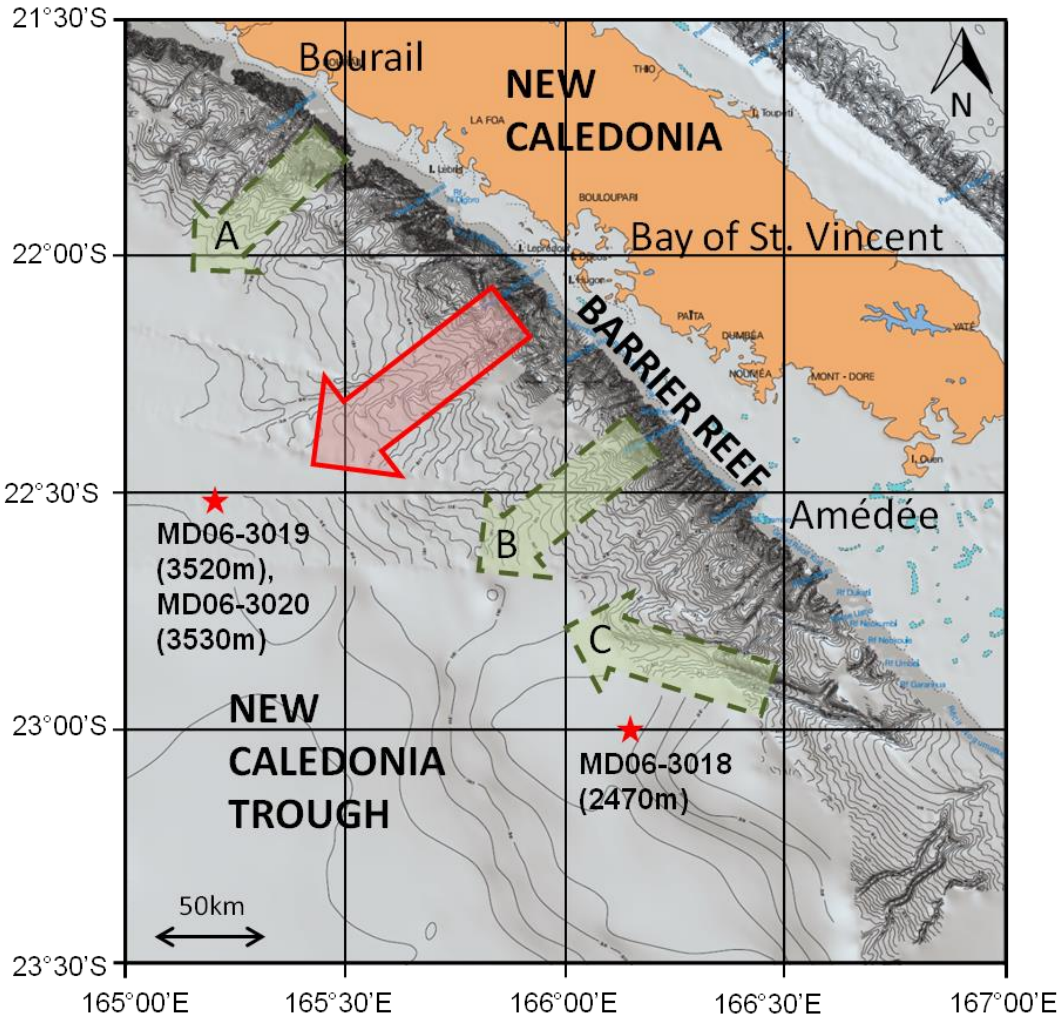

Figure 6.3 Map of the New Caledonia Trough showing the location of the numerous canyons which incise the western slope of the island and the location of the cores used in the production of this thesis. Also shown is the expected proximal source of turbidite deposits to deep sea sediment core MD06-3019 (solid red arrow) and the location of potential sources of more distal, finer grained turbidite (dashed green arrows). (Bathymetry from the ZoNéCo program [*Foucher et al.*, 2006].)

It is possible to use XRF data for elements associated with terrigenous material to see if any patterns occur to suggest a temporal change in source area for turbidites in core MD06-3019. For example, the ophiolite complex in the south of the island is strongly associated with nickel (Ni) and iron (Fe) deposits (which are mined for their economic value) whereas the Permo-mesozoic basement, flysch and Poya Terrane to the North are not. By examining the concentration of Ni and Fe in turbidites down-core, it is possible to investigate the changing importance of the relative supply of terrigenous material from the south of the island. Analysis of this data, though, does not indicate a statistically significant difference between the Ni and Fe XRF counts of turbidite layers in different sections of the core (see *Table 6.10* and *Table 6.11*). Therefore, there is no indication that the turbidite source area has changed to the South over the period covered by the core.

Mann-Whitney U test for temporal variations in MD06-3019 turbidite XRF Ni Counts			
Group 1	**Group 2**	**Mann-Whitney U Value**	**Two-tailed P value**
MIS11-Holocene n= 26 Median= 560 counts	MIS22-MIS11 n= 28 Median= 620 counts	286	0.180 (Cannot reject null-hypothesis)
MIS22-MIS11 n= 28 Median= 620 counts	1.26Ma-MIS22 n= 21 Median= 640 counts	310	0.757 (Cannot reject null-hypothesis)
MIS11-Holocene n= 26 Median=560 counts	1.26Ma-MIS22 n= 21 Median= 640 counts	341	0.150 (Cannot reject null-hypothesis)

Table 6.10 Comparison of the XRF Ni count (reflecting contribution of sediments from the ophiolite complex in the south of Grande Terre) of turbidites deposited in different time periods using a Mann-Whitney U test. α=0.05 for rejection of the null hypothesis (that the median turbidite XRF Ni count is the same in the two time periods).

Mann-Whitney U test for temporal variations in MD06-3019 turbidite XRF Fe Counts			
Group 1	**Group 2**	**Mann-Whitney U Value**	**Two-tailed P value**
MIS11-Holocene n= 26 Median= 12,600 counts	MIS22-MIS11 n= 28 Median= 14,30 counts	338	0.660 (Cannot reject null-hypothesis)
MIS22-MIS11 n= 28 Median= 14,300 counts	1.26Ma-MIS22 n= 21 Median= 11,800 counts	214	0.107 (Cannot reject null-hypothesis)
MIS11-Holocene n= 26 Median= 12,600 counts	1.26Ma-MIS22 n= 21 Median= 11,800 counts	257	0.741 (Cannot reject null-hypothesis)

Table 6.11 Comparison of the XRF Fe count (reflecting contribution of sediments from the ophiolite complex in the south of Grande Terre) of turbidites deposited in different time periods using a Mann-Whitney U test. α=0.05 for rejection of the null hypothesis (that the median turbidite XRF Fe count is the same in the two time periods).

6.5.3.2 Turbidite transport dynamics

The second option is that, that there has been a consistent level of shallow water carbonate production along the New Caledonia margin since 1.26Ma; but, this has not, due to some unknown transport effect: perhaps due to changes in flow intensity, been recorded in MD06-3019. However, this does not seem to be a plausible explanation for the pattern we see. It is unclear why there would be a reduction in turbidite flow intensity (as a result of the export of less material from the upper slope) if carbonate production on the shelf was consistent during the whole time period. It also requires the presence of a barrier reef to be postulated during a time period where from both the findings of this study and borehole work [*Cabioch et al.*, 2008; *Montaggioni et al.*, 2011] there is little evidence of one. Additionally, this barrier reef is required merely so that unknown transport processes can be called into

effect in order that its existence is not recorded at the MD06-3019 core site during the middle period of the record.

With only one record of turbidite sedimentation in the New Caledonia Trough over the last 1.26Myrs it is impossible to entirely rule out the possibility that the patterns of turbidite deposition we see are not due to a transport signal. However, given the evidence collected it seems unlikely. Additionally, comparisons with turbidites in the nearby (<100m) short gravity core MD06-3020 (see Chapter 4 §4.4) do show local coherence in the timing of deposits with MD06-3019 sediments back to MIS5 (~120ka). Rather the most probable explanation of temporal changes in turbidite deposition at core site MD06-3019 is evolution in sediments at the source location.

6.5.4 Source signal: Changes in shallow water carbonate production

The final hypothesis is that temporal changes in shallow water carbonate production and supply along the west New Caledonia margin over the last 1.26Ma can explain the observed patterns of turbidite deposition in core MD06-3019. Temporal variations in reef growth due to changes in sea-level, temperature, salinity etc. are well known and have been noted on timescales commensurate with this study on the Belize Barrier Reef and in the Gulf of Papua [*Gischler et al.*, 2010; *Droxler and Jorry*, 2013]. This study proposes that shallow water carbonate communities of similar extent to the modern day New Caledonia Barrier Reef existed during the period 1.26Ma- MIS23, there was then a significant reduction in shelf carbonate production between MIS23-MIS11, before the establishment of the modern barrier reef at MIS11 which has continued until the present day. This explanation, unlike those previously discussed, requires fewer assumptions.

The proposed expansion of the barrier reef at ~MIS11 agrees with the borehole studies of *Cabioch et al.* (2008) *Montagionni et al.* (2011). By contrast, they state that prior to this period there were no significant reef developments on the western New Caledonia margin and rather it acted as a carbonate ramp/ unrimmed shelf. Possible reasons for this discrepancy occur due to difficulties in investigating early periods of reef growth via boreholes drilled through modern day reef crests. These problems include erosion of previous reefs, large uncertainties in dating and possible lateral movement of the reef crest position (see Chapter 1 §6.2). These sources of uncertainty would be amplified if there had been a gap of ~500kyr between the most recent period of significant reef growth and the previous occurrence.

Changes in reef abundance may also provide an explanation to the variations in turbidite grain size, width and frequency. With a barrier reef present this not only acts as a source of more coarse grained material but also provides a barrier to sediment export to the shelf edge/upper slope [*Cotillon et al.*, 1990; *Dunbar and Dickens*, 2003; *Dubois et al.*, 2008]. This would likely result in fewer turbidites, but those that did occur would be of a greater size and thus carry coarse grained material further. By contrast without the presence of a barrier reef, material could be more easily transported to the shelf edge and consequently more frequent, but smaller events could be expected to occur in agreement with the observation of turbidite frequency. (Variations in the content, grain size, width and frequency of turbidite deposits in core MD06-3019 with respect to glacial- interglacial cycles and possible reef extent are examined in more detail in Chapter 7.)

Overall, whilst it is not possible to rule out the possibility that either dissolution or transport process are responsible for the pattern of turbidite deposition observed in sediment core MD06-3019, neither is considered the most likely explanation. Rather these changes are attributed to variations in shallow shelf carbonate production over the 1.26Myr period covered by the MD06-3019 turbidite record. If this explanation is accepted, the question arises as to what influences shallow shelf carbonate

production over this time period. Possible controls such as sea surface temperature and changes in relative sea-level are, therefore, explored in the next section.

6.6 Controls on shallow water carbonate production

Numerous factors impact on the growth of shallow shelf carbonate producers, with different organisms requiring different conditions and have varying tolerance limits to deviations from these ideal hydrographic and physical settings. Factors include geographic-tectonic, physico-chemical, hydrodynamic and biological variables. (See Appendix 4 for a detailed literature review of the various conditions required for tropical coral reef growth.)

Previous research provides good estimates as to the variation of some of these conditions over the last 1.26Myrs, such as regional SST [*Russon et al.*, 2010] and global eustatic sea-level [*Miller et al.*, 2005]. However, other factors, such as nutrient levels and aragonite saturation state, remain poorly constrained over period. Here the impact of changes in the most accurately quantified variables (SST and eustatic sea-level) on coral reef production over the last 1.26Myrs are explored. *Figure 6.4* shows the changes in the turbidite record of MD06-3019 as well as a regional mean annual SST reconstruction from the western New Caledonia margin using core MD06-3018 [*Russon et al*., 2010] (which is located only ~100km from MD06-3019) and the global eustatic sea-level record [*Miller et al*., 2005].

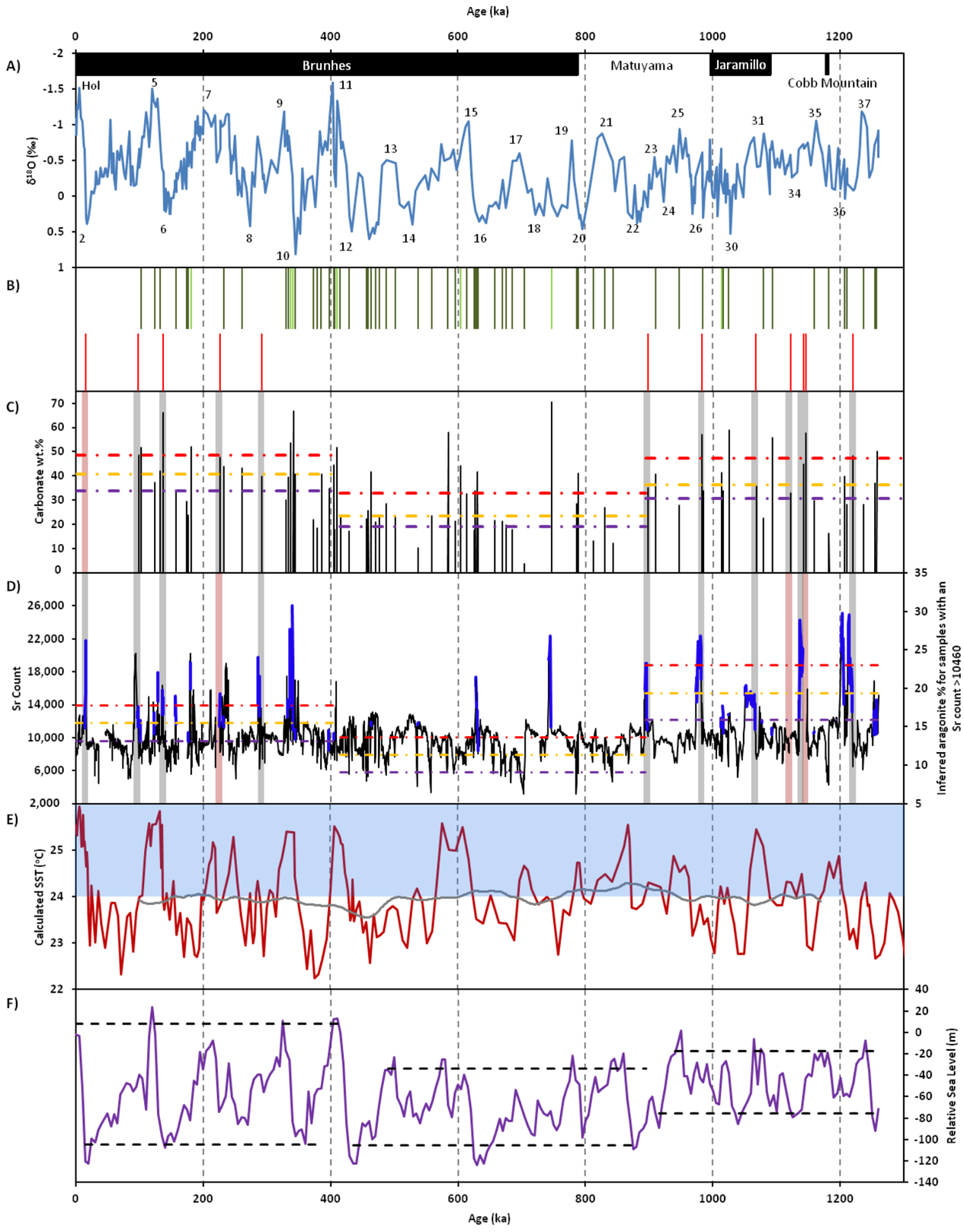

Figure 6.4 A) $\delta^{18}O$ record for MD06-3019 obtained from G. *ruber* foraminifera.
B) Positions of sandy layers. Red: coarse, dark green: dark fine layers, pale green: light fine layers.
C) Carbonate wt. % values for sandy layers with upper quartile (red), median (yellow) and lower quartile (purple) shown for each section. Shaded grey areas show coarse layer positions (red when data missing)
D) XRF Sr counts as a proxy for aragonite. LHS axis: Sr counts. RHS axis: for blue coloured portions of the record- inferred aragonite content of sandy layers with a count value > $\mu_{carbonate\ ooze}+\sigma_{carbonate\ ooze}$ calibrated using XRD. Background aragonite values ~1.3%. Upper quartile, median and lower quartile for Sr counts shown for each section.
E) *Russon et al.*'s 2010 SST reconstruction from MD06-3018 for the New Caledonia area. Grey line shows 200kyr running mean. Blue shaded area represents the temperatures at which extensive coral reef growth can occur.
F) *Miller et al.*'s 2005 global sea-level reconstruction from stacked records. Dotted lines represent average maximum interglacial relative sea-level for the three different time periods.

6.6.1 Changes in Mean Annual Sea Surface Temperature

Changes in sea surface temperatures (SSTs) are known to be a limiting factor controlling coral reef growth. Generally, tropical corals require a minimum annual SST of 18^{o}C. Temperatures between 18-24^{o}C allow for reduced growth and an SST range of 24-34^{o}C is required for extensive growth and barrier reef building activity [*Isern et al.*, 1996; *Kleypas et al.*, 1999; *Montaggioni and Braithwaite*, 2009]. The role of temperature has been highlighted as a potential limiting factor on coral reef growth along the western margin of New Caledonia [*Cabioch*, 2003, *Cabioch et al.*, 2008; *Montaggioni et al.*, 2011]. They postulate that only after MIS11 did climatic conditions become optimal for luxuriant reef growth during highstand periods.

Russon et al. (2010) derived a mean annual SST record for the western New Caledonia margin, using Mg/Ca measurements on planktic G. *ruber* foraminifera from deep sea sediment core MD06-3018 (see *Figure 6.3*). This record provides a high resolution, local reconstruction of mean annual SST changes over the full 1.26Myr period covered by core MD06-3019 (see *Figure 6.4E*). (See Appendix 4 for information on the selection of the SST record used for comparison to changes in MD06-3019 turbidites.)

Reconstructed glacial-interglacial mean annual SST changes round New Caledonia are ~2-3^{o}C with a long term average of 23.9±0.5 ^{o}C since 1.26Ma. Mean annual temperatures for the whole record, during both interglacials and glacials are consistently above the required minimum (18^{o}C) for coral reef growth and all nearly all interglacials have a mean annual temperature greater than 24^{o}C, the temperature required for extensive coral reef growth [*Isern et al.*, 1996]. The exceptions to this being the interglacial periods MIS13, where the temperature is below this threshold and MIS27, 29 and 33; where due to significant noise in the δ^{18}O record between MIS35-27 for core MD06-3019, from which the chronology was derived, it is difficult to establish the precise dates of these events and thus their corresponding SSTs. Since MIS11 mean annual interglacial temperatures have been consistently

higher than previous periods, which could be consistent with the claim of *Cabioch et al.* (2008) and *Montaggioni et al.* (2011) that temperature may have been a limiting factor on reef growth prior to MIS11. Reconstructed mean annual interglacial SSTs since MIS11 have an average of 25.6 ± 0.6ºC; whereas prior to MIS 11, the average reconstructed mean annual interglacial SST value was 24.6 ± 1.0 ºC. These SSTs are only ~1ºC cooler on average and thus close to the analytical uncertainties. During MIS15, 21 and 31 mean annual temperatures reached comparable levels to those post MIS 11 (~25.5ºC), but there are no obviously associated peaks in either turbidite carbonate or aragonite content. Nor is there any obvious consistent or significant decrease in mean annual interglacial temperatures in the period MIS22-MIS11 compared to prior to MIS22, when this thesis argues for an increased level of carbonate production. In summary, there is no clear relationship between the reconstructed mean annual SST record and either the carbonate or aragonite content of turbidites deposited in sediment core MD06-3019.

6.6.2 Changes in Seasonal Sea Surface Temperatures

Whilst mean interglacial SSTs are consistently greater than the 24ºC threshold for extensive coral reef growth [*Isern et al.*, 1996], it is important to consider the effect of seasonal variation. If regional austral winter SSTs drop below the threshold for significant periods of weeks to months, this may cause coral stress and thus reduced growth rates. Transfer function estimates of winter and summer season SSTs were made by Russon in his PhD thesis (2010) for the *Russon et al.* (2010) SST record using the Modern Analogue Technique (MAT) [*Prell*, 1985] and a global training data set (n = 61) [*Imbrie and Kipp*, 1971]. Estimates of SST seasonal amplitude vary from 6±2.2ºC for glacial periods and 3.5 ± 2.2ºC during interglacial periods (see *Figure 6.5*) [*Russon*, 2010].

Estimated summer and winter temperatures for the western New Caledonian margin over the last 1.26Myr can be derived from these seasonality estimates and compared to modern day seasonal temperatures (see *Table 6.12*). Throughout the record

average summer and winter SSTs for interglacial periods lie within the modern range. However, glacial summer and winter SSTs, though within error coinciding with modern temperatures, tend to be on average 0.5-1.5 ^{o}C cooler than modern values and may have fallen below the 18^{o}C limit for coral production [*Isern et al.*, 1996]. Significant levels of carbonate production are only likely to occur during interglacial high stands and the later stages of transgressions, when the shallow shelf is flooded [*Schlager et al.*, 1994]. Therefore, the effect of lower temperatures preventing coral reef growth during glacials is unlikely to have had a significant impact on the total amount of coral reef production when examined over several glacial to interglacial cycles.

Overall, given the similarity between modern and previous average interglacial mean and seasonal SSTs, it is not thought that variations in SST is likely to be the principal control on inferred changes in carbonate production along the western New Caledonia margin over the last 1.26Myrs.

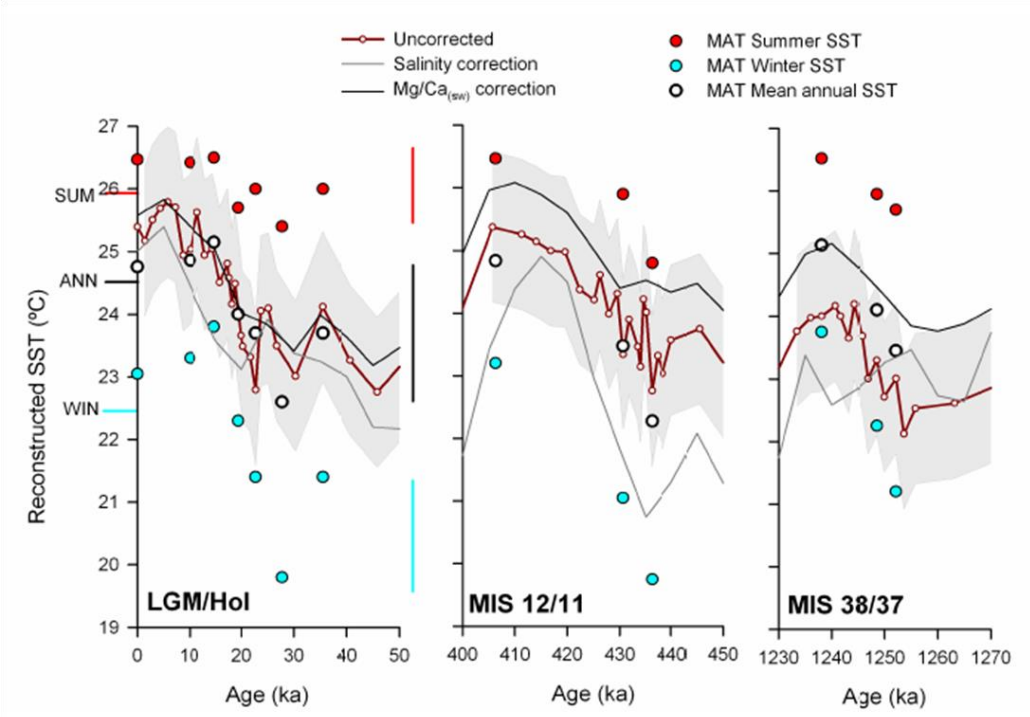

Figure 6.5 Comparison of Mg/Ca-derived and MAT-derived SST estimates across the LGM/Hol, MIS 12/11 and MIS 38/37 terminations. Red line: shows the uncorrected Mg/Ca SST data, at 1-2kyr resolution. Grey line: shows salinity corrected data, at 5kyr resolution. Black line shows $Mg/Ca_{(sw)}$ corrected data, at 5kyr resolution. Grey shaded area shows $\pm 2\sigma_r$ reproducibility error envelope for the uncorrected Mg/Ca-derived SST reconstruction. On the LGM/Hol plot, horizontal bars at the axis show WOA2005 SST values for 0m depth at the core-site [*Locarnini et al.*, 2006]. Vertical bars show statistical uncertainties on the MAT-derived SST estimates; the statistical uncertainty for the mean-annual SST estimate was calculated using standard error propagation formulae. (From *Russon*, 2010)

Time period		Average SST	Estimated summer SST	Estimated winter SST
		°C		
Modern		24.5	26-28	21-23
MIS11-Holocene	**Interglacial**	25.6 ± 0.6	27.4 ± 1.7	23.9 ±1.7
	Glacial	22.6 ± 0.6	25.6 ± 1.7	19.6 ± 1.7
MIS22-MIS11	**Interglacial**	24.9 ± 0.5	26.7 ± 1.6	23.2 ± 1.6
	Glacial	23.3 ± 0.5	26.3 ± 1.6	20.3 ± 1.6
1.26Ma-MIS 22	**Interglacial**	24.3 ± 0.5	26.1 ± 1.6	22.6 ± 1.6
	Glacial	23.0 ± 0.4	26.0 ± 1.5	20.0 ± 1.5

Table 6.12 Modern summer and winter SST values for the western New Caledonian margin [*Cabioch et al.*, 1995] and estimates for the last 1.26Myr [*Russon*, 2010].

6.6.3 Sea-level change

Global sea-level has fluctuated dramatically (~+10 to -120m) over the Quaternary due to glacial-interglacial climate cycles (eustatic sea-level change) [*Waelbroeck et al.*,2002; *Lea et al.*, 2002; *Siddall et al.*, 2003; *Miller et al.*, 2005; *Rohling et al.*,2009; *Siddall et al,.* 2010; *Elderfield et al.*,2012; *Bates et al*, 2014] and this has led to significant changes in the extent, nature and distribution of reef habitats [*Montaggioni and Braithwaite*, 2009]. The effect of this sea-level change on reef development at a particular locality depends on the relative sea-level: the interaction between eustatic sea-level, subsidence/uplift rates and margin morphology in individual locations [*Hubbard et al.*, 1988; *Montaggioni and Braithwaite*, 2009]. Variations in relative sea-level not only affect the amount of suitable substrate available for coral reef settlements, but also the rate at which sea-level change occurs can control reef development [*Neumann and MacIntyre*, 1985]. If relative sea-level rise outstrips the production rate of reefs they may drown, alternatively slow sea-level rise or sea-level fall causes a reduction in accommodation space and so limits reef growth [*Montaggioni and Braithwaite*, 2009].

Unlike the *Russon et al.* (2010) SST reconstruction there is no relative sea-level curve for the western New Caledonia margin or even a eustatic curve obtained from

the locality. For this thesis, therefore, the global *Miller et al*. (2005) eustatic sea-level curve (see *Figure 6.4F*) has been used to make a comparison between sea-level change and evolution in the nature of turbidite deposits observed in MD06-3019. (See Appendix 4 for information on the selection of sea-level reconstruction used in this work.)

A prominent feature of the eustatic sea-level record is the reduction in the height of highstand sea-levels for interglacials between MIS23-13. These lower temperature, lower sea-level highstands are known as the 'lukewarm interglacials' [*Masson-Delmotte et al.*, 2010; *Jaccard et al.*, 2013]. There is also a significant drop in glacial sea-level from MIS22 onwards, which is attributed to a large expansion of the Antarctic Ice Sheet [*Elderfield et al.*, 2012].

The modern western New Caledonia margin is characterised by a shallow shelf, with an average lagoon depth of ~18m, and a steeply dipping slope from the shelf break down into the deep basin, and thus is classified as an escarpment margin [*Le Roy et al.*, 2008]. However, the evolution of the morphology of the margin over the last 1.26Myr remains poorly constrained (see Chapter 7). Thus the simplest assumption, that net subsidence has been matched by net accumulation at the shelf edge, such that the height and profile of the shelf have remained relatively constant, is used here. A relative sea-level drop of -70 to -130m would mean that during any glacial period since 1.26Ma the shelf would be entirely exposed, and any carbonate production would be limited to a narrow band on the steep slope [*Schlager et al.*, 1994]. However, the variation in highstand sea-level (see *Figure 6.4F*) could have had a significant impact on the amount of carbonate production on the shelf. This is because the relatively shallow dip of the shelf means that flooding during transgressions can work as a threshold process. Once sea-level has risen the past shelf-break, the shallow shelf quickly floods and carbonate production can take off. However, at any level, regardless as to whether this is 2m or 120m, below the

threshold carbonate production would be limited to a narrow band on the slope [*Schlager et al.*, 1994].

This evolution in reconstructed relative sea-level fits well with the timing of changes in turbidite deposition in core MD06-3019 (see *Figure 6.4*). It is therefore thought that changes in the height of sea-level during inter-glacial periods are likely to have had a significant effect on the level of carbonate production on the shallow shelf, which in turn is responsible for the temporal variations seen in turbidite deposition in core MD06-3019. It is proposed that higher sea-levels during some interglacial periods prior to MIS23 allowed significant carbonate production (comparable to the last 400ka) to occur during certain interglacials, with a significant reduction of carbonate production between MIS22-MIS12 as the relative height of interglacial sea-level fell; before the documented expansion of the barrier reef during the long, warm, high sea-level MIS11 period. *Figure 6.6* provides a cartoon explanation of the possible effect of sea-level change on the space available for carbonate production over the last 1.26Myr.

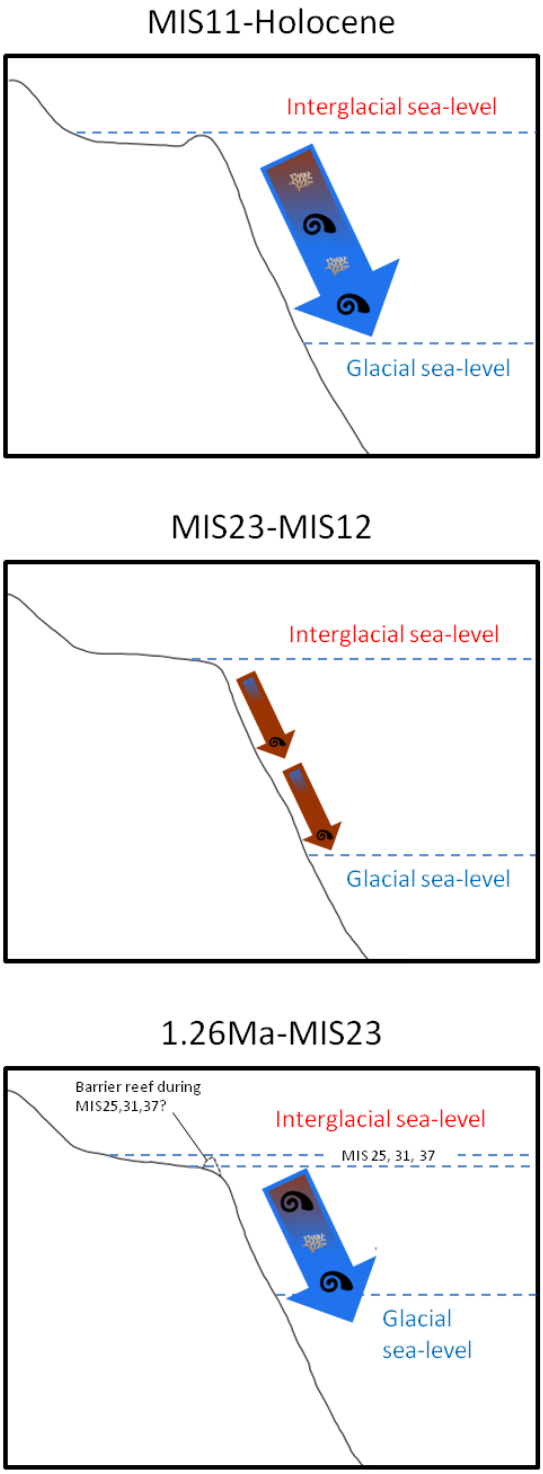

Figure 6.6 Cartoon (not to scale) showing the effect of changing glacial-interglacial sea-level on the area available for shallow water carbonate production on the western New Caledonia margin over the last 1.26Myr. Arrows represent the proposed effect of these changes in shallow water production on on turbidites in terms of turbidite composition (blue indicates greater carbonate content, brown indicated greater siliciclastic content, symbols indicate greater or lesser bioclasts content), volume (size of arrow) and frequency (number of arrows).

6.6.4 Support for the sea-level change control hypothesis

Figure 6.6 in the previous section provides a basic working hypothesis, illustrating how changes in sea-level may have affected coral reef production on the western New Caledonia margin since 1.26Ma. The flooding of the shallow shelf is likely to be a threshold process and the shelf has the potential to flood quickly once sea-level passes a critical level. Thus small scale differences (±5m) in sea-level could cause significant variation in the amount of carbonate production possible. Therefore, accurate, relative sea-level information and a knowledge of the evolution of the margin morphology is needed to prove the hypothesis that sea-level would have been a significant control on shallow water carbonate production over the last 1.26Myr.

The *Miller et al.*, (2005) eustatic sea-level curve does not provide the relative sea-level curve for the New Caledonia area, which is dependent on the interaction between subsidence rates, sediment accumulation and eustatic sea-level change. For example, MIS5 relative sea-level for the area is believed to have peaked at +6m compared to modern day values [*Frank et al.*, 2006]. However, values from the *Miller et al*. (2005) eustatic sea-level curve place the sea-level at +24m, similarly the *Elderfield et al.* (2012) curve places MIS5 sea-level at ~ +18m and the *Bates et al.* (2014) reconstructions vary from -11m to +14m depending on location. Subsidence rates, based on U/Th dates on fossil corals, are available back to MIS5 (125ka) for the west New Caledonian margin. This work yields estimates ranging from 0.03-0.2cm/kyr [*Cabioch et al*., 1995; *Frank et al.*, 2006] depending on location. However, by comparison with magnetostratigraphic results these subsidence rates do not yield accurate values for reef accumulation when applied to older reef units [*Cabioch et al.*, 2008]. Additionally, subsidence is known to be non-uniform along the margin (see Chapter 2 §2.4.1) [*Cabioch et al.*, 1995; *Frank et al.*, 2006; *Andréfouët et al.*, 2009]. Such discrepancies are likely to result from differential temporal and geographical tectonic movements affecting the New Caledonian mainland during the late Quaternary [*Cabioch et al.*, 2008]. It is impossible, therefore, to provide a reliable relative sea-level curve over the last 1.26Myrs spanned by core MD06-3019.

The history of margin morphology over the last 1.26Myr, which sea-level interacts with, is also poorly constrained. *Cabioch et al.* (2008) and *Montaggioni et al.* (2011) describe the margin before MIS11 as an 'open shelf margin, i.e. a ramp or non-rimmed platform', but the slope and extent of this open shelf margin is unknown. The history of the development of the lagoon is also open to debate; some authors have suggested that lagoon sediments date back to the Mid-Pleistocene [*Lafoy et al.*, 2000]. Others have argue that the lagoon was only flooded during MIS5 (or perhaps MIS7) with the barrier reef presumably being a fringing reef between MIS11 until that point [*Le Roy et al.*, 2008].

The exact nature of the interaction between eustatic sea-level change and the western New Caledonia margin is unknown. However, the plausibility of the hypothesis that variations in the amplitude of glacial-interglacial sea-level change have been a significant control on carbonate production levels on the New Caledonia margin is supported by work conducted on other modern day tropical reefs such as in Belize and the Gulf of Papua [*Gischler et al.*, 2010; *Droxler and Jorry*, 2013].

Gischler et al., (2010) cite high-amplitude eustatic sea-level fluctuations as being the major control on Pleistocene facies variation in Belize (see *Figure 6.7*). Their reef borehole records show a dominance of mollusc rich wakestones and coral packstones and marls at the base. These are thought to have been deposited prior to ~900ka during the high sea-levels of MIS25, 31 and 37 [*Gischler et al.*, 2010] (see *Figure 6.7*). The sediment cores are then dominated by siliciclastic sediments laid down during the mid-Pleistocene; a period of comparatively low sea-level highstands MIS23- MIS13 [*Miller et al.*, 2005], when the shelf is believed to have been generally sub-aerially exposed [*Gischler et al.*, 2010]. Finally, the upper most sediments return to carbonate deposits with coral reef packstones and grainstones, deposited during highstands since MIS11. *Gischler et al*. (2010) hypothesise that the

long highstand of MIS11 allowed the development of the modern barrier reef along former glacial siliciclastic shorelines at the shelf edge.

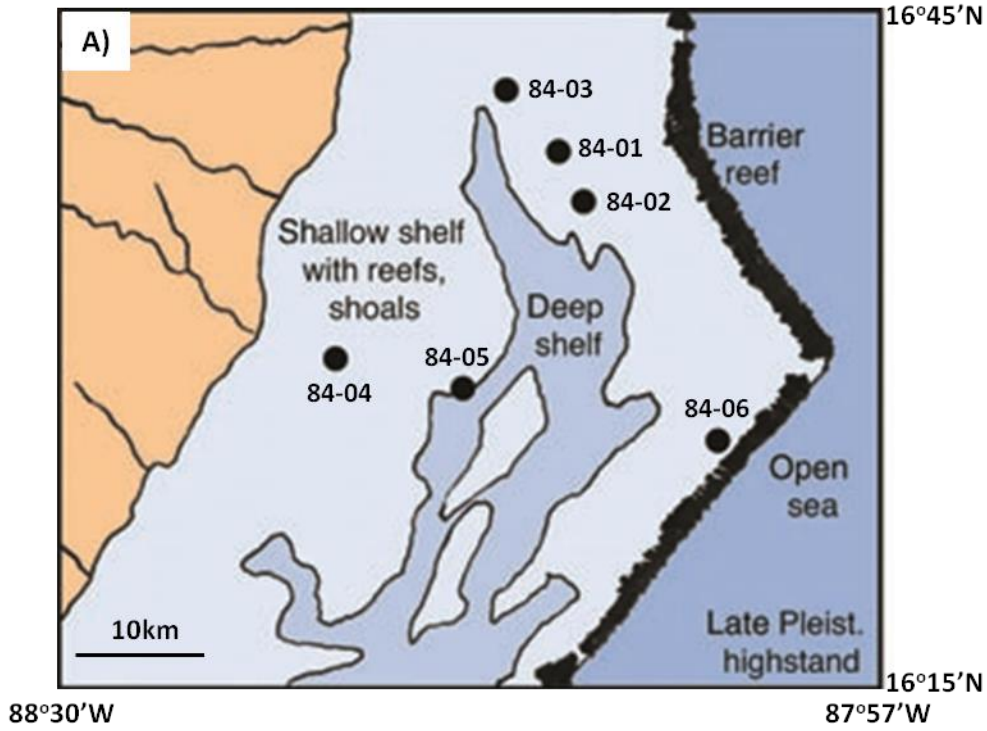

Figure 6.7 A) Sketch map of part of the modern day Belize margin (showing the positions of borehole records used in the production of the stratigraphic model of the area [*Gischler et al.*, 2010]. Peach: land areas, light blue: shallow shelf with reefs and shoals, middle blue deeper shelf, dark blue: open Caribbean Sea and black: barrier reef. **(**From *Gischler et al.*, 2010.)

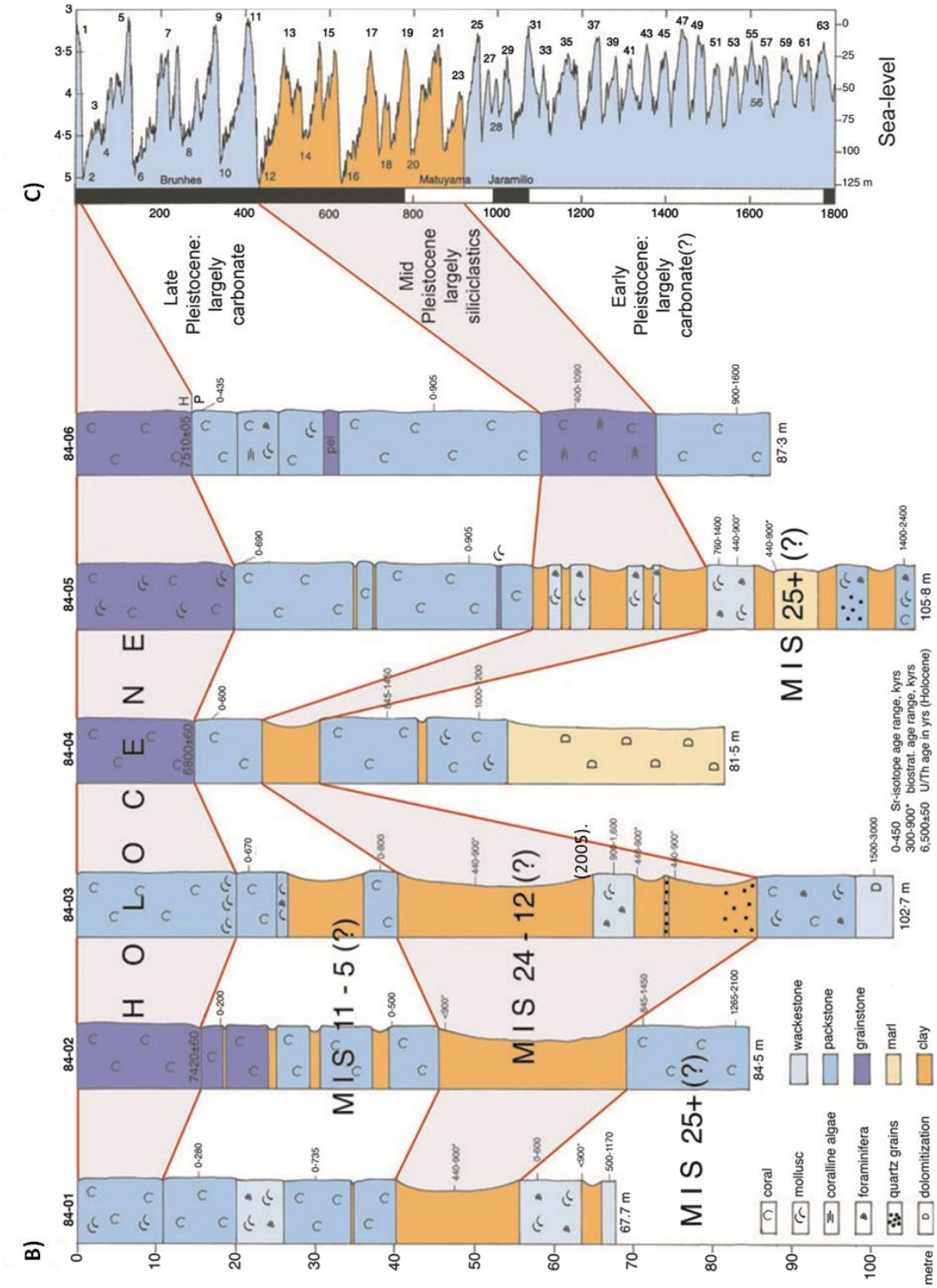

Figure 6.7 B) Stratigraphic model for reef boreholes taken from the Belize margin. **C)** Pleistocene sea-level curve of *Lisiecki and Raymo* (2005). (From *Gischler et al.*, 2010.)

Similarly *Droxler and Jorry* (2013) comment that during the late Pliocene and Quaternary, short-lived reefal platforms and barriers were able to grow along the Gulf of Papua shelf edge during intervals of high-amplitude sea-level transgression. They attribute former reef developments seen in seismics profiles of the Gulf of Papua to the high sea-level interglacials of MIS31 and MIS47/49 (see *Figure 6.8).*

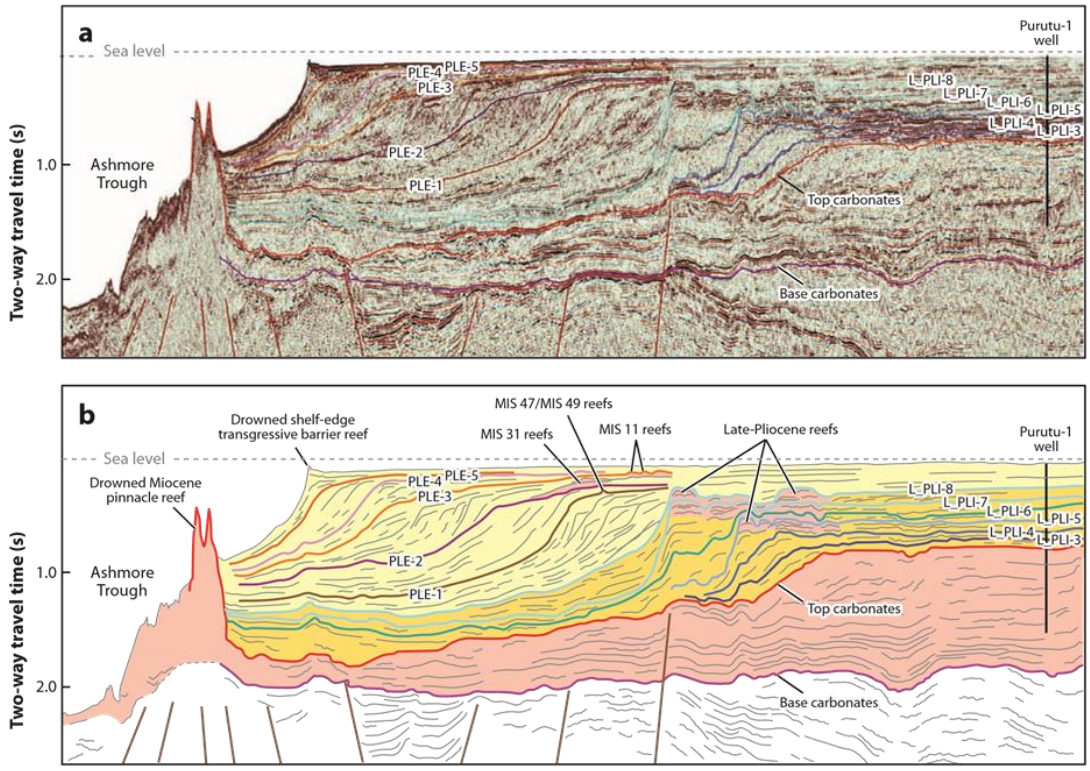

Figure 6.8 A) Seismic profile showing late-Pliocene (L_PLI) and Pleistocene (PLE) sequences developed along the Gulf of Papua shelf edge (after *Tcherepanov et al.*, 2010). **B)** Interpreted seismic profile. PLE-1is thought to correspond to units deposited between 2.7 to 1.6 Myr, PLE-2 to those between 1.5 to 1.1 Myr; PLE-3 to approximately 1.0 to 0.6 Myr; PLE-4 between 0.6- 0.33 and PLE-5 0.33Myr-present. (From *Droxler and Jorry*, 2013.)

Overall, given the concurrence of timing in the evolution of the eustatic sea-level curve and the changes in turbidite deposition, it is proposed that variations in glacial-interglacial sea-level change over the last 1.26Myr has been a significant control on the evolution of carbonate production on the western New Caledonia margin.

6.7 Conclusions

There is a significant evolution in the nature of turbidite deposits in core MD06-3019 over the 1.26Myr record. Compared to 1.26Ma- MIS22 and MIS11-Holocene, the period MIS22-MIS11 contains no coarse grained turbidites, only fine grained; an increased frequency of turbidite deposition but an overall reduction in turbidite accumulation rate and a significant reduction in total carbonate and aragonite content. Additionally, the nature of turbidites deposited during the periods 1.26Myr-MIS22 and MIS11-present are largely indistinguishable from each other. This supports the work of previous borehole studies in the area, which proposed that the New Caledonian Barrier Reef (NCBR) evolved from an open carbonate ramp with patch reefs into a rimmed shelf at around MIS11 [*Cabioch et al.*, 2008; *Montaggioni et al.*, 2011]. However, the additional change in the nature of turbidite deposition at MIS22, suggests a more complex picture in earlier periods than that proposed by previous work. Therefore, overall these results only partially support hypothesis 1 (outlined in Chapter 1); since whilst a change in the composition of turbidite deposition was seen at MIS11, this was not the only evolution in the record as had been predicted.

Given that this study only examined one sediment core from the New Caledonia Trough, it is impossible to rule out a scenario whereby transport or dissolution processes were responsible for the observed pattern of turbidite deposition. However, there is a substantial body of evidence which supports the claim that the observed changes in the nature of turbidite deposition are due to variations in the abundance of shallow shelf carbonate material through time. This work suggests that shallow water carbonate production decreased substantially during the period MIS23-MIS13. It is hypothesised that the principal control on this is glacial-interglacial sea-level change, since there is a clear relationship between available sea-level curves [*Miller et al.*, 2005; *Siddall et al,.* 2010; *Elderfield et al.*,2012; *Bates et al.*, 2014] and the timing of changes in the nature of turbidite deposition in sediment core MD06-3019. However,

other possible controls such as sea surface temperatures, though thought unlikely, cannot be entirely excluded at this stage.

Overall the results of this chapter do not appear to support hypothesis 2 (outlined in Chapter 1), that the main control on coral reef growth along the western New Caledonia margin was SST. Rather the proposed model of the evolution in carbonate production on the west New Caledonian margin is that: 1) prior to MIS23 sea-level was high enough during at least certain interglacial periods for significant carbonate production to occur on the shelf (either as an un-rimmed carbonate platform or with barrier reef development at the shelf edge). 2) From MIS23 the climate proceeded into the period of 'lukewarm' interglacials with lower sea-levels. It is hypothesised that during this period sea-level did not rise enough during highstands to flood the shelf sufficiently (if at all) to allow for significant shallow water carbonate production. 3) The high sea-levels of the long, warm MIS11then allowed for the expansion of the barrier reef and its continuation during subsequent interglacial periods until the current day.

Chapter 7: A 1.26Myr record of mixed siliciclastic-carbonate turbidite deposition in the New Caledonia Trough

7.1 Chapter Abstract

Hypotheses outlining the processes of sediment shedding on pure siliciclastic and carbonate margins due to changes in sea-level are well established (the ‘lowstand’ and ‘highstand’ hypotheses respectively). By contrast, studies on mixed siliciclastic-carbonate margins are far less common and yield differing hypotheses as to how sediment shedding occurs in relation to glacial-interglacial sea-level change. Additionally, much of this work is focused on fine grained sediment shedding and does not include the likely significant contribution of turbidite deposition to sediment accumulation in slope and basin settings.

This work provides the first quantitative analysis of deep sea turbidite sedimentation in the New Caledonia Trough over the last 17 glacial-interglacial cycles (~1.26Myr) from the study of sediment core MD06-3019. It is unprecedented in analysing a

turbidite record covering the last million years, sourced from a mixed siliciclastic-carbonate margin. By providing evidence from a longer record of sedimentation than has previously been investigated, on a margin where deep sea turbidite deposition has not previously been studied, this work will help to contribute towards a greater understanding of how sediment shedding to the deep sea from mixed margins via turbidites operates. This chapter investigates the role of possible controls, such as glacial-interglacial sea-level change and variations in shallow shelf carbonate production, on turbidite sedimentation. The significance of patterns in the timing and frequency of turbidite events recorded in sediment core MD06-3019 were assessed via Monte Carlo analysis and temporal changes in the content and layer width of turbidites by Mann-Whitney U tests.

Results show that there is a clear evolution in the nature of turbidite deposits in core MD06-3019 over the 1.26Myr record. Compared to periods 1.26Ma- MIS23 (910ka) and MIS11 (~400ka) - present, the interval MIS23-MIS11 (~910ka-400ka) contains no coarse grained turbidites, only fine grained; shows a significant reduction in the carbonate and aragonite content of turbidites; as well as a decrease in layer width. It is proposed that these variations are due to a substantial reduction in shallow water carbonate production between MIS23-MIS13, as a result of changes in the amplitude of glacial-interglacial sea-level change (see Chapter 6).

The repeated clustering of turbidite events within ±4kyr of each other occurs throughout the MD06-3019 record, in all phases of glacial-interglacial cycles and is a significant feature. These clusters are possibly due to seismic activity either on land or in the lagoon due to faults in the peridotite nappe, which forms the south of Grande Terre, or on the nearby arc trench system of the New Hebrides, approximately 200-300km west of New Caledonia.

In contrast to previous studies [*Jorry et al.*, 2008; *Webster et al.*, 2012; *Puga-Bernabéu et al.*, 2014], over the complete 1.26Myr MD06-3019 record there does not appear to be any relationship between the timing, frequency, content, grain size or layer width of turbidites and their depositional timing in relation to glacial-interglacial cycles. This finding holds across the record as a whole and during shorter sub-periods, delineated by different levels of carbonate production or amplitudes of glacial-interglacial sea-level change, which may be expected to have produced different glacial-interglacial patterns of turbidite sedimentation. Possible reasons for this apparent lack of relationship between turbidite deposition and glacial-interglacial sea-level change include: the distal position of sediment core MD06-3019 from the western New Caledonian margin which means that not all gravity flow events were necessarily recorded at the site, the storage and mixing of sediments on the outer shelf/ upper slope on 10kyr time scales before export as turbidites to the deep sea and the influence of seismic events in triggering turbidites which may 'mask' glacial-interglacial sea-level change driven patterns in turbidite deposition.

For sediment core MD06-3019 this means broad scale patterns in turbidite content, grain size and width on a 100kyr time scales may help to elucidate changes on the shallow shelf. However, it is not possible to identify temporal changes in turbidite deposition on glacial-interglacial timescales in relation to variations in the amplitude of sea-level change, shallow-shelf carbonate production, margin morphology or sediment routing.

7.2 Introduction

The previous chapter made use of the temporal changes in the content of turbidites deposited in deep sea core MD06-3019, on a 400-500kyr timescale, to make inferences as to the history of carbonate production on the western New Caledonia margin over the last 1.26Myr. This chapter aims to investigate, on orbital timescales, how the timing and content of turbidite deposition in the New Caledonia Trough has responded to glacial-interglacial sea-level cycles, changes in amplitude of these cycles and variations in morphology and carbonate production of the shallow shelf.

7.2.1 Highstand versus lowstand shedding on pure siliciclastic or carbonate margins

The development of sequence stratigraphy began in the 1970s and provides an understanding of how changes in sea-level affect the export of material from the shallow shelf to the deep sea [*Vail et al.,* 1977]. Initially, the same principles were applied to both siliciclastic and carbonate margins; however, there are fundamental differences in the assumptions that need to be made for the different systems [*Handford and Loucks,* 1993]. In siliciclastic systems sediment is of extrabasinal origin, delivered by fluvial and deltaic systems which drain land updip from the basin. However, carbonate sediments are not necessarily delivered but rather can be produced in the basin by organic and inorganic processes [*James,* 1979]. Today it is accepted that while traditional sequence stratigraphy applies to siliciclastic margins, differing processes control the export of material on carbonate platforms. Whilst there is some disagreement, it is generally considered that the 'highstand shedding' hypothesis for carbonate platforms [*Schlager, Reijmer and Droxler,* 1994] is as robust as the 'lowstand shedding' hypothesis for siliciclastic margins. It is important that the difference in sediment export from carbonate and siliciclastic margins is understood, so as errors do not occur in the interpretation of past sediments with respect to sea-level changes. It should also be noted for both systems that individual locations may show variations from the basic hypothesis due to differences in topography and other regional controls.

The ‘lowstand shedding’ hypothesis for pure siliciclastic margins proposes that most sediment is shed to the adjacent basins during lowstand periods (see *Figure 7.1)*:

1. During highstands sediment is deposited on the flooded inner shelf and only very fine grained sediment is exported out to the continental rise.
2. During lowstands sediment is carried, via rivers, across the exposed continental shelf and deposited directly on the outer shelf and upper slope. Turbidites then carry this material out to the continental rise and abyssal plain. In addition to this, sediments from the previous highstand are now exposed to erosion, further increasing sediment supply to the outer shelf and upper slope.

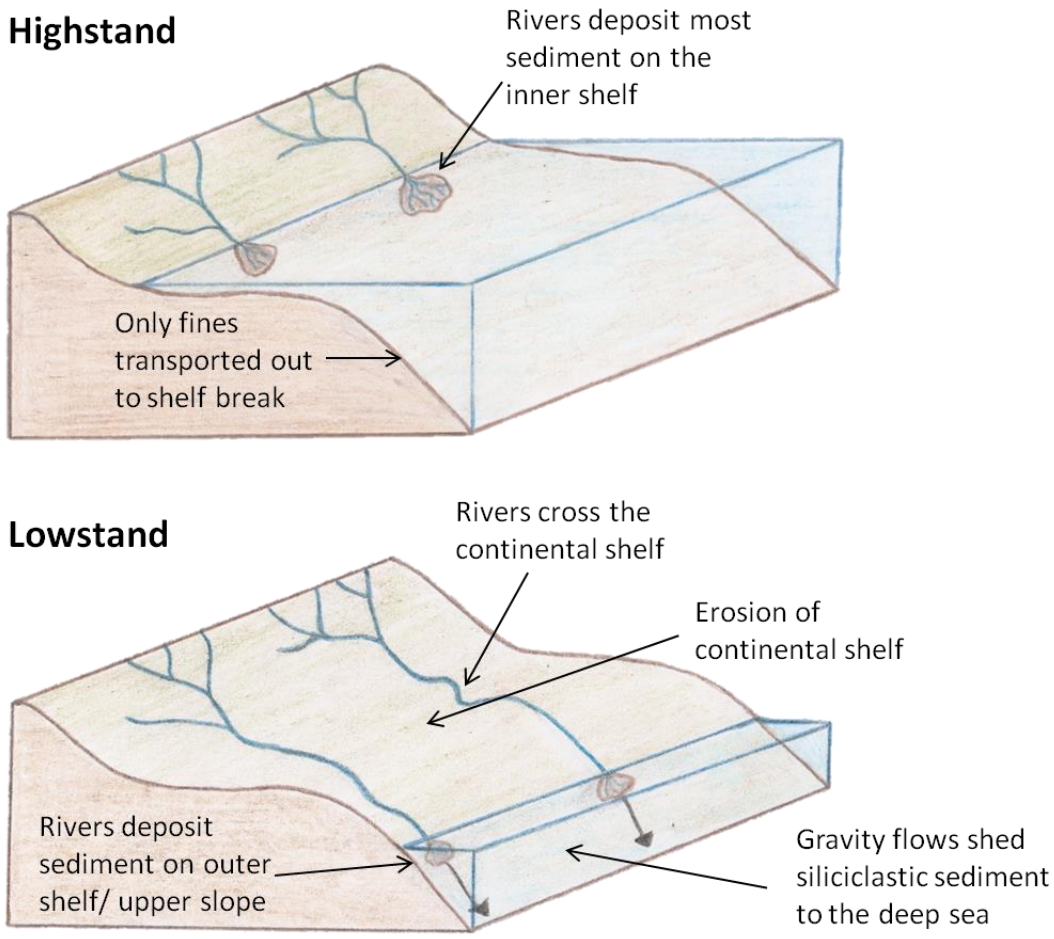

Figure 7.1 Cartoon (not to scale) illustrating the lowstand shedding hypothesis for pure siliciclastic margins.

The ‘highstand shedding’ hypothesis for pure carbonate systems proposes that most sediment is shed from the shallow shelf to the surrounding basins during highstand periods [*Droxler and Schlager*, 1985; *Schlager, Reijmer and Droxler*, 1994] (see *Figure 7.2*):

1. During highstands the shallow shelf is flooded, this causes a large increase in carbonate production compared to glacial periods. This production exceeds carbonate accumulation, both at the rim and in areas of lower production in the lagoon. This excess material is then exported to adjacent basins and thick deposits, associated with highstands, are seen both in shallow and deep sediment records. This increase in sediment export occurs concurrently with flooding of the carbonate bank rather than the period of fastest sea-level rise. (If, however, the platform is drowned carbonate production and export ceases.)
2. During lowstands the shelf is exposed leading to a significant reduction in carbonate production. The highstand sediment platform is also rapidly lithified, in low-latitude areas, as sea-level falls and it is exposed to fresh water; this limits the amount mechanical erosion that can occur. Extant Holocene carbonate platforms show evidence of extensive lithification in less than 1,000years [*Halley and Harris*, 1979]. Export of sediments to adjacent basins is thus reduced, though not necessarily stopped, and deposits are dominated by pelagic input.

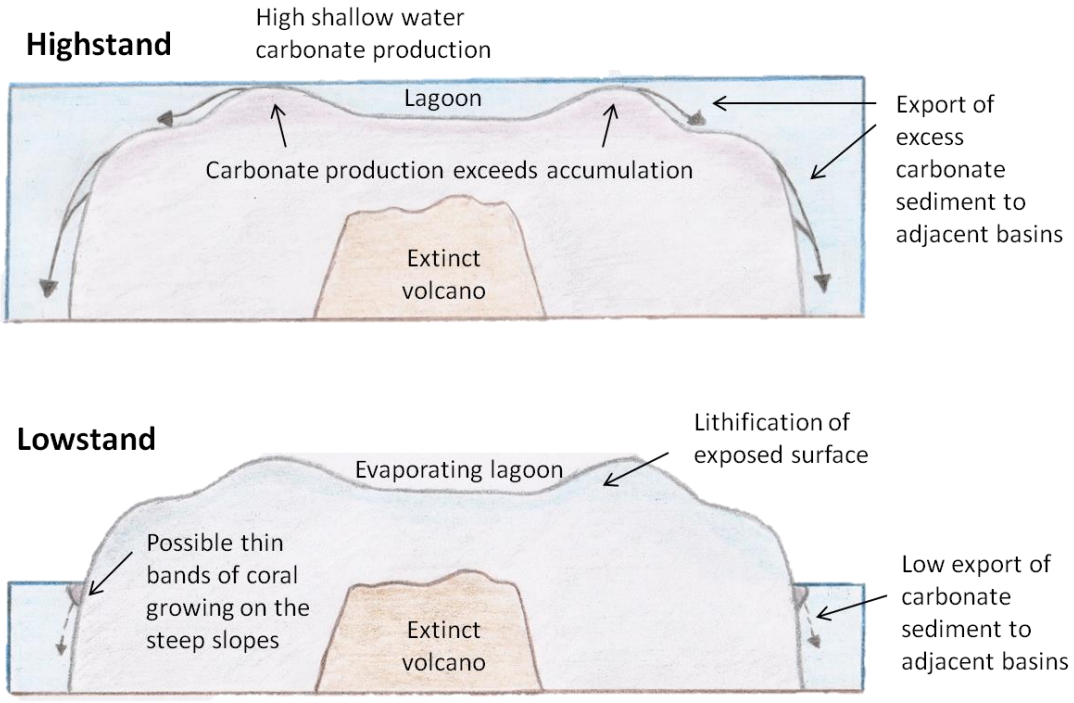

Figure 7.2 Cartoon (not to scale) illustrating the highstand shedding hypothesis for pure carbonate margins, in this case an atoll.

The 'highstand shedding' hypothesis has been shown to occur during the Quaternary for all tropical rimmed pure carbonate systems studied to date, in the Bahamas [*Droxler and Schlager*, 1985; *Schlager, Reijmer and Droxler*, 1994], Caribbean [*Hanna and Moore*, 1979] and Maldives [*Paul et al.*, 2012]. The phenomenon is seen in both the aragonite content of periplatform carbonate ooze, bulk sedimentation rates as well as turbidite frequency and accumulation rates. Though the topography of the platform top and margin can significantly affect the basic trend, carbonate platforms are generally very flat and so are flooded or exposed very quickly once sea-level passes a critical level [*Droxler and Schlager*, 1985]. Also compared to siliciclastic margins they frequently build rimmed platforms associated with reefs and sand shoals and hence the shelf break is more pronounced. Thus rimmed platforms operate two contrasting modes, connected by extremely rapid transitions: highstands when the platform top is flooded and lowstands when the top is exposed and sea-level impinges further down the slope, though whether this is 10m or 100m

below has little effect on sediment export since the platform is exposed either way. By comparison siliciclastic margins tend to have a steeper, more uniform shelf gradient and thus the system is less sensitive to movements in sea-level.

7.2.2 Sediment shedding on mixed siliciclastic-carbonate margins

Numerous studies have been conducted on sediment shedding from both pure carbonate [*Hanna and Moore*, 1979; *Droxler and Schlager*, 1985; *Schlager, Reijmer and Droxler*, 1994; *Paul et al.*, 2012] and siliciclastic systems [*Vail et al.*, 1977; *Vail*, 1987; *Haq et al.*, 1987; *Posamentier and Vail*, 1988]. Work has also been conducted on some ancient mixed siliciclastic and carbonate systems such as the Devonain reef complex of the Canning Basin, Western Australia [*Southgate et al.*, 1993] and the Permian Capitan Formation in Guadalupe Mountains of west Texas and New Mexico [*Silver and Todd*, 1969; *Meissner*, 1972; *Reeckmann*, 1985; *Borer and Harris*, 1991; *Brown and Loucks*, 1993; *Melim and Scholle*, 1995]; the study of which lead to the concept of reciprocal sedimentation with basinal deposition of highstand carbonates and lowstand siliciclastics. However, remarkably few studies have examined late Quaternary sediment accumulation in basins along mixed siliciclastic-carbonate margins; this is despite the expectation that special sequences of siliciclastic and carbonate turbidites will occur in basins along tropical mixed margins [*Jorry et al.*, 2008]. *Mount* (1985) suggests that this reluctance to study mixed siliciclastic-carbonate systems is rooted in the pedagogical belief that carbonate production on shallow shelves is inhibited by the influx of siliciclastic material and thus the two sediments should not and do not commingle. However, the occurrence of mixed siliciclastic and carbonate sediments in both modern and ancient systems, whilst not abundant, shows that such systems are not just geological oddities [*Mount*, 1984; *Mount*, 1985].

Studies that have been conducted on Quaternary mixed siliciclastic-carbonate margins produce a variety of hypotheses as to how sediment shedding occurs. Whilst all agree that carbonate shedding is greatest during highstands, the timing of

maximum siliciclastic deposition in the deeper basin is still a matter of debate. The first, and perhaps most intuitive hypothesis, is the 'reciprocal shedding model'; whereby the margin shows alternately highstand carbonate shedding and lowstand siliciclastic shedding [*Handford and Loucks*, 1993; *Schlager et al.*, 1994; *Ferro et al.*, 1999]. By contrast, others argue for the 'trangsressive shedding model' based on results from off the Great Barrier Reef [*Dunbar et al.*, 2000; *Dunbar and Dickens*, 2003; *Page et al.*, 2003]. This model predicts that the highest fluxes of siliciclastic material to the slope and deep basin occur during the later stages of transgressions. The pattern is thought to be the result of siliciclastic material, that was deposited and trapped on the shelf behind the topographic high of karstified barrier reefs during lowstands, being mobilised due to reflooding and wave driven currents. Finally, *Francis et al*. (2007), who also studied the Great Barrier Reef, argued for a 'coeval shedding model' where the highest fluxes of both carbonate and siliciclastic material occur at the same time during highstands, though the accumulation of carbonate is higher than siliciclastics.

It is noted, however, that these models of sediment shedding on mixed siliciclastic-carbonate margins have been focused almost exclusively on fine grained material deposited as hemipelagic or pelagic sediments. Thus they overlook the likely significant contribution of turbidite deposition to sediment accumulation in slope and basin settings and it remains uncertain whether the patterns of sediment shedding to the deep sea via turbidites, or other mass wasting events, are in phase with the export of fines [*Webster et al.*, 20012; *Puga-Bernabéu et al.*, 2014].

More recently a limited number of studies have examined the pattern of Late Quaternary turbidite deposition along mixed margins in relation to sea-level; for example in the Pandora Trough, Gulf of Papua [*Jorry et al.*, 2008] and along the Great Barrier Reef on the north-eastern Australian margin [*Webster et al.*, 2012; *Puga-Bernabéu et al.*, 2014]. These studies highlight the importance of understanding the variable physiography of mixed siliciclastic-carbonate margins in

order to be able to correctly interpret patterns of deep water turbidite deposition along a mixed margin in a sequence stratigraphic context. In the Pandora Trough siliciclastic turbidites are seen to be associated with low sea-level periods and calciturbidites with sea-level highs and periods of shallow shelf reflooding [*Jorry et al.*, 2008]. It is important to note though, that in the Pandora Trough study the sources of the siliciclastic and carbonate sediments are from separate areas. By contrast, no such simple temporal pattern of turbidite deposition was observed along the Great Barrier Reef, where the supply of siliciclastic sediment to the basin is modulated by the presence of the carbonate factory on the shelf in between [*Webster et al.*, 2012; *Puga-Bernabéu et al.*, 2014]. Instead, a wide a variety of turbidite sedimentation patterns are associated with the changing morphology along the margin and how this interacts with fluctuations in sea-level. Calciturbidites dominate in regions with more open-marine conditions at the outer-shelf and where canyons are either slope-confined or less abundant (Palm Passage) [*Puga-Bernabéu et al.*, 2014]. The bathymetry of the region affects when turn-on and maintenance of carbonate production occurs and thus the availability of carbonate sediment to be supplied to the deep. For instance, it is noted by *Harper et al.* (2015) for the central GBR that periods of highest carbonate export are not necessarily linked with the peak of highstand sea-level, due to reef drowning, but rather when the largest proportion of the shelf is in the photic zone. By contrast, siliciclastic and mixed turbidites are associated with canyons which indent the shelf-break and well developed shelf-edge barrier reefs which can block and store sediment on the shelf behind them (Ribbon Reef). Turbidite deposition is sustained while the sea-level position allows a connection to the shelf and sediment bypasses through inter-reef passages and canyons [*Puga-Bernabéu et al.*, 2014]. There is no apparent link between turbidite thickness and sea-level position.

7.2.3 A new study of sediment shedding on a mixed siliciclastic-carbonate margin: New Caledonia

As has been noted in the previous section, studies on the variation of sediment shedding from Quaternary mixed carbonate-siliciclastic margins in relation to sea-

level change are relatively scarce. Those that there are frequently only consider variations in fine grained sedimentation and do not take into account the contribution of turbidites to deep sea sedimentation [*Ferro et al.*, 1999; *Dunbar et al.*, 2000; *Dunbar and Dickens*, 2003; *Francis et al.*, 2007; *Page et al.*, 2003]. Additionally, apart from one exception (which examines sediment records back to 300ka, ~MIS9) [*Dunbar et al.*, 2003], none of the studies investigate sediment shedding prior to MIS3 (~60ka). This means that even those who have examined turbidite deposition have not able to make the required quantitative statistical analyses of patterns of deposition over multiple cycles in order to ascertain whether the patterns they observe are actually associated with sea-level change. Furthermore, the differing patterns of turbidite sedimentation related to variation in margin morphology highlight the necessity of understanding how to adapt generic models to account for variable margin physiography [*Puga-Bernabéu et al.*, 2014]. Therefore, in order to create a comprehensive sedimentation model for mixed carbonate-siliciclastic margins a better knowledge of turbidite deposition and timing is required [*Puga-Bernabéu et al.*, 2014].

Together this means that currently there is no definitive explanation for what controls sediment shedding from mixed margins either for fine grained or turbidite sediments and the role of submarine canyons in delivering turbidites to the deep sea is also poorly understood. *Puga-Bernabéu et al.* (2014) highlight the importance of future work which examines turbidite deposition in other locations world-wide and over several glacial-interglacial cycles, in order to increase our understanding of sediment shedding on mixed margins.

Despite research in the 1980s by *Cotillon et al*., there is relatively little known about the Quaternary turbidite deposition system in the New Caledonia Trough, in terms of turbidite frequency, size, lateral extent, composition and triggering mechanisms (see Chapter 2). This chapter aims to begin to fill this gap by providing the first quantitative analysis of the nature and frequency of turbidite sedimentation in the

New Caledonia Trough over the last 17 glacial-interglacial cycles (~1.2Myr) from the analysis of sediment core MD06-3019.

This study has four principal aims:

1. To examine the major trends in the timing, nature and content of turbidite deposition in the New Caledonia Trough over the last 1.26Myr.
2. To establish if there are any apparent links between glacial-interglacial sea-level change and the timing, grain size, content or layer width of turbidites deposited in deep sea core MD06-3019.
3. To investigate if there is any evidence of temporal change in the MD06-3019 record of turbidite deposition with respect to glacial-interglacial cycles, which indicates the variation in the amplitude of glacial-interglacial cycles since 1.26Ma.
4. To investigate if there is any evidence of temporal change in the MD06-3019 record of turbidite deposition with respect to glacial-interglacial cycles, to support different hypotheses of margin history: contraction of carbonate production during highstands after MIS25, establishment of the barrier reef system at MIS11, flooding of the lagoon at MIS5 and rerouting of the lowstand shelf fluvial system at MIS2 [*Cabioch et al.*, 2008; *Le Roy et al.*, 2008; *Montaggioni et al.*, 2011].

7.3 Controls on sediment production, supply and shedding along the western New Caledonia margin

As noted in §2.2 a wide a variety of turbidite sedimentation patterns are associated with differing margin morphologies and how these morphologies interact with fluctuations in sea-level [*Puga-Bernabéu et al*., 2014]. Therefore, in order to make informed hypotheses as to how sediment shedding via turbidites to the deep sea occurs on mixed siliciclastic-carbonate margins, it is necessary to have a good understanding of the history of the margin over the time period being studied.

However, for the western New Caledonian margin the history of the timing, extent and nature and shallow shelf carbonate production; the morphology of the margin (open carbonate ramp vs. rimmed shelf, presence or absence of a lagoon, presence or absence of slope canyons etc.); the orientation of fluvial drainage systems supplying terrigenous sediment and the position of relative sea-level and therefore its interaction with the margin are not well constrained over the last 1.26Myrs. Previous work provides some information on the history of the area, but there is not always consensus between authors on these topics [*Lafoy et al*., 2000; *Chevillotte et al.*, 2005; *Cabioch et al*., 2008; *Le Roy et al.*, 2008; *Montaggioni et al.*, 2011].

Reef borehole studies by *Cabioch et al.* (2008) and *Montaggioni et al.* (2011), as well as evidence from this thesis, supports the existence of a barrier reef on the western New Caledonian margin, during highstands, since MIS11. During lowstands the shelf is believed to be sub-aerially exposed and carbonate production on the barrier reef suspended. Prior to this time *Cabioch et al.* (2008) and *Montaggioni et al.* (2011) argue for consistent carbonate deposition during interglacial highstands, on an open, shallow water margin, i.e. a ramp or non-rimmed shelf margin. However, results from this thesis suggest that the history of carbonate production on the New Caledonia margin is more complex than initially hypothesised (see Chapter 6). It is proposed that rather than a simple one step history, there was a period of increased

carbonate production, more akin to the present day, during highstands since at least 1.26Ma (the base of the core) until MIS25 (~950ka). There then followed a substantial reduction in shallow shelf carbonate production during highstands between MIS23-MIS13, before the modern day barrier reef was established at MIS11.

From barrier reef borehole studies *Cabioch et al.* (2008) and *Montaggioni et al.* (2011), propose an open carbonate ramp prior to MIS11 (when they cite a rimmed shelf developing), but give no quantification as to its width or slope. From bathymetric and seismic data surveys of the western New Caledonian margin *Lafoy et al.* (2000) dates the appearance of the lagoon to the Mid-Pleistocene (~550ka); whereas *La Roy et al.* (2008) argue that the lagoon is a more recent feature with initial flooding not occurring until MIS7 (~200ka), before full flooding at MIS5 (~125ka). This later interpretation suggests that for the highstands of MIS11, MIS9 and MIS7 the barrier reef was essentially an extensive fringing reef. The work of *Chevillotte et al.* (2005) and *Le Roy et al.* (2008) also suggest that the lowstand fluvial drainage networks that cut across the lagoonal area and through passes in the barrier reef are not older than MIS6. Furthermore, they argue that prior to MIS2 these channels ran parallel to the barrier reef system, transporting their sediment load from the St. Vincent Bay area to the pass of Mato, some 100km south, at the southern most tip of Grande Terre (see *Figure 6.3*). They proposed that it is only since the Last Glacial Maximum, due to the progressive tilt of the lagoon, that the channels have migrated to be orientated perpendicular to the barrier reef and terrigenous sediment supplied through local passes to the upper slope along the entirety of the western New Caledonia margin.

7.4 Analytical Methodology

7.4.1 Analysis of the timing and frequency of deposition of turbidite layers in core MD06-3019: Monte-Carlo simulations

In order to assess the significance of patterns in the timing and frequency of turbidite deposition in deep sea sediment core MD06-3019 a series of Monte Carlo simulation tests have been conducted. The real pattern of turbidite deposition in the core has been compared with thousands of simulated turbidite deposition patterns, which place turbidites randomly. If any aspect of the pattern of actual turbidite deposition lies outside the 5-95% interval of what would be expected from a random distribution, then it is said to be a significant feature and thought likely to have some controlling mechanism behind its occurrence, rather than being a purely stochastic feature. In order to fulfil the four aims three different sets of Monte Carlo simulations were set up. Full details of the parameters used for each Monte-Carlo simulation are available in the digital only Supplementary Data.

Simulation Set 1: A stochastic system? (Aim 1)

Initially, an entirely stochastic system was assumed and the frequency of deposition of all layers over the whole time period was analysed. A Monte-Carlo simulation, of 5,000 repeats, was set up to generate 79 randomly distributed layers across a 1.26Myr time period. The number of layers present in 400, 200 and 100kyr moving windows was then calculated and the distribution of results with time for these simulated layers was then compared to the actual distribution of turbidites in the MD06-3019 record. Layers that were clustered close to each other (±4kyrs), and conceivably related to a single 'trigger' event, were then combined into single points and the distribution re-assessed.

The significance of the gap in coarse layer deposition between 899-292ka was then examined. A Monte-Carlo simulation, of 5,000 repeats, was set up to generate 12 randomly distributed layers (corresponding to the 12 coarse layers in the MD06-3019

record) across a 1.26Myr time period. The number of layers present in 600, 400, 200 and 100kyr moving windows was then calculated and the distribution of results with time for these simulated layers was then compared to the actual distribution of coarse grained turbidites in the MD06-3019 record.

Simulation Set 2: Effect of glacial-interglacial sea-level change on turbidite deposition (Aim 2)

Given the work of *Jorry et al* (2008), *Webster et al.* (2012) and *Puga-Bernabéu et al.*, (2014) it is predicted that the timing and content of turbidites deposited in the deep sea on mixed carbonate-siliciclastic margins will not be entirely stochastic. An obvious possible controlling mechanism is glacial-interglacial sea-level changes, patterns related to which would not have been picked up in the purely stochastic simulation, due to the varying length of cycles. Therefore the timing of turbidite deposition was next examined in relation to glacial- interglacial sea-level change, to investigate whether sea-level appears to be a controlling factor on the deposition of turbidite layers.

Whilst the general global pattern of glacial-interglacial sea-level is known, there is no relative sea-level record specifically for the western New Caledonia margin. The modern day shelf break is at about 70m water depth but there is no well constrained information on subsidence rates, sedimentation rates, margin morphology, the timing of flooding and exposure of the shelf or the rate of change of sea-level rise/fall over the last 1.26Myr. Thus determining the position of the relative-sea level through time and how this interacted with margin morphology is very difficult, even when making frequent and significant assumptions based on the limited data for subsidence and sedimentation rates that we have for the Western New Caledonian margin. Alternatively a simplistic, though unrealistic, model can be used, in which it is assumed that the shelf break has remained at approximately the same position with the same margin morphology throughout the period studied, through a balance of subsidence and sedimentation. In each case a eustatic sea-level curve rather than a

local relative sea-level curve has to be used, even though these records can vary significantly between authors and are known to be incorrect for New Caledonia even in the recent past (MIS5) [*Waelbroeck et al*., 2002; *Lea et al.* 2002; *Siddall et al.*, 2003; *Rohling et al.*, 2009; *Miller et al.*, 2005; *Elderfield et al.*, 2012; *Siddall et al.*, 2010 and *Bates et al*., 2014]. Since neither model is particularly satisfactory or can yield results that can be considered robust, this problem was addressed by testing the sensitivity of results to changes in the definition of glacial, transgression (transition from a glacial to an interglacial), interglacial and regression (transition from an interglacial to glacial) periods. Four definitions were employed (see *Figure 7.3*):

i. **50:50** - the midpoint between the peak and trough $\delta^{18}O$ values marks the cut off between an interglacial and a glacial period.
ii. **33:33:33** - the amplitude between peak and trough $\delta^{18}O$ values is split into thirds. The top third is assigned to an interglacial, the middle to a transition and the lowest to a glacial.
iii. **25:50:25** - the amplitude between peak and trough $\delta^{18}O$ values is split into quarters. The top quarter is assigned to an interglacial, the middle two quarters a transition and the lowest to a glacial.
iv. **10:80:10** - the amplitude between peak and trough $\delta^{18}O$ values is split into tenths. The top tenth is assigned to an interglacial, the middle eight tenths to a transition and the lowest tenth to a glacial.

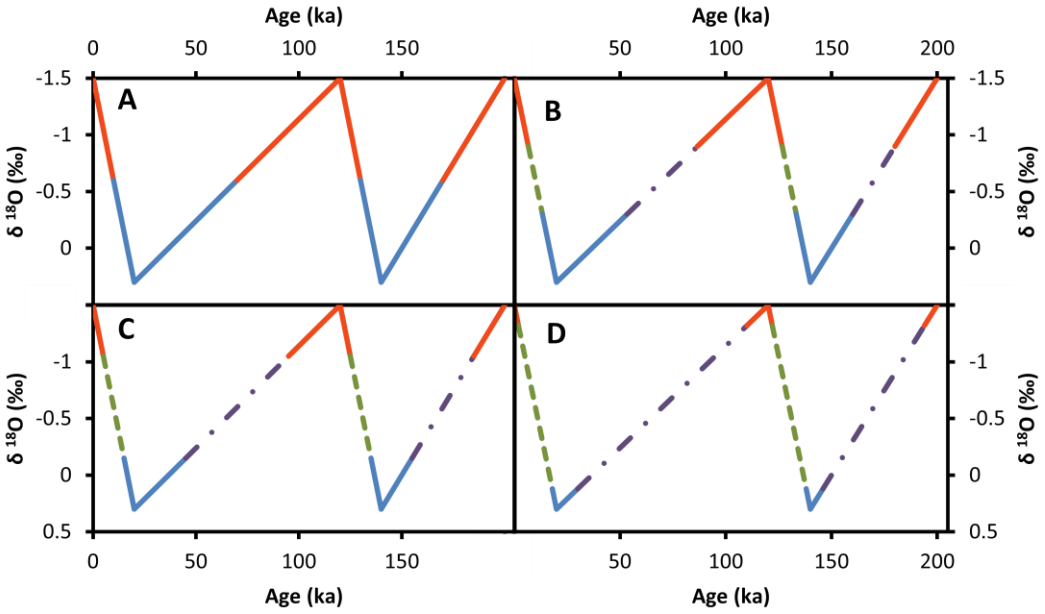

Figure 7.3 Showing the subdivision of a simplified glacial-interglacial record for the last 200kyr for differing definitions of climate regimes. Red- interglacial, green- transgression, blue- glacial, purple- regression. A) 50:50 division between glacials and interglacials, B) 33:33:33 division between glacials, transgressions, interglacials and regressions, C) 25:50:25 division between glacials, transgressions, interglacials and regressions and D) 10:80:10 division between glacials, transgressions, interglacials and regressions.

For each definition the record was partitioned, the periods spent in each climate regime recorded and turbidite layers assigned as glacial, transgression, interglacial or regression deposits.

For each definition a Monte-Carlo simulation, of 5,000 repeats, was set up to generate 79 randomly distributed layers across a 1.26Myr time period. The distribution of the number of layers deposited in each climate regime was then compared to the actual data from MD06-3019.

The reliability of the $\delta^{18}O$ record is reduced between ~1160-1100ka (MIS35-28) and the assignment of time to each climate regime becomes difficult during this period

(see Chapter 3 §6.1). Therefore, for each of the four definitions of glacial-interglacial cycle division the Monte-Carlo simulation was adjusted to remove these periods of time and the turbidite layers deposited during them. The simulations were then rerun to test the sensitivity of results to the exclusion of this time period.

For each of the four definitions of glacial-interglacial cycles division the Monte-Carlo simulation was adjusted and repeated to test for the significance of clustered layers, which are conceivably related to a single 'trigger' event, on the distribution. Layers which fell within ± 4kyr of each other, in the same climate regime, were combined into single layers. The simulations were then rerun to test the sensitivity of results to the clustering of layers.

Simulation Set 3: Effect of changes in the amplitude of glacial-interglacial sea-level cycles, carbonate production and margin morphology on turbidite deposition in relation to glacial-interglacial cycles (Aims 3 and 4)

Next it was investigated whether proposed changes in the amplitude of glacial-interglacial sea-level cycles [*Miller et al.*, 2005], shallow shelf carbonate production [*Frank et al.*, 2006; *Cabioch et al.*, 2008; *Andréfouët et al.*, 2009; *Montaggioni et al.*, 2011] and margin morphology [*Lafoy et al.*, 2000; *Chevillotte et al.*, 2005; *Le Roy et al.*, 2008] appear to have modulated the pattern of turbidite deposition on glacial-interglacial timescales in core MD06-3019. The record was split into sections based on the proposed time of change in the controlling factor and the differences in the relationship between turbidite deposition and glacial-interglacial cycles in each system examined.

To investigate how changes in the amplitude of glacial-interglacial sea-level and proposed variations in carbonate production (including the presence or absence of a barrier reef) may affect turbidite deposition in the deep sea, the record was split into three sections:

1) Start of MIS11 – Holocene (barrier reef expansion [*Cabioch et al.*, 2008, *Montaggionni et al*., 2011] and increase in the height of interglacial sea-level)
2) Start of MIS23 - end of MIS12 to MIS11 transgression (proposed period of significantly reduced carbonate production, see Chapter 6 and reduction in the height of interglacial sea-levels)
3) 1.26Ma – end of MIS24 to MIS23 transgression (proposed period of higher carbonate production and possible barrier reef existence, see Chapter 6 and increased height of interglacial sea-levels.)

As was seen in the work of *Cotillon et al.* (1990) on turbidites off the eastern New Caledonia margin there can be a delay of 10-15kyr in the material from the shallow shelf reaching the deep sea in turbidites. A similar delay was proposed in Chapter 4 §5.1 to account for the lag in the disappearance and reappearance of coarse grained turbidites in core MD06-3019 in relation to changes in the amplitude of glacial-interglacial sea-level. Therefore the record was split into divisions based on the presence or absence of coarse grained turbidites rather than the timing of MIS stages to take into account this possible delay. The divisions were:

1) 292ka- present
2) 898-293ka
3) 1260-899ka

For each time period Monte-Carlo simulations, for 5,000 repeats, were done for each of the four different definitions of climate regime, adjusted as necessary for the number of turbidite layers present and the time spent in each climate regime. This simulated data was then compared to the actual data from core MD06-3019. These results were then once again tested for their sensitivity to clustered layers and inclusion of periods of the record where the assignment of climate regime was difficult.

Unfortunately, investigation into the effect of the proposed flooding of the lagoon at MIS 5 and re-routing of the shallow shelf drainage systems during MIS2 [*Le Roy et al.*, 2008] on turbidite deposition is not possible, due to the low frequency of turbidite deposition since MIS5.

7.4.2 Analysis of the temporal variation of turbidite content, grain size and width in core MD06-3019: Mann-Whitney tests

Turbidite composition was analysed via coulometry for average total bulk carbonate content (see Chapter 6) and by XRF [Sr] measurements, as a proxy to obtain the inferred aragonite content (see Chapter 5). The grain size and width of each turbidite layer was assessed by eye during initial examination of the core (see Chapter 4).

Aim 1- Patterns of content, grain size and width of turbidites across the complete 1.26Myr MD06-3019 record

Temporal evolution since 1.26Ma in the width and total carbonate and aragonite content of the turbidites was assessed via the non-parametic Mann-Whitney U test, to see if certain time periods have significantly wider layers or turbidites with higher carbonate or aragonite content. The non-parametric Mann-Whitney U test is required since the distributions being considered are strongly non-normal. For a two-tailed test an alpha value of 0.05 was set for rejection of the null-hypothesis (that there is no difference in the median layer width, carbonate or aragonite content of the different populations). The turbidite record was split into 3 sections: 1.26Ma-MIS23 (~1.26Ma-910ka), MIS23-MIS11 (~910-400ka) and MIS11-Holocene (~400ka-present). This division was based on changes in the climate system, i.e. the occurrence of the ‘lukewarm interglacials’ (boundaries at MIS23 and MIS11) [*Masson-Delmotte et al.*, 2010; *Jaccard et al.*, 2013]; which was proposed in the previous chapter as being a principal controlling mechanism behind changes in carbonate production in the area. However, sensitivity tests were also conducted

using section boundaries defined by changes in sedimentation in the core, i.e. the presence/ absence of coarse turbidites (boundaries at ~900 and 300ka).

Aim 2- The effect of glacial-interglacial change on the content, grain size and width of MD06-3019 turbidites across the complete 1.26Myr record

Variations in the layer width and carbonate and aragonite content of turbidites deposited in different stages of glacial-interglacial cycles across the whole 1.26Myr record was examined. This was assessed via the non-parametic Mann-Whitney U test to see if certain time periods of glacial-interglacial cycles have significantly wider layers, or turbidites with higher carbonate or aragonite content. The non-parametric Mann-Whitney U test is required since the distributions being considered are strongly non-normal. For a two-tailed test an alpha value of 0.05 was set for rejection of the null-hypothesis (that there is no difference in the median layer width, carbonate or aragonite content of the different populations). Sensitivity tests were conducted to examine the effect of changes in the definition of climate regime and the removal of periods of time where the assignment of marine isotope stages was doubtful.

Additionally, the record was examined for bias in the sedimentation of different grain size turbidites during different periods of the glacial-interglacial cycle. The proportion of different grain size turbidite deposited in each stage of the glacial-interglacial cycle was also compared to the overall pattern of turbidite deposition and the amount of time spent in each phase of the glacial-interglacial cycle.

Aim 3 and 4- The effect of evolution in the amplitude of glacial-interglacial sea-level change, shallow shelf carbonate production, sediment routing and margin morphology on glacial-interglacial patterns of turbidite deposition in MD06-3019

Finally, it was investigated whether proposed changes in the amplitude of glacial-interglacial sea-level cycles [*Miller et al.*, 2005], shallow shelf carbonate production [*Frank et al*., 2006; *Cabioch et al.*, 2008; *Andréfouët et al.*, 2009; *Montaggioni et al.*, 2011] and margin morphology [*Lafoy et al.*, 2000; *Chevillotte et al.*, 2005; *Le Roy et al.*, 2008] appear to have modulated the pattern of turbidite deposition on glacial-interglacial timescales in core MD06-3019. As per the previous section for *Simulation Set Three*, the record was split into sections based on the proposed time of change in the controlling factor and the differences in relationship between median turbidite content and width with glacial-interglacial cycles in each period examined. It was not, however, possible to conduct Mann Whitney U tests on these values due to the very low numbers of turbidite layers present in each population.

Unfortunately, investigation into the effect of the proposed flooding of the lagoon at MIS 5 and re-routing of the shallow shelf drainage systems during MIS2 [*Le Roy et al.*, 2008] on turbidite deposition is not possible, due to the low frequency of turbidite deposition since MIS5.

7.5 Results

For full details on the depositional ages, widths, grain size and content of the individual turbidites in sediment core MD06-3019, see Chapters 3, 4 and 6, Appendix 6 and the digital only Supplementary Data. *Figure 3.6* shows the temporal pattern of turbidite deposition in sediment core MD06-3019 in relation to the stable isotope record of glacial-interglacial climate change.

7.5.1 Timing of turbidite deposition in sediment core MD06-3019 since 1.26Ma- a stochastic system?

Initially, the timing of deposition of all turbidite layers in sediment core MD06-3019 (see *Figure 3.6*) was compared, via Monte Carlo analysis, to the random distribution of layers expected for an entirely stochastic system (Simulation Set 1).

When assessed the minimum, median and maximum numbers of turbidites occurring in the 100 and 200 kyr moving windows lie within the 5-95% interval ($\mu_{rand}\pm2\sigma_{rand}$) for a random distribution (see *Figure 7.4*). The same is true for the minimum and median number of turbidites within the 400kyr moving window. However, the value for the maximum number of turbidites in a 400kyr window lies outside the $\mu_{rand}+2\sigma_{rand}$ value; this high maximum number of turbidites within a 400kyr period is a result of the repeated clustering of turbidite layers (see *Figure 7.4*). When turbidite layers that are clustered within ± 4kyr of one another are grouped together into single layers and the analysis repeated, this feature of the record disappears (see *Figure 7.5*). Then the minimum, median and maximum numbers of turbidites occurring in the 100, 200 and 400 kyr moving windows all lie within the region $\mu_{rand}\pm2\sigma_{rand}$ and the pattern of turbidite deposition appears to be stochastic.

Next the ~600kyr break in the deposition of coarse turbidite layers in MD06-3019 between ~900ka-300ka was examined. Results show that whilst a 100, 200 or 400kyr gap in the record is not a significant result with respect to what would be expected in a stochastic system, a 600 kyr gap is a significant absence (see *Figure 7.6*).

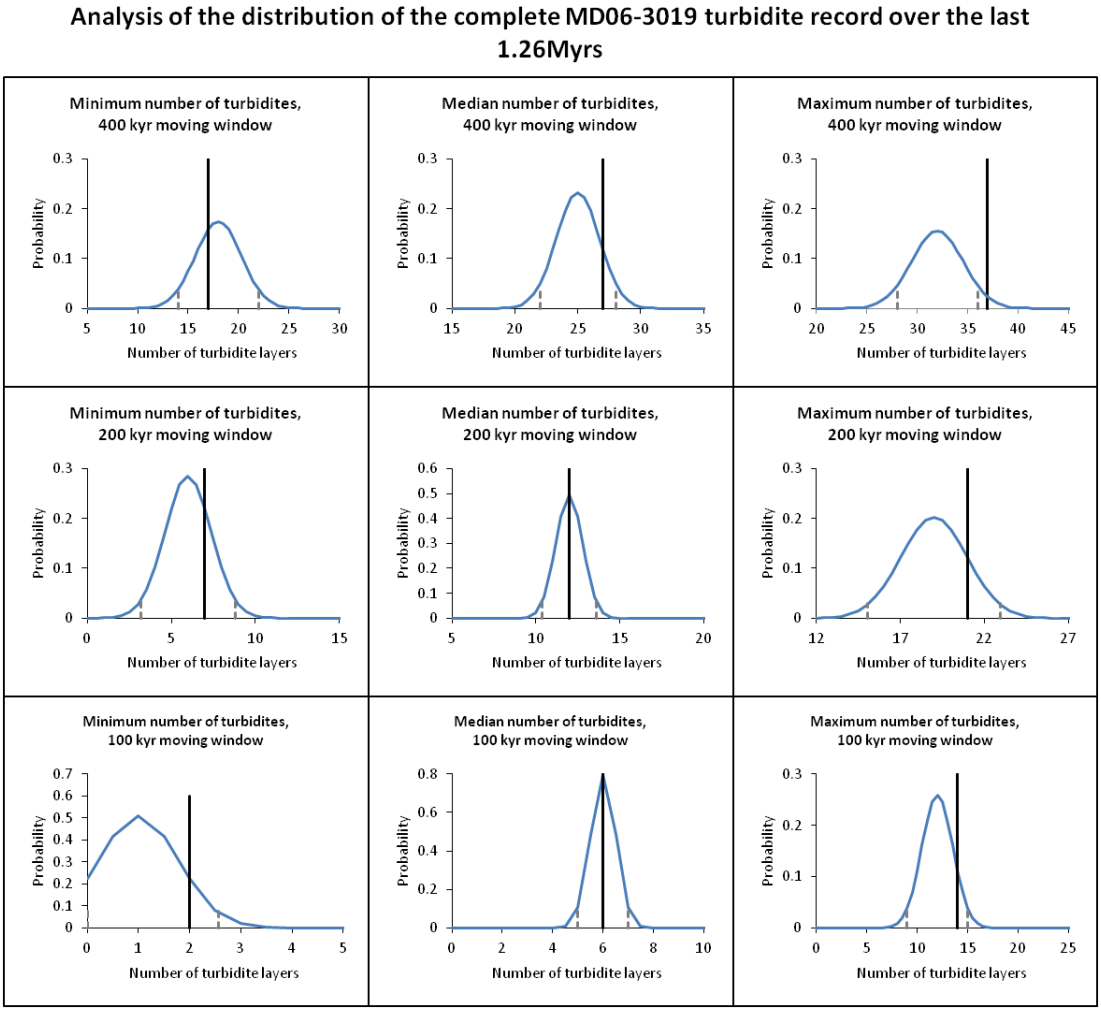

Figure 7.4 Results of Monte Carlo analysis, using 100, 200 and 400kyr moving windows, comparing the features of the complete MD06-3019 turbidite record (black lines), against an expected random distribution for a stochastic system (blue lines). Grey dotted lines represent $\mu_{rand} \pm 2\sigma_{rand}$ for each distribution. If a result lies either $> \mu_{rand} + 2\sigma_{rand}$ or $< \mu_{rand} - 2\sigma_{rand}$ from the generated random distribution, then it is considered to be significant and thought likely to have some controlling mechanism behind its occurrence, rather than being a purely stochastic feature.

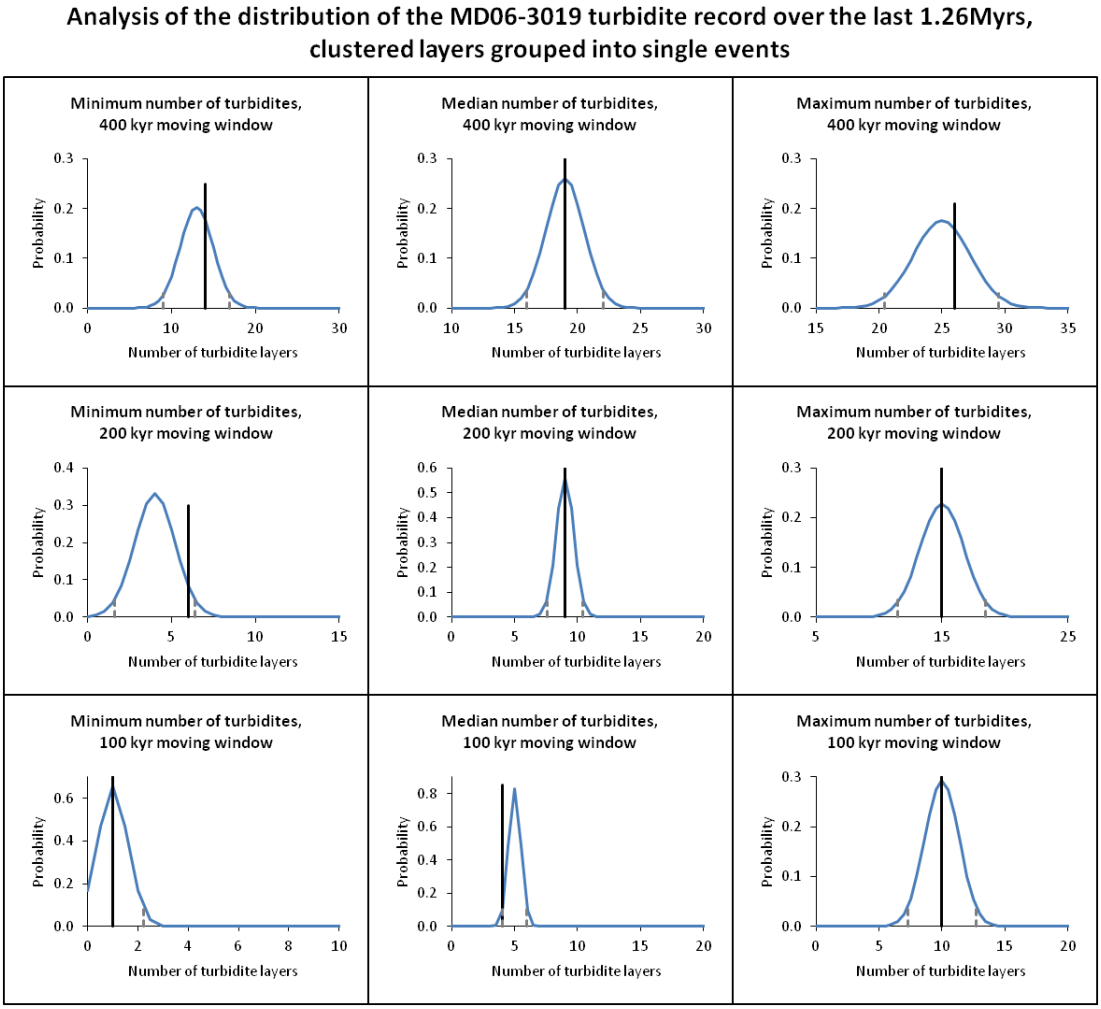

Figure 7.5 Results of Monte Carlo analysis, using 100, 200 and 400kyr moving windows, comparing the features of the MD06-3019 turbidite record where turbidite events which occurred within ±4kyrs of each other have been grouped into single events (black lines), against an expected random distribution for a stochastic system (blue lines). Grey dotted lines represent $\mu_{rand} \pm 2\sigma_{rand}$ for each distribution. If a result lies either $> \mu_{rand} + 2\sigma_{rand}$ or $< \mu_{rand} - 2\sigma_{rand}$ from the generated random distribution, then it is considered to be significant and thought likely to have some controlling mechanism behind its occurrence, rather than being a purely stochastic feature.

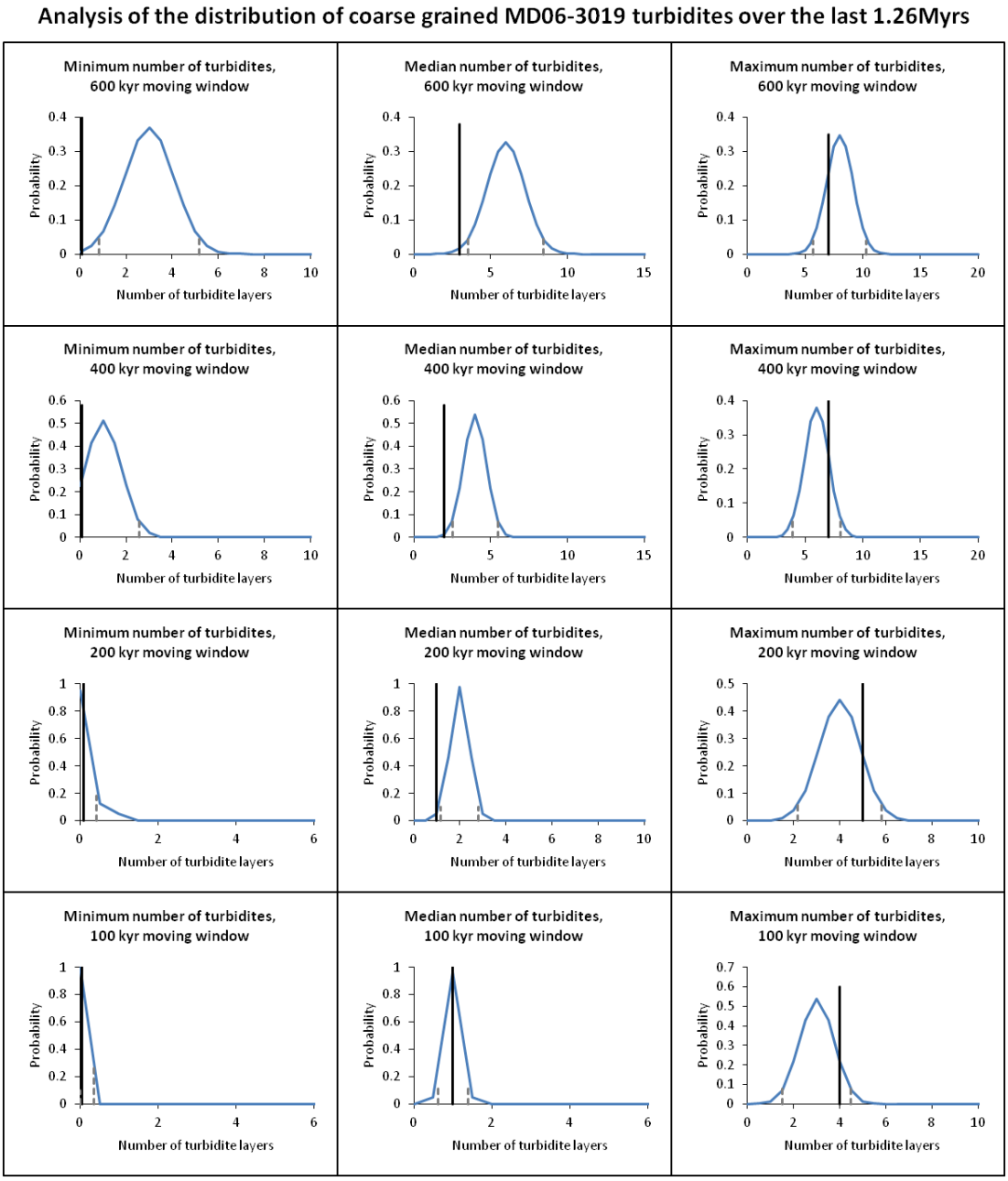

Figure 7.6 Results of Monte Carlo analysis, using 100, 200, 400 and 600kyr moving windows, comparing features of the MD06-3019 coarse grained turbidite distribution (black lines), against an expected random distribution for a stochastic system (blue lines). Grey dotted lines represent $\mu_{rand} \pm 2\sigma_{rand}$ for each distribution. If a result lies either $>\mu_{rand}+2\sigma_{rand}$ or $<\mu_{rand}-2\sigma_{rand}$ from the generated random distribution, then it is considered to be significant and thought likely to have some controlling mechanism behind its occurrence, rather than being a purely stochastic feature.

7.5.2 Timing of turbidite deposition in sediment core MD06-3019 with respect to glacial-interglacial cycles since 1.26Ma

Given the work of *Jorry et al* (2008), *Webster et al.* (2012) and *Puga-Bernabéu et al.*, (2014) it is predicted that the timing and content of turbidites is likely to be controlled by glacial-interglacial sea-level changes. Therefore, the timing of turbidite deposition is next examined in relation to glacial- interglacial sea-level change (*Simulation Set 2*).

The exact values depend on the definitions being used, but when the complete record of 79 turbidites deposited since 1.26Ma is analysed there are proportionally more layers deposited during interglacials and regressions compared to glacials and transgressions (see *Figure 7.7).* It also appears that more turbidites are deposited close to the glacial-transgression definition boundary than the interglacial-regression divide; hence the greater sensitivity of this category to changes in regime definition.

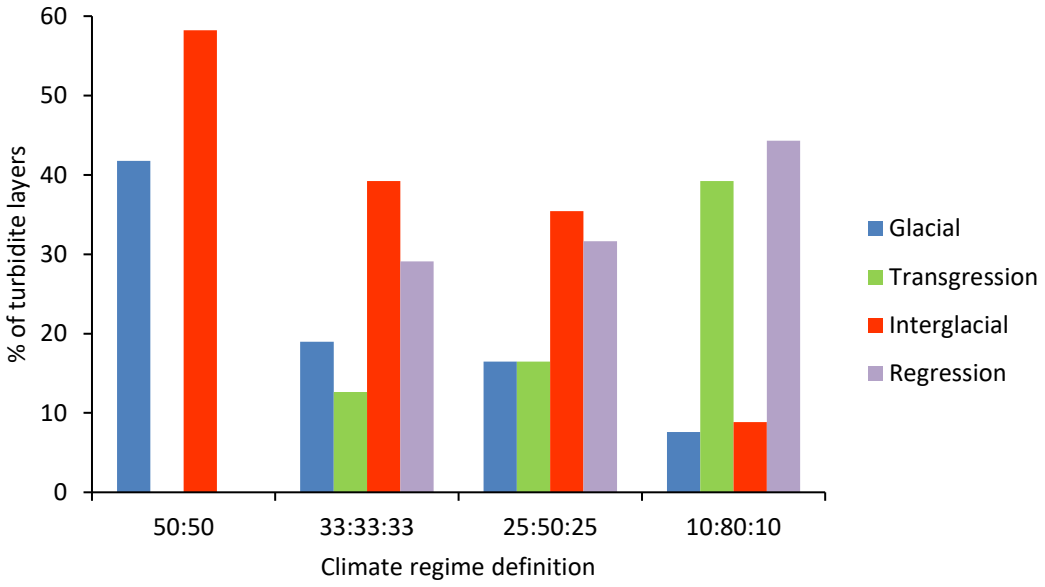

Figure 7.7 Change in the proportion of turbidite layers deposited during different stages of glacial-interglacial cycles for the complete MD06-3019 record using different definitions of climate regimes.

The climate system does not spend an equal amount of time in each stage of the glacial-interglacial cycle (glacial, trangsression, interglacial and regression). Therefore, in order to assess the significance of these results it is necessary to consider the distribution of turbidites within a framework that takes into account the amount of time spent in each phase of glacial-interglacial cycles. For the complete record of 79 turbidites over 1.26Myr, Monte-Carlo simulations were generated with reference to the amount of time the record spends in each glacial-interglacial cycle phase, using the four different definitions of climate regime (50:50, 33:33:33, 25:50:25, 10:80:10). These results show that compared to a random distribution the number of layers deposited during interglacials and transgressions is marginally higher than would be expected, whereas the number of turbidites deposited during glacials is slightly lower than would be predicted (the number of regression turbidites is about as expected) (see *Figure 7.8* and *Table 7.1*). However, none of these results are sufficiently outside (either $>\mu_{rand}+2\sigma_{rand}$ or $<\mu_{rand}-2\sigma_{rand}$) the expected random distribution to be considered significant and therefore likely to have some controlling mechanism behind their occurrence (see *Figure 7.8* and *Table 7.1*).

Comparison of the number of turbidite layers in MD06-3019 deposited during different periods of the glacial-interglacial cycle against a generated random distribution				
Climate definition	**Climate Regime**			
	Glacial	**Transgression**	**Interglacial**	**Regression**
50:50	$\mu_{rand}-2\sigma_{rand} \leq x < \mu_{rand}-\sigma_{rand}$	N/A	$\mu_{rand}+1\sigma_{rand}<x\leq \mu_{rand}+2\sigma_{rand}$	N/A
33:33:33	$\mu_{rand}-2\sigma_{rand} \leq x < \mu_{rand}-\sigma_{rand}$	$\mu_{rand} \pm \leq 1\sigma_{rand}$ (high)	$\mu_{rand} \pm \leq 1\sigma_{rand}$ (high)	$\mu_{rand} \pm \leq 1\sigma_{rand}$ (high)
25:50:25	$\mu_{rand}-2\sigma_{rand} \leq x < \mu_{rand}-\sigma_{rand}$	$\mu_{rand} \pm \leq 1\sigma_{rand}$ (high)	$\mu_{rand}+1\sigma_{rand}<x\leq \mu_{rand}+2\sigma_{rand}$	$\mu_{rand} \pm \leq 1\sigma_{rand}$ (low)
10:80:10	$\mu_{rand} \pm \leq 1\sigma_{rand}$ (low)	$\mu_{rand}+1\sigma_{rand}<x\leq \mu_{rand}+2\sigma_{rand}$	$\mu_{rand} \pm \leq 1\sigma_{rand}$ (mean)	$\mu_{rand}-2\sigma_{rand} \leq x < \mu_{rand}-\sigma_{rand}$

Table 7.1 Comparison of the actual number of layers deposited in sediment core MD06-3019 during different stages of glacial-interglacial cycles, against a random distribution generated based on the amount of time spent in each climate regime. Blue shading: indicates a result that is between $2\sigma_{rand}$ -$1\sigma_{rand}$ below μ_{rand}, green shading: indicates a result that is within $\pm1\sigma_{rand}$ of μ_{rand} and yellow shading: indicates a result that is $2\sigma_{rand}$- $1\sigma_{rand}$ above μ_{rand}. For results that lie within $\mu_{rand} \pm1\sigma_{rand}$, it is indicated whether the result is actually the random mean or slightly higher or lower.

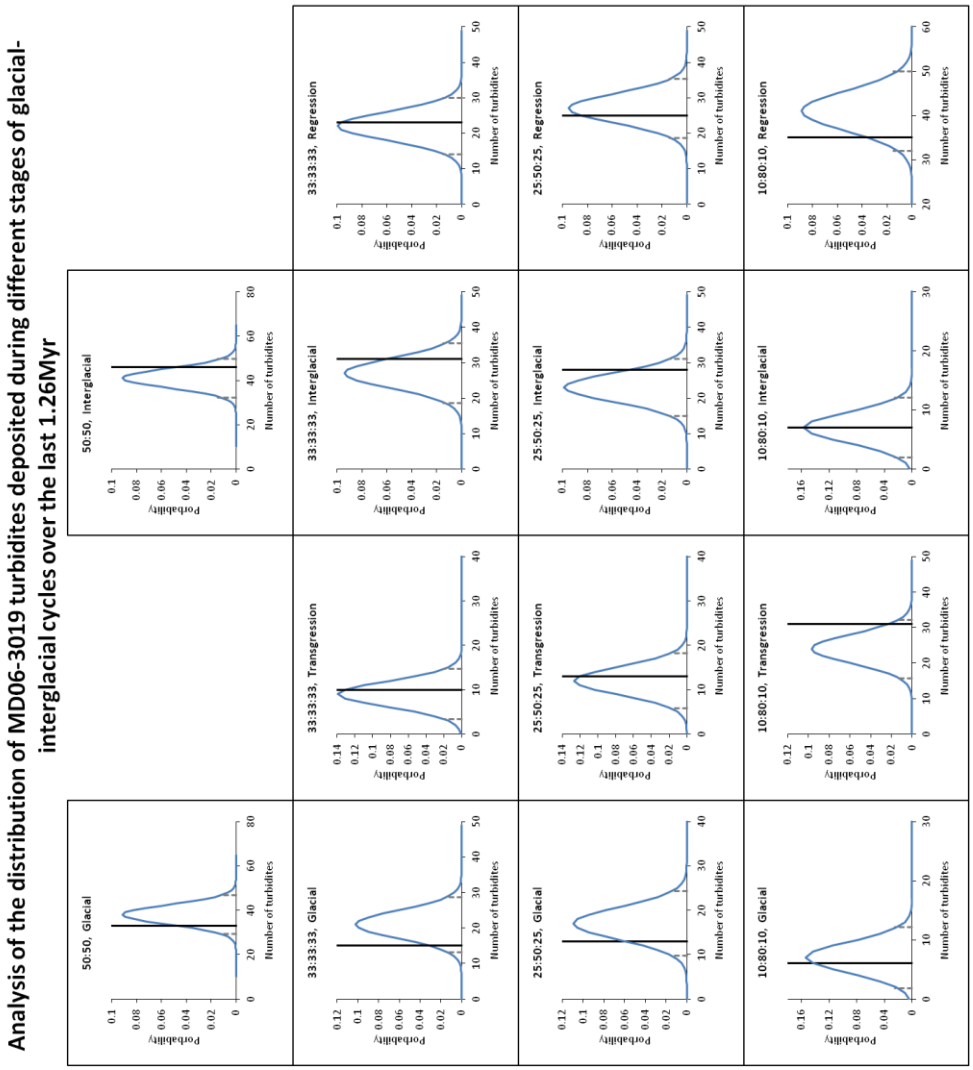

Figure 7.8 Comparison of the actual number of layers deposited over the complete MD06-3019 record in different stages of glacial-interglacial cycles (black lines), against the generated random distribution based on the amount of time spent in each climate regime using different climate definitions (blue lines). Grey dotted lines represent $\mu_{rand} \pm 2\sigma_{rand}$ for each distribution. If a result lies either $> \mu_{rand} + 2\sigma_{rand}$ or $< \mu_{rand} - 2\sigma_{rand}$ from the generated random distribution, then it is considered to be significant and thought likely to have some controlling mechanism behind its occurrence, rather than being a purely stochastic feature.

Sensitivity tests were conducted to assess the effect of removal of time periods where the assignment of marine isotope stages was problematic and clusters of turbidites by combining them into single layers (for full results of these sensitivity tests see digital only Supplementary Data). The results of these tests show that the Monte Carlo simulation results are not generally sensitive to either factor and that the same pattern of slightly higher than expected numbers of turbidites being deposited during interglacials and transgressions, slightly lower numbers during glacials and expected numbers during regressions holds throughout. The only significant change occurs for the 33:33:33 definition of climate, where when clustered layers are combined into single points the number of layers deposited during glacial periods slips into being less than $2\sigma_{rand}$ below the mean for the expected random distribution. However, clustering of layers does not appear to be a phenomenon particularly associated with glacial periods (see *Table 7.2*).

Number of clustered turbidite layer events in core MD06-3019 during different periods of the glacial-interglacial cycle				
Glacial-interglacial definition	**Climate Regime**			
	Glacial	**Transgression**	**Interglacial**	**Regression**
50:50	5	N/A	7	N/A
33:33:33	2	2	4	3
25:50:25	2	4	3	4
10:80:10	1	7	-	5

Table 7.2 Numbers of clustered layer events occurring in different stages of glacial-interglacial cycles, using four different definitions of climate regime.

7.5.3 Evolution in the timing of turbidite deposition in sediment core MD06-3019 with respect to glacial-interglacial cycles since 1.26Ma

Proposed changes in the amplitude of glacial-interglacial sea-level cycles [*Miller et al.*, 2005], and shallow shelf carbonate production [*Frank et al*., 2006; *Cabioch et al.*, 2008; *Andréfouët et al.*, 2009; *Montaggioni et al.*, 2011] may be expected to have modulated the pattern of turbidite deposition in core MD06-3019 since 1.26Ma. Therefore, the record was split into sections based on the proposed time of change in the controlling factors and the differences in relationship between turbidite deposition and glacial-interglacial cycles in each system examined (*Simulation Set 3*).

Initially, the MD06-3019 record was split into three sections (1.26Ma- MIS23, MIS23-MIS11 and MIS11- Holocene) based on changes in the amplitude of glacial-interglacial cycles and the apparent concurrent changes in shallow shelf production [*Miller et al.*, 2005; *Cabioch et al.*, 2008; *Montaggioni et al.*, 2011]. The number of turbidites deposited during glacial, transgression, interglacial and regression periods was then ascertained for each of the three sections. Results presented here are given for the 25:50:25 definition of glacial-interglacial cycles. This was chosen since it is not a definition at either extreme and the timing it yields for the Holocene inundation of the western New Caledonia shallow shelf (initial flooding at ~12ka and full flooding at 8ka) is consistent with estimates given in previous work [*Le Roy et al.*, 2008]. Though the exact numbers vary based, on the climate definition used, the basic pattern of deposition remains consistent.

Initial results (using the 25:50:25 climate definition) of the absolute number of turbidites deposited during the middle period of the MD06-3019 record, MIS23-MIS11, seems to show an approximate doubling of the number of turbidites deposited during glacial periods and reduction of between half and a third in the amount of transgression turbidites (see *Figure 7.9*).

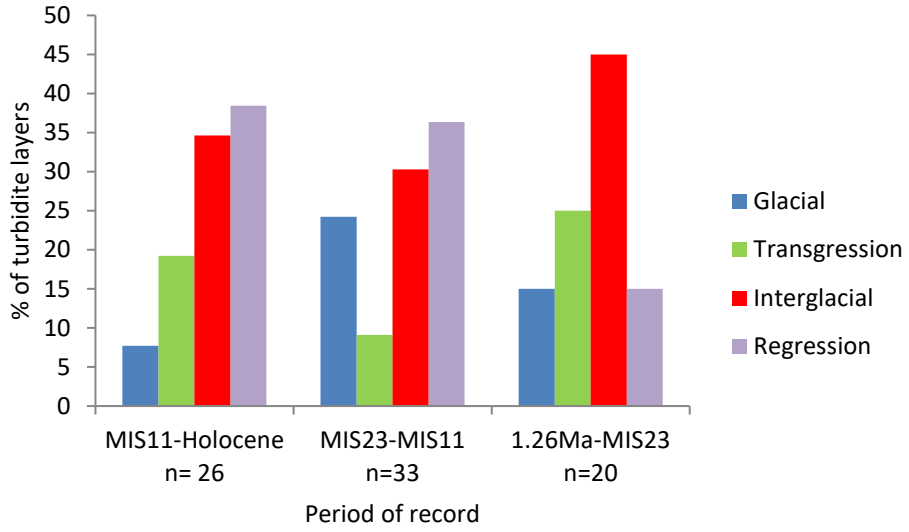

Figure 7.9 Proportional numbers of turbidites deposited in different stages of the glacial-interglacial cycle during different periods of the MD06-3019 record, using the 25:50:25 definition of climate regime. The numbers of turbidites deposited is given for each period of the record.

As noted in the previous section it is, however, necessary to consider this result in relation to the amount of time spent in each stage of the glacial-interglacial cycle, since the shape and length of cycles is non-uniform over the period studied. When tested for significance, with reference to the length of time spent in each stage of a glacial-interglacial cycle, a rather different pattern of turbidite deposition emerges for sediment core MD06-3019. During the middle period MIS23-MIS11 compared to 1.26Ma-MIS23 and MIS11-present there appears to be a marginal decrease in the numbers of turbidites deposited during glacials, transgressions and interglacials and an increase in the number deposited during regressions (see *Table 7.3* and *Figure 7.10*). However, none of these are significant changes and there is no significant deviation from what would be expected based on a random distribution for any individual period of the record. In fact, despite the increase in absolute numbers of turbidite layers deposited during glacial stages in the period MIS23-MIS11, there are still marginally fewer than would be expected based on random chance given the length of time spent in glacial stages; the same as in the rest of the record.

Comparison against a random distribution of the number of turbidite layers deposited in different stages of the glacial-interglacial cycle during different periods of the MD06-3019 record				
	Climate Regime			
	Glacial	**Transgression**	**Interglacial**	**Regression**
Whole Record	$\mu_{rand}-2\sigma_{rand} \leq x < \mu_{rand}-\sigma_{rand}$	$\mu_{rand} \pm \leq 1\sigma_{rand}$ (high)	$\mu_{rand}+1\sigma_{rand}<x\leq \mu_{rand}+2\sigma_{rand}$	$\mu_{rand} \pm \leq 1\sigma_{rand}$ (low)
MIS11-Holocene	$\mu_{rand} \pm \leq 1\sigma_{rand}$ (low)	$\mu_{rand}+1\sigma_{rand}<x\leq \mu_{rand}+2\sigma_{rand}$	$\mu_{rand} \pm \leq 1\sigma_{rand}$ (high)	$\mu_{rand} \pm \leq 1\sigma_{rand}$ (low)
MIS23-MIS22	$\mu_{rand} \pm \leq 1\sigma_{rand}$ (low)	$\mu_{rand} \pm \leq 1\sigma_{rand}$ (low)	$\mu_{rand} \pm \leq 1\sigma_{rand}$ (mean)	$\pm \leq 1\sigma_{rand}$ (high)
1.2Ma-MIS23	$\mu_{rand} \pm \leq 1\sigma_{rand}$ (low)	$\mu_{rand} \pm \leq 1\sigma_{rand}$ (mean)	$\mu_{rand}+1\sigma_{rand}<x\leq \mu_{rand}+2\sigma_{rand}$	$\mu_{rand}-2\sigma_{rand} \leq x < \mu_{rand}-\sigma_{rand}$

Table 7.3 Comparison of the actual number of layers deposited in sediment core MD06-3019 during different stages of glacial-interglacial cycles, in different periods of the MD06-3019 record, against a generated random distribution. Results are given for the 25:50:25 definition of climate regime. Blue shading: indicates a result that is between $2\sigma_{rand}$ -$1\sigma_{rand}$ below μ_{rand}, green shading: indicates a result that is within $\pm1\sigma_{rand}$ of μ_{rand} and yellow shading: indicates a result that is $2\sigma_{rand}$ - $1\sigma_{rand}$ above μ_{rand}. For results that lie within $\mu_{rand} \pm1\sigma_{rand}$, it is indicated whether the result is actually the random mean or slightly higher or lower.

Sensitivity tests show that the results obtained are not significantly affected by altering the definition of climate regimes, grouping clustered layers into single events or removing periods of the record where assignment of marine isotope stages was difficult (see digital only Supplementary Data). The overall pattern remains consistent between trials and generally no result for any glacial-interglacial stage in any time period is significant when compared to a random distribution. Only in a few trials are the numbers of glacial turbidites deposited during the middle section (MIS23-MIS11) low enough to be considered significant, principally when clustered layers have been combined.

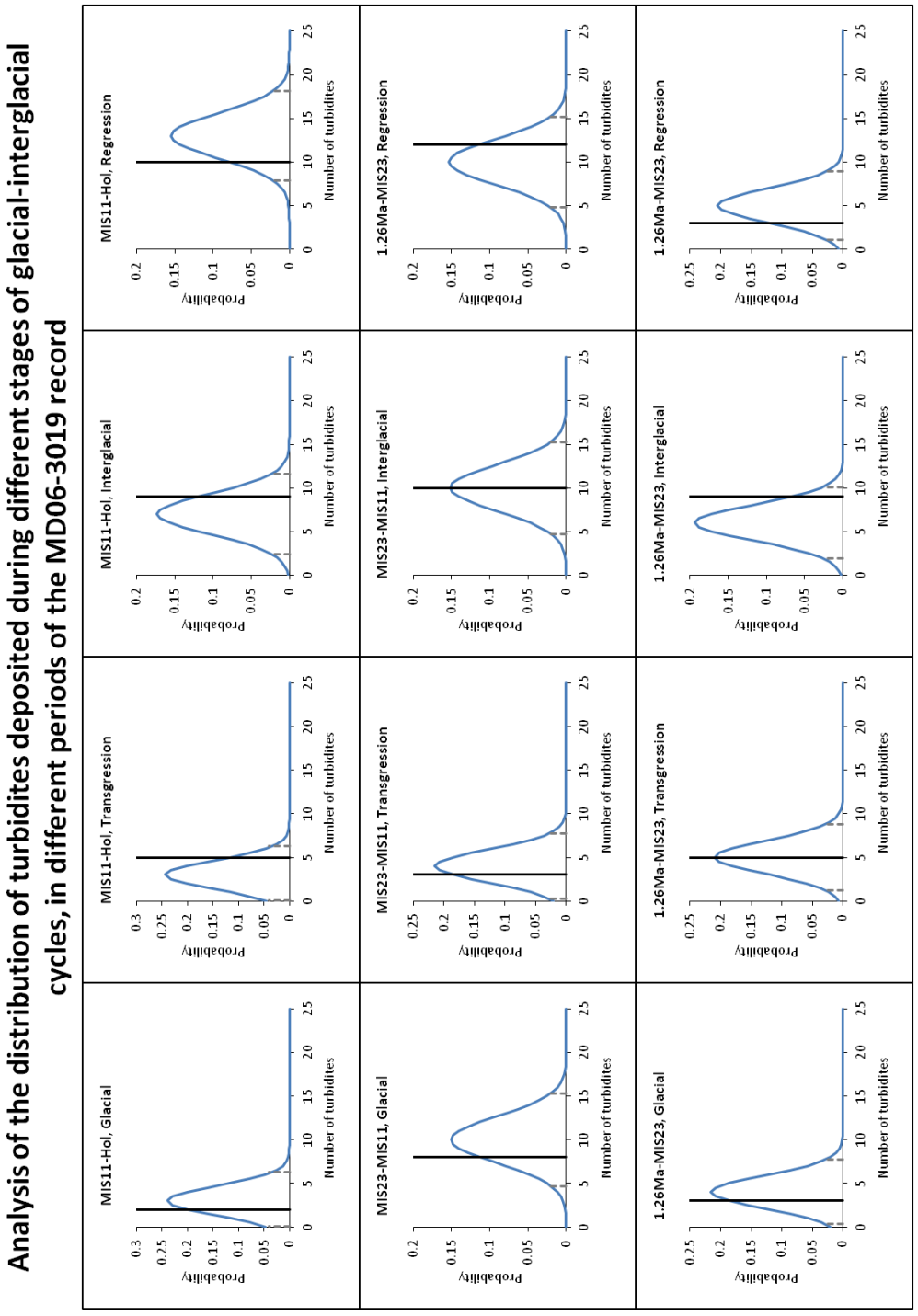

Figure 7.10 Comparison of the actual number of layers deposited during different stages of glacial-interglacial cycles (black lines), in different periods of the MD06-3019 record, against a generated random distribution (blue lines). Grey dotted lines represent $\mu_{rand} \pm 2\sigma_{rand}$ for each distribution. Results given are for the 25:50:25 definition of climate regimes. If a result lies either $> \mu_{rand} + 2\sigma_{rand}$ or $< \mu_{rand} - 2\sigma_{rand}$ from the generated random distribution, then it is considered to be significant and thought likely to have some controlling mechanism behind its occurrence, rather than being a purely stochastic feature.

The MD06-3019 record was also split into three sections again, but this time based on the presence or absence of coarse grained turbidites rather than the timing of marine isotope stages (1260-899ka, 898-293ka and 292ka- present). This is to take into account the possible delay between changes in carbonate production and sea-level amplitude and this being recorded in turbidites in the New Caledonia Trough. A similar pattern is obtained to that seen previously with a marginal decrease in the numbers of turbidites deposited during glacials in the middle period (898-293ka) and an increase in the number deposited during regressions (see digital only Supplementary Data). Changes in the numbers of turbidites deposited during transgressions and interglacials, in different periods of the record does not show any particular pattern. Once again sensitivity tests show that the results are not significantly affected by changing the definitions of climate regimes, grouping clustered layers into single events or removing periods of the record where assignment of marine isotope stages was difficult (see digital only Supplementary Data). The overall pattern remains consistent between trials and generally no result for any glacial-interglacial stage, in any time period, is significant when compared to a random distribution. Only in a few trials are the numbers of turbidites deposited during glacial periods in the middle section (898-293ka) low enough to be considered significant, principally when clustered layers have been combined.

7.5.4 Evolution in turbidite content, grain size and layer width in sediment core MD06-3019 since 1.26Ma

As has been noted previously in Chapter 4 § 4 and Chapter 6 § 4 there are noticeable patterns in the content, grain size and layer width of turbidites deposited in MD06-3019 over the last 1.26Myr.

Whilst fine grained turbidites are present throughout the core, coarse grained turbidites only occur between ~1.26Ma-900ka and ~300ka-present. This 600kyr gap in deposition is seen to be a statistically significant result when compared against a stochastic system (see *Figure 7.6*).

The total weight % (wt.%) carbonate content of turbidites in core MD06-3019 varies between 4-71%, shows a statistically significant reduction in the overall total carbonate content of turbidite layers deposited between MIS23-11compared to the 1.26Ma- MIS23 and MIS11-Holocene periods (see *Table 6.3* and *Table 6.4 and Figure 7.11*). Similarly the average aragonite content of turbidite layers is also seen to vary with timing of deposition. There is a statistically significant reduction in the measured XRF Sr count value, as a proxy for aragonite, of turbidite layers in the middle section of the core between MIS23-MIS11 compared to the base and top (see *Table 6.5, Table 6.6, Table 6.7* and *Figure 6.2*). Additionally, the reduction in total average carbonate and aragonite content of turbidite layers between MIS23-MIS11 is not merely due to the lack of coarse grained layers in this period (see *Table 6.3, Table 6.5, Table 6.7* and *Table 6.8*). An assessment of the sensitivity of the above results (that there is a significant reduction in aragonite and calcite content of turbidites in turbidites deposited between MIS23 and MIS11, ~900-400ka) to the position of section boundaries was also conducted. Results of these sensitivity tests show that the significance of the reduction of carbonate and aragonite content of turbidite layers in the middle period is not sensitive to small changes (of the order of 20-100kyr) in the section boundaries (see Chapter 6 § 4.2). (Full results of these sensitivity tests may be found in the digital only Supplementary Data.)

The pattern of temporal changes in turbidite widths does not follow so clear a pattern as the changes in turbidite content and grain size. Whilst there is a clear reduction in the mean width of turbidites between MIS23- MIS11 compared to the periods before and afterwards, this is not seen in the median widths (see *Table 7.4*). Mann Whitney tests do show a significant drop in layer width for the middle section compared to the period MIS11-present; however, this is not seen when comparing the middle period to 1.26Ma-MIS23 (see *Table 7.4*). Sensitivity tests as to the effect of changing section boundaries by 20-100kyr, do not materially affect the results. (Full results of these sensitivity tests may be found in the digital only Supplementary Data.)

Mann-Whitney U test for temporal variations in MD06-3019 turbidite width			
Group 1	**Group 2**	**Mann-Whitney U Value**	**Two-tailed P value**
MIS11-Holocene n= 27 Median= 6.0cm Mean= 8.0cm	MIS23-MIS11 n= 32 Median= 2.5cm Mean= 3.0cm	613	0.0006 (Reject null hypothesis)
MIS23-MIS11 n= 32 Median= 2.5cm Mean= 3.0cm	1.26Ma-MIS23 n= 20 Median= 2.5cm Mean= 7.0cm	381	0.2585 (Cannot reject null hypothesis)
MIS11-Holocene n= 27 Median= 6.0cm Mean= 8.0cm	1.26Ma-MIS23 n= 20 Median= 2.5cm Mean= 7.0cm	229	0.3843 (Cannot reject null hypothesis)

Table 7.4 Comparison of the widths of turbidites deposited in different time periods using a Mann-Whitney U test. α=0.05 for rejection of the null hypothesis (that the median turbidite width is the same in the two time periods).

7.5.5 Relationship between turbidite content, grain size and layer width and glacial-interglacial cycles

Next, the relationship between turbidite grain size, content and layer width was investigated in relation to depositional timing within glacial-interglacial cycles. Results presented here are given for the 25:50:25 definition of glacial-interglacial cycles. This was chosen since it is not a definition at either extreme and the timing it yields for the Holocene inundation of the western New Caledonia shallow shelf (initial flooding at ~12ka and full flooding at 8ka) is consistent with estimates given in previous work [*Le Roy et al.*, 2008]. However, sensitivity tests as to the effect of using different climate cycle definitions (10:80:10, 33:33:33 and 50:50) and removal of periods of the record where the climate assignment of marine isotope stages was difficult has also been conducted. These tests show that the results presented here are not significantly affected by changes in definition of glacial-interglacial cycles or removal of periods of the record where climate assignment was more problematic. (Full results of these sensitivity tests may be found in the digital only Supplementary Data.)

As was seen in § 4.2 overall there are a slightly greater number of layers deposited during interglacial periods and a slightly lower number in glacial periods than would be expected by random chance. During transgression and regression periods approximately the expected number of layers were deposited. When split into different layer types (see Chapter 4 §4.1) dark fine grained layers follow this overall pattern well, but the results from coarse and light fine grained layers are more varied (see *Table 7.5*). However, there are only 12 coarse grained layers and 7 light fine layers compared to 60 dark fine layers; this means that the relative percentages yielded for the number of layers in each climate period for coarse grained and light fine grained layers are subject to higher uncertainties.

Percentage of each turbidite type in MD06-3019 that is deposited in each sea-level regime over the complete 1.26Myr record				
Turbidite type	**Glacial** (274ka, 21%)	**Transgression** (190ka, 15%)	**Interglacial** (367ka, 29%)	**Regression** (430ka, 34%)
All layers (n= 79)	16% (13/79)	16% (13/79)	35% (28/79)	32% (25/79)
Coarse grained (n= 12)	17% (2/12)	17% (2/12)	42% (5/12)	25% (3/12)
Dark fine grained (n= 60)	17% (10/60)	15% (9/60)	33% (20/60)	35% (21/60)
Light fine grained (n= 7)	14% (1/7)	29% (2/7)	43% (3/7)	14% (1/7)

Table 7.5 Distribution of different turbidite layer types, based on grain size, deposited in each climate regime over the whole 1.26Myr record. Climate regimes assigned using the 25:50:25 definition. The total time spent in ka and as a percentage of the complete 1.26Myr record is given for each climate regime.

The carbonate content of turbidites, averaging at ~35 wt.%, does not appear to vary significantly depending on depositional timing with respect to glacial-interglacial cycles (see *Table 7.6* and *Table 7.7*). The median aragonite content of turbidites deposited during glacials is higher than those deposited during other periods and the aragonite content of turbidites deposited during regression slightly lower than average (see *Table 7.6*). However, when analysed via Mann-Whitney tests there is no significant difference in the aragonite content of turbidite layers deposited during different stages of glacial-interglacial cycles (see *Table 7.8*).

The median turbidite layer width also does not appear to vary significantly with depositional timing with respect to glacial-interglacial cycles (see *Table 7.6* and *Table 7.9*).

Median carbonate and aragonite content and layer width of MD06-3019 turbidite layers in different climate regimes over the complete 1.26Myr record				
	Glacial (274kyr, 21%)	**Transgression** (190kyr, 15%)	**Interglacial** (367kyr, 29%)	**Regression** (430kyr, 34%)
Carbonate content	36 wt.%	39 wt.%	36 wt.%	31wt.%
Aragonite content	12,100 XRF [Sr] counts (15.7%)	10,200 XRF [Sr] counts (13.9%)	10,300 XRF [Sr] counts (13.9%)	9,200 XRF [Sr] counts (13.9%)
Layer width	2cm	4cm	3 cm	3cm

Table 7.6 Median carbonate and aragonite content and layer width for turbidites over the whole 1.26Myr record for each climate regime. Climate regimes assigned using the 25:50:25 definition. Aragonite content is presented as the XRF [Sr] count followed by the equivalent inferred maximum aragonite content using the calibration developed in Chapter 5. For those layers with a Sr count below the cut off for the XRF-XRD calibration a maximum aragonite value of 13.9% (the equivalent aragonite value for the lowest Sr count value in the calibration) is given.

Mann-Whitney U test for variations in MD06-3019 turbidite $CaCO_3$ wt.% content with respect to glacial-interglacial cycles			
Group 1	**Group 2**	**Mann-Whitney U Value**	**Two-tailed P value**
Glacial n= 12 Median= 37 wt%	Transgression n= 13 Median= 34 wt%	68	0.6031 (Cannot reject null hypothesis)
Glacial n= 12 Median= 37 wt%	Interglacial n= 28 Median= 35 wt%	164	0.9203 (Cannot reject null hypothesis)
Glacial n= 12 Median= 37 wt%	Regression n= 25 Median= 26 wt.%	167	0.5892 (Cannot reject null hypothesis)
Transgression n= 13 Median= 34 wt%	Interglacial n= 28 Median= 35 wt%	202	0.5823 (Cannot reject null hypothesis)
Transgression n= 13 Median= 34 wt%	Regression n= 25 Median= 26 wt.%	205	0.1971 (Cannot reject null hypothesis)
Interglacial n= 28 Median= 35 wt%	Regression n= 25 Median= 26 wt.%	275	0.1835 (Cannot reject null hypothesis)

Table 7.7 Comparison of the total wt. carbonate content of turbidites deposited in different periods of glacial-interglacial cycles using a Mann-Whitney U test. α=0.05 for rejection of the null hypothesis (that the median turbidite carbonate content values are the same in the two time periods).

Mann-Whitney U test for variations in MD06-3019 turbidite XRF Sr counts with respect to glacial-interglacial cycles			
Group 1	**Group 2**	**Mann-Whitney U Value**	**Two-tailed P value**
Glacial n= 13 Median= 10,400	Transgression n= 13 Median= 10,200	66	0.3576 (Cannot reject null hypothesis)
Glacial n= 13 Median= 10,400	Interglacial n= 26 Median= 9,700	209	0.2380 (Cannot reject null hypothesis)
Glacial n= 13 Median= 10,400	Regression n= 24 Median= 9,000	214	0.0673 (Cannot reject null hypothesis)
Transgression n= 13 Median= 10,200	Interglacial n= 26 Median= 9,700	178	0.8026 (Cannot reject null hypothesis)
Transgression n= 13 Median= 10,200	Regression n= 24 Median= 9,000	182	0.4179 (Cannot reject null hypothesis)
Interglacial n= 26 Median= 9,700	Regression n= 24 Median= 9,000	261	0.3271 (Cannot reject null hypothesis)

Table 7.8 Comparison of XRF Sr count values for turbidites deposited in different periods of glacial-interglacial cycles using a Mann-Whitney U test. α=0.05 for rejection of the null hypothesis (that the median turbidite XRF Sr count values are the same in the two time periods).

Mann-Whitney U test for variations in MD06-3019 turbidite layer width with respect to glacial-interglacial cycles			
Group 1	**Group 2**	**Mann-Whitney U Value**	**Two-tailed P value**
Glacial n= 13 Median= 2.0cm	Transgression n= 13 Median= 4.0cm	100	0.4593 (Cannot reject null hypothesis)
Glacial n= 13 Median= 2.0cm	Interglacial n= 28 Median= 3.0cm	169	0.7263 (Cannot reject null hypothesis)
Glacial n= 13 Median= 2.0cm	Regression n= 25 Median= 3.0cm	153	0.7795 (Cannot reject null hypothesis)
Transgression n= 13 Median= 4.0cm	Interglacial n= 28 Median= 3.0cm	207	0.4902 (Cannot reject null hypothesis)
Transgression n= 13 Median= 4.0cm	Regression n= 25 Median= 3.0cm	186	0.4777 (Cannot reject null hypothesis)
Interglacial n= 28 Median= 3.0cm	Regression n= 25 Median= 3.0cm	349	0.9840 (Cannot reject null hypothesis)

Table 7.9 Comparison of the widths of turbidites deposited in different periods of glacial-interglacial cycles using a Mann-Whitney U test. α=0.05 for rejection of the null hypothesis (that the median turbidite width is the same in the two time periods).

7.5.6 Evolution in the relationship between turbidite content and layer width and glacial-interglacial cycles over the last 1.26Ma

Finally, turbidites deposited in MD06-3019 were investigated to see if proposed changes in the amplitude of glacial-interglacial sea-level cycles [*Miller et al.*, 2005] and shallow shelf carbonate production [*Cabioch et al.*, 2008; *Montaggioni et al.*, 2011] have modulated their glacial-interglacial variations in content and layer width over the 1.26Myr period covered by the core.

For all phases of the glacial-interglacial cycle there is a reduction in the carbonate and aragonite content of turbidites layers between MIS23-MIS11 compared to the periods MIS11- Holocene and 1.26Ma-MIS23 (see *Table 7.10* and *Table 7.11*). However, as with the results for the record taken as a whole there is no clear pattern that any stage of the glacial-interglacial cycle has consistently higher or lower carbonate or aragonite content; nor that there is an obvious evolution in these patterns with time. Similarly, there is no clear evolution in the widths of turbidite layers deposited in different periods of the MD06-3019 in relation to glacial-interglacial cycles (see *Table 7.12*).

Median wt.% $CaCO_3$ of MD06-3019 turbidite layers deposited in different climate regimes during different periods of the MD06-3019 record				
	Climate Regime			
	Glacial	Transgression	Interglacial	Regression
Whole Record	34%	39%	36%	31%
MIS11-Holocene	41%	54%	37%	36%
MIS23-MIS22	34%	18%	29%	22%
1.2Ma-MIS23	39%	35%	39%	45%

Table 7.10 Median carbonate content of turbidite layers deposited in core MD06-3019 in different climate regimes, during different periods of the record. Climate regimes assigned using the 25:50:25 definition.

Median XRF [Sr] counts of MD06-3019 turbidite layers deposited in different climate regimes during different periods of the MD06-3019 record				
	Climate Regime			
	Glacial	Transgression	Interglacial	Regression
Whole Record	12,100 (15.7%)	10,200 (13.9%)	10,300 (13.9%)	9,200 (13.9%)
MIS11-Holocene	12,900 (16.5%)	13,200 (16.8%)	10,800 (13.9%)	9,900 (13.9%)
MIS23-MIS22	10,500 (13.9%)	6,300 (13.9%)	7,600 (13.9%)	7,600 (13.9%)
1.2Ma-MIS23	16,000 (19.9%)	9,500 (13.9%)	12,100 (15.7%)	12,000 (15.5%)

Table 7.11 Median XRF [Sr] counts for turbidite layers deposited in core MD06-3019 in different climate regimes, during different periods of the record. Climate regimes assigned using the 25:50:25 definition. Aragonite content is presented as the XRF [Sr] count followed by the equivalent inferred maximum aragonite content using the calibration developed in Chapter 5. For those layers with a Sr count below the cut off for the XRF-XRD calibration a maximum aragonite value of 13.9% (the equivalent aragonite value for the lowest Sr count value in the calibration) is given.

Median layer width of MD06-3019 turbidites deposited in different climate regimes during different periods of the MD06-3019 record				
	Climate Regime			
	Glacial	Transgression	Interglacial	Regression
Whole Record	2cm	4cm	3cm	2.5cm
MIS11-Holocene	4cm	9.5cm	3cm	6cm
MIS23-MIS22	2cm	4cm	2.5cm	2.5cm
1.2Ma-MIS23	11cm	2.5cm	4cm	2cm

Table 7.12 Median layer width of turbidites deposited in core MD06-3019 in different climate regimes, during different periods of the record. Climate regimes assigned using the 25:50:25 definition.

7.6 Discussion

7.6.1 Turbidite deposition in sediment core MD06-3019 over the last 1.26Myrs

Aim 1: To provide a descriptive record of the timing, nature and content of turbidite deposition in core MD06-3019 over the last 1.26Myr

The 79 turbidite layers deposited in sediment core MD06-3019 seem at a basic level to be random when compared to a stochastic system, apart from two features: the repeated clustering of turbidite layers and the ~600kyr absence of coarse grained turbidites between ~900-300ka (see *Figure 7.4, Figure 7.5* and *Figure 7.6*).

The repeated clustering of turbidite events within ±4kyr of each other occurs throughout the MD06-3019 record and in all phases of glacial-interglacial cycles. Clusters tend to occur for small to middle sized turbidites (up to 4cm and 15cm respectively) but include one large event of 27cm. Along active margins such clustering of turbidites has been linked to earthquake events with the size of the turbidite being closely related to the magnitude of the rupture [*Goldfinger et al.*, 2012]. Whilst the western New Caledonia margin is itself a passive margin, the area experiences significant present-day tectonic activity both on land and offshore [*Régnier et al.*, 1999]. On land events rarely exceed a magnitude of 5 on the Richter scale and are generally confined to the top 5km of the crust, probably as a result of faulting in the peridotite nappe [*Le Roy et al.*, 2008]. In recent years a cluster of earthquakes has also been recorded in the south of the lagoon, near the pass of Mato, which were between 5 and 6 on the Richter scale. Additionally, seismic activity from the nearby subduction of the Australian plate eastwards under the Pacific plate, along the arc trench system of the New Hebrides approximately 200-300km west of New Caledonia, also causes quakes in the area on monthly-yearly time scale, of a magnitude between 5-7 on the Richter scale [*www.earthquaketrack.com*]. These seismic events may possibly act as triggers for turbidite flows to the deep basin, though the exact mechanism is unknown. It is possible that clusters of turbidites are

due to clusters of seismic events or alternatively a single earthquake may create a meta-stable slope which is then later subject to multiple failures.

A possible explanation for the absence of coarse grained turbidites between ~900-300ka has been outlined in Chapter 6. As well as the change in grain size, a concurrent decrease in the width, accumulation rate and carbonate and aragonite content of turbidite layers also occurs. It is proposed that these variations in the turbidite record are probably due to the changes in the level of carbonate production on the shallow shelf. For the periods 1.26Ma-MIS23 and MIS11-present the presence of a barrier reef would not only acts as a source more coarse grained material but also provides a barrier to sediment export to the shelf edge/upper slope [*Cotillon et al.,* 1990; *Dunbar and Dickens,* 2003; *Dubois et al.,* 2008]. This would likely result in fewer turbidites, but those that did occur would be of a greater size and thus carry coarse grained material further. By contrast, without the presence of a barrier reef, during the middle period (MIS23-11), material could be easily transported to the shelf edge and consequently more frequent, but smaller events could be expected to occur in agreement with the observation of turbidite frequency.

7.6.2 The effect of glacial-interglacial cycles on turbidite deposition in sediment core MD06-3019

Aim 2: To examine the e*ffect of glacial-interglacial cycles on turbidite deposition in sediment core MD06-3019 over the complete 1.26Myr record*

Whilst the 'highstand' and 'lowstand shedding models' for carbonate and siliciclastic margins respectively are commonly accepted, there is less consensus on how shedding on mixed siliciclastic-carbonate margins operates on glacial-interglacial timescales. Various suggestions such as the 'reciprocal' [*Handford and Loucks,* 1993; *Schlager et al.,* 1994; *Ferro et al.,* 1999], 'transgressive' [*Dunbar et al.,* 2000; *Dunbar and Dickens,* 2003; *Page et al.,* 2003] and 'coeval shedding models' [*Francis et al.,* 2007] have been proposed. However, these hypotheses were based on

studies of hemipelagic and pelagic sediments and did not include the likely significant contribution of turbidite deposition to sediment accumulation in the slope and basin settings.

The only morphological analogous studies of turbidite sedimentation in the deep sea on mixed margins were conducted on the Ribbon Reef, which is situated along the northern stretch of the Great Barrier Reef, Australia [*Webster et al.*, 2012; *Puga-Bernabéu et al.*, 2014]. The morphology of the Ribbon Reef region is similar to that of the western New Caledonia margin being comprised of a narrow (<50 km) flat shelf, which is rimmed by an extensive shelf-edge reef barrier system. The shelf break is at 70 m water depth and the steep (>6^{o}) continental slope is deeply excavated by shelf-incised canyons. The connection of the Ribbon Reef Canyons with the shelf is influenced by the Ribbon Reefs and the inter-reef passages between them, which are locally connected to shelf-palaeochannels [*Puga-Bernabéu et al.*, 2014]. Studies on the Ribbon Reefs support a form of the transgressive shedding model, where the period where sea-level intersects with the shelf edge canyons is an important factor in determining turbidite production. Results showed a dominance of carbonate (>60 wt.% $CaCO_3$) and siliciclastic turbidites (<40 wt.% $CaCO_3$) during glacial periods; siliciclastic, mixed (40-60 wt.% $CaCO_3$) and carbonate turbidites during transgressions and carbonate and mixed turbidites during interglacial periods. Overall, the authors concluded that the deposition of turbidites was controlled by the position of sea-level and its interaction with the margin morphology. This led to there being many more carbonate turbidites deposited during transgression and interglacials, when the height of the sea-level allowed for carbonate production to be switched on. The presence of siliciclastic and mixed turbidites was principally attributed to the presence of the barrier reefs (which block and store siliciclastic sediment behind them and concentrate sediment fluxes through the inter-reef passages) and shelf incising canyons (which preferentially capture siliciclastic sediments stored or bypassing the shelf). During a transgression sea-level crosses the shelf break and intersects with reef-passages, allowing mobilisation of sediment on the shelf, via tides and wind driven currents, for export to the deep sea via canyons.

However, these results were only obtained from turbidites deposited over the last 60kyr and the changes in turbidite deposition were not quantitatively assessed.

For the complete MD06-3019 sediment core record there is no obvious significant pattern in the timing, content, grain size or layer width of turbidites in relation to glacial-interglacial cycles. Results do not appear to support the traditional reciprocal model [*Handford and Loucks*, 1993; *Schlager et al.*, 1994; *Ferro et al.*, 1999; *Jorry et al.*, 2008] since there is no reduction in the average carbonate content of turbidites deposited during glacial periods, indeed glacial and interglacial average carbonate values are the same for MD06-3019 turbidites (see *Table 7.6* and *Table 7.7*). Nor do results appear to support the 'transgressive model' suggested by *Dunbar et al.*, 2000, *Dunbar and Dickens*, 2003, *Page et al.*, 2003, *Webster et al.*, 2012, *Puga-Bernabéu et al.*, 2014 and *Harper et al.*, 2015, where the time spent crossing the shelf edge is critical of siliciclastic turbidite production. There is no predicted drop in the average carbonate content of turbidites deposited during transgression periods to suggest an in increase in siliciclastic deposition, indeed there is an apparent marginal increase compared to all other phases of the glacial-interglacial sea-level cycle(see *Table 7.6* and *Table 7.7*). Nor is there a significant increase in the average carbonate during interglacial periods (see *Table 7.6* and *Table 7.7*).

There is however, perhaps some support for the 'coeval' model [*Francis et al.*, 2007]; since, relative to the amount of time spent in each period of the glacial-interglacial cycle there are more turbidites deposited during interglacials and fewer in glacials than would be expected (see *Table 7.5*). Though, these results are not considered as significant when examined against a random distribution (see *Table 7.1*). In the coeval model for the GBR by *Francis et al.*, 2007 it is proposed that during the Holocene, in narrow shelf areas (<50km), up to 13% of the annual terrigenous riverine sediment supplied to the margin may be deposited in the Queensland Trough. Mechanisms for sediment transport across the shelf are poorly constrained but river plumes during large floods, nepheloid layers, tidal currents,

cyclones and mushroom jets are suggested as possible means of transporting sediment out to the deeper basin [*Francis et al.,* 2007]. The New Caledonia lagoon is relatively narrow, at around 10-20km along the western margin (see *Figure 2.5*) and although terrigenous sediment supply to the lagoon is thought to be minimal, especially in the sand fraction; it is noted that high sediment river plumes and resuspension of sediment during is cyclones and storm events does occur and transports terrigenous material further out towards the shelf edge (see Chapter 2 §2.2). It possible therefore that results seen for sediment core MD06-3019 are due to an increase in humidity and thus precipitation and erosion during interglacial periods and vice versa during glacials, which causes increased turbidite deposition during interglacial periods. However, whilst this occurs concurrently with glacial-interglacial sea-level change, the two mechanisms are not directly linked. Additionally, the slight reduction in turbidites deposited during glacial periods may be due to rivers initially depositing eroded siliciclastic material on the exposed shelf and aggrading, due to the topographic barrier of karstified highstand reefs, before passes are eroded through and material can be more easily be transported out to the outer shelf/ upper slope [*Francis et al.,* 2007; *Puga-Bernabéu et al.,* 2014].

Overall, this suggests that glacial-interglacial sea-level is not the principal controlling factor in establishing the timing of turbidite deposition in the deep sea along the western New Caledonian margin. Different processes can be seen to increase the chance of slope failure happening during both highstand and lowstand conditions. For example, during highstands prograding shelf and slope edges can cause over steepening and thus slope failure. By contrast, sea-level fall during lowstands and transgressions causes erosion and undercutting of the shelf edge shoreline by waves and currents, as well as cyclic wave loading causing pulsating pore pressures which can result in slope failure. However, *Handford and Loucks* (1993) note that slope failure is not constrained by sea-level and can occur at any time if sediments are ready for gravity failure and triggering mechanisms exist. It is possible that sea-level does have an effect on turbidite deposition in the New Caledonia trough, but this is masked by other mechanisms which initiate gravity flow events. As was proposed in

the previous section earthquakes may act as triggers. The timing of these events, whilst not entirely stochastic when considered in respect to the fault system they are associated with, do not have any relationship with glacial-interglacial change and thus complicate the turbidite record observed. If seismic events did exert a significant control on turbidite deposition on the western New Caledonian margin this may explain the apparent lack of correlation between turbidite width and timing relative to glacial-interglacial cycles. Rather the size of the turbidite event would depend on the amount of sediment available to be mobilised and the size of the triggering earthquake [*Blumberg et al.*, 2008; *Goldfinger et al.*, 2012]. The former may be affected by changes in the degree of sediment supplied to the upper slope during glacial-interglacial cycles, but sediment 'starvation' does not occur to the same extent on mixed margins as it does on pure siliciclastic or carbonate ones.

The content of turbidite layers may show little variation over glacial-interglacial cycles due to possible mixing and storage on the shallow shelf and upper slopes before deposition in the deep sea. It has not been possible to independently date the carbonate material present in turbidite layers in order to examine the time lag between growth and final deposition in the deep sea. For turbidites on the eastern side of New Caledonia *Cotillon et al*. (1990) observed a time lag of 10-15kyr between the age of carbonate material present within a turbidite layer and the depositional age of the layer itself. If there were merely a consistent offset between the age of material deposited and the age of turbidites itself this may be corrected for fairly easily. However, it is likely that mixing has occurred between material during storage on the outer shelf or upper slope, before deposition in the deep sea and that the growth ages of material deposited within a single layer are variable. Along the western margin of New Caledonia drowned terraces, associated with previous periods of reef growth, provide possible areas for the storage and mixing of material before export to the deep sea back until the Mid-Pleistocene [*Flamand*, 2006]. These terraces, which are present along the whole barrier reef slope, are 10s of metres wide and present down to ~120m water depth. Similar locations may have existed further back in the MD06-3019 record. Though the volume of material able to be stored on

these terraces individually would be unable to account for the size of turbidites seen at core site MD06-3019, they do represent areas for potential storage and mixing before later export to the deep sea. The problems of storage and mixing of sediment before deposition would not affect hemipelagic or pelagic records of sedimentation on mixed margins, since sediment export operates via a different mechanism.

7.6.3 The effect of changes in shallow-shelf carbonate production, margin morphology and the amplitude of sea-level change on turbidite deposition in sediment core MD06-3019

Aim 3 and 4: To examine the effect of changes in sea-level amplitude, shallow shelf carbonate production, shelf morphology and sediment routing on glacial-interglacial turbidite deposition in sediment core MD06-3019

From previous work it is to be expected that changes in glacial-interglacial sea-level cycles, shallow shelf carbonate production, sediment routing and margin morphology would have an effect on the glacial-interglacial pattern of deep sea turbidite deposition; though the exact nature of these changes remains the subject of research. The work of *Puga-Bernabéu et al.* (2014) on turbidite deposition along different areas of the Great Barrier Reef highlights the need to consider margin morphology when making interpretations of turbidite deposition in the deep sea. Whilst their study examined spatial changes along the Great Barrier Reef, there are proposed temporal changes on the western new Caledonian margin which may be expected to have affected turbidite deposition across the period in an analogous way. For example, the contraction of carbonate production during highstands after MIS25, establishment of the barrier reef system at MIS11, flooding of the lagoon at MIS5 and rerouting of the lowstand shelf fluvial system at MIS2 [*Cabioch et al.*, 2008; *Le Roy et al.*, 2008; *Montaggioni et al.*, 2011]. Indeed, if there were significant temporal variations this could account for why no obvious pattern of glacial-interglacial turbidite deposition was observed for the MD06-3019 record as a whole; since different temporal depositional patterns would be averaged out. Therefore, the

patterns of glacial-interglacial turbidite deposition were examined in different periods of the MD06-3019 record.

The proportional increase in glacial turbidites during the middle period of the record between MIS23-MIS11 may have been indicative of the shelf acting more like a siliciclastic margin with lowstand shedding showing a greater dominance (see *Figure 7.9*). This would have supported the hypothesis presented in the previous chapter of lower carbonate production during the period MIS23-MIS11. However, when this feature of the record was analysed with respect to the amount of time spent in glacial periods this pattern disappears. Instead, generally, when compared to random distributions there are no significant patterns of deposition at any period of the MD06-3019 record, during any stage of the glacial-interglacial cycle. During the middle period MIS23-MIS11 compared to 1.26Ma-MIS23 and MIS11-present there appears to be a marginal decrease in the numbers of turbidites deposited during glacials, transgressions and interglacials and an increase in the number deposited during regressions (see *Table 7.3* and *Figure 7.10*). However, none of these are statistically significant changes. In fact, despite the increase in numbers of turbidite layers deposited during glacial stages in the period MIS23-MIS11, there are still marginally fewer than would be expected based on random chance; the same as in the rest of the record. Similarly, no clear patterns were observed when the MD06-3019 record was analysed to see if there were any changes in turbidite content or width, in relation to glacial-interglacial cycles, that could be associated with changes in shallow shelf carbonate production or sea-level change amplitude.

Overall, there are no clear changes in any feature of turbidite deposition between the periods 1.26Ma-MIS23, MIS23-MIS11 or MIS11-present, with respect to glacial interglacial cycles; which suggest that any of the ‘reciprocal’, ‘transgressive’ or ‘coeval’ shedding models appear to operate more strongly in one period than another. It is, however, implausible to argue from this evidence that neither changes in sea-level amplitude, shallow shelf carbonate production or margin morphology affect

deep sea turbidite deposition. Rather, there are a number of other feasible explanations. As mentioned previously, it is possible that the effect of glacial-interglacial sea-level change on turbidites is masked by seismic events acting as triggers for gravity flows. Additionally, due to the distal position of sediment core MD06-3019 from the western New Caledonian margin, it almost certainly does not receive material from all turbidite events. Therefore, the record examined is both incomplete and may not contain enough turbidites to make a reliable assessment of the effect of changes in shallow-shelf carbonate production, margin morphology and variations in sea-level amplitude on glacial-interglacial turbidite deposition. Furthermore, the problem of sediment mixing and the time lag between deposition on the outer shelf/ upper slope and export as turbidites to the deep sea may provide another complication to the record.

For sediment core MD06-3019 this means broad scale patterns in turbidite content, grain size and width on a 100kyr time scales may help to elucidate changes on the shallow shelf. However, it is not possible to identify temporal changes in turbidite deposition on glacial-interglacial timescales in relation to variations in sea-level change amplitude, shallow-shelf carbonate production or margin morphology and sediment routing. This highlights the need for similar studies in the future to use multiple sediment cores, from both more proximal and distal positions from the margin, in order to better understand the controlling factors for turbidite deposition on mixed margins.

7.7 Conclusions

This chapter provides the first quantitative analysis of turbidite sedimentation in the New Caledonia Trough over the last 17 glacial-interglacial cycles (~1.2Myr) from the analysis of sediment core MD06-3019. In doing so it helps to contribute to the relatively limited body of work that has been conducted on sediment shedding to the deep sea from mixed margins via turbidites.

There is a clear evolution in the nature of turbidite deposits in core MD06-3019 over the 1.26Myr record. Compared to 1.26Ma- MIS23 and MIS11-Holocene, the period MIS23-MIS11 contains no coarse grained turbidites, only fine grained; shows a significant reduction in the carbonate and aragonite content of turbidites, as well as a reduction in layer width and turbidite accumulation rate. It is proposed that the observed changes in the nature of turbidite deposition are due variations in the abundance of shallow shelf carbonate material through time. Shallow water carbonate production is believed to have decreased substantially during the period MIS23-MIS11, due to changes in the amplitude of glacial-interglacial sea-level change (see Chapter 6).

The repeated clustering of turbidite events within ±4kyr of each other occurs throughout the MD06-3019 record, in all phases of glacial-interglacial cycles and is a significant feature. These clusters are possibly due to seismic activity in the area.

In contrast to previous studies [*Jorry et al.*, 2008; *Webster et al.*, 2012; *Puga-Bernabéu et al.*, 2014], over the complete 1.26Myr MD06-3019 record there does not appear to be any relationship between the timing, frequency, content, grain size or layer width of turbidites and their depositional timing in relation to glacial-interglacial cycles. This finding holds across the record as a whole and during shorter sub-periods, delineated by different levels of carbonate production or amplitudes of

glacial-interglacial sea-level change, which may be expected to have produced different glacial-interglacial patterns of turbidite sedimentation. Possible reasons for this apparent lack of relationship between turbidite deposition and glacial-interglacial sea-level change include: the distal position of sediment core MD06-3019 from the western New Caledonian margin which means that not all gravity flow events are recorded at the site, the storage and mixing of sediments on the outer shelf/ upper slope on 10kyr time scales before export as turbidites to the deep sea and the influence of seismic events in triggering turbidites which may 'mask' glacial-interglacial sea-level change driven patterns in turbidite deposition.

For sediment core MD06-3019 this means broad scale patterns in turbidite content, grain size and width on a 100kyr time scales may help to elucidate changes on the shallow shelf. However, it is not possible to identify temporal changes in turbidite deposition on glacial-interglacial timescales in relation to variations in sea-level change amplitude, shallow-shelf carbonate production or margin morphology and sediment routing. Overall, the results of this chapter do not appear to support hypothesis 3 (outlined in Chapter 1), that the record of turbidite deposition MD06-3019 would change at MIS11 (~400ka), due to the expansion of the barrier reef, from a pattern more reflecting low-stand siliciclastic shedding to one reflecting high stand carbonate shedding.

Chapter 8: Perspectives

8.1 Rationale, Motivation and Aims

The rationale and motivation behind this PhD stemmed from the, as yet, unexplained changes that occurred during the Mid-Pleistocene Transition (MPT), when the dominant time period of glacial-interglacial cycles shifted from ~41kyrs to ~100kyrs [*Raymo et al.*, 1997; *Berger et al.*, 1999; *Paillard and Parrenin*, 2004; *de Garidel-Thoron et al.*, 2005; *Medina-Elizalde and Lea*, 2005; *McClymont and Rosell-Melé*, 2005; *Raymo et al.*, 2006; *Clark et al.*, 2006; *Siddall et al.*, 2010; *McClymont et al.*, 2013; *Bates et al.*, 2014]. These changes in global climate are approximately concurrent with an apparent global expansion of tropical reef growth [*Alexander et al.*, 2001*; Multer et al.*, 2002*; Braithwaite et al.*, 2004; *Yamamoto et al.*, 2006; *Cabioch et al.*, 2008*; Gischler et al.*, 2010; *Montaggioni et al.*, 2011]. A possible link between the MPT and this expansion of tropical reef growth has been proposed via modifications in the global carbon cycle: phases of rapid reef growth in shallow water areas being associated with increased release of carbon dioxide to the atmosphere. Tropical coral reef production in shallow water areas is neither the

triggering mechanism for deglaciations, nor entirely responsible for glacial-interglacial atmospheric CO_2 differences. However, reefs are still potentially an important factor in explaining glacial-interglacial CO_2 cycles, being amplifiers of glacial-interglacial climate change and potentially contributing significantly to CO_2 emissions during the later phases of deglaciations [*Kleypas*, 1997; *Vecsei and Berger*, 2004; *Ridgewell et al*, 2003; *Hinestrosa et al.*, 2015].

Most previous investigations of Quaternary tropical reefs have been conducted via borehole studies and frequently have dating uncertainties of the order of hundreds of kyrs (see Chapter 1§6.2). These uncertainties are, therefore, not only larger than the length of a glacial-interglacial cycle (100/41kyr) but are also significant when compared to the length of the MPT as a whole 1,200-500ka (as defined by *Head and Gibbard* (2005)). This means that any inferences made about the relationship between reef expansion and specific changes in the climate system are not well constrained. This thesis set out to attempt to tackle this issue of poorly constrained dating by developing a new methodology for investigating reef history, using sediments shed from the shallow shelf to the deep sea as turbidites. This provides a complementary source of information on reef history from within a secure time framework.

8.2 Overall Conclusions

Deep sea sediment core MD06-3019 was chosen as a study site, being located in the eastern Coral Sea, approximately ~110km offshore from the main island of New Caledonia and its associated barrier reef. The core is principally composed of pelagic ooze but also contains 79 mixed siliciclastic-carbonate turbidites, deposited since 1.26Ma, which contain sediments exported from the shallow shelf, including reefal material. An age model for the core was developed via orbital tuning of the pelagic $\delta^{18}O$ record; this has allowed the depositional ages of turbidites to be given to ±10kyrs, an order of magnitude better than previous studies on coral reefs.

The results of this thesis show that there are significant variations in the nature of turbidite deposition recorded in deep sea sediment core MD06-3019 over the last 1.26Myrs. In the middle section of the core, between ~900-400ka, compared to the periods either side, there is: an absence of coarse grained turbidites, a reduction in the turbidite accumulate rate, yet an increase in turbidite event frequency, a reduction in total carbonate and aragonite content of turbidites and a reduction in the occurrence of coral bearing layers. This evolution in the turbidite record has been hypothesised to be due to variations in the rate of shallow shelf carbonate production and export over time, probably as a result of changes in the amplitude of interglacial highstands. It is proposed that prior to MIS23 (~900ka) sea-level was high enough, during certain interglacial periods at least (MIS25, 31, 37), for significant carbonate production to occur on the shelf (either as an un-rimmed carbonate platform or with barrier reef development at the shelf edge). From MIS23 the climate proceeded into a period of 'lukewarm' interglacials with lower sea-levels. It is suggested that during this period sea-level did not rise enough during highstands to flood the shelf sufficiently (if at all) to allow for significant shallow water carbonate production. The high sea-levels of the long, warm MIS11 then allowed for the expansion of the barrier reef and its continuation during subsequent interglacial periods until the current day.

Consistent with the work of previous researchers [*Cabioch et al.*, 2008; *Montaggioni et al.*, 2011], results from this thesis, support the proposed expansion of the New Caledonia Barrier Reef on the western margin at around 400ka (MIS11). However, changes in the nature of the MD06-3019 turbidite record around 900ka (MIS23/22) suggests that the history of carbonate production on the shelf may be more complex than was thought hitherto. This thesis proposes a previous period of more luxuriant coral reef growth prior to 900ka, at least during certain sea-level highstands (MIS25, 31,37), more akin to the modern day. With reference to global patterns of tropical reef growth during the Quaternary this hypothesis is in line with some previous models of reef growth, such as on the Belize margin and the Gulf of Papua [*Gischler et al.*, 2010; *Droxler and Jorry*, 2013], though not those for the Great Barrier Reef,

Florida Keys or Ryukyu Barrier Reef [*Alexander et al.*, 2001; *Multer et al.*, 2002; *Braithwaite et al.*, 2004; *Dubois et al.*, 2008, *Yamamoto et al*., 2010]. Possible causes for these discrepancies arise due to the limitations of both previous studies and the new methodology, developed in this thesis. Core reef borehole studies suffer from loss and alteration of material via erosion and diagenesis, large uncertainties in their age models and limited spatial resolution (see Chapter 1§6.2). By contrast, studies using deep sea turbidites are removed from the source area being investigated and though receiving material from a wide spatial area, turbidites only provide snapshot windows into the history of the shallow shelf, with an added unknown time lag factor.

Overall, this thesis is unique in providing a long term history of deep water turbidite sedimentation on a mixed siliciclastic- carbonate margin over an unprecedented 1.26Myrs. Additionally, this work provides evidence of features in the history of carbonate deposition on the shallow shelf round Grande Terre that have not been seen before in previous borehole studies.

8.3 Assessment of the methodology

The main advantage of the method developed in this thesis is the significant reduction in age uncertainty of events. The core (and the turbidites it contains) can be accurately dated using correlation of oxygen isotope curves from the background carbonate ooze (see Chapter 3 § 5). Age model uncertainties for the turbidites dated in sediment core MD06-3019 are of the order of ±10 kyr (see Chapter 3 § 6.2). This is a small compared to that of previous methodologies (of the order of 100kyrs, see *Table 1.1*) and relative to the length of climate cycles [*Lisiecki and Raymo*, 2005] and the MPT [*Head and Gibbard*, 2005]. Palaeoceanographic proxies can be compared directly to reef history, since both data sets are derived from the same sediment core. This allows for comparison of the timing of events which is simply impossible with traditional borehole methods. In addition, because turbidite material is sourced from a wide area along the coast, the method is able to provide

information on reef history over a larger spatial area than single reef boreholes. Thus reef growth at a laterally shifted position to the modern day barrier reef, which may be missed by boreholes drilled exclusively through the current reef crest, should still be recorded in the turbidite record.

However, as with any methodology there are limitations and here these occur by being removed from the actual locus of the reef. Unlike insitu reef boreholes, this method is limited to the analysis of the material that reaches the deep sea. This removal from the source creates an added 'unknown' when making interpretations on reef history from the nature of the turbidites: are the patterns we see due to changes in the source (i.e. growth or demise of the barrier reef) or transport related (e.g. changes in the canyon systems that feed the turbidites to the deep sea)? Turbidites also only provide 'snap shot windows' of information and there is no control on when these windows are placed; though the distribution of turbidites may have the potential to provide information on shelf history in its own right. Another constraint is that whilst we can accurately date the turbidite events, this may not be an accurate representation of the reef at that time. As has been noted by previous authors, there can be a time lag of 10-15kyrs between the age of carbonate material present within a turbidite layer and the depositional age of the layer itself [*Cotillon et al*., 1990]. Additionally, the spread of ages of material within a single layer is also unknown.

The work presented in this thesis is a trial of a new methodology and a number of the limitations it suffers from could be significantly reduced in future studies by the simple expedient of using more than one core during the investigation of a single margin. By comparing the turbidite records of sediment cores taken from varying locations in the basin, both laterally and with depth, it is possible to ascertain with greater certainty which patterns in the turbidite record are due to changes in production on the shallow shelf, rather than transport processes or dissolution. Additionally, if the grain size of deposits allows (i.e. enough coarse grained material), radiocarbon or U/Th dating on shallow shelf bioclasts found within

turbidites would allow for the quantification of the residence time experienced by sediments on the shallow shelf and upper slope before deposition in deep sea. This would also provide an estimate of the average spread of growth ages for the material within one layer. This may allow for 'correction' of the turbidite events for the time deposition to the period of shallow shelf history they represent.

Overall, the method shows significant promise for future use in investigations of tropical reef history; both as an independent research method for reef history in its own right, but also to provide complementary data to traditional borehole studies, by quantifying reef history with greater temporal accuracy prior to the last two glacial-interglacial cycles.

8.4 Future Work

8.4.1 Future work- New Caledonia

A number of avenues for future work are related to unanswered questions raised by this thesis about the western New Caledonia margin. The acquisition and analysis of more turbidite bearing deep sea cores from the New Caledonia Basin is required in order to ascertain that temporal patterns in the nature of turbidite deposition observed in MD06-3019 are due to changes on the shallow shelf and not transport or dissolution signals.

With only the single sediment core MD06-3019 being investigated, it has not been possible to identify any significant changes in the nature of turbidite deposition during different phases of glacial-interglacial cycles. This may be a result of: the distal position of sediment core MD06-3019 from the western New Caledonian margin which means that not all gravity flow events are recorded at the site; the storage and mixing of sediments on the outer shelf/ upper slope on 10kyr time scales before export as turbidites to the deep sea or the influence of seismic events in

triggering turbidites which may ‘mask’ glacial-interglacial sea-level change driven patterns in turbidite deposition. Additional turbidite containing cores would help to distinguish between these possibilities and assist in our understanding of turbidite shedding on mixed margins in relation to glacial-interglacial sea-level change. Indeed, more generally, any investigations into the canyon and turbidite systems of the margin would be welcome in this under-researched topic.

Other areas for further investigation include better constraining the nature of carbonate production prior to 900ka and whether previous phases of barrier reefs were present. An in-depth study of the shallow shelf, large benthic foraminifera found in MD06-3019 turbidites could prove useful in the reconstruction of past shallow water carbonate production and the local climate for the western New Caledonian margin. These foraminifera species are particularly sensitive to depth, substrate, shallow water environment and climate [*Hallock and Glenn*, 1986; *Baccaert*, 1987; *Hottinger*, 1993; *Hottinger*, 1997; *Langer and Hottinger*, 2000]. Thus their distribution thorough time can be used to inform reconstructions of the evolution of carbonate production on the shallow shelf [*Montaggioni and Vénec-Pyré*, 1993]. Further work with additional boreholes and seismic lines of the reef and lagoon areas will help provide a better understanding of the margin morphology during earlier periods of the Pleistocene. As part of this PhD a two week exploratory 2D modelling study, using DIONISOS, of evolution on the shelf was conducted. However, it was not possible to accurately reproduce mixed siliciclastic-carbonate turbidite shedding to the deep sea for the western New Caledonia margin. This was partially due to the difficulties of modelling the complex mixed system in 2D but also as a result of poor constraints on previous margin subsidence and production rates. However, in the future 3D modelling could be a useful tool in helping to constrain the history of the margin over the Quaternary.

8.4.2 Future work- Global Scale

Results from this thesis suggest that changes in the amplitude of eustatic glacial-interglacial sea-level change may have played a significant role in determining the history of the New Caledonia Barrier Reef since 1.26Ma. Since these changes have a global impact, unlike local sea surface temperatures or nutrient variations, it may be predicted that other tropical reefs worldwide may also show a more luxuriant phase of carbonate production prior to 900ka, in a similar way to the New Caledonia margin. Given the potential of the methodology developed in this thesis, the next step is to apply it to investigate the history of other tropical coral reefs worldwide on both pure and mixed margins. This will not only help provide complementary information to the studies already conducted in these areas but may also help illuminate as yet unknown evolutions in their histories. Of course, the evolution of individual margins depends on a whole host of factors, not just eustatic sea-level. However, if it is generally found that there is a global pattern of higher carbonate production during highstands prior to MIS23, a significant reduction between MIS23-MIS11, before a re-expansion at MIS11 this would be an exciting finding. It would not only help support the hypothesis that changes in glacial-interglacial sea-level is a significant factor in determining reef growth world-wide, but also has significant implications for the relationship between global reef production, the carbon cycle and climate during earlier periods of the Quaternary. Unfortunately, high resolution CO_2 records from ice-cores only cover the last 800kyr [*Lüthi et al.*, 2008]. This makes it difficult to constrain the relationship between atmospheric CO_2 changes, evolution in global coral reef growth and variations in ocean circulation, ice-volume (location and extent) and surface and deep ocean temperatures which have all been proposed as contributory mechanisms behind the MPT. Thus the Mid-Pleistocene Transition and the role of reefs during this period remains an open and deeply interesting question.

References

Achituv, Y. and Dubinsky, Z. (1990) Evolution and zoogeography of coral reefs; In Z. Dubinsky (editor) 'Ecosystems of the world 25. Coral Reefs', Chapter 1, p. 1-9, Elsevier, Amsterdam

Alexander, I., Andres, M., Braithwaite, C., Braga, J., Cooper, M., Davies, P., Elderfield, H., Gilmour, M., Kay, R., Kroon, D., McKenzie, J., Montaggioni, L., Skinner, A., Thompson, R., Vasconcelos, C., Webster, J., and Wilson, P. (2001) New Constraints on the origin of the Australian Great Barrier Reefs: Results from an international project of deep coring; Geology, v. 29, p. 483-486

Allwood, A., Walter, M., Kamber, B., Marshall, C. and Burch, I. (2006) Stromatolite reef from the Early Archaean era of Australia; Nature, v. 441, p. 714-718.

Alory, G., Vega, A., Ganachaud, A. and Despinoy, M. (2006) Influence of upwelling, subsurface stratification, and heat fluxes on coastal sea surface temperature off southwestern New Caledonia; Journal of Geophysical Research, v. 111, C07023, p. 1-9

Anderson, R., Fleisher, M. Lao, Y. and Winckler, G. (2008) Modern $CaCO_3$ preservation in equatorial Pacific sediments in the context of late-Pleistocene glacial cycles; Marine Chemistry, v. 111, p. 30-46

Andréfouët, S., Muller-Karger, F., Robinson, J., Kranenburg, C., Torres-Pulliza, D., Spraggins, S. and Murch, B. (2006) Global assessment of modern coral reef extent and diversity for regional science and management applications: a view from space; Proceedings of the 10th International Coral Reef Symposium, v. 1, p. 1732-1745

Andréfouët, S., Cabioch, G., Flamand, B. and Pelletier, B. (2009) A reappraisal of the diversity of geomorphological and genetic processes of New Caledonian coral reefs: a synthesis from optical remote sensing, coring and acoustic multibeam observations; Coral Reefs, v. 28, p. 691-707

Anthony, K. and Connolly, S. (2004) Environmental limits to growth: Physiological niche boundaries of corals along turbidity-light gradients; Oecologia, v. 141, p.373-384

Archer, D. (1991) Equatorial Pacific calcite preservation cycles: production or dissolution; Paleoceanography, v. 6(5), p. 561-571

Baccaert, J. (1987) Distribution patterns and taxonomy of benthic foraminifera in the Lizard Island reef complex, northern Great Barrier Reef, Australia; PhD thesis, Liege University, Belgium

Bak, R. and Elgershuizen, J. (1976) Patterns of oil-sediment rejection in corals; Marine Biology, v. 37, p. 105-113

Baldwin, S., Rawling, T. and Fitzgerald, P. (2007) Thermochronology of the New Caledonian high pressure terrane-Implications for the middle Tertiary plate boundary process in the SW Pacific; Geological Society of America Special Paper 419, p. 117-134

Barker, S., Archer, D., Booth, L., Elderfield, H., Henderiks, J. and Rickaby, R. (2006) Globally increased pelagic carbonate production during the Mid-Brunhes dissolution interval and the CO_2 paradox of MIS11; Quaternary Science Reviews, v. 25, p. 3278-3293

Bates, S., Siddall, M. and Waelbroeck, C. (2014) Hydrographic variations in deep ocean temperature over the mid-Pleistocene transition; Quaternary Science Reviews, v. 88, p. 147-158

Berger, A., Li, X. and Loutre, M. (1999) Modelling northern hemisphere ice volume over the last 3 Ma; Quaternary Science Reviews, v.18, p.1-11

Berger, W. (1982) Increase of Carbon Dioxide in the Atmosphere During Deglaciation: the Coral Reef Hypothesis; Naturwissenschaften, v. 69, p. 87-88

Berner, R., Lasaga, A. and Garrels, R. (1983) The Carbonate-silicate geochemical cycle and its effect on atmospheric carbon dioxide over the past 100 million years; American Journal of Science, v. 283, p.641-683

Blumberg, S., Lamy, F., Arz, H., Echtler, H., Wiedicke, M., Haug, G. and Oncken, O. (2008) Turbiditic trench deposits at the South-Chilean active margin: A Pleistocene-Holocene record of climate and tectonics; Earth and Planetary Science Letter, v. 268, 526-539

Boardman, M. and Neumann, A. (1984) Sources of periplatform carbonates: Northwest Providence Channel, Bahamas; Journal of Sedimentary Petrology, v. 54(4), p. 1110-1123

Boardman, M., Neumann, A., Baker, P., Dulin, L., Kenter, R., Hunter, G. and Kiefer, K. (1986) Banktop responses to Quaternary fluctuations in sea level recorded in periplatform sediments; Geology, v. 14(1), p. 28-31

Borer, J. and Harris, P. (1991) Lithofacies and cyclicity of the Yates Formation, Permian Basin: Implications for reservoir heterogeneity; American Association of Petroleum Geologists Bulletin, v. 75, p. 726-779

Bosscher, H. and Schlager, W. (1992) Computer simulation of reef growth; Sedimentology, v. 39(3), p. 503-512

Braithwaite, C., Dalmasso, H., Gilmour, M., Harkness, D., Henderson, G., Kay, R., Kroon, D., Montaggioni, L. and Wilson P. (2004) The Great Barrier Reef: The chronological record from a new borehole; Journal of Sedimentary Research, v. 74, p. 298-310

Broecker, W. and van Donk, J. (1970) Insolation changes, ice volumes, and the O^{18} record in deep-sea cores; Reviews of Geophysics, v. 8(1), p. 169-198

Brown, A. and Loucks, R. (1993) Influence of sediment type and deposition processes on stratal patterns in the Permian Basin-margin Lamar Limestone, McKittrick Canyon, Texas; In: R.G. Loucks and G.F. Sarg (Eds.), 'Carbonate Sequence Stratigraphy'. American Association of Petroleum Geologists, Memoir 57, p. 133-156.

Cabioch, G. (2003) Postglacial reef development in the South-West Pacific: case studies from New Caledonia and Vanuatu; Sedimentary Geology, v. 159, p. 43-59

Cabioch, G., Montaggioni, L. and Faure, G. (1995) Holocene initiation and development of New Caledonian fringing reefs, SW Pacific; Coral Reefs, v. 14, p. 131-140

Cabioch, G., Correge, T., Turpin, L., Castellaro, C. and Recy, J. (1999) Development patterns of fringing and barrier reefs in New Caledonia (southwest Pacific); Oceanologica Acta, v. 22(6), p. 567-578

Cabioch, G., Montaggioni, L., Thouveny, N., Frank, N., Sato, T., Chazottes, V., Dalamasso, H., Payri, C., Pichon M. and Sémah, A.M., (2008) The chronology and structure of the western New Caledonia barrier reef tracts; Palaeogeography, Palaeclimatoloy, Palaeoecology, v. 268, p. 91-105

Calder, N. (1974) Arithmetic of ice ages; Nature, v. 252, p.216-218

Cande, S. and Kent, D. (1995) Revised calibration of the geomagnetic polarity timescale for the Late Cretaceous and Cenozoic; Journal of Geophysical Research, v. 100 (B4), p. 6093-6095

Chalker, B. (1981) Simulating light-saturation curves for photosynthesis and calcification by reef-building corals; Marine Biology, v. 63, p. 135-141

Chardon, D. and Chevillotte, V. (2006) Morphotectonic evolution of the New Caledonia ridge (Pacific Southwest) from post-obduction tectonosedimentary record; Tectonophysics, v. 420, p. 473-491

Chardon, D., Austin, J., Cabioch, G., Pelletier, B., Saustrup, S. and Sage, F. (2008) Neogene history of the northeastern New Caledonia continental margin from multichannel reflection seismic profiles; Comptes Rendus Geocience, v. 340, p. 68-73

Chevillotte, V., Douillet, P., Cabioch, G., Lafoy, Y., Lagabrielle, Y. and Maurizot, P. (2005) Évolution géomorphologique de l'avant-pays du Sud-Ouestde la Nouvelle-Calédonie durant les derniers cycles glaciaires; Comptes Rendus Géoscience, v. 337, p. 695-701

Clark, P., Archer, D., Pollard, D., Blum, J., Rial, J., Brovkin, V., Mix, A., Pisias, N. and Roy, M. (2006) The middle Pleistocene transition: characteristics, mechanisms, and implications for long-term changes in atmospheric pCO_2; Quaternary Science Reviews, v.25, p. 3150-3184

Clavier, J., Chardy, P. and Chevillon, C. (1995) Sedimentation of particulate matter in the South-West lagoon of New Caledonia: spatial and temporal patterns; Estuarine Costal and Shelf Science, v. 40, p. 281-294

Cluzel, D., Aitchison, J. and Picard, C. (2001) Tectonic accretion and underplating of mafic terranes in the Late Eocene intraoceanic fore-arc of New Caledonia (Southwest Pacific) : geodynamic implications; Tectonophysics, v. 340, p. 23-59

Coles, S. and Jokiel, P. (1992) Effects of salinity on coral reefs. In D.W. Connell and D.W. Walker (editors), 'Pollution in tropical aquatic systems', Chapter 6, p. 147-166, CRC Press, Boca Raton

Collot, J., Malahoff, A., Recy, J., Latham, G. and Missegue F. (1987) Overthrust emplacement of New Caledonia ophiolite: geophysical evidence; Tectonics, v. 6(3), p. 215-232

Cooper, T., Uthicke, S., Humphrey, C and Fabricius, K. (2007) Gradients in water column nutrients, sediment parameters, irradiance and coral reef development in the Whitsunday Region, central Great Barrier Reef; Estuarine Coastal and Shelf Science, v. 74, p. 458-470

Copper, P. (1994) Ancient reef ecosystems expansion and collapse; Coral Reefs, v. 13, p.3-11

Cotillon, P., Rigolot, P., Coustillas, F., C., Laurin, B., Liu, D.J., Pannetier, W., Pascal, A. and Rio, M. (1989a) Pentes et bassins au large de la Nouvelle-Calédonie (Sud -Ouest Pacifique); Oceanologica Acta, v. 12(2), p. 131-140

Cotillon, P., Liu, J.D., Gaillard, C. and Evin, J. (1989b) Evolution du taux de sédimentation au cours des derniers 30 000 ans aux abords de la Nouvelle-Calédonie (SW Pacifique): résultants de datations au radiocarbon et par la courbe de l'oxygène 18: Bulletin de la Société Géologique de France, v. 4, p. 881-884

Cotillon, P., Coustillas, F., Gaillard, C., Laurin, B., Liu, D.J., Pannetier, W., Pascal, A., Pascal, F., Rigolot, P., Rio, M., Tribouillard, N. and Vincent, E. (1990) Grands traits de la sedimentation actuelle et récente sur les pentes et dans les bassins au large de la Nouvelle-Calédonie (SW Pacifique): résultats géologiques de la campagne Biocal; Oceanologica Acta, v. Spécial 10, p. 341-359

Coudray, J. (1976) Recherches sur le Néogene et le Quaternaire marins de la Nouvelle-Calédonie; contribution de l'étude sédimentologique à la connaissance de l'histoire Géologique post-éocene. In: Expédition française sur les récifs coralliens de la Nouvelle-Calédonie; volume Huitième; Thèse Doct. D'Etat, Montpellier, 1-275

Cramer, B., Toggweiler, J., Wright, J., Katz, M. and Miller, K. (2009) Ocean overturning since the Late Cretaceous: Inferences from a new benthic foraminiferal isotope compilation; Paleoceanography, v. 24(4), PA4216

Cravatte, S., Kestenare, E., Eldin, G., Ganachaud, A., Lefèvre, J., Marin, F., Menkes, C. and Aucan, J. (2015) Regional circulation around New Caledonia from two decades of observations; Journal of Marine Systems, v. 148, p. 249-271

de Garidel-Thoron, T., Rosenthal, Y., Bassinot, F. and Beaufort, L. (2005) Stable sea surface temperatures in the western Pacific warm pool over the past 1.75 million years; Nature, v. 433, p.294-298

DeConto, R. and Pollard, D. (2003) Rapid Cenozoic glaciation of Antarctica induced by declining atmospheric CO_2; Nature, v. 421, p. 245-249

Delcroix, T. and Lenormand, O., (1997) ENSO signals in the vicinity of New Caledonia, South Western Pacific; Oceanologica Acta, v. 20, p. 481-491

Done, T. (1992b) Effects of tropical cyclone waves on ecological and geomorphological structures of the Great Barrier Reef; Continental Shelf Research, v. 12, p. 859-872

Droxler, A. and Schlager, W. (1985) Glacial versus interglacial sedimentation rates and turbidite frequency in the Bahamas; Geology, v. 13, p. 799-802

Droxler, A. and Jorry, S. (2013) Deglacial origin of barrier reefs along low-latitude mixed siliciclastic and carbonate continental shelf edges; Annual Review of Marine Science, v. 5, p. 165-190

Dubois, J., Launay, J. and Récy, J. (1974) Uplift movements in New Caledonia-Loyalty Islands area and their plate tectonics interpretation; Tectonophysics, v. 24(1-2), p. 133-150

Dubois, N., Kindler, P., Spezzaferri, S. and Coric, S. (2008) The initiation of the Southern central Great Barrier Reef: New multiproxy data from Pleistocene distal sediments from the Mario Plateau (NE Australia); Marine Geology, v. 280, p. 223-233

Dunbar, G., Dickens, G. and Carter, R. (2000) Sediment flux across the Great Barrier Reef Shelf to the Queensland Trough over the last 300ky; Sedimentary Geology, v. 133, p. 49-92

Dunbar, G. and Dickens, G. (2003) Late Quaternary shedding of shallow-marine carbonate along a tropical mixed siliciclastic-carbonate shelf: Great Barrier Reef, Australia; Sedimentology, v. 50, p. 1061-1077

Elderfield, H., Ferretti, P., Greaves, M., Crowhurst, S., McCave, I.N., Hodell, D. and Piotrowski, A. (2012) Evolution of Ocean Temperature and Ice Volume Through the Mid-Pleistocene Climate Transition, Science, v. 337, p. 704-709

Emery, D. (1996) Carbonate systems. In: Emery, D., Myers, K.J. (Eds.), 'Sequence Stratigraphy'. Blackwell Science Ltd, p. 211-237

Emiliani, C. (1955) Pleistocene temperatures, Journal of Geology, v. 63(6), p. 538-578

Encyclopaedia Britannica, 2012

Farrell, J. and Prell, W. (1989) Climatic change and $CaCO_3$ preservation: an 800,000 year bathymetric reconstruction from the central equatorial Pacific Ocean; Paleoceanography, v. 4(4), p. 447-466

Ferro, C., Droxler, A., Anderson, J., Mucciarone, D. (1999) Late Quaternary Shift of Mixed Siliciclastic-carbonate Environments Induced by Glacial Eustatic Sea-level Fluctuations in Belize; in Advances in Carbonate Sequence Stratigraphy: Application to Reservoirs, Outcrops and Models, SEPM Special Publication No. 63, p. 385-411

Flamand, B. (2006) Les pentes externes du récif barrière de la Grande Terre de Nouvelle-Caledonie: morphologie, lithologie, contrôle de la tectonique et de l'eustatisme; PhD Thesis, Ecole Doctrale des Sciences de la Mer, Université de Bretagne Occidentale, Brest, France, p. 1-241

Flamand, B., Cabioch, G., Payri, C. and Pelletier, B. (2008) Nature and biological composition of the New Caledonian outer barrier reef slopes; Marine Geology, v. 250, p. 157-179

Foucher, J. P., Charlou, J. L., Harmegnies F., Wirrmann D., Sémah A. M., Chaduteau C. and Roussel E. (2006) Rapport des travaux de la champagne ZoNéCo 12, Campagne AUSFAIR/ZoNéCo 12 à bord du N/O Marion Dufresne (12 au 26 février 2006)

Francis, J., Dunbar, G., Dickens, G., Sutherland, I. and Droxler, A. (2007) Siliciclastic sediment across the north Queensland margin (Australia): A Holocene perspective on reciprocal versus coeval deposition in tropical mixed siliciclastic-carbonate systems; Journal of Sedimentary Research, v. 77, p. 572-586

Frank, N., Turpin, L., Cabioch, G., Blamart, D., Tressens-Fedou, M., Colin, C. and Jean-Baptiste, P. (2006) Open system U-series ages of corals from a subsiding reef in New Caledonia: Implications for sea level changes, and subsidence rate; Earth and Planetary Science Letters, v. 349, p. 271-289

Ghent, E., Roddick, J. and Black, P. (1994) $^{40}Ar/^{39}Ar$ dating of white micas from the epidote to the omphacite zones, northern New Caledonia; tectonic implications; Canadian Journal of Earth Sciences, v. 31(6), p. 995-1001

Gilbert, G. (1900) Rhythms and geologic time, Science; v. 11(287), p. 1001-1012

Gischler, E., Ginsburg, R., Herrle, J. and Prasad, S. (2010) Mixed carbonate and siliciclastics in the Quaternary of southern Belize: Pleistocene turning points in reef development controlled by sea-level change; Sedimentology, v. 57, p. 1049-1068

Goldfinger, C., Morey, A., Nelson, C., Gutierrez-Pastor, J., Johnson, J., Karabanov, E., Chaytor, J. and Eriksson, A. (2007) Rupture lengths and temporal history of significant earthquakes on the offshore and north coast segments of the Northern San Andreas Fault based on turbidite stratigraphy; Earth and Planetary Science Letters, v. 254, p. 9-27

Goldfinger, C., Nelson, C., Morey, A., Johnson, J., Patton, J., Karabanov, E., Gutiérrez-Pastor, J., Eriksson, A., Gràcia, E., Dunhill, G., Enkin, R., Dallimore, A. and Vallier, T. (2012) Turbidite Event History- Methods and Implications for Holocene Paleoseismicity of the Cascadia Subduction Zone; In: 'Earthquake Hazards of the Pacific Northwest Coastal and Marine Regions', USGS Professional Paper 1661, Robert Kayen (editor)

Goldner, A., Herold, N. and Huber M. (2014) Antarctic glaciation caused ocean circulation changes at the Eocene-Oligocene transition; Nature, v. 511, p.574-577

Gouriou, Y. and Delcroix, T. (2002) Seasonal and ENSO variations of sea surface salinity and temperature in the South Pacific Convergence Zone during 1976-2000; Journal of Geophysical Research, v. 107 (C12), 8011

Grigg, R. (1982) Darwin Point: A threshold for atoll formation; Coral Reefs, v. 1, p. 29-34

Grossman, E. and Fletcher, C. III (2004) Holocene reef development where wave energy reduces accommodation space, Kailua Bay, Windward Oahu, Hawaii, U.S.A; Journal of Sedimentary Research, v. 74, p. 49-63

Hallcock, P. and Glenn, C. (1986) Larger foraminifera: a tool for paleoenvironmental analysis of Cenozoic carbonate depositional facies; Palaios, v.1, p. 55-65

Halley, R. and Harris, P. (1979) Freshwater cementation of a one thousand year old oolite; Journal of Sedimentary Petrology, v. 49, p.969-988

Handford, C. and Loucks, R. (1993) Carbonate Depositional Sequences and Systems Tracts- Responses of Carbonate Platforms to Relative Sea-Level Changes; In: R.G. Loucks and G.F. Sarg (Eds.), 'Carbonate Sequence Stratigraphy'. American Association of Petroleum Geologists, Memoir 57, p. 3-41

Hanna, J. and Moore, C. (1979) Quaternary temporal framework of reef to basin sedimentation, Grand Cayman, B.W.I.; Geological Society of America Annual Meeting, Abstract Programs, 11: 438

Haq, B., Hardenbol, J. and Vail, P. (1987) Chronology of fluctuating sea levels since the Triassic; Science, v. 235, p. 1156-1166

Harper, B., Puga-Bernabéu, A., Droxler, A., Webster, J., Gischler, E., Tiwari, M., Lado-Insua, T., Thomas, A., Morgan, S., Jovane, L. and Rôhl, U. (2015) Mixed carbonate-siliciclastic sedimentation along the Great Barrier Reef upper slope: a challenge to the reciprocal sedimentation model; Journal of Sedimentary Research, v. 85, p. 1019-1036

Haug, G., Tiedemann, R., Zahn, R. and Ravelo, A. (2001) Role of Panama uplift on oceanic freshwater balance; Geology, v. 29(3), p. 207-210

Hays, J., Saito, T., Opdyke, N. and Burckle, L. (1969) Pliocene-Pleistocene sediments of the equatorial Pacific: Their paleomagnetic, biostratigraphic and climatic record; Geological Society of America Bulletin, v. 80(8), p. 1481-1514

Hays, J., Imbrie, J. and Shackleton, N. (1976) Variations in the Earth's Orbit: Pacemaker of the Ice Ages; Science, v.194, p. 1121-1132

Head, M. and Gibbard, P. (2005) Early-Middle Pleistocene Transitions: an overview and recommendation for the defining boundary; in 'Early-Middle Pleistocene Transitions: The Land-Ocean Evidence', edited by M. J. Head and P. L. Gibbard, p. 1-18, Geological Society

Hénin, C. and Cresswell, G. (2005) Upwelling along the western barrier reef of New Caledonia; Marine and Freshwater Research, v. 56(7), p. 1005-1010

Hennekam, R. and de Lange, G. (2012) X-ray fluorescence core scanning of wet marine sediments: methods to improve quality and reproducibility of high resolution paleoenvironmental records; Limnology and oceanography: methods, v. 10(12), p. 991-1003

Hinestrosa, G., Webster, J. and Beaman, R. (2015) Drowned reefs as agents of climate change: New constraints from the shelf-edge of the Great Barrier Reef, Australia; Conference abstract from the 31st International Association of Sedimentologists Meeting, Krakow, Poland

Hottinger, L. (1983) Processes determining the distribution of larger foraminifera in space and time; Utrecht Micropaleontological Bulletin, v. 30, p. 239-253

Hottinger, L. (1997) Shallow benthic foraminiferal assemblages as signals for depth of their deposition and their limitations; Bulletin de la Société Géologique de France, v.168(4), p. 491-505

Hubbard, D. (1988) Controls of modern and fossil reef development: Common ground for biological and geological research; Proceedings of the Sixth International Coral Reef Symposium, Townsville, Australia, v. 1, p. 243-252

Hubbard, D., Burke, R. and Gill, I. (1998) Where's the reef: The role of framework in the Holocene; Carbonates and Evaporites, v. 13(1), p. 3-9

Huybers, P. and Aharonson, O., (2010) Orbital tuning, eccentricity, and the frequency modulation of climatic precession; Paleoceanography, v. 25, PA4228

Imbrie, J., and Kipp, N. (1971) A new micropaleontological method for quantitative paleoclimatology: application to a late Pleistocene Caribbean core; in 'The Late Cenozoic Glacial Ages', edited by K. K. Turekian, p. 71-181, Yale University Press, New Haven

Imbrie, J. and Imbrie, J (1980) Modeling the Climate Response to Orbital Variations; Science, v.207, p.943-953

Imbrie, J., Hays, J., Martinson, D., McIntyre, A., Mix, A., Morley, J., Pisias, N., Prell, W. and Shackleton, N. (1984) The orbital theory of Pleistocene climate: Support from a revised chronology of the marine $\delta^{18}O$ record; In 'Milankovitch and Climate; Understanding the Response to astronomical Forcing', Volume 2 edited by A. Berger et al., p. 269-305, D. Riedel, Dordrecht, Netherlands

Imbrie, J., Berger, A., Boyle, E., Clemens, S., Duffy, A., Howard, W., Kukla, G., Kutzbach, J., Martinson, D., McIntyre, A., Mix, A., Molfino, B., Morley, J., Peterson, L., Pisias, N., Prell, W., Raymo, M., Shackleton, N. and Toggweiler, J. (1993) On the Structure and Origin of Major Glacial Cycles; Paleoceanography, v. 8(6), p. 699-735

Isern, A., McKenzie, J. and Feary, D. (1996) The role of sea-surface temperature as a control on carbonate platform development in the western Coral Sea; Palaeogeography Palaeoclimatology Palaeoecology, v. 124(3-4), p. 247-272

Jaccard, S., Hayes, C., Martíez-Garda, A., Hodell, D., Anderson, R., Sigman, D. and Haug, G. (2013) Two Modes of Change in Southern Ocean Productivity Over the Past Million Years; Science, v. 339, p. 1419-1423

James, N. (1979) Facies models 9. Introduction to carbonate facies models; In R. G. Walker (editor), 'Facies Models: Geoscience', Canada Reprint Series 1, p. 105-107

Jorry, S., Droxler, A., Mallarino, G., Dickens, G., Bentley, S., Beaufort, L., Peterson L. and Opdyke B. (2008) Bundled turbidite deposition in the central Pandora Trough (Gulf of Papua) since Last Glacial Maximum: Linking sediment nature and accumulation to sea level fluctuation at millennial timescale; Journal of Geophysical Research, v. 113, F01S19, p. 1-15

Katz, M., Cramer, B., Toggweiler, J., Esmay, G., Liu, C., Miller, K., Rosenthal, Y., Wade, B. and Wright, J. (2011) Impact of Antarctic Circumpolar Current evolution on late middle Eocene to early Oligocene ocean structure; Science, v. 332, p.1076-1079

Kennedy, D., and Woodroffe, C. (2002) Fringing reef growth and morphology: A review; Earth Science Reviews, v. 57, p. 255-277

Kennett, J. (1977) Cenozoic Evolution of Antarctic Glaciation, the Circum-Antarctic Ocean, and their Impact on Global Paleoceanography; Journal of Geophysical Research, v. 82(27), p. 3843-3860

Kessler,W. and Cravatte, S. (2013a) Mean circulation of the Coral Sea; Journal of Geophysical Resarch: Oceans, v. 118, p. 6385-6410

Kinsey, D. and Davies, P. (1979) Effects of elevated nitrogen and phosphorous on coral reef growth; Limnology and Oceanography, v. 24(5), p. 935-940

Kleypas, J. (1997) Modelled estimates of global reef habitat and carbonate production since the Last Glacial Maximum; Paleoceanography, v. 12(4), p. 533-545

Kleypas, J., McManus, J. and Meñez, L. (1999) Environmental Limits to Coral Reef Development: Where Do We Draw the Line?; American Zoologist, v. 39, p.146-159

Klingelhoefer, F., Lafoy, Y., Collot, J., Cosquer, E., Géli, L., Nouzé, H. and Vially, R. (2007) Crustal structure of the basin and ridge system west of New Caledonia (southwest Pacific) from wide-angle and reflection seismic data; Journal of Geophysical Research, v. 112, B11102, p. 1-18

Lafoy, Y., Auzende, J.M., Smith, R. and Labails, C. (2000) Évolution géologique post-Pléistocène moyen du domaine lagonaire Néo-Calédonien méridional; Comptes Rendus de l'Académie des Sciences, Sér. IIA, Earth Planetary Sciences, v. 330 (4), p. 265-272

Lagabrielle, Y., Maurizot, P., Lafoy, Y., Cabioch, G., Pelletier, B., Régnier, M., Wabete, I. and Calmant S. (2005) Post-Eocene extensional tectonics in Southern New Caledonia (SW Pacific): Insights from onshore fault analysis and offshore seismic data; Tectonophysics, v. 403(1-4), p. 1-28

Lambeck, K., Esat, T. and Potter, E.K (2002) Links between climate and sea levels for the past three million years; Nature, v. 419, p.199-207

LaMontagne, R., Murray, R., Wei, K.-Y., Leinen, M. and Wang, C.-H. (1996) Decoupling of carbonate preservation, carbonate concentration, and biogenic accumulation: A 400-kyr record from the central equatorial Pacific Ocean; Paleoceanography, v.11(5), p. 553-562

Langer, M. and Hottinger, L. (2000) Biogeography of selected "larger" foraminifera; Micropaleontology, v.46, supplement no.1, p. 105-126

Laskar, J., Robutel, P., Joutel, F., Gastineau, M., Correia, A. and Levrard, B. (2004) A long-term numerical solution for the insolation quantities of the Earth; Astronomy and Astrophysics, v. 428(1), p. 261-285

Lawrence, K. and Herbert, T. (2005) Late Quaternary sea-surface temperatures in the western Coral Sea: Implications for the growth of the Australian Great Barrier Reef ; Geology, v. 33, p. 677-680

Le Roy, P., Cabioch, G., Monod, B., Lagabrielle, Y., Pelletier, B and Flamand, B. (2008) Late Quaternary history of the Nouméa lagoon (New Caledonia, South West Pacific) as depicted by seismic stratigraphy and multibeam bathymetry. A modern model of tropical rimmed shelf; Paleogeography, Paleoclimatology, Paleoecology, v. 270, p. 29-45

Lea, D., Pak, D. and Spero, H. (2000) Climate Impact of Late Quaternary Equatorial Pacific Sea Surface Temperature Variations; Science, v. 289, p. 1719-1724

Lea, D., Martin, P., Pak, D. and Spero, H. (2002) Reconstructing a 350ky history of sea level using planktonic Mg/Ca and oxygen isotope records from a Cocos Ridge core; Quaternary Science Reviews, v. 21, p. 283-293

Lisiecki, L. and Raymo, M. (2005) A Pliocene-Pleoistocene stack of 57 globally distributed benthic $\delta^{18}O$ records; Paleoceanography, v.20, PA1003

Locarnini, R., Mishonov, A., Antonov, J., Boyer T. and Garcia, H. (2006),World Ocean Atlas 2005, Volume 1, p. 1-182, U.S. Government Printing Office, Washington, D.C.

Löwmark, L., Hong, W.L., Yui, T.F. and Hung, T.F. (2005) A test of different factors influencing the isotopic signal of planktonic foraminifera in surface sediments from the northern South China Sea; Marine Micropaleontology, v. 55, p. 49-62

Lüthi, D., Le Floch, M., Bereiter, B., Blunier, T., Barnola, J.M., Siegenthaler, U., Raynaud, D., Jouzel, J., Fischer, H., Kawamura, K. and Stocker, T. (2008) High-resolution carbon dioxide concentration record 650,000-800,000 years before present; Nature, v. 453, p. 379-382

Magand, O. (1999) Recherche et définition des signatures géochimiques (métaux lourds et lanthanides) des sources terrigènes du lagon sud-ouest de Nouvelle-Calédonie; Masters Thesis, Université Aix-Marseille II, France, p.1-48

Martinson, D., Pisias, N., Hays, J., Imbrie, J., Moore, T. and Shackleton, N. (1987) Age Dating and the Orbital Theory of the Ice Ages: development of a High-Resolution 0 to 300,000-Year Chronostratigraphy; Quaternary Research, v. 27, p. 1-29

Masson-Delmotte, V., Stenni, B., Pol, K., Braconnot, P., Cattani, 0., Falourd, S., Kageyama, M., Jouzel, J., Landais, A., Minster, B., Barnola, J.M., Chappellaz, J., Krinner, G., Johnsen, S., Röthlisberger, R., Hansen, J., Mikolajewicz, U. and Otto-Bliesner, B. (2010) EPICA Dome C record of glacial and interglacial intensitites; Quaternary Science Reviews, v. 29, p. 113-128

Maurizot, P. and Vendé-Leclerc, M. (2009) New Caledonia geological map, scale 1/500 000, Direction de l'Industrie, des Mines et de l'Energie - Service de la Géologie de Nouvelle-Calédonie, Bureau de Recherches Géologiques et Minières. Explanatory note by Maurizot, P. and Collot, J., 2009

Maurizot, P. and Collot, J. (2009) Explanatory note of the geological map of New Caledonia, scale 1/500 000, Direction de l'Industrie, des Mines et de l'Energie - Service de la Géologie de Nouvelle-Calédonie, Bureau de Recherches Géologiques et Minières

Mazaud, A. (2005) User-friendly software for vector analysis of the magnetization of long sediment cores; Geochemistry Geophysics Geosystems, v. 6, Q12006

McClymont, E. and Rosell-Melé, A. (2005) Links between the onset of modern Walker circulation and the mid-Pleistocene climate transition; Geology, v. 33, p. 389-392

McClymont, E., Sosdian, S., Rosell- Melé, A. and Rosenthal, Y. (2013) Pleistocene sea-surface temperature evolution: Early cooling, delayed glacial intensification, and implications for the mid-Pleistocene climate transition; Earth Science Reviews, v.123, p. 173-193

McGee, W. (1892) Comparative chronology; American Anthropology, p. 327-344

Medina-Elizalde, M. and Lea, D. (2005) The Mid-Pleistocene Transition in the Tropical Pacific; Science, v. 310, p.1009-1012

Meissner, F. (1972) Cyclic sedimentation in Middle Permian strata of the Permian Basin; In: J.G. Elam and S. Chuber (Eds.) 'Cyclic Sedimentation in the Permian Basin', 2nd Edition. West Texas Geological Society Publication 72-60, p. 203-232

Melim, L. and Scholle, P. (1995) The forereef facies of the Permian Capitan formation: the role of sediment supply versus sea-level changes; Journal of Sedimentary Research, v. B65(1), p. 107-118

Mielke, J.E. (1979) Composition of the Earth's crust and distribution of the elements. In: Siegel, F.R. (Ed.), Review of Research on Modern Problems in Geochemistry.UNESCO Report, Paris, p. 13-37

Milankovitch, M. (1948) Ausbau Und Gegenwartiger Stand Der Astronomischen Theorie Der Erdgeschichtlichen Klimate; Experientia, v. 4(11), p. 413-418

Miller, K., Kominz, M., Browning, J., Wright, J., Mountain, G., Katz, M., Sugarman, P., Cramer, B., Christie-Blick, N. and Pekar, S. (2005) The Phanerozoic record of Global Sea-Level Change; Science, v. 310, p. 1293-1298

Milliman, J. (1993) Production and Accumulation of Calcium Carbonate in the Ocean: Budget of a Nonsteady State; Global Biogeochemical Cycles, v. 7(4), p. 927-957

Molnar, P. (2008) Closing of the Central American seaway and the ice age: a critical review; Paleoceanography, v. 23(1), PA2201

Montaggioni, L. (2005) History of Indo-Pacific coral reef systems since the last glaciation: Development patterns and controlling factors; Earth Science Reviews, v. 71, p. 1-75

Montaggioni, L and Braithwaite, C (2009) Quaternary coral reef systems: history development processes and controlling factors. Developments in Marine Geology, v. 5, p. 1-532

Montaggioni, L., Cabioch, G., Thouveny, N., Frank, N., Sato, T. and Sémah, A.M. (2011) Revisiting the Quaternary development history of the western New Caledonian shelf system: From ramp to barrier reef; Marine Geology, v. 280, p. 57-75

Montaggioni, L. and Vénec-Pyré (1993) Shallow-water foraminiferal taphocoenoses at site 821: implications for the Pleistocene evolution of the central Great Barrier Reef shelf, northeastern Australia; Proceedings of the Ocean Drilling Program, Scientific Results, v. 133, p. 365-378

Mount, J. (1984) Mixing of siliciclastic and carbonate sediments in shallow shelf environments; Geology, v. 12, p. 432-435

Mount, J. (1985) Mixed siliciclastic and carbonate sediments: a proposed first-order textural and compositional classification; Sedimentology, v. 32, p.435-442

Multer, H., Gischler, E., Lundberg, J., Simmons, K. and Shinn, E. (2002) Key Largo Limestone Revisited: Pleistocene Shelf-edge Facies, Florida Keys, USA; Facies, v. 46, p. 229-272

Neumann, A. and MacIntyre, I. (1985) Reef response to sea level rise: keep-up, catch-up or give-up; Proceedings of the 5th International Coral Reef Congress 3, Tahiti, p. 105-110

Nicet, J. and Delcroix, T. (2000) ENSO-Related Precipitation Changes in New Caledonia, Southwestern Tropical Pacific: 1969-98; American Meteorological Society, Notes and Correspondence, v. 128, p. 3001-3006

Opdyke, B. and Walker, J. (1992) Return of the coral reef hypothesis: Basin to shelf partitioning of $CaCO_3$ and its effect on atmospheric CO_2; Geology, v. 20, p. 733-736

Ouillon, S., Douillet, P., Lefebvre, J., Le Gendre, R., Jouon, A., Bonneton, P., Fernandez, J., Chevillon, C., Magand, O., Lefèvre, J., Le Hir, P., Laganier, R., Dumas, F., Marchesiello, P., Bel Madani, A., Andréfouët, S., Panché, J. and Fichez, R. (2010) Circulation and suspended sediment transport in a coral reef lagoon: The south-west lagoon of New Caledonia; Marine Pollution Bulletin, v.61, p.269-296

Owen, M., Day, S. and Maslin, M., (2007) Late Pleistocene submarine mass movements: occurrence and causes; Quaternary Science Reviews, v. 26, p. 958-978

Pagani, M., Huber, M., Liu, Z., Bohaty, S. M., Henderiks, J., Sijp, W., Krishnan, S. and DeConto, R. (2011) The Role of Carbon Dioxide During the Onset of Antarctic Glaciation; Science, v. 334, p. 1261-1264

Page, M., Dickens, G. and Dunbar, G. (2003) Tropical view of Quaternary sequence stratigraphy: Siliciclastic accumulation on slopes east of the Great Barrier Reef since the Last Glacial Maximum; Geology, v. 31(11), p. 1013-1016

Paillard, D. (1998) The timing of Pleistocene glaciations from a simple multiple-state climate model; Nature, v. 391, p. 378-381

Paillard, D. (2001) Glacial Cycles: Toward a New Paradigm; Reviews of Geophysics, v. 39(3), p. 325-346

Paillard, D. and Perrenin, F. (2004) The Antarctic ice sheet and the triggering of deglaciations; Earth and Planetary Science Letters, v. 227. p. 263-271

Paillard, D., Labeyrie, L. and Yiou, P. (1996) Macintosh program performs timeseries analysis, Eos Transactions AGU, v. 77, p. 379

Pandolfi, J. (2011) The Paleoecology of Coral Reefs. In Coral Reefs: An Ecosystem in Transition (1st edition), Springer

Pandolfi, J. and Jackson, J. (2007) Broad-scale patterns in Pleistocene coral reef communities from the Caribbean: Implications for ecology and management; In: R. B. Aronson (editor.), Geological approaches to coral reef ecology, p. 201-236, New York: Springer

Parrenin, F. and Paillard, D. (2012) Termination VI and VIII (~530 and ~720kyr NP) tell us the importance of obliquity and precession in the triggering of deglaciations; Climate of the Past, v. 8, p. 2031-2037

Patterson, R. and Fishbein, A. (1989) Re-examination of the statistical methods used to determine the number of point counts needed for micropaleontological quantitative research; Journal of Paleontology, v. 63(2), p. 245-248

Paul, A., Reijmer, J., Fürstenau, J., Kinkel, H. and Betzler, C. (2012) Relationship between Late Pleistocene sea-level variations, carbonate platform morphology and aragonite production (Maldives, Indian Ocean), Sedimentology, v. 59, p. 1640-1658

Pelletier, B. (2006) Geology of the New Caledonia region and its implications for the study of the New Caledonian biodiversity; In 'Compendium of marines species from New Caledonia', (C. Payri and B. Richer de Forges Editors), Forum BIOdiversité des Ecosystèmes Coralliens, 30 octobre -4 novembre 2006, Nouméa, Nouvelle-Calédonie. Doc. Sci. Tech. IRD, II 7, Octobre 2006, p. 17-30

Petit, J., Jouzel, J., Raynaud, D., Barkov, N., Barnola, J., Basile, I., Bender, M., Chappellaz, J., Davis, M., Delaygue, G., Delmotte, M., Kotlyakov, V., Legrand, M., Lipenkov, V., Lorius, C., Pépin, L. and Ritz, C. (1999) Climate and atmospheric history of the past 420,000 years from the Vostok ice core, Antarctica; Nature, v.399, p. 429-436

Pilkey, O. and Goodell, H. (1963) Trace elements in recent mollusk shells; Limnology and Oceanography, v. 8(2), p. 137-148

Posamentier, H. and Vail, P. (1988) Eustatic controls on clastic deposition II-sequence and systems tract models, In C.K. Wilgus, B.S. Hastings, C.G.St.C. Kendall, H.W. Posamentier, C.A. Ross and J.C. Van Wagoner (editors), 'Sea Level Changes: An Integrated Approach', SEPM Special Publication No.42, p.125-154

Prell, W. (1985) The stability of low-latitude sea surface temperatures: an evaluation of the CLIMAP reconstruction with emphasis on the positive SST anomalies; US Department of Energy, Washington, DC

Puga-Bernabéu, A., Webster, J., Beaman, R., Reimer, P. and Renema, W. (2014) Filling the gap: A 50ky record of mixed carbonate-siliciclastic turbidite deposition from the Great Barrier Reef, Marine and Petroleum Geology, v. 50, p. 40-50

Purdy, E. and Bertram, G. (1993) Carbonate concepts, from the Maldives, Indian Ocean; American Association of Petroleum Geologists, Studies in Geology, v. 34, p. 1-56

Pye, K. (2007) Geological and Soil Evidence: Forensic Applications; CRC Press, Taylor Francis Group, Boca Raton, Florida, USA, p. 105

Rawling, T. (1998) Oscillating orogenesis and exhumation of high-pressure rocks in New Caledonia, SW Pacific; PhD Thesis, Department of Earth Sciences, Monash University, Melbourne, Australia, p. 1-272

Raymo, M. (1994) The initiation of northern-hemisphere glaciation; Annual Review of Earth and Planetary Sciences, v. 22, p.353-383

Raymo, M. and Ruddiman, W. (1992) Tectonic forcing of late Cenozoic Climate; Nature, v. 359(6391), p.117-122

Raymo, M., Oppo, D. and Curry, W. (1997) The mid-Pleistocene climate transition: A deep sea carbon isotopic perspective; Paleoceanography, v. 12(4), p. 546-559

Raymo, M., Lisiecki, L. and Nisancioglu, K. (2006) Plio-Pleistocene Ice Volume, Antarctic Climate, and the Global $\delta^{18}O$ Record; Science, v.313, p. 492-495

Reeckmann, S. (1985) geology of the foreslope to basinal transition. Permian Reef Complex, McKittrick Canyon, Guadalupe Mountains: Special Study for Guadalupe Mountains National Park, 21

Régnier, M., Van de Beuque, S., Baldassari, C. and Tribot Laspiere, G. (1999) La sismicité du Sud de la Nouvelle Calédonie: implications structurales; Comptes Rendus de l'Académie des Sciences, v. 329(2), p.143-148

Reymer, J.J.G., Schlager, W.. and Droxler, A.W. (1988) Site 632: Pliocene-Pleistocene sedimentation cycles in a Bahamian basin; In: J.A. Austin Jr., W. Schlager et al. (Editors), Proceedings of the Ocean Drilling Program, Scientific Results Leg 101. Ocean Drilling Program, College Station (TX), p. 213-220

Reimer, P., Baillie, M., Bard, E., Bayliss, A., Beck, J., Blackwell, P., Bronk Ramsey, C., Buck, C., Burr, G., Edwards R., Friedrich, M., Grootes, P., Guilderson, T., Hajdas, I., Heaton, T., Hogg, A., Hughen, K., Kaiser, K., Kromer, B., McCormac, F., Manning, S., Reimer, R., Richards, D., Southon, J., Talamo, S., Turney, C., van der Plicht, J. and Weyhenmeyer, C. (2009) INTCAL09 and MARINE09 radiocarbon age calibration curves, 0-50,000 years cal BP; Radiocarbon, v. 51(4), p. 1111-1150

Richter, T., van der Gaast, S., Koster, B., Vaars, A., Gieles, R., de Stigter, H., de Haas, H. and van Weering, T. (2006) The Avaatech XRF Core Scanner: technical description and applications to NE Atlantic sediments; Geological Society, London, Special Publications, v. 267, p. 39-50

Rickaby, R., Elderfield, H., Roberts, N., Hillenbrand, C.-D. and Mackensen, A. (2010) Evidence for elevated alkalinity in the glacial Southern Ocean; Paleoceanography, v.25, PA1209

Ridgwell, A., Watson, A., Maslin, M. and Kaplan, J. (2003) Implications of coral reef buildup for the controls on atmospheric CO_2 since the Last Glacial Maximum; Paleoceanography, v. 18(4), 1083

Rohling, E., Grant, K., Bolshaw, M., Roberts, A., Siddall, M., Hemleben, Ch. And Kucera, M. (2009) Antarctic temperature and global sea level closely coupled over the past five glacial cycles; Nature Geoscience, v. 2, p. 500-504

Rothwell, R.G., Hoogakker, B., Thomson, J., Croudace, I. and Frenz, M. (2006) Turbidite emplacements on the southern Balearic Abyssal Plain (western Mediterranean Sea) during Marine Isotope Stages 1-3; an application of ITRAX XRF scanning of sediment cores to lithostratigraphic analysis; Geological Society, London, Special Publications, v. 267, p. 79-98

Rougerie, F. (1986) Le lagon sud-ouest de Nouvelle-Calédonie : spécificité hydrologique, dynamique et productivité; PhD thesis, ORSTOM, p. 1-231

Russon, T. (2010) The paleoceanography of the southern Coral Sea across the Mid-Pleistocene Transition; PhD Thesis, University of Edinburgh, UK, p. 1-262

Russon, T., Elliot, M., Kissel, C., Cabioch, G., De Deckker, P. and Corrège (2009) Middle-late Pleistocene deep water circulation in the southwest subtropical Pacific; Paleoceanography, v. 24, PA4205

Russon, T., Elliot, M., Sadekov, A., Cabioch, G., Corrège, T. and De Deckker, P. (2010) Inter-hemispheric asymmetry in the early Pleistocene Pacific warm pool; Geophysical Research Letters, v. 37, L11601

Sanders, D. and Baron-Szabo, R. (2005) Scleractinian assemblages under sediment input: Their characteristics and relation to the nutrient input concept; Palaeogeography, Palaeoclimatology, Palaeoecology, v. 216, p. 139-181

Schlager, W., Reijmer, J. and Droxler, A. (1994) Highstand shedding of carbonate platforms; Journal of Sedimentary Research, v. B64(3), p. 270-281

Schlitzer, R. (2007), Ocean Data View, http://odv.awi.de

Sexton, P. and Barker, S. (2012) Onset of 'Pacific-style' deep-sea sedimentary carbonate cycles at the mid-Pleistocene transition; Earth and Planetary Science Letters, v. 321-322, p. 81-94

Shackleton, N. J. (2000) The 100,000-year ice-age cycle identified and found to lag temperature, carbon dioxide, and orbital eccentricity; Science, v. 289(5486), p. 1897-1902

Shackleton, N. (1967) Oxygen Isotope Analyses and Pleistocene Temperatures Re-assessed; Nature, v. 215, p. 15-17

Shackleton, N., Backman, J., Zimmerman, H., Kent, D., Hall, M., Roberts, D., Schnitker, D., Baldauf, J., Desprairies, A., Homrighausen, R., Huddlestun, P., Keene, J., Kaltenback, A., Krumsiek, K., Morton, A., Murray, J. and Westberg-Smith, J. (1984) Oxygen isotope calibration of the onset of ice-rafting and history of glaciation in the North Atlantic region; Nature, v. 307, p. 620-623

Shackleton, N., Berger, A. and Peltier, W. (1990) An alternative astronomical calibration on the Lower Pleistocene time scale based on ODP site 677; Transactions of the Royal Society of Edinburgh, Earth Sciences, v. 81, p, 2511-3261

Shannon, R. (1976) Revised effective ionic radii and systematic studies of interatomic distances in halides and chaleogenides; Acta Crystallographica, v. 32, p. 751-767

Siddall. M., Rohling, E., Almogi-Labin, A., Hemleben, Ch,. Melschner, D., Schmelzer, I. and Smeed, D. (2003) Sea-level fluctuations during the last glacial-cycle; Nature, v.423, p. 853-858

Siddall, M., Hönisch, B., Waelbroeck, C. and Huybers, P. (2010) Changes in deep Pacific temperature during the mid-Pleictocene transition and Quaternary; Quaternary Science Reviews, v.29, p.170-181

Sigman, D. and Boyle, E. (2000) Glacial/interglacial variations in atmospheric carbon dioxide; Nature, v.490, p. 859-869

Silver, B. and Todd, R. (1969) Permian cyclic strata, northern Midland and Delaware Basins, west Texas and southeastern New Mexico; American Association of Petroleum Geologists Bulletin, v. 53, p. 2223-2251

Silverman, J., Lazar, B., and Erez, J. (2007) Effect of aragonite saturation, temperature, and nutrients on the community calcification rate of a coral reef; Journal of Geophysical Research, v. 112, C05004

Skinner, L. and McCave, I. (2003) Analysis and modelling of gravity- and piston coring based on soil mechanics; Marine Geology, v. 199, p. 181-204

Sosdian, S. and Rosenthal, Y. (2009) Deep-Sea Temperature and Ice Volume Changes Across the Pliocene-Pleistocene Climate Transitions; Science, v. 325, p. 306-310

Southgate, P., Kennard, J., Jackson, M., O'Brien, P. and Sexton, M. (1993) Reciprocal lowstand clastic and highstand carbonate sedimentation, subsurface Devonian reef complex, Canning Basin, Western Australia; In R.G. Loucks and G.F. Sarg (Eds.), 'Carbonate Sequence Stratigraphy: Recent Developments and Applications', AAPG Special Volumes, Chapter 6

Spalding, M., Green, E. and Ravilious, C. (2001) World Atlas of Coral Reefs; UNEP-WCMC publishing, Cambridge, p. 1-436

Spandler, C., Rubatto, D. and Hermann J. (2005) Late Cretaceous-Tertiary tectonics of the southwest Pacific: Insights from U-Pb sensitive, high-resolution ion microprobe (SHRIMP) dating of eclogite facies rocks from New Caledonia; Tectonics, v. 24, TC3003

Stuiver, M., and Braziunas T. (1993) Modelling atmospheric ^{14}C influences and ^{14}C ages of marine samples back to 10,000 BC; Radiocarbon, v. 35, p. 137-189

Tcherepanov, E., Droxler, A., Lapointe, P., Mohn, K. and Larsen, O. (2010) Siliciclastic influx and burial of the Cenozoic carbonate system in the Gulf of Papua; Marine Petroleum Geology, v. 27, p. 533-54

Thomson, J., Crudeli, D., de Lange, G., Slomp, C., Erba, E., Corselli, C. and Calvert, S. (2004) Florisphaera profunda and the origin and diagenesis of carbonate phases in eastern Mediterranean sapropel units; Paleoceanography, v. 19, PA3003, p.1-19

Thomson, J., Croudace, W. and Rothwell, R. (2006) A geochemical application of ITRAX scanner to a sediment core containing eastern Mediterranean sapropel unit; Geological Society, London, Special Publications, v. 267, p. 39-50

Thouveny, N., Moreno, E., Delanghe D., Candon, L., Lancelot, Y. and Shackleton N. (2000) Rock magnetic detection of distal ice-rafted debris: clue for the identification of Heinrich layers on the Portuguese margin; Earth and Planrtary Science Letters, v. 180, p. 61-75

Tudhope, A., and Scoffin, T. (1984) The effects of Callianassa bioturbation on the preservation of carbonate grains in Davies Reef Lagoon, Great Barrier Reef, Australia; Journal of Sedimentary Petrology, v. 54, p. 1091-1096

Vail, P. (1987) Seismic stratigraphy interpretation using sequence stratigraphy, Part 1; Seismic stratigraphy interpretation procedure; In A.W. Bally (editor), 'Atlas of Seismic Stratigraphy': AAPG Studies in Geology 27, v. 1, p.1-10

Vail, P., Mitchum Jr, R., Todd, R., Widmier, J., Thompson III, S., Sangree, J., Bubb, J. and Hatlelid, W. (1977) Seismic stratigraphy and global changes of sea level, In C.E. Payton (editor), 'Seismic Stratigraphy- Applications to Hydrocarbon Exploration': AAPG Memoir 26, p. 49-212

van der Plas, L. and Tobi, A. (1965) A chart for judging the reliability of point counting results; American Journal of Science, v. 263, p. 87-90

Vecsei, A. and Berger, W. (2004) Increase of atmospheric CO_2 during deglaciation: Constraints on the coral reef hypothesis from patterns of deposition; Global Biogeochemical Cycles, v.18, GB1035, p.1-7

Waelbroeck, C., Labeyrie, L., Michel, E., Duplessy, J., McManus, J., Lambeck, K., Balbon, E. and Labracherie, M. (2002) Sea-level and deep water temperature changes derived from benthic foraminifera isotopic records; Quaternary Science Reviews, v. 21, p. 295-305

Webster, J. (1999) The response of coral reefs to sea level change: Evidence from the Ryukyu Islands and the Great Barrier Reef; Unpublished Ph.D. thesis, University of Sydney, p. 1-328

Webster, J., Beaman, R., Puga-Bernabéu, Á., Ludman, D., Renema, W., Wust, R., George, N., Reimer, P., Jacobsen, G. and Moss, P. (2012) Late Pleistocene history of turbidite sedimentation in a submarine canyon off the northern Great Barrier Reef, Australia; Palaeogeography, Paleoclimatology, Palaeoecology, v. 331-331, p.75-89

Weltje, G.J. and Tjallingii, R. (2008) Calibration of XRF core scanners for quantitative geochemical logging of sediment cores: Theory and application; Earth and Planetary Science Letters, v. 274, p. 423-438

Wood, R. (1998) The ecological evolution of reefs; Annual Review of Ecology Systematics, v. 29, p. 179-206

www.earthquaketrack.com

Yamamoto, K., Iryu, Y., Sato, T., Chiyonobu, S., Sagae, K. and Abe, A. (2006) Responses of coral reefs to increased amplitude of sea-level changes at the Mid-Pleistocene Climate Transition; Paleoeography, Paleoclimatology, Paleoecology, v. 241, p. 160-175

Yu, J and Elderfield, H. (2007) Benthic foraminiferal B/Ca ratios reflect deep water carbonate saturation state; Earth and Planetary Science Letters, v.258, p. 73-86

Zachos, J., Pagani, M., Sloan, L., Thomas, E. and Billups, K., (2001) Trends, Rhythms, and Aberrations in Global Climate 65Ma to Present; Science, v. 292, p. 686-693

Appendices

Appendix 1: Underlying principles of experimental methods

A1.1 Coulometry measurements for bulk carbonate content

Carbonate coulometry is a method used to obtain the total wt.% carbonate content of samples. It is an analytical technique that determines the amount of CO_2 transformed during an electrolysis reaction by measuring the amount of electricity (in coulombs) consumed. Since it is an absolute method, based on Faraday's law, it doesn't require any calibration; thus it is both simple but also has high precision and accuracy.

Carbonate coulometry results in this thesis were obtained using a UIC Inc CM5012 CO_2 coulometer which uses the coulometric titration method (see *Figure A.1*). The sample vial is connected to the coulometer and the system is initially purged for three minutes of any atmospheric carbon dioxide, using a CO_2 free carrier gas (CO_2 removed by a pre-scrubber). The analysis is then initiated by the addition of 8ml of 2N perchloric acid into the sample flask and the sample is heated to 60ºC (to ensure fast reaction times); this causes the dissolution of inorganic carbon and the production of CO_2. The CO_2-free carrier gas then transports the reaction products through to the post-scrubber (to remove any other gases) and then on to the coulometer titration cell, where analysis takes place.

The coulometer cell is partially filled with a blue aqueous medium containing ethanolamine and a colorimetric pH indicator. As the carbon dioxide is absorbed by the solution, it reacts with the ethanolamine to form a strong acid; which in turn causes the indicator colour to fade. The titration current automatically turns on and electrically produces a base which neutralises the solution, until it returns it to its original blue colour. The amount of electricity (in coulombs) required to return the solution back to its original colour (and pH) is then determined by calculating the integral of the titration current over time. This current is directly proportional to the amount of evolved CO_2 dissolved in the titration cell and by simple stoichiometric

computation can be converted to the equivalent mass of CO_2. This in turn can be converted to the total original mass of $CaCO_3$ in the sample, using the relative molecular weights of the different molecules ($CaCO_3$= 100g/mol, CO_2= 40g/mol).

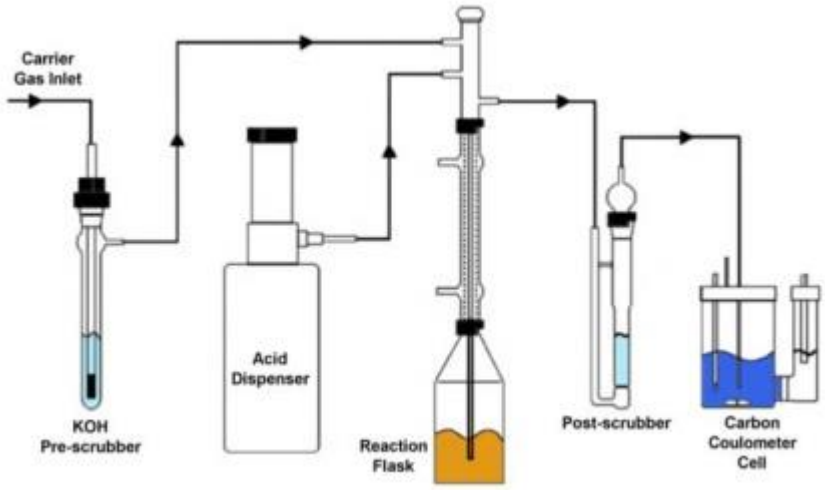

Figure A.1 Schematic of the set up of a titration coulometer.

A1.2 X-ray fluorescence analysis

X-ray fluorescence analysis is a method used to analyse the concentration of major and trace elements in samples.

X-rays are part of the electromagnetic spectrum, which is comprised of radio waves, microwaves, infra-red radiation, visible light, ultra violet light, X-rays and gamma rays in increasing order of energy (normally expressed in kilo electron volts: keV) and decreasing wavelength (normally expressed in nanometres: nm) (see *Figure A.2*). Since X-rays have short wavelengths between 0.01-10nm, they also have a correspondingly high energy between 0.1-100keV.

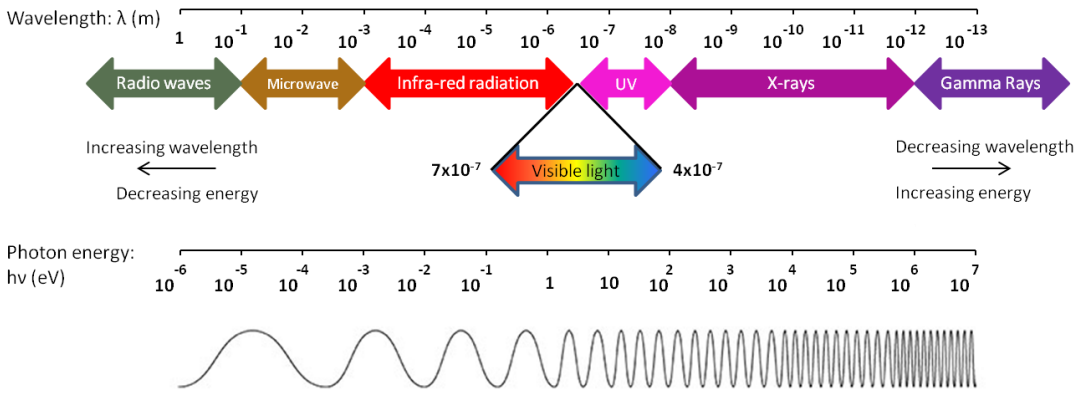

Figure A.2 Schematic of the electromagnetic spectrum, showing the varying wavelengths and energies of the different types of waves.

The process of X-ray fluorescence is due to changes occurring within an atom. A stable atom is comprised of a nucleus of protons (positively charged) and neutrons (neutral charge) with electrons (negatively charged) orbiting in 'shells' (see *Figure A.3*). These shells are arranged in increasing levels of discrete energy with distance from the nucleus. Electrons can be lost from an atom, in a process called ionisation, when provided with enough energy to escape the pull of the nucleus (an energy

greater than the ionisation potential). Those electrons in the inner shells have a lower binding energy and thus are more readily released.

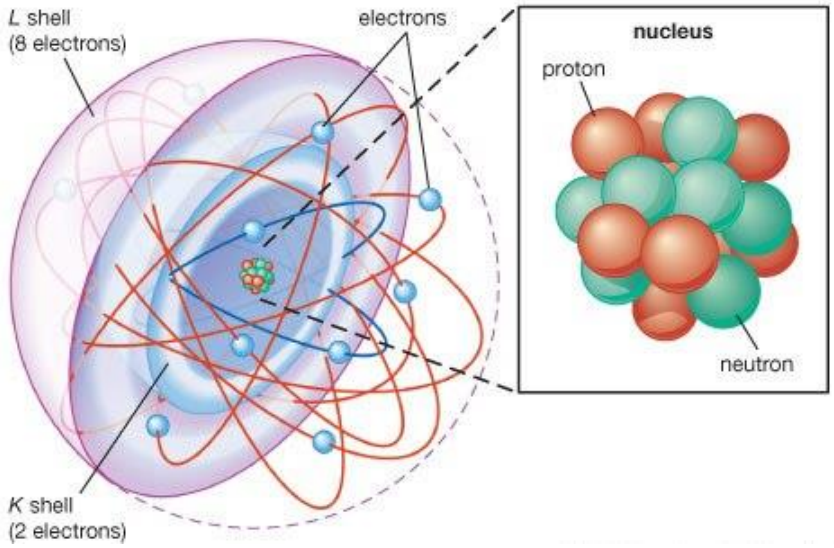

Figure A.3 Atomic structure of an atom showing protons and neutrons in the nucleus with electrons orbiting in shells. Only the first two electron shells, K and L, are shown here. Additional shells, labelled sequentially, occur on the outside of these for larger atoms. (Reproduced from Encyclopaedia Britannica, 2012.)

When a high energy incident X-ray collides with an atom, an electron can be ejected from a low energy shell (e.g. K) and a space is created (see *Figure A.4*). This creates an instability in the atom and an electron from a higher energy shell 'falls' to fill the space. As the electron falls a secondary X-ray (fluorescence photon) is released, with an energy equivalent to the difference in energy between the two electron shells. The energy levels of these secondary emitted X-rays are characteristic of particular elements. This is because the discrete energy of different electron shells is unique to individual atoms and there are only a limited number of ways an electron can fall within an atom, for instance L to K, M to K or M to L (see *Figure A.4*). By analysing the spectrum of wavelengths of X-rays emitted from an irradiated sample it is possible to ascertain its chemical makeup.

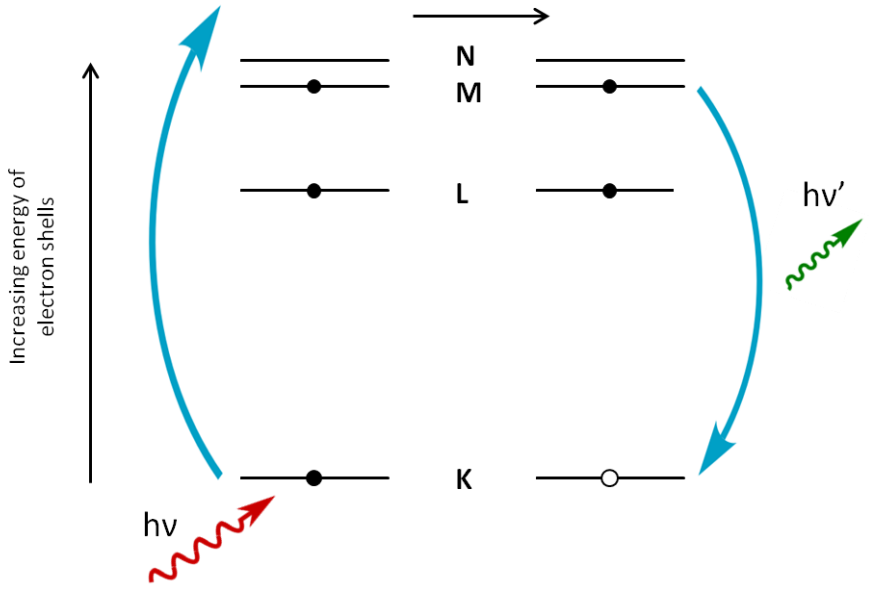

Figure A.4 An X-ray with energy hν is absorbed by an atom, ionising an electron in the lowest energy K shell. This creates a space which is filled by another electron falling from the higher energy M shell. As this electron falls it releases a secondary X-ray with an energy of hν', which is equal to the energy difference between the M and L shells.

In X-ray fluorescence analysis a sample is illuminated by an intense incident X-ray beam, normally from a Rhodium target. The energy of this beam varies (typically between 10-60keV) depending on the elements being analysed for; heavier elements require a greater energy to be ionised. Some of the incident energy is scattered but the rest is absorbed by the sample in a way that depends on its chemistry. The emitted secondary X-rays are separated by a wavelength dispersive spectrometer, where photons are divided by diffraction on a single crystal before being detected. This allows the separation of a complex emitted X-ray spectrum into characteristic wavelengths for each element present. A detector (typically gas flow proportional for long wavelength emissions and scintillation for short wavelength emissions) then measures the intensity of the emitted beam, which corresponds to an element's concentration in the sample.

Typically, samples for X-ray fluorescence analysis are required to be powdered and pressed into a tablet or mixed with a chemical flux, heated and cast into homogeneous glass. This process is destructive to samples, time consuming, comparatively expensive and means that only a limited number of measurements can be conducted. By contrast, this thesis employs the use of X-ray fluorescence core scanning; which is cheaper, non-destructive, significantly reduces sample preparation time and increases sampling resolution. In this method the split core is simply prepared to give a flat, clean surface using a glass slide and the detector moves along the core length, measuring at set intervals (usually of 1cm).

A1.3 X-ray diffraction analysis

X-ray powder diffraction is a semi-destructive, analytical technique for the identification and quantitative determination of various crystalline phases within a sample.

When a crystal interacts with an incident X-ray beam it produces characteristic diffraction patterns, due to constructive interference, when the conditions satisfy Bragg's Law: $n\lambda=2d \sin \theta$ (see *Figure A.5*). This law relates the wavelength of incident X-ray to the diffraction angle and the lattice spacing in a crystalline sample. Due to the random orientation of the powdered material it is necessary to scan through a range of 2θ angles in order that all possible diffraction directions of the lattice are obtained. Conversion of the diffraction peaks to d-spacings allows identification of the mineral, since each mineral has a unique set of lattice spacings. Typically this is achieved by comparison with standard reference patterns.

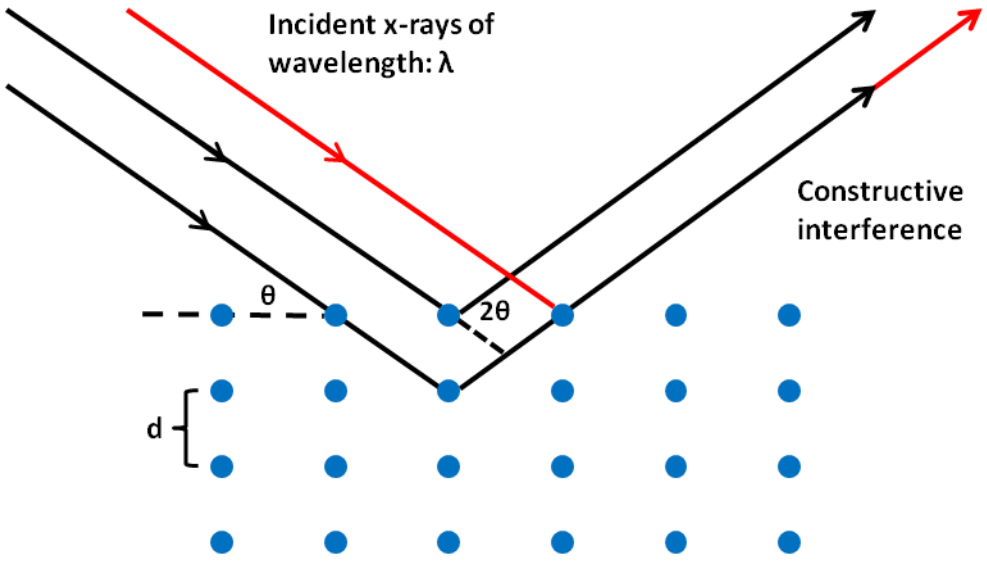

Figure A.5 Sketch of a crystal lattice illustrating Bragg's Law. Blue circles-atoms, d-lattice spacing, θ- angle of incident radiation and λ- wavelength of incident radiation.

Typically samples are ground to a homogenised powder (grain size <10μm) in order to expose all orientations of the crystal lattice to the X-ray beam. Samples are then loaded into sample holders and a flat surface prepared. Once the sample is illuminated by the X-ray beam the detector will scan through a range of 2θ angles (typically 5-70^{o}), measuring the intensity of the diffracted X-ray. This data is then processed and the spectrum obtained is matched to a reference database, in order to identify the phases present. An estimation of the relative proportions of the minerals in multiphase specimens can be obtained by comparing the peak intensities of the different identified phases. Or alternatively, and more accurately, as was used in this thesis, via the Rietveld method. Once the mineral phases present in a sample have been identified, this method then uses full pattern analysis to model the data until the best fit to the experimental data is obtained.

Appendix 2: Variation in Apparent Sedimentation Rates due to Coring Methods

A2.1 Introduction

Sediments are subjected to a myriad of natural processes that can cause discrepancies between the actual sedimentation rate occurring at a given time and the perceived sedimentation for that period, obtained at a later date via examination of preserved sediments. For example: dissolution, compaction, winnowing and for sediment cores MD06-3019 and MD06-3020, erosion by turbidite flows can all reduce the calculated sedimentation rate by removal of sediment. Therefore the sedimentation rates obtained from sediment cores should always be treated as 'apparent' rather than 'absolute'.

In addition to this apparent sedimentation rates can be affected by processes associated with the coring methodology. Sediments drilled by Calypso corers (particularly in the upper 10-15m) can be subject to significant extension, being 1.5-3 times longer than the same sequences recovered by conventional piston cores from the same site [*Thouveny et al.*, 2000; *Skinner and McCave*, 2003; *Rothwell et al.*, 2006]. By contrast, gravity coring can lead to sediment compaction and an apparent decrease in sedimentation rates. Therefore the ratio of thickness to time does not necessarily accurately represent the real sedimentation rate. Evidence of this expansion of sediments in the upper parts of core MD06-3019 (Calypso piston core) can be seen by comparison to the nearby (less than 100m away) MD06-3020 (gravity core) (see *Figure A.7*). Modelling, using the principles of soil mechanics, of the effects of piston and gravity corers on the dimensional accuracy of soft marine sediment cores has attributed this 'over-sampling' by piston coring to cable rebound, causing upward piston acceleration [*Skinner and McCave*, 2003].

A2.2 MD06-3020 age model

MD06-3020 age model was principally developed via tuning of the $\delta^{18}O_{planktic}$ curve to the local MD06-3018 $\delta^{18}O_{planktic}$ record using Analyseries software [*Paillard et al.*, 1996] (see *Figure A.6*). Further to this, comparisons of sedimentary features such as the pattern of turbidite deposition and colour changes in the background pelagic ooze with MD06-3019 helped inform the chronology. MD06-3020, unlike MD06-3018 and MD06-3019, is a short core and has not been the subject of such intensive study. The $\delta^{18}O_{planktic}$ record is of a lower resolution and there are no magnetic measurements or radiocarbon dates.

Both the amplitude and absolute values of the MD06-3020 $\delta^{18}O_{planktic}$ record are very similar to those for the planktic MD06-3018 record. The orbital age model yields an average apparent sedimentation rate of 1.45cm/kyr. The planktic stable isotope sampling resolution, based on the core model is ~ 6.8kyr, therefore a 1cm thick sample of pelagic ooze therefore represents ~680 years.

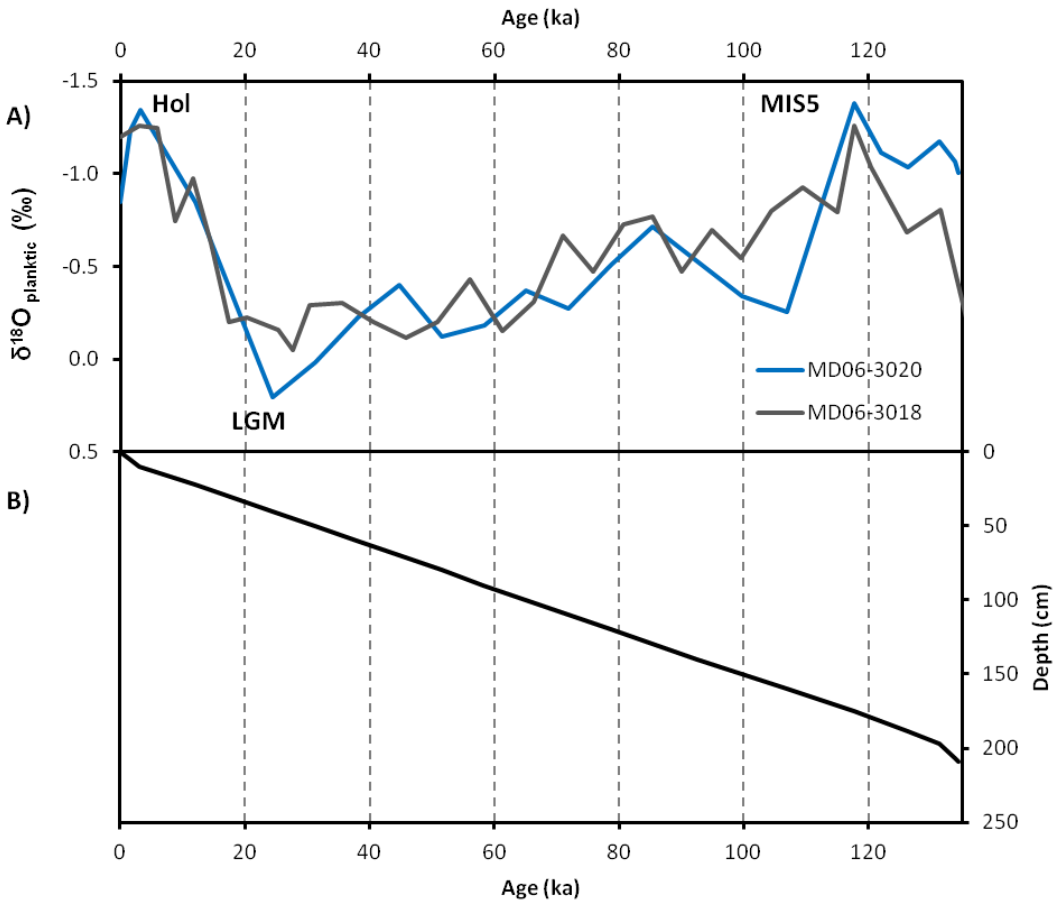

Figure A.6 A) Comparison between the $\delta^{18}O_{planktic}$ records of the tuned MD06-3020 and the reference MD06-3018. Numbers are the assigned marine isotope stages, LGM= Last Glacial Maximum (MIS2), Hol= Holocene (MIS1). B) Line showing the MD06-3020 age model as derived from MD06-3018.

A2.3 Comparison of apparent sedimentation rates between MD06-3019 and MD06-3020

The age model for sediment core MD06-3019 yields apparent average sedimentation rates of 3.7cm/kyr between 0-1825cm, 2.0cm/kyr between 1825cm to base (see *Figure A.7*). By contrast the age model for sediment core MD06-3020 yields an average apparent sedimentation rate of 1.5cm/kyr over the 214cm length (see *Figure A.7*).

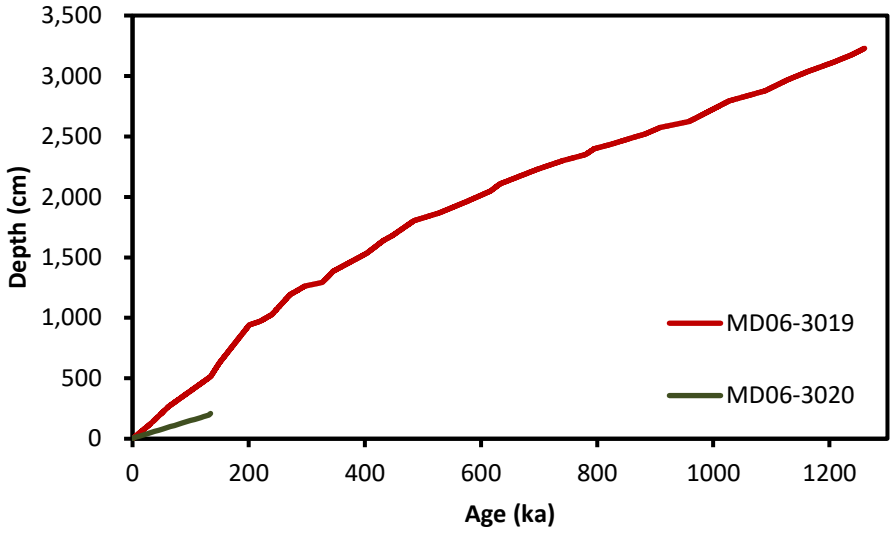

Figure A.7 Comparison of age models obtained for sediment cores MD06-3019 and MD06-3020.

This suggests that sediment extension due to the Calypso coring process creates a greater than two-fold difference (3.7cm/kyr versus 1.5cm/kyr) in apparent sedimentation rates between sediments at the top of cores MD06-3019 and MD06-3020. Therefore the sedimentation rates obtained for MD06-3019 (or MD06-3020) should not be taken as absolute values. *Skinner and McCave* (2003) comment on the importance of recognising the sampling effects of each coring method and their variability down core in order that artefacts are not interpreted as sedimentary signals. It is to be emphasised however, that stratigraphic order is preserved and structural deformation is limited to the edge of the cores [*Thouveny et al.*, 2000].

Appendix 3: Carbonate dissolution in the New Caledonia Trough

A3.1 Carbonate Dissolution

The bulk carbonate content of the pelagic ooze from cores MD06-3018 (128 samples, 86 measured previously by Tom Russon for his PhD) and MD06-3019 (201 samples) was measured via coulometry (see Chapter 4 §3.2 for methodology). Core MD06-3018 is characterised by a having a relatively consistent carbonate content, with a mean and standard deviation of 75±5 wt.% for the whole length of the core (see *Figure A.8C*). By contrast there are significant variations in the bulk carbonate content of the background pelagic ooze in core MD06-3019, which ranges between 18-84 wt.% (see *Figure A.8B*). This variation in carbonate content can be seen visually in the changing colour of the sediments in core MD06-3019. Periods of high carbonate content are associated with pale cream- light brown coloured sediments and periods of lower carbonate content are associated with darker, often olive green tinged sediments. This variation in the carbonate content of the pelagic ooze in core MD06-3019 is seen to vary approximately in phase with glacial-interglacial changes in climate, particularly since 1Ma; with higher carbonate content seen during glacial periods and lower carbonate content seen during interglacial periods (see *Figure A.8B*).

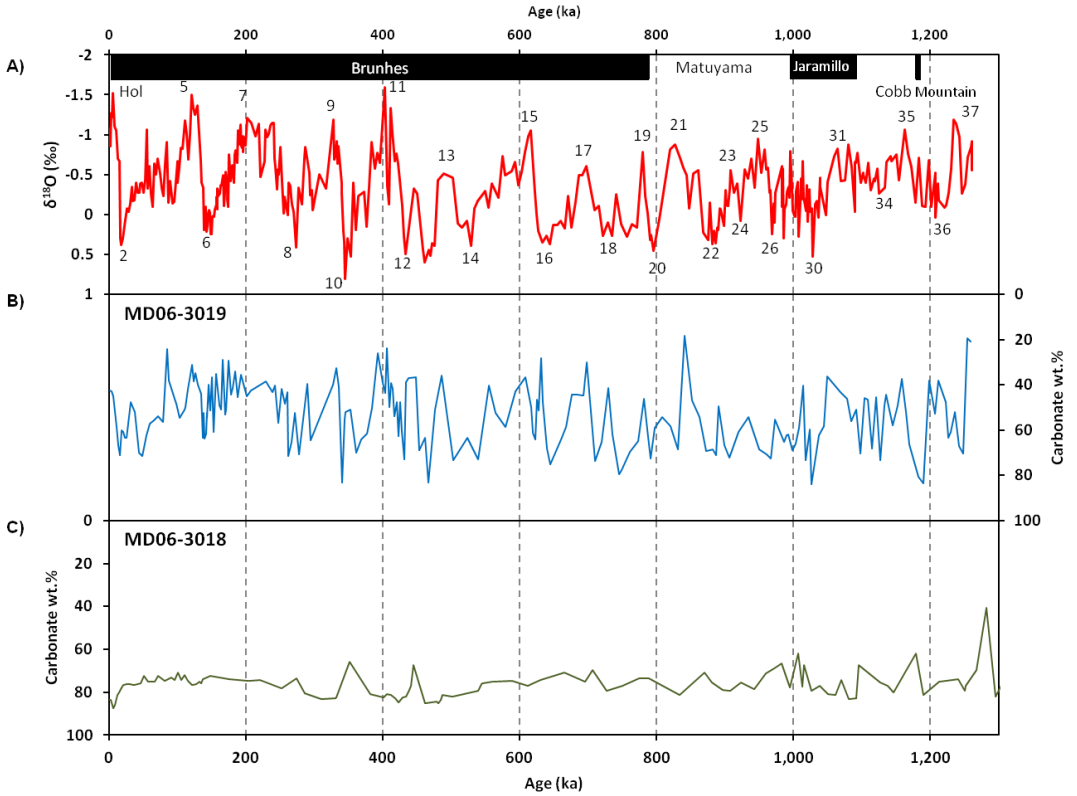

Figure A.8 A) $\delta^{18}O$ record for MD06-3019, obtained from G. *ruber* foraminifera. **B)** Total carbonate wt.% record for MD06-3019 pelagic ooze samples. **C)** Total carbonate wt. % record for MD06-3018 pelagic ooze samples.

The carbonate content of deep sea sediments can be affected by three different processes: changes in planktic carbonate productivity levels, alterations in the supply of siliciclastic detrital material or varying degrees of carbonate dissolution. Cores MD06-3018 and MD06-3019 are only ~110km apart (see Chapter 2, *Figure 2.5*), therefore the effects of differential productivity and dilution by detrital material are assumed to be small. The two cores are, however, separated by just over 1000m in depth (2470m- MD06-3018 and 3520m- MD06-3019) and thus the variations in total carbonate are interpreted as being the result of varying dissolution through time. The shallower site, MD06-3018, is postulated to be above the lysocline throughout the whole time period and thus shows no cyclic dissolution patterns in total carbonate content. By contrast the deeper core, MD06-3019, appears to be significantly affected by movements of the calcite compensation depth (CCD) and shows a pronounced variation in total carbonate content in phase with climate oscillations.

Furthermore, these variations in MD06-3019 total carbonate content are also in phase with the cyclicity of carbonate content in sediments in the open Pacific Ocean.

Deep-sea sediments from the Pacific Ocean show an increase in carbonate content during glacials and a decrease during interglacials, which is anti-correlated to the pattern seen in Atlantic Ocean sediments [*Farrell and Prell*, 1989; *Archer*, 1991; *LaMontagne et al.*, 1996; *Anderson et al.*, 2008; *Rickaby et al.*, 2010; *Sexton and Barker*, 2012]. These cycles in carbonate content are sometimes attributed to changes in shallow water production [*Archer*, 1991; *LaMontagne et al.*, 1996]; however, due to their wide spatial synchronicity they are generally thought to reflect changes in carbonate preservation, as a result of glacial-interglacial variations in ventilation and water mass reorganisation [*Farrell and Prell*, 1989; *Yu and Elderfield*, 2007; *Anderson et al.*, 2008; *Rickaby et al.*, 2010; *Sexton and Barker*, 2012]. The 'Pacific-style' phasing of the carbonate record is thought to have begun around 1.1Ma and involved a two-fold switch, during which glacial carbonate preservation became increasingly better, whilst concurrently interglacial preservation became consistently poorer [*Sexton and Barker*, 2012]. It is suggested that during glacials a consistent strengthening of deep water ventilation within the Pacific sector of the Southern Ocean caused Pacific carbonate dissolution to diminish. Whilst a contemporaneous weakening of the very well ventilated 'upstream' North Atlantic Deep Water during interglacials caused Pacific carbonate dissolution 'downstream' to intensify [*Sexton and Barker*, 2012].

Future work on cores MD06-3018 and MD06-3019 to further support the hypothesis that the differences in their pelagic carbonate content is due to their relative positions with respect to the mobile lysocline, would include measurements of B/Ca on benthic foraminifera as a proxy for the CO_3^{2-} concentration of the waters they were formed in [*Yu and Elderfield*, 2007]. This would enable a comparison of the varying carbonate saturation state of the waters of the New Caledonia Trough both vertically and temporally. Comparisons to previous studies of changes in deep water circulation in

the area [*Russon et al.*, 2009] could also prove useful in further refining the hypothesis.

A3.2 Carbonate content and XRF Sr count cyclicity in MD06-3019 pelagic ooze

A consequence of the high variation in the pelagic carbonate content of MD06-3019 sediments is believed to be seen in the concurrent considerable variation in pelagic ooze XRF Sr count values; 9,200 ± 1,300. This variation in the pelagic ooze can make it difficult to identify turbidite layers with low aragonite content in core MD06-3019 (see Chapter 5 §5.1). The Sr record for the pelagic ooze alone, with sandy layer data removed, shows a cyclicity which is broadly in phase with the pronounced changes in the overall carbonate content of the core (18-84%), (see *Figure A.9B*). These variations are also generally in phase with changes in climate, showing higher values during glacial periods and lower values during interglacials. The nearby shallower core, MD06-3018, whilst showing some variation (some of which seems to be concurrent with climate changes, for example: a prominent increase in both aragonite and total carbonate from around 15ka to present) does not appear to show the same cyclic variation in carbonate content, (see *Figure A.9C*). For MD06-3018 both the overall average carbonate content (75±5 wt.%) and Sr counts (11,600±900) are higher and there is less variation compared to MD06-3019.

In contrast, the average aragonite values obtained via XRD analysis for MD06-3018 are not any higher than those for MD06-3019 (1.4±0.2% compared to 1.3±0.5 %). It is postulated therefore, that the cyclicity in Sr values seen in the carbonate ooze in MD06-3019 is due to the large variations in calcite content of samples and not changes in aragonite, the mineral Sr is principally associated with. Whilst Sr is not present in calcite at the same high concentrations as it is in aragonite (1,000 ppmv versus 8,000 ppmv), it would, in the absence of aragonite, contribute significantly to the Sr count value of a sample. This would account for why a cyclicity is seen in the

Sr count values for MD06-3019 in the absence of any apparent aragonite variation and both the lack of cyclicity in MD06-3018 and the higher average values.

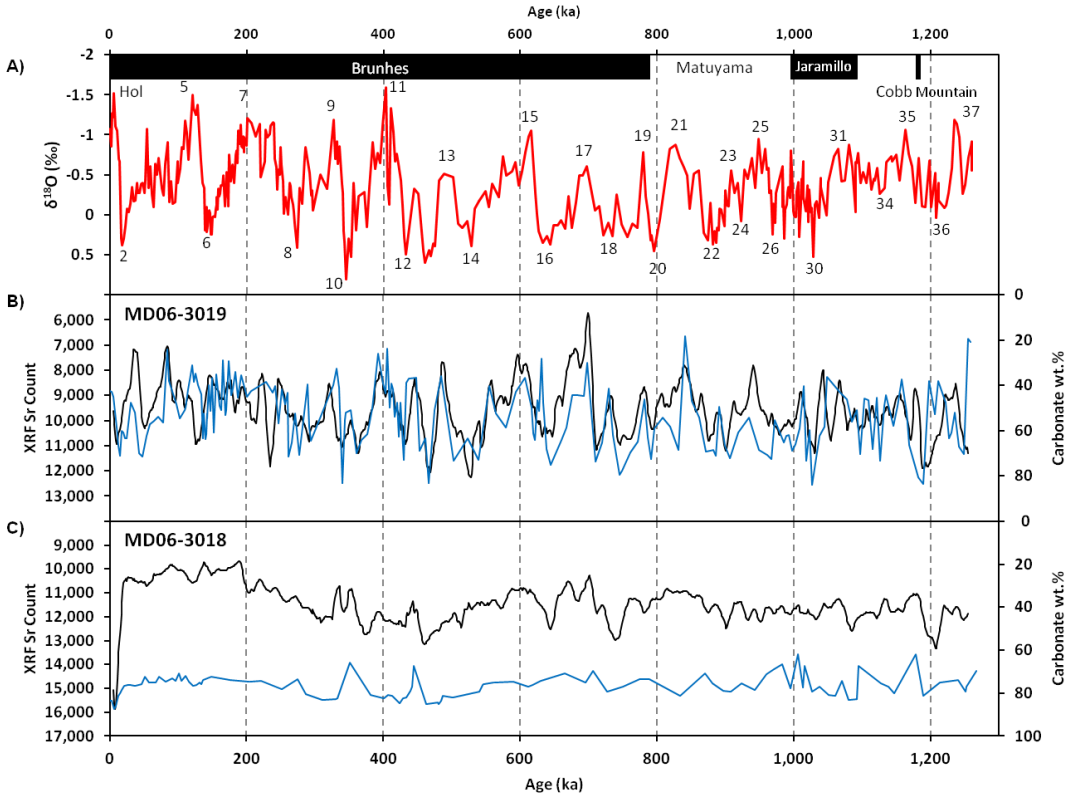

Figure A.9 A) Oxygen isotope stratigraphy for core MD06-3019. **B)** 10kyr running mean XRF Sr count (black) and total carbonate wt. % variation (blue) for core MD06-3019. **C)** 10kyr running mean Sr count (black) and total carbonate wt. % variation (blue) for core MD06-3018.

Appendix 4: Controls on shallow water carbonate production

A4.1 Literature review of controls on shallow water carbonate production

Factor	Coral reef limits	Notes	References
Sea surface temperature (°C)	• 24-34: annual minima and minima for extensive growth[1,2,3] • 18-24: annual minima for reduced growth, due to coral stress[1,2] • 16-18, 34-36: few days exposure[3]	• SST is controlled by the seasons, upwelling, currents and glacial-interglacial climate change. • Coral reefs are currently mainly confined to the tropics, 23.5°N or S of the equator, but the detail of their world distribution is strongly influenced by currents and substrate availability [3].	[1]*Isern et al.*, 1996; [2]*Kleypas et al.*, 1999; [3]*Montaggioni and Braithwaite*, 2009
Sea surface salinity (PSU)	• 23-42 (Continuous) [2,3,4] • 20 (< 1 day exposure) [4]	• SSS varies with seasons (evaporation/ precipitation), upwelling, currents, ENSO and glacial-interglacial climate change. • Generally grow in areas of 'normal' marine salinity (35-36psu) but relatively tolerant to variations [3]. • SSS changes not thought to have been a limiting factor in coral reef growth at a regional scale over the Pleistocene period [3].	[4]*Coles and Jokiel*, 1992; [2]*Kelypas et al.*, 1999; [3]*Montaggioni and Braithwaite*, 2009
Nutrients (µmol l^{-1})	• Reefs generally occur in low nutrient conditions[3] • ≤2.0 NO_3? [5] • ≤0.2 PO_4? [5]	• Nutrients vary with dust and sediment supply (causing iron enrichment), currents, glacial-interglacial climate (dust flux) and circulation change, ENSO variations and upwelling. • At high nutrient concentrations the growth of microalgae is enhanced and they compete with reef corals for space. Bioerosion is also intensified. However, reefs can persist under mesotrophic to eutrophic conditions [3].	[5]*Kinsey and Davies*, 1979; [3]*Montaggioni and Braithwaite*, 2009
Water clarity	• < 100mgl^{-1} of sediment input[10]	• Water clarity is dependent on dust and sediment input, currents, wind driven waves, tides, storms/cyclones/hurricanes/typhoons. • High sediment input is detrimental to reef framework growth [10, 3]. This is due to reduced light penetration and thus lower reef photosynthesis; but also due to reefs being smothered in sediment [7]. • Sediment load is an important control on coral species distribution and reef development [9]. Some reefs are more tolerant of high turbidity than others, depending on their ability to trap and remove sediment [6, 8, 3]. • Fast growing framework builders, such as branching Acropora are only weakly tolerant of chronic turbidity; however, Porites, which have smaller polyps, can be very effective in removing clays and silts and thus dominate in shallow, turbid–water communities [6, 8, 3].	[6]*Bak and Elgershuizen*, 1976; [7]*Bosscher and Schlager*, 1992; [8]*Tudhope and Scoffin*, 1994; [9]*Anthony and Connolly*, 2004; [10]*Sanders and Baron-Szabo*, 2005; [3]*Montaggioni and Braithwaite*, 2009
Light availability (µE$m^{-2}s^{-1}$)	• 50-450[11] • 30-40% of surface (limits reefs)[13] • <8% of surface (limits corals) [14]	• Light availability varies as a function of latitude, water clarity (governed by dust and sediment input, waves, tides and currents) and depth (dependent on antecedent topography and relative sea-level, including rate of change) [2]. • Corals have minimum light requirements for photosynthesis, below which photosynthesis rapidly declines. Light attenuation explains reduced calcification at depth, but depending on water clarity reefs can grow at different depths in different locations [12]. • Light availability is thought to be a possible limiting factor on reef growth at higher latitudes [2].	[11]*Chalker*, 1981; [12]*Grigg*, 1982; [13]*Achituv and Dubinsky*, 1990; [14]*Cooper et al.*, 2007, [2]*Kleypas et al.*, 1999
Aragonite saturation state (Ω-arag)	• 3.1-4.1[2, 15]	• Levels of aragonite saturation in the ocean are controlled by temperature and the pCO_2 of the atmosphere. This varies with the seasons, the temperature of the location, relative levels of evaporation and precipitation, upwelling and on glacial to interglacial timescales[3]. • Reefs require waters that are aragonite supersaturated in order to calcify [2,15,3].	[2]*Kleypas et al.*, 1999; [15]*Silverman et al.*, 2007, [3]*Montaggioni and Braithwaite*, 2009

Factor	Coral reef limits	Notes	References
Storms/ cyclones/ hurricanes and typhoons		• Frequency of such events varies widely with ENSO and glacial-interglacial cycles [3]. • Such events are important limiting factors in coral colonisation and growth, due to catastrophic mechanical disturbance of communities, as well as sediment generation and deposition [17]. • Levels of destruction depends on the shape and size of the coral species and/or colony and how well it is attached to the underlying substrate. Young corals are smaller, provide less resistance to flow and thus are less likely to be damaged [3]. • If communities are completely destroyed the area can be 'reset' and new communities develop; however if damage is lower survivors may recover and re-establish the community structure [16].	[16]*Done*, 1992b; [17]*Grossman and Fletcher*, 2004; [3]*Montaggioni and Braithwaite*, 2009
Biotic controls		• There are many biotic controls on reef development including: the distribution and recruitment of coral larvae, diversity of communities, species saturation, competition, predation, symbiosis and disease. These factors can all be influenced by variations in SST, SSS, wave energy, turbidity, currents etc. [18, 3].	[18]*Pandolfi and Jackson*, 2007; [3]*Montaggioni and Braithwaite*, 2009
Antecedent topography		• The antecedent topography available for coral colonisation depends on geography and varies with glacial-interglacial changes in sea-level. • Prior topography is important since suitable nurseries are needed for species. Shelf edges, banks and seamounts provide the best refuges and centres of dispersal for coral larvae [22]. • Reefs often develop on top of elevations in the antecedent topography, including previous beach edges and river deposits on shelves [21]. • The slope of the substrate can control the types of pioneering corals that grow and thus coral communities [20]. • Reefs preferentially colonise limestone karst surfaces and rough lava flows; whereas smooth surfaced, metasedimentary outcrops and unconsolidated sediments are less suitable [19].	[19]*Cabioch et al.*, 1995; [20]*Webster*, 1999; [21]*Gischler et al.*2010; [22]*Droxler and Jorry*, 2013
Subsidence/ uplift		• Subsidence/ uplift can affect the degree of accommodation space available for reef growth and thus reef structure and spatial relationships to previous reef units (see Chapter 2 §2.4.1)[3, 24]. • Increased subsidence rates leads to greater vertical reef accumulation[23]. Lack of accommodation space is thought to be a limiting factor on reef growth[25] and affects reef architecture. Low subsidence rates can cause increased lateral reef growth to occur[3]. • Variations in subsidence rate can lead to differences in the degree of reef accumulation at different locations over the same time period[26].	[23]*Braithwaite et al.*, 2004; [24]*Cabioch et al.*, 1999; [25]*Kennedy and Woodroffe*, 2002; [3]*Montaggioni and Braithwaite*, 2009; [26]*Montaggioni et al*., 2011
Sea-level		• During the Quaternary sea-level fluctuated dramatically (~+10 to -120m) on orbital timescales[29]; this lead to significant changes in the extent, nature and distribution of reef habitats during this period[3]. • The effect of these sea-level changes on reef development depends on the interaction between eustatic sea-level changes, subsidence/uplift rates and margin morphology in individual locations [27, 30]. • However, during all glacial- lowstands (when sea-level fell by 70-120m below present), shallow shelves became sub-aerially exposed and carbonate production was limited to relatively narrow bands on the slope[28].	[27]*Hubbard*, 1988; [28]*Schlager et al.*, 1994; [29]*Waelbroeck et al.*, 2002; [3]*Montaggioni and Braithwaite*, 2009; [30]*Puga- Bernabéu et al.*, 2014

Table A.1 Summary of the controls on and conditions required (including tolerance limits) for tropical coral reef growth.

A.4.2 Choice of record used for reconstruction:

Sea surface temperature reconstruction choice

There are a number Quaternary sea surface temperature records for the Pacific [*Lea et al.*, 2000; *Lawrence and Herbert*, 2005, *Russon et al.*, 2010]. However, the *Lea et al.* (2000) record only covers the last 450kyr and the *Lawrence and Herbert* (2005) the last 780kyr. Additionally, neither of the reconstructions were obtained from near New Caledonia, rather coming from the Cocos Ridge and Ontong Java Plateau [*Lea et al.*, 2000] and the Western Coral Sea, near the Central Great Barrier Reef [*Lawrence and Herbert*, 2005]. By contrast, the *Russon et al*. (2010) SST curve is derived from core MD06-3018 on the western New Caledonia margin. Using Mg/Ca measurements on planktic foraminifera it provides a high resolution, local reconstruction of SST changes over the full 1.26Myr period covered by core MD06-3019 (see Chapter 6, *Figure 6.4E*). Therefore this record was used to consider the potential effect of changing temperatures on the history of carbonate production along the western New Caledonia margin over the last 1.26Myr.

Sea-level reconstruction choice

There are a number of global eustatic sea-level curves covering the Quaternary period, such as *Waelbroeck et al*. (2002), *Lea et al.* (2002), *Siddall et al.* (2003), *Rohling et al.* (2009), *Miller et al.*, (2005), *Elderfield et al.* (2012), *Siddall et al.* (2010) and *Bates et al*. (2014). The first four of these only cover the last 450 kyrs, 350kyrs, 470 kyrs and 520kyrs respectively and thus are not long enough for use this study. However, the last four studies do provide sea-level reconstructions which cover the complete 1.26Myr period covered by sediment core MD06-3019. These studies differ in resolution and the approach by which they obtain their past sea-level estimates; but, overall, there is a good coherence in the pattern of sea-level change since 1.26Ma between different reconstructions.

The *Miller et al*. (2005) reconstruction is based on a review of Phanerozoic sea-level changes, since 543 Ma, on various time scales and presents a new sea-level record

for the past 100Myr. The last three aforementioned studies [*Elderfield et al.*, 2012, *Siddall et al.*, 2010; *Bates et al.*, 2014] utilise $\delta^{18}O_{benthic}$ measurements from foraminifera in order to produce their sea-level reconstructions. Foraminiferal $\delta^{18}O_{benthic}$ records contain both temperature and seawater $\delta^{18}O$ composition components. The latter of which reflects a combination of the signal from global changes in ice volume (sea-level) and local hydrographic features, due to the influences of different water masses. The *Elderfield et al.* (2012) investigates sediment core ODP1123 taken from the Chatham Rise, east of New Zealand at 41°47.15'S, 171°29.94'W. This study uses Mg/Ca measurements, as a proxy for temperature, in order to separate out the temperature component of the $\delta^{18}O_{benthic}$ record to produce a relative sea-level curve. By contrast *Siddall et al.* (2010) and *Bates et al.* (2014) use previously published $\delta^{18}O_{benthic}$ records, then obtain the sea-level component of this curve via non-linear transfer functions. These transfer functions have been estimated by examining past sea-level and $\delta^{18}O_{benthic}$ records from the last two glacial cycles, with additional information from the Mid-Pleistocene [*Siddall et al.*, 2010]. *Siddall et al.* (2010) produce their sea-level reconstruction based on the *Shackleton et al.* (1990) composite $\delta^{18}O$ record from the east equatorial Pacific. *Bates et al.* (2014) use 10 $\delta^{18}O$ records from the Pacific, Atlantic and Indian Oceans, including the *Elderfield et al.* (2012) record.

For this thesis the *Miller et al.* (2005) curve was chosen (see Chapter 6, *Figure 6.4F*). It was made by 'stacking' (combining) records from different sites and thus should better represent the global eustatic sea-level, since local features and errors from single records will be averaged out. All curves show a similar broad pattern in the variations of the amplitude of sea-level change with glacial-interglacial cycles. However, the individual reported absolute relative sea-levels (compared to the present day) can differ significantly from record to record and from known relative sea-levels for the western New Caledonian margin at that time. For example, MIS5 sea-level is believed to have peaked at +6m, compared to modern day values, for the western margin of New Caledonia [*Frank et al.*, 2006]. However, values from the *Miller et al*. (2005) place the level at +24m, similarly the *Elderfield et al.* (2012) curve places MIS5 sea-level at ~18m and the *Bates et al.* (2014) reconstructions vary

from -11m to 14m depending on the original $\delta^{18}O$ record used. Therefore caution should be exercised in the consideration of 'absolute' eustatic sea-level values.

Appendix 5: Core photographs and sedimentary logs MD06-3018, MD06-3019 and MD06-3020

A5.1 MD06-3018

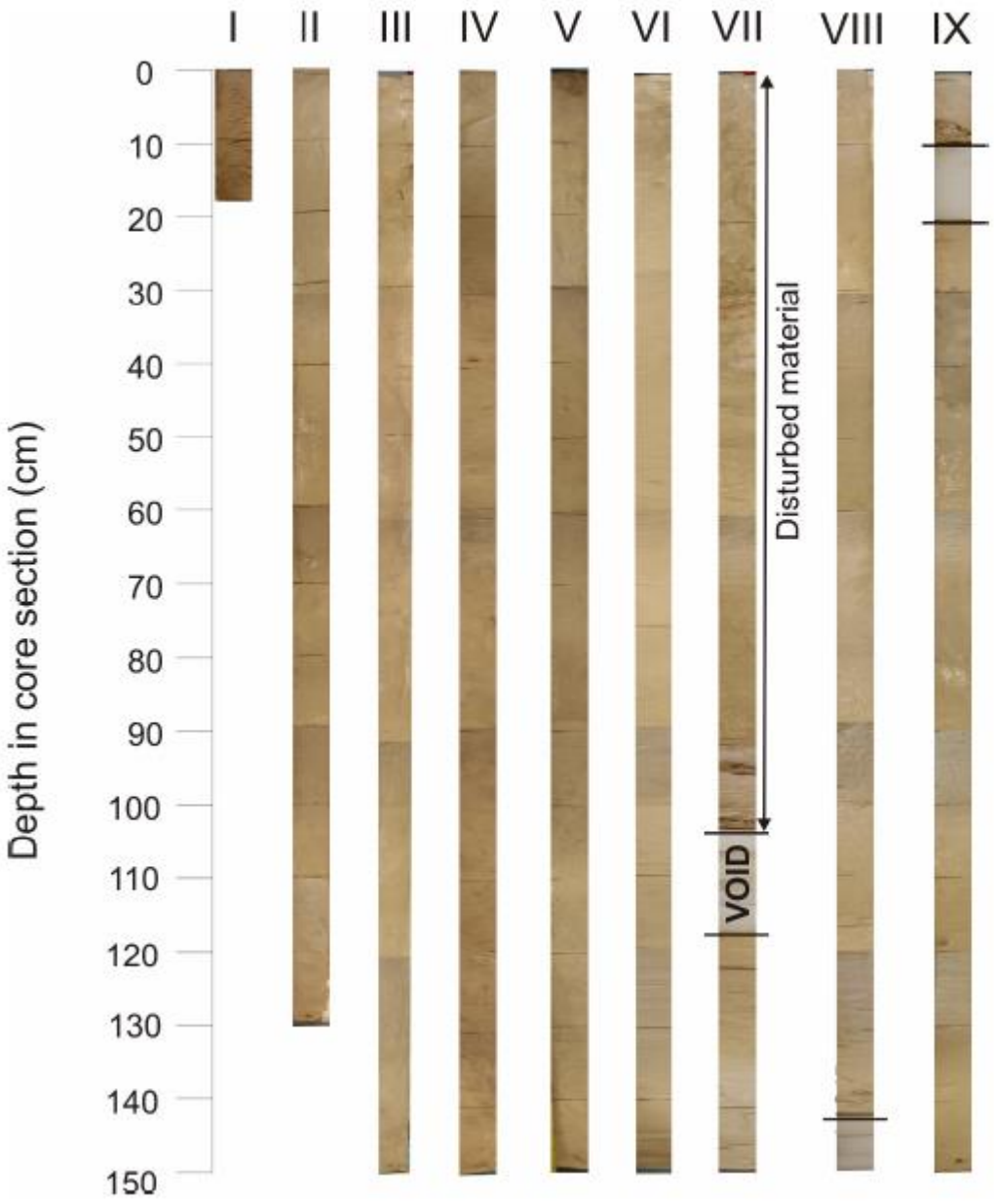

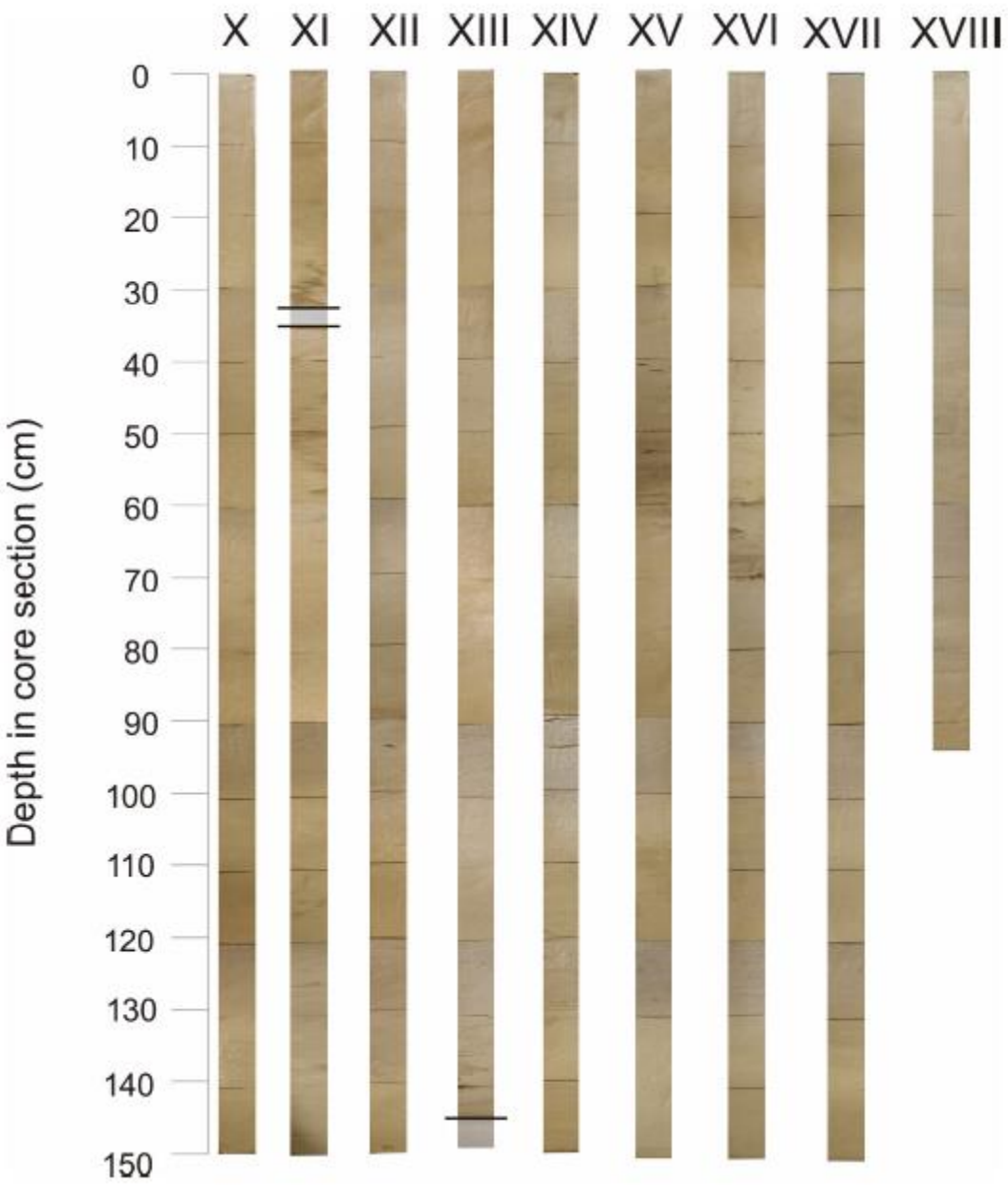

Figure A.10 Core photographs of MD06-3018 core sections. Fine dark lines every 10cm are an artefact from core sampling. Each photograph is a composite of three images, stitched together electronically, leading to some colour artefacts. The bold black lines show the extent of the voids in the core, for example in section VII. There are internal voids in sections VII, IX and XI as well as voids at the end of sections VIII and XIII. The grey colours of these sections arises from the presence of the polypropylene material that was used to infill the voids and support the sediment.

A5.2 MD06-3019

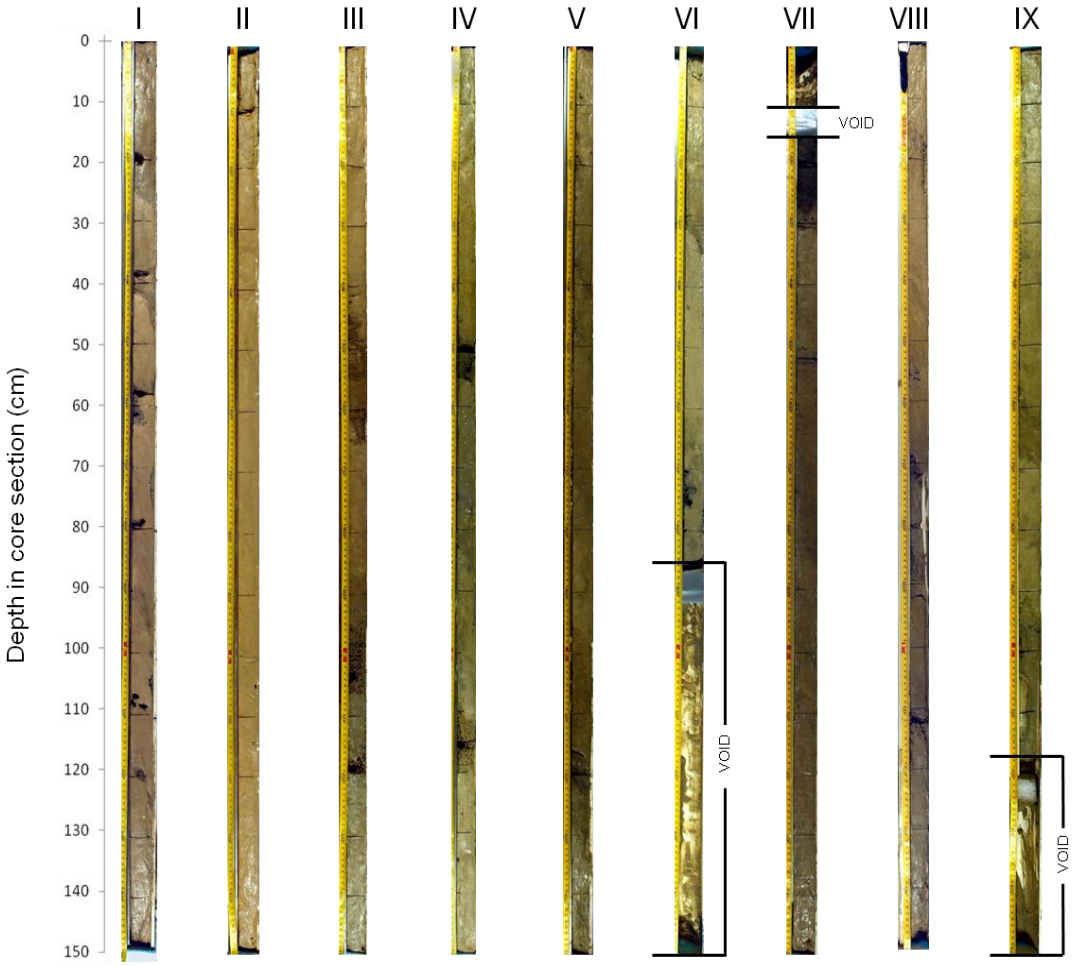

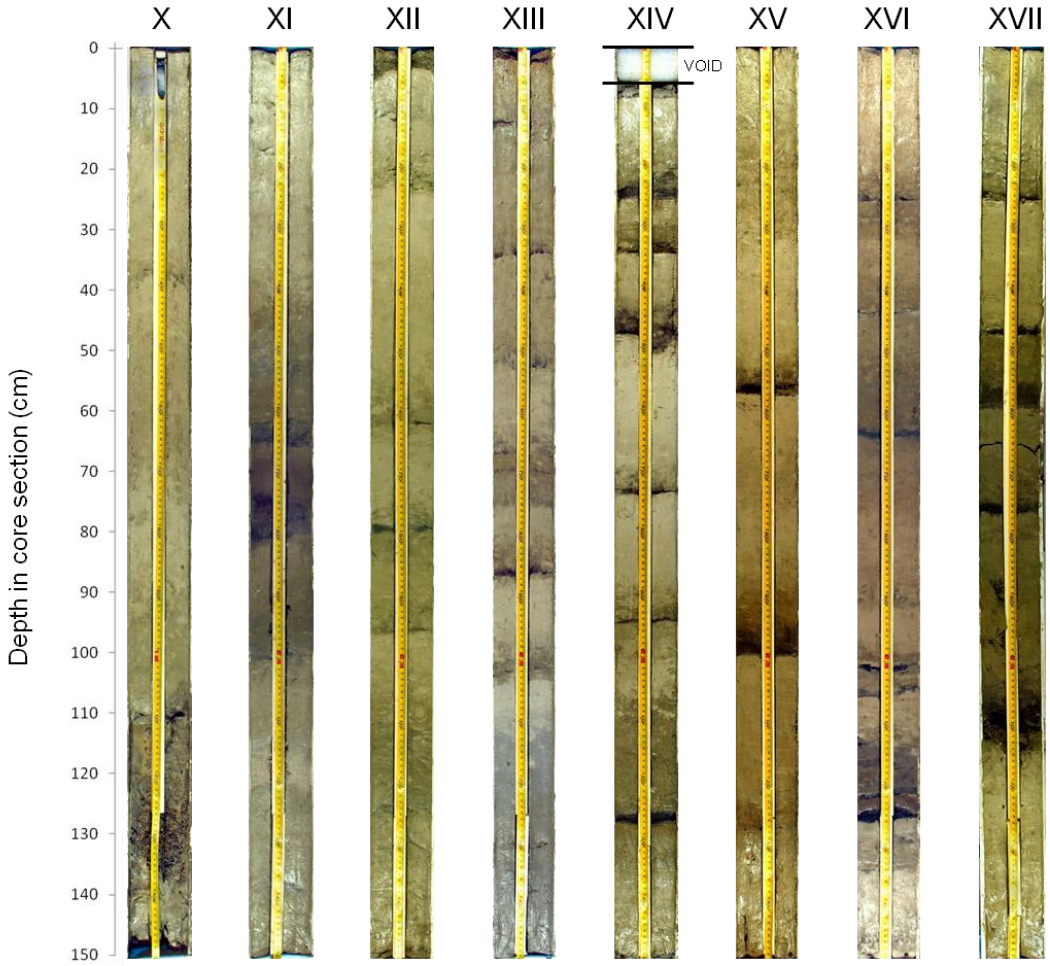
X
XI
XII
XIII
XIV
XV
XVI
XVII
VOID
Depth in core section (cm)
0
10
20
30
40
50
60
70
80
90
100
110
120
130
140
150

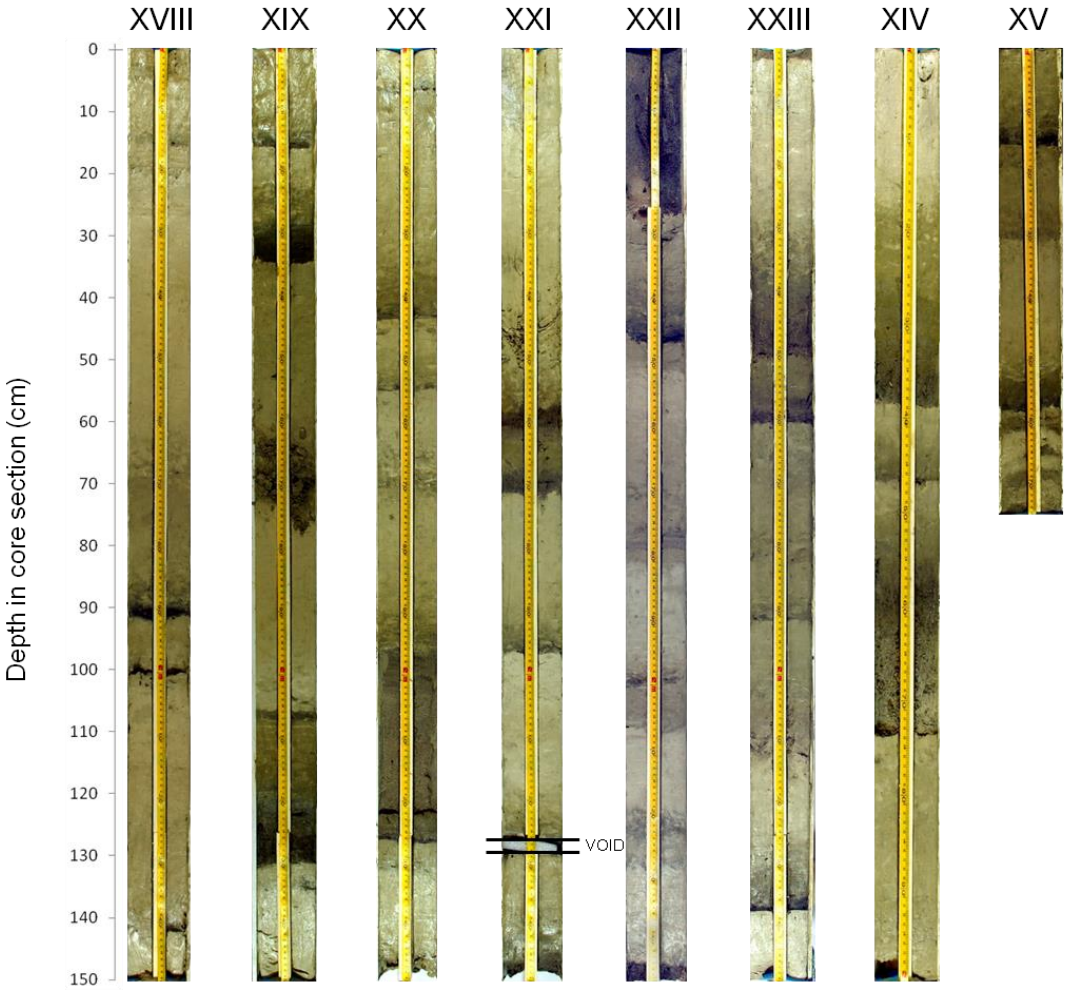

Figure A.11 Core photographs of MD06-3019 core sections. Fine dark lines every 10cm in sections I-IX are an artefact from core sampling. The bold black lines show the extent of the voids in the core, for example in section VI. There is an internal void in section XXI (3126-3129cm) and voids at the end of sections VI (835-900cm), VII (900- 916cm), IX (1320-1350cm) and XIV (1950-1956cm).

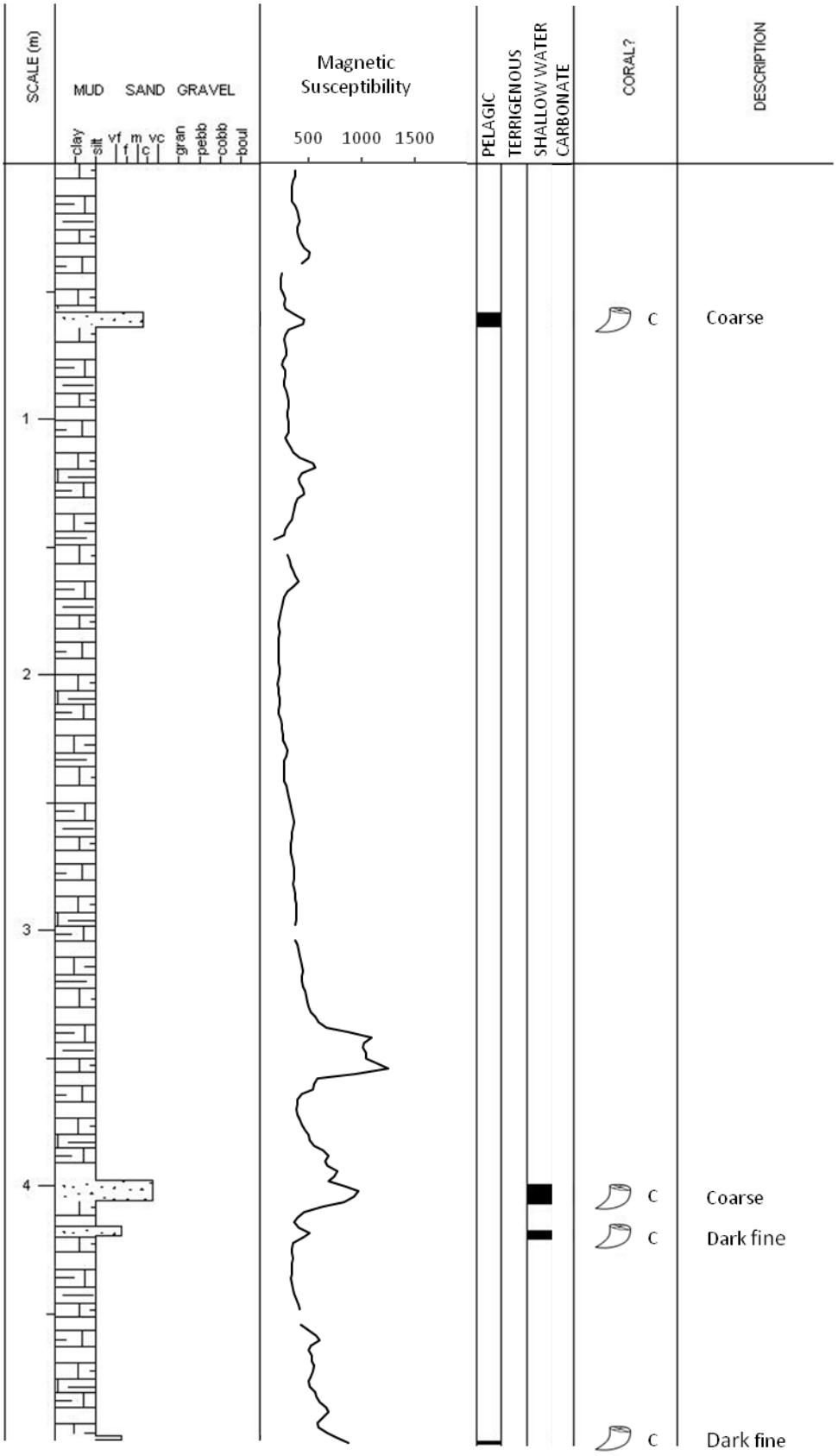
SCALE (m)
MUD
SAND
GRAVEL
clay
silt
vf
f
m
c
vc
gran
pebb
cobb
boul
Magnetic Susceptibility
500
1000
1500
PELAGIC
TERRIGENOUS
SHALLOW WATER CARBONATE
CORAL?
DESCRIPTION
1
2
3
4
C
Coarse
C
Coarse
C
Dark fine
C
Dark fine

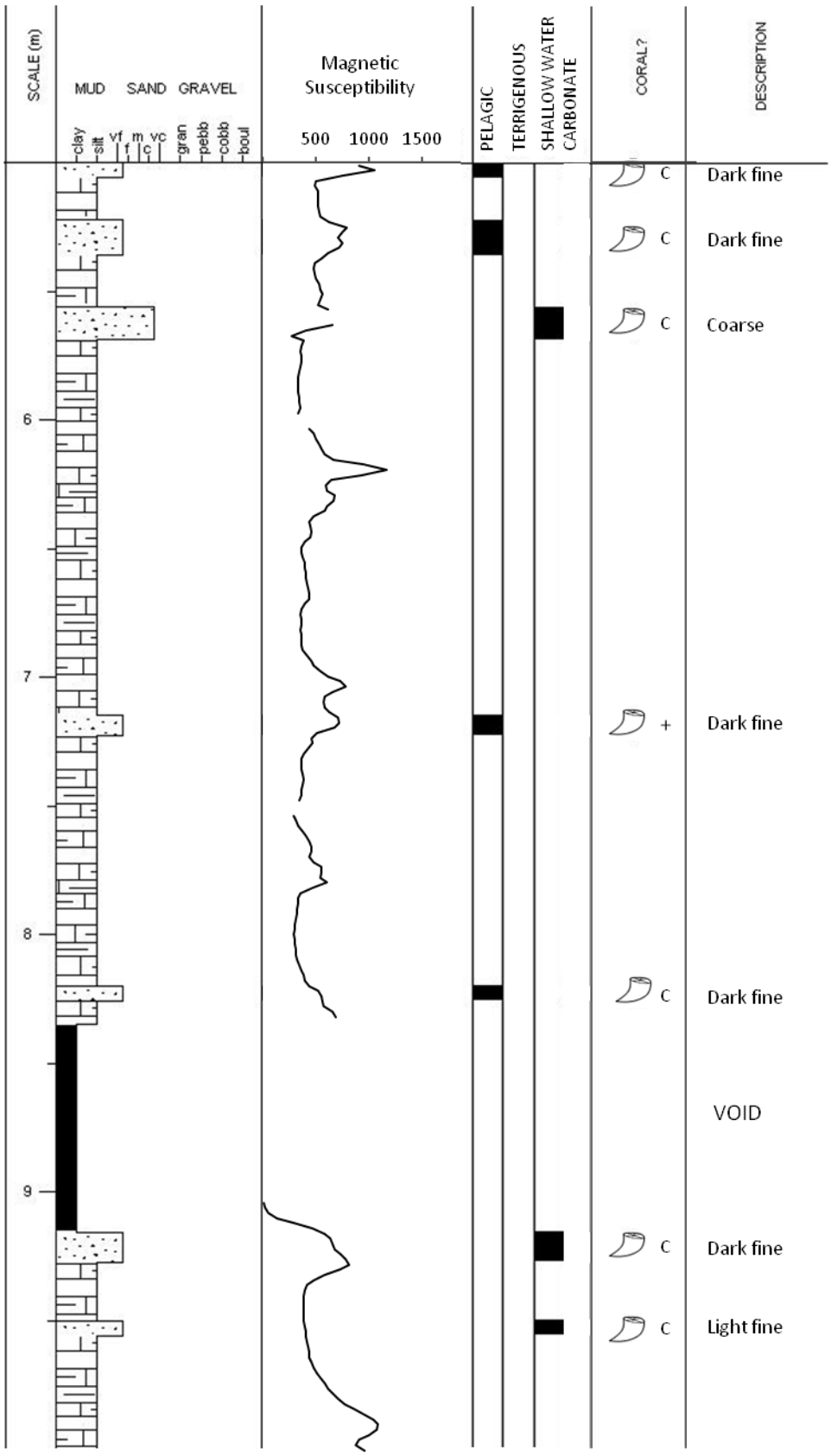
SCALE (m)
MUD
SAND
GRAVEL
clay
silt
vf
f
m
c
vc
gran
pebb
cobb
boul
Magnetic Susceptibility
500
1000
1500
PELAGIC
TERRIGENOUS
SHALLOW WATER CARBONATE
CORAL?
DESCRIPTION
6
7
8
9
C
C
C
+
C
C
C
Dark fine
Dark fine
Coarse
Dark fine
Dark fine
VOID
Dark fine
Light fine

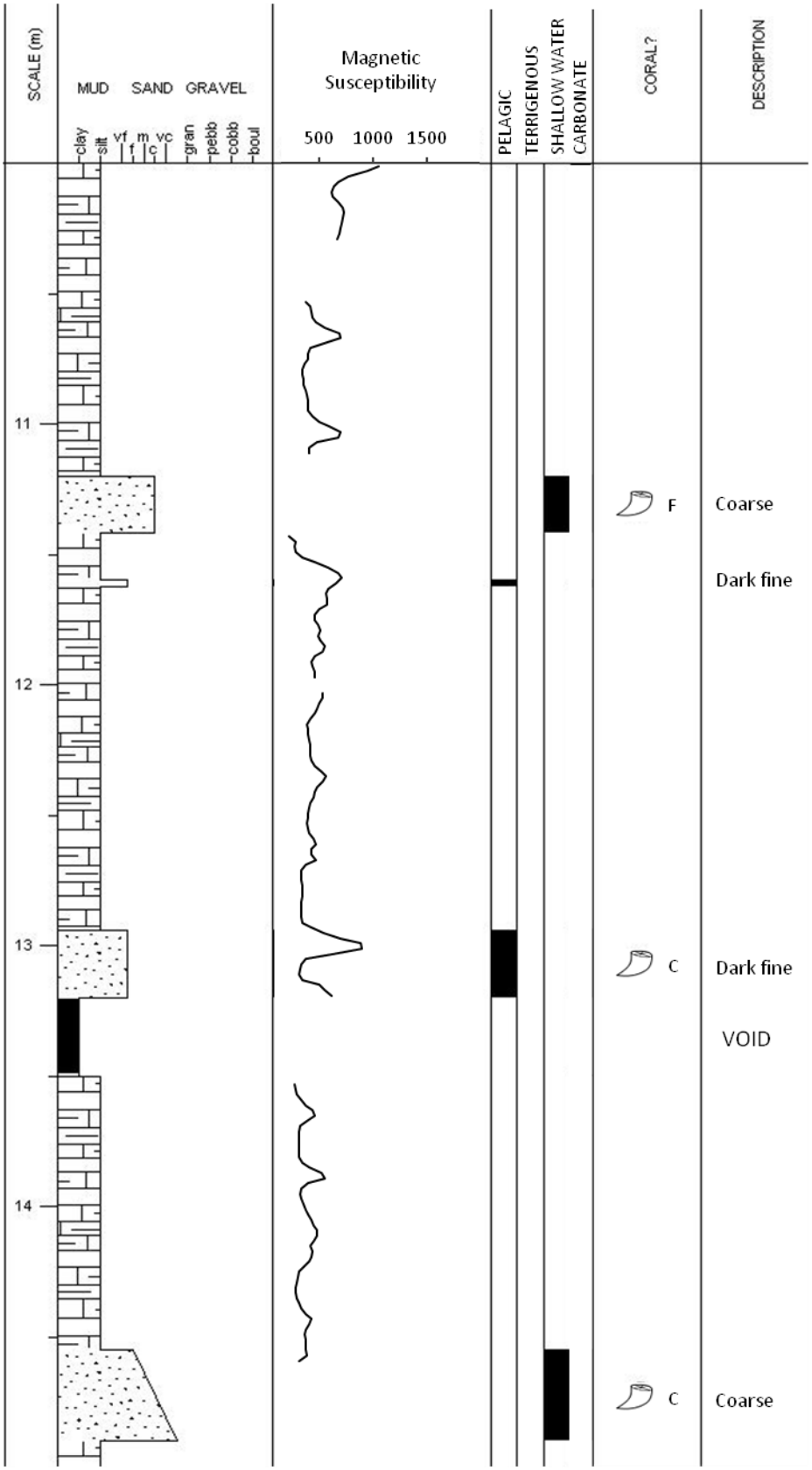
SCALE (m)
MUD
SAND
GRAVEL
clay
silt
vf
f
m
c
vc
gran
pebb
cobb
boul
Magnetic Susceptibility
500
1000
1500
PELAGIC
TERRIGENOUS
SHALLOW WATER CARBONATE
CORAL?
DESCRIPTION
11
12
13
14
F
Coarse
Dark fine
C
Dark fine
VOID
C
Coarse

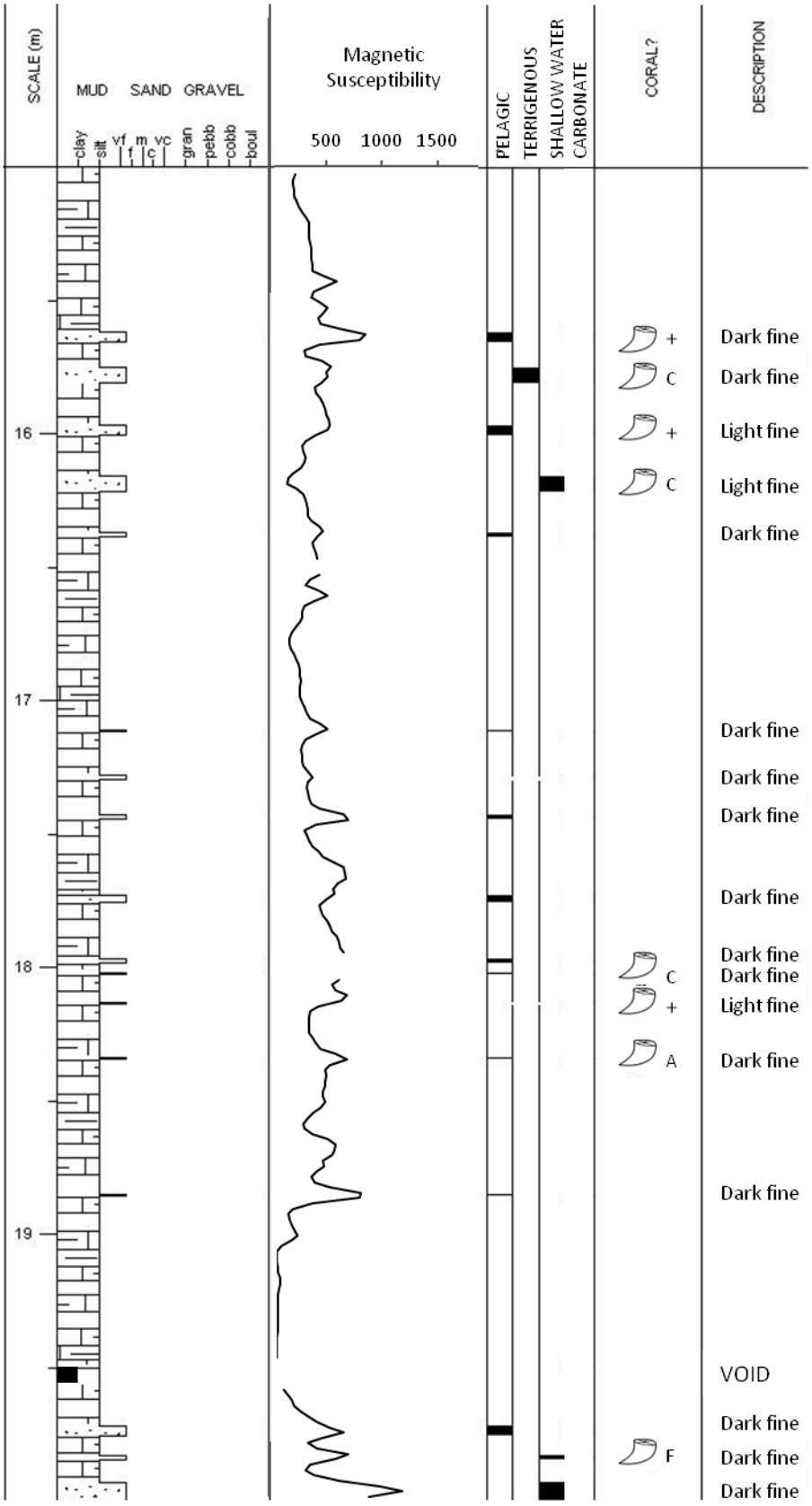
SCALE (m)
MUD
SAND
GRAVEL
clay
silt
vf
f
m
c
vc
gran
pebb
cobb
boul
Magnetic Susceptibility
500
1000
1500
PELAGIC
TERRIGENOUS
SHALLOW WATER CARBONATE
CORAL?
DESCRIPTION
16
17
18
19
+
C
+
C
A
F
Dark fine
Light fine
VOID

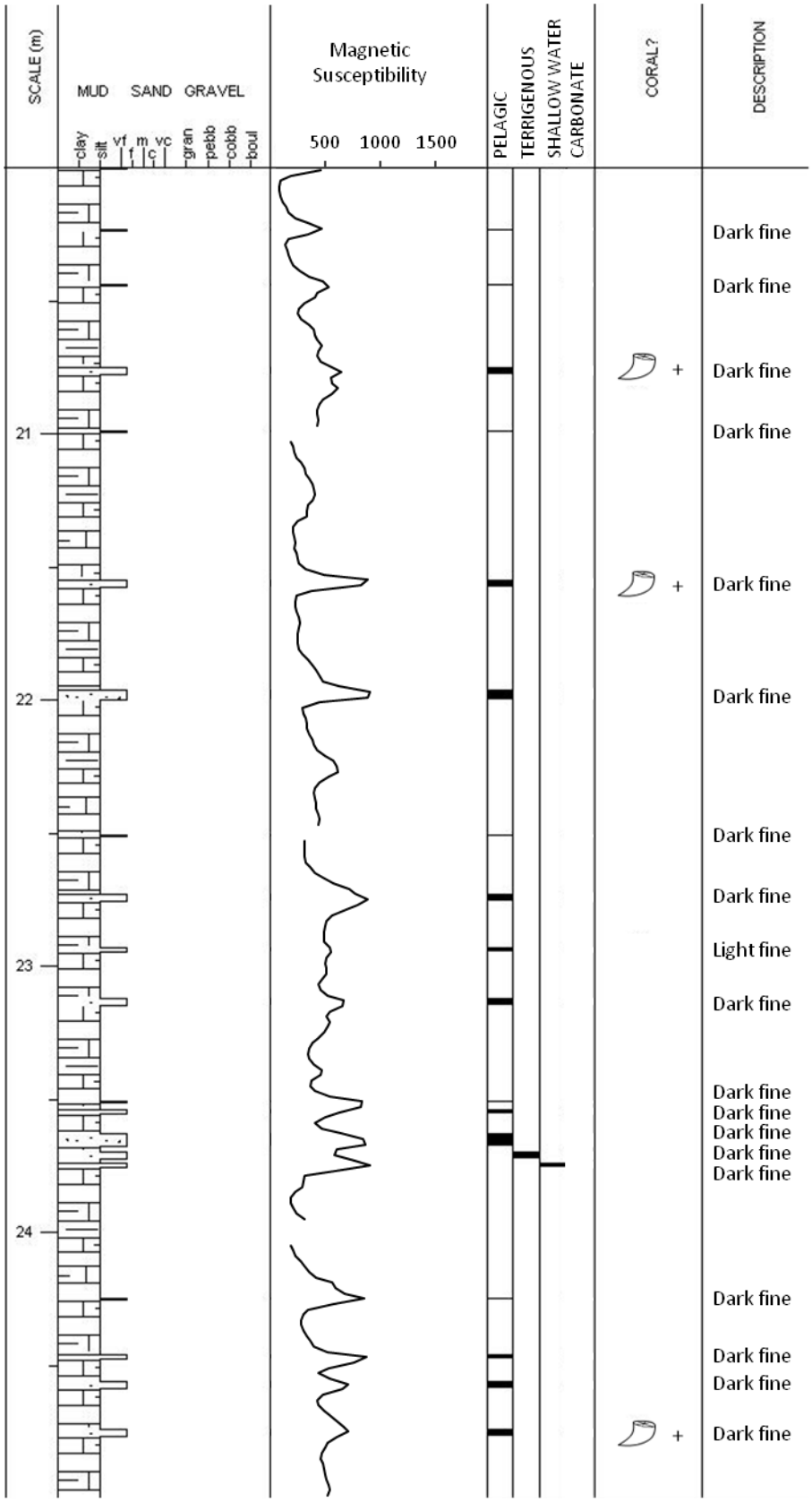
SCALE (m)
MUD
SAND
GRAVEL
clay
silt
vf
f
m
c
vc
gran
pebb
cobb
boul
Magnetic Susceptibility
500
1000
1500
PELAGIC
TERRIGENOUS
SHALLOW WATER CARBONATE
CORAL?
DESCRIPTION
21
22
23
24
Dark fine
Dark fine
+
Dark fine
Dark fine
+
Dark fine
Dark fine
Dark fine
Light fine
Dark fine
Dark fine
Dark fine
Dark fine
Dark fine
Dark fine
Dark fine
Dark fine
Dark fine
+
Dark fine

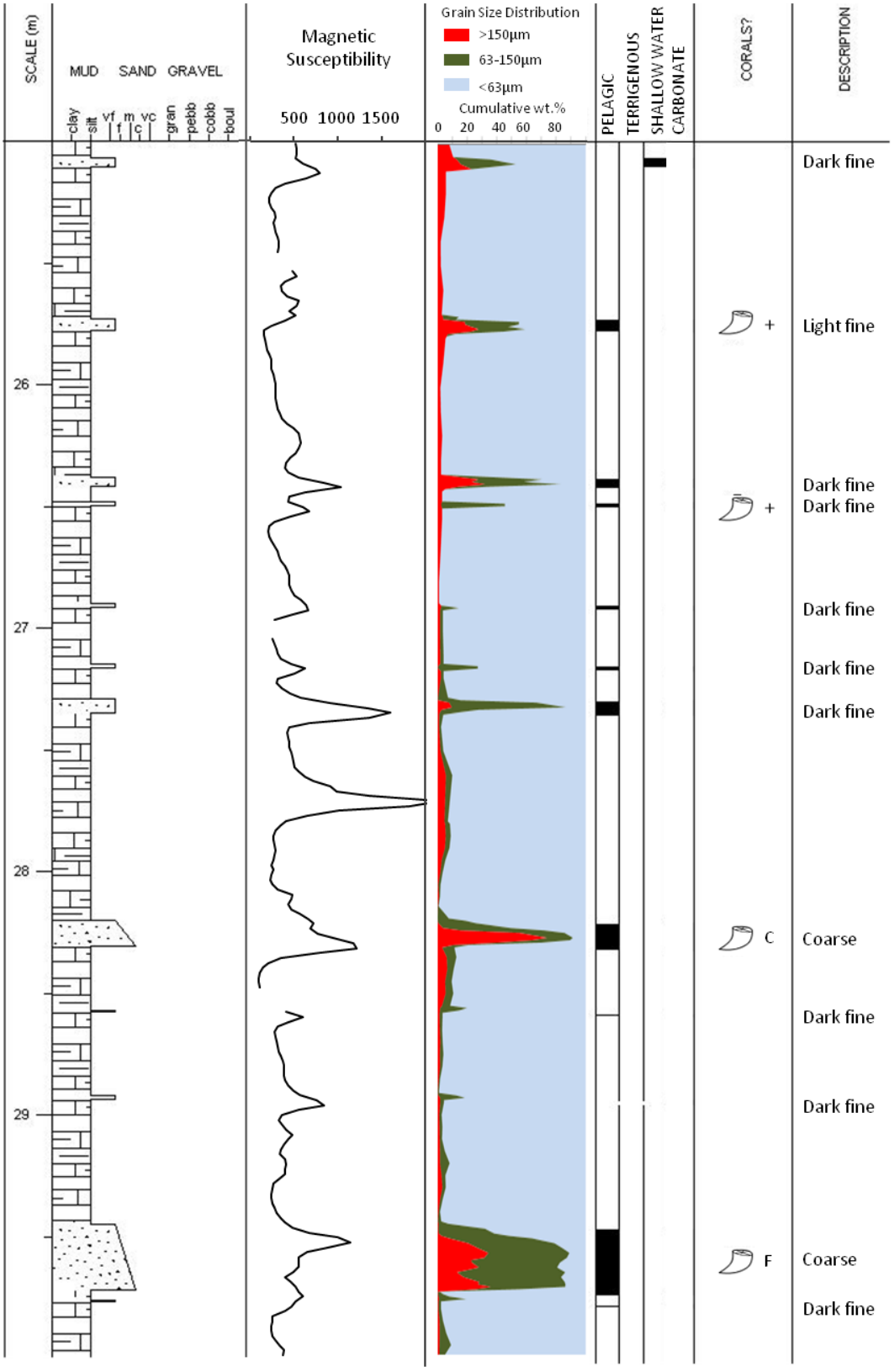
SCALE (m)
MUD
SAND
GRAVEL
clay
silt
vf
f
m
c
vc
gran
pebb
cobb
boul
Magnetic Susceptibility
500 1000 1500
Grain Size Distribution
>150µm
63-150µm
<63µm
Cumulative wt.%
0 20 40 60 80
PELAGIC
TERRIGENOUS
SHALLOW WATER CARBONATE
CORALS?
DESCRIPTION
26
27
28
29
Dark fine
Light fine
Dark fine
Dark fine
Dark fine
Dark fine
Dark fine
Coarse
Dark fine
Dark fine
Coarse
Dark fine
+
+
C
F

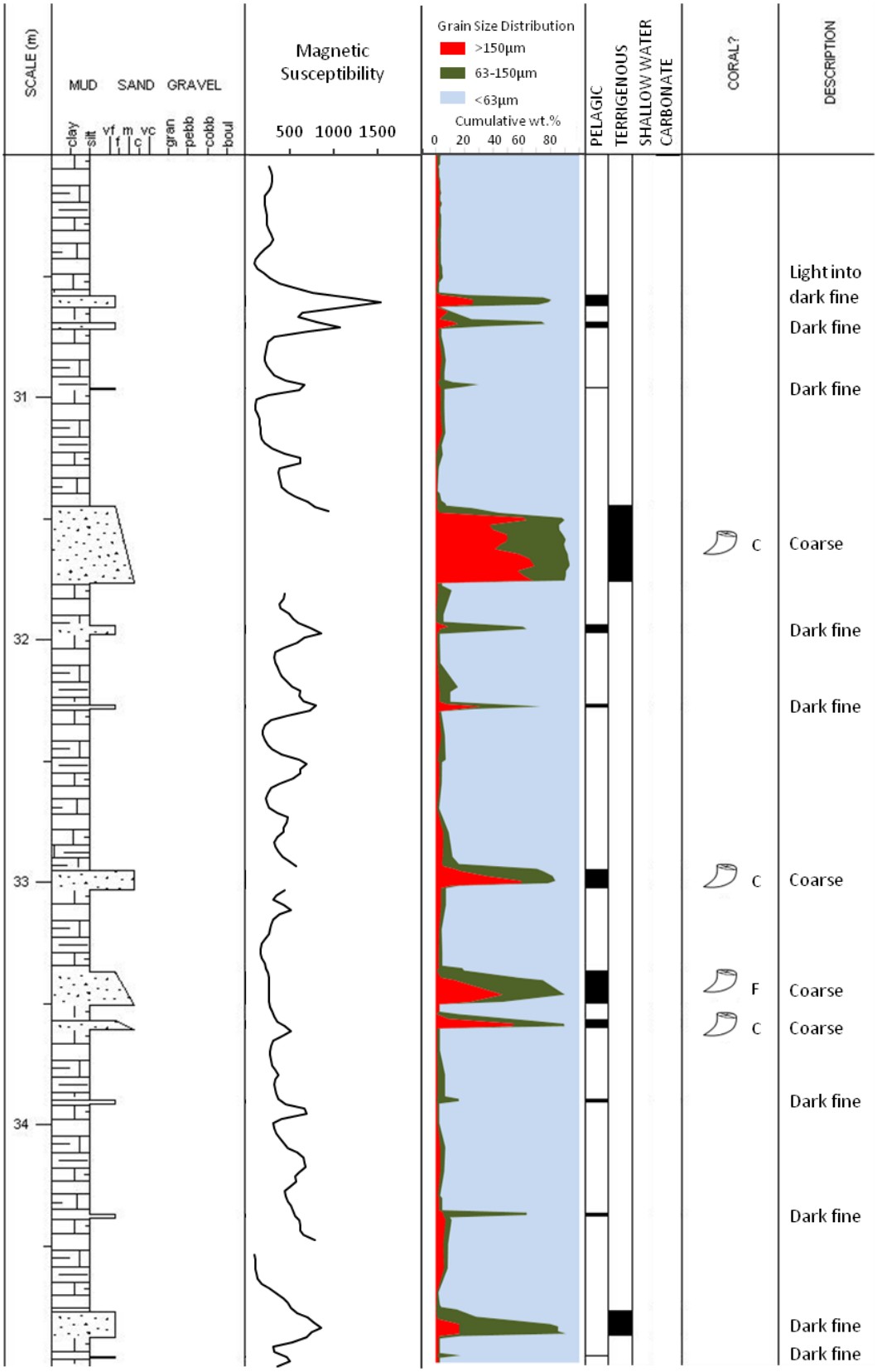
SCALE (m)
MUD
SAND
GRAVEL
clay
silt
vf
f
m
c
vc
gran
pebb
cobb
boul
Magnetic Susceptibility
500 1000 1500
Grain Size Distribution
>150µm
63-150µm
<63µm
Cumulative wt.%
0 20 40 60 80
PELAGIC
TERRIGENOUS
SHALLOW WATER CARBONATE
CORAL?
DESCRIPTION
31
32
33
34
Light into dark fine
Dark fine
Dark fine
C
Coarse
Dark fine
Dark fine
C
Coarse
F
Coarse
C
Coarse
Dark fine
Dark fine
Dark fine
Dark fine

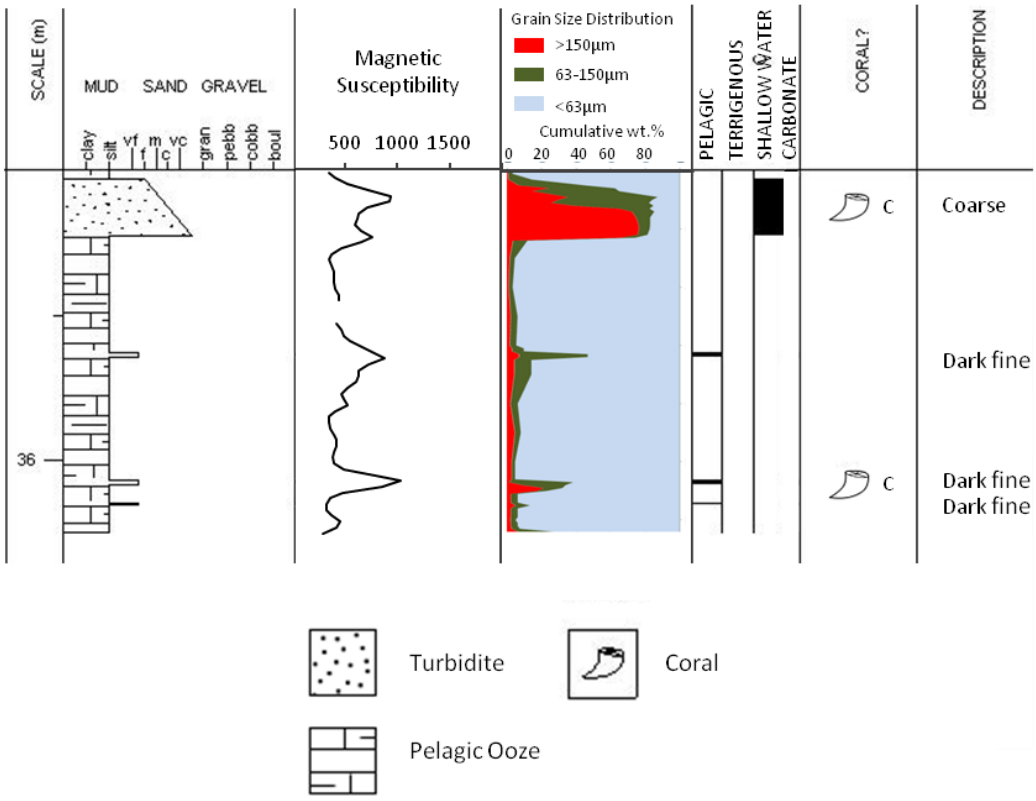

Figure A.12 Stratigraphic logs for core MD06-3019 showing lithology, qualitative grain size, magnetic susceptibility, the compositional component with the highest percentage, coral content and layer type. A coral symbol is given when any coral was found in a sample, the abundance of coral is indicated by the following letters: A- abundant (>10% of shallow water grains), C- common (1-10% shallow water grains), F- few (<1% shallow water grains), R-rare (<0.1% shallow water grains) and + - present but not counted or not enough grains to provide an accurate idea of abundance. From 25m to base logs of grain size cumulative wt.% are provided for size fractions <63µm, 63-150µm and >150µm. This was not possible further up the core due to missing data, where weight measurements were not recorded by previous researchers who sampled the core.

A5.3 MD06-3020

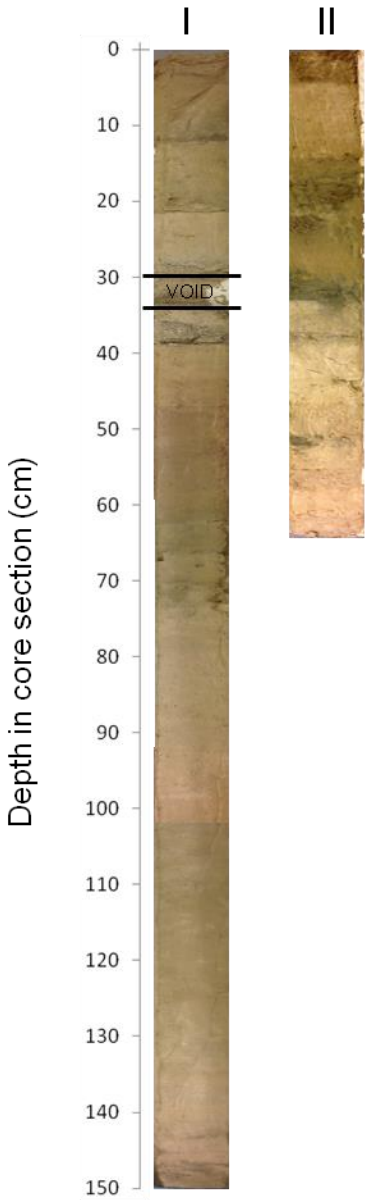

Figure A.13 Core photographs of MD06-3020 core sections. The photograph for section I is a composite of three images, stitched together electronically, leading to some colour artefacts. There is an internal void in section I (29-34cm), the bold black lines highlight its extent.

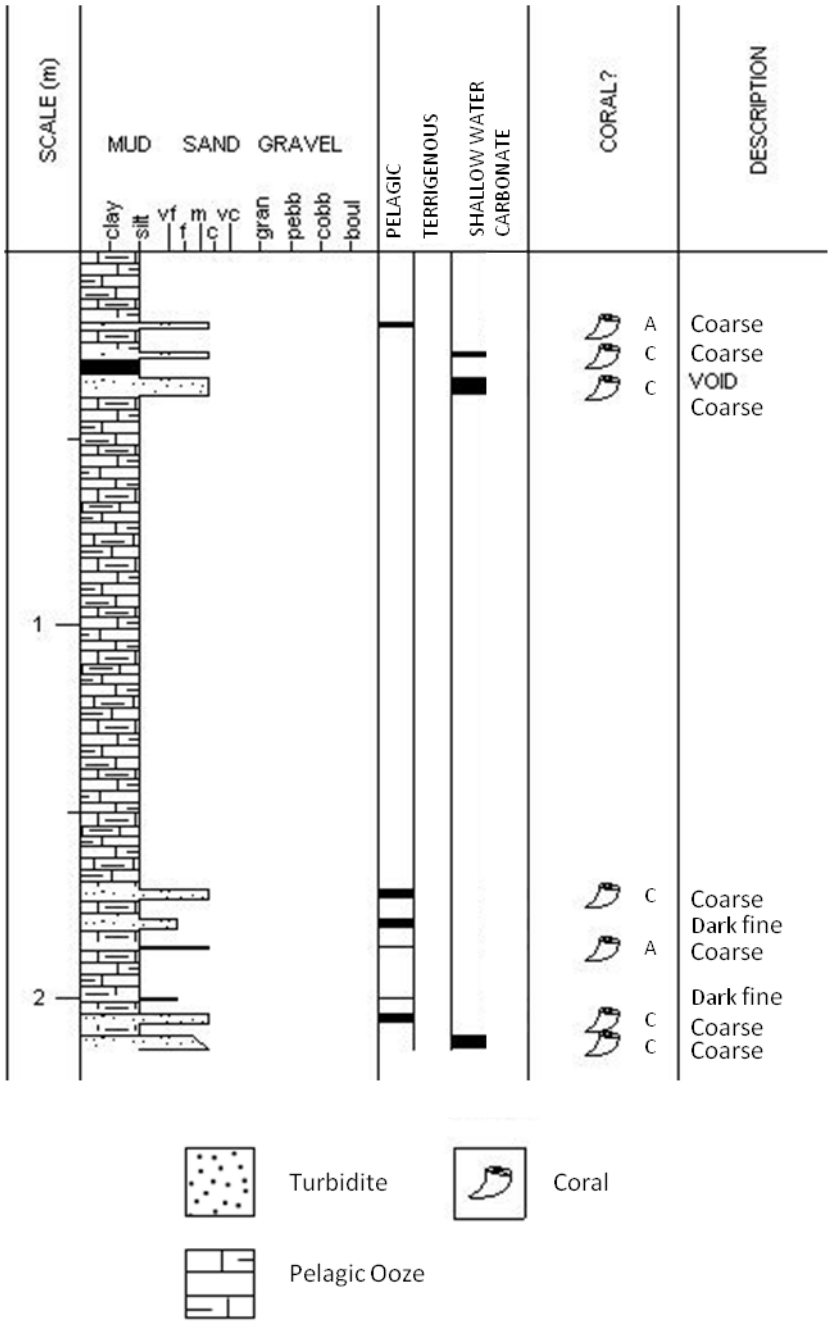

Figure A.14 Stratigraphic logs for core MD06-3020 showing lithology, qualitative grain size, the compositional component with the highest percentage, coral content and layer type. A coral symbol is given when any coral was found in a sample, the abundance of coral is indicated by the following letters: A- abundant (>10% of shallow water grains), C- common (1-10% shallow water grains), F- few (<1% shallow water grains), R-rare (<0.1% shallow water grains) and + - present but not counted or not enough grains to provide an accurate idea of abundance.

Appendix 6: MD06-3019 and MD06-3020 Turbidite Descriptions

A6.1 MD06-3019 turbidite ages and descriptions

MD06-3019 Turbidite Layer Summary												
Raw layer depth down-core	**Corrected layer depth down-core**	**Age**	**Turbidite layer type**	**Turbidite layer width**	**Additional Notes**	**Number of layers point counted**	**Number of grains point counted**	**Planktic**	**Terrigenous**	**Shallow water carbonate**	**Miscellaneous**	**Coral abundance**
(cm)	**(cm)**	**(ka)**		**(cm)**				**(%)**	**(%)**	**(%)**	**(%)**	**(% of shallow water material)**
58-64	58-64	16	Coarse grained	6	Does not continue across the whole core width.	7	5,576	**74**	5	21	0	3
398-406	398-406	98	Coarse grained	8	Coarse sand; fines up.	5	2,989	1	30	**69**	1	2
416-420	416-420	102	Dark fine grained	4	Mainly fine sand, though fines up from medium coarse sand in the bottom 2 cm.	2	1,065	9	34	**57**	0	2
498-506	498-506	124	Dark fine grained	8	Fines up; mid-dark brown colour.	4	2,608	**58**	33	8	0	4
522-536	522-536	132	Dark fine grained	14	Very fine sand.	4	611	**85**	4	11	0	3
556-569	556-569	137	Coarse grained	13	Fines up; grains of mixed colour and not well rounded.	4	2,943	6	38	**56**	0	4
715-723	715-723	158	Dark fine grained	8	Very fine grained; moderately dark coloured sand.	6	1,386	**83**	11	6	0	1
820-826	820-826	173	Dark fine grained	6	Dark fine grained sand, with some larger (2mm diameter) white clasts present.	2	403	**41**	26	33	0	2
916-928	835-847	177	Dark fine grained	12	Mainly dark coloured, mid-fine grained sand.	3	1,644	11	43	**46**	0	9
950-956	869-875	181	Light fine grained	6		3	865	12	39	**49**	0	6
1120-1142	1039-1061	227	Coarse grained	22	Mid-brown colour; mid-coarse to fine grained sand, poorly sorted.	10	3,834	25	26	49	0	2
1160-1163	1079-1082	232	Dark fine grained	3	Mid-dark brown colour.	2	**108**	**85**	11	4	0	0
1294-1320	1213-1239	261	Dark fine grained	26		5	2,443	**41**	25	34	0	3

MD06-3019 Turbidite Layer Summary												
Raw layer depth down-core	**Corrected layer depth down-core**	**Age**	**Turbidite layer type**	**Turbidite layer width**	**Additional Notes**	**Number of layers point counted**	**Number of grains point counted**	**Planktic**	**Terrigenous**	**Shallow water carbonate**	**Miscellaneous**	**Coral abundance**
(cm)	**(cm)**	**(ka)**		**(cm)**				**(%)**	**(%)**	**(%)**	**(%)**	**(% of shallow water material)**
1455-1490	1344-1379	292	Coarse grained	35	Fines up; very coarse sand/ gravel at base (often 5-8mm diameter grains), with clear whole bioclasts, fines up to medium coarse sand at top.	11	4,931	13	40	**47**	0	4
1562-1566	1451-1455	330	Dark fine grained	4		3	357	**46**	32	22	1	4
1575-1581	1464-1470	333	Dark fine grained	6		2	978	35	**39**	26	0	5
1597-1601	1486-1490	337	Light fine grained	4	Very fine grained sand; light grey colour.	2	785	**84**	9	6	1	4
1616-1622	1505-1511	341	Light fine grained	6	Generally light coloured sand grains, but some darker terrigenous material.	4	720	27	35	**38**	0	4
1637-1639	1526-1528	345	Dark fine grained	2	Dark grey-black colour, does not continue across whole core diameter.	1	**48**	**98**	0	2	0	0
1711-1712	1600-1601	373	Dark fine grained	1		1	**23**	**87**	9	4	0	0
1728-1730	1617-1619	379	Dark fine grained	2		0	**0**	N/A	N/A	N/A	N/A	N/A
1743-1745	1632-1634	385	Dark fine grained	2		1	**58**	**88**	3	9	0	0
1773-1776	1662-1665	398	Dark fine grained	3		1	**22**	**64**	27	9	0	0
1797-1799	1686-1688	405	Dark fine grained	2		1	**55**	**89**	5	5	0	0
1802-1803	1691-1692	407	Dark fine grained	1		2	318	**51**	24	25	0	6
1813-1814	1702-1703	410	Light fine grained	1		0	**0**	N/A	N/A	N/A	N/A	N/A
1834-1835	1723-1724	415	Dark fine grained	1		1	596	**40**	34	26	0	13

MD06-3019 Turbidite Layer Summary												
Raw layer depth down-core (cm)	**Corrected layer depth down-core (cm)**	**Age (ka)**	**Turbidite layer type**	**Turbidite layer width (cm)**	**Additional Notes**	**Number of layers point counted**	**Number of grains point counted**	**Planktic (%)**	**Terrigenous (%)**	**Shallow water carbonate (%)**	**Miscellaneous (%)**	**Coral abundance (% of shallow water material)**
1885-1886	1774-1775	429	Dark fine grained	1		1	339	**97**	1	2	0	0
1972-1976	1855-1859	457	Dark fine grained	4	Reasonably sharp base; grey-brown colour.	2	**25**	**92**	0	8	0	0
1983-1985	1866-1868	459	Dark fine grained	2	Reasonably sharp base; grey-brown colour.	2	480	9	2	**89**	0	0
1993-2001	1876-1884	464	Dark fine grained	8	Reasonably sharp base; dark brown colour.	4	2,402	25	0	**75**	0	0
2023-2024	1906-1907	470	Dark fine grained	1	Dark brown colour.	1	**298**	**94**	3	3	0	0
2044-2045	1927-1928	476	Dark fine grained	1	Dark brown colour.	1	**89**	24	7	**70**	0	0
2075-2078	1958-1961	488	Dark fine grained	3	Medium fine grained sand; grey-black colour.	2	**169**	**52**	19	29	0	16
2099-2100	1982-1983	502	Dark fine grained	1		1	**110**	**60**	17	23	0	0
2155-2158	2038-2041	537	Dark fine grained	3	Sharp base.	3	1,031	**97**	0	2	0	8
2196-2200	2079-2083	559	Dark fine grained	4	Sharp base.	3	**83**	**83**	4	13	0	0
2251-2252	2134-2135	584	Dark fine grained	1		1	**67**	**97**	1	1	0	0
2273-2276	2156-2159	596	Dark fine grained	3	Medium brown colour.	2	459	**99**	0	1	0	0
2294-2295	2177-2178	604	Light fine grained	1		2	476	**96**	2	2	0	0
2312-2315	2195-2198	614	Dark fine grained	3		1	**136**	**98**	1	1	0	0
2351-2352	2234-2235	625	Dark fine grained	1		1	**171**	**96**	4	0	0	0
2354-2356	2237-2239	626	Dark fine grained	2		2	**256**	**100**	0	0	0	0

MD06-3019 Turbidite Layer Summary												
Raw layer depth down-core	**Corrected layer depth down-core**	**Age**	**Turbidite layer type**	**Turbidite layer width**	**Additional Notes**	**Number of layers point counted**	**Number of grains point counted**	**Planktic**	**Terrigenous**	**Shallow water carbonate**	**Miscellaneous**	**Coral abundance**
(cm)	**(cm)**	**(ka)**		**(cm)**				**(%)**	**(%)**	**(%)**	**(%)**	**(% of shallow water material)**
2363-2368	2246-2251	630	Dark fine grained	5	Fines up.	4	**143**	**77**	20	3	0	0
2370-2373	2253-2255	631	Dark fine grained	3		1	**27**	15	**81**	4	0	0
2374-2376	2257-2259	632	Dark fine grained	2		2	**241**	17	6	**78**	0	0
2425-2426	2308-2309	658	Dark fine grained	1	Dark brown colour.	2	340	**99**	0	1	0	0
2446-2448	2329-2331	669	Dark fine grained	2		2	**92**	**95**	4	1	0	0
2456-2459	2339-2342	675	Dark fine grained	3	Very fine grained; medium brown colour.	3	**107**	**85**	4	11	0	0
2474-2477	2357-2360	685	Dark fine grained	3		2	**175**	**56**	29	15	0	4
2507-2511	2390-2394	704	Dark fine grained	4	Very dark brown; very fine grained sand.	3	1,246	10	0	**90**	0	0
2573-2578	2456-2461	747	Light fine grained	5	Fine grained sand; light coloured- same colour as surrounding pelagic ooze though with some darker coloured grains.	5	1,779	**96**	1	3	0	4
2638-2642	2521-2525	787	Dark fine grained	4		2	694	**92**	5	3	0	0
2648-2650	2531-2533	789	Dark fine grained	2		1	**219**	**99**	0	0	0	100
2690-2692	2573-2575	813	Dark fine grained	2		2	431	**99**	0	1	0	0
2715-2717	2598-2600	831	Dark fine grained	2	Mid-brown to grey colour; very fine sand; sharp base but top bioturbated.	1	**29**	**93**	7	0	0	0

MD06-3019 Turbidite Layer Summary												
Raw layer depth down-core	**Corrected layer depth down-core**	**Age**	**Turbidite layer type**	**Turbidite layer width**	**Additional Notes**	**Number of layers point counted**	**Number of grains point counted**	**Planktic**	**Terrigenous**	**Shallow water carbonate**	**Miscellaneous**	**Coral abundance**
(cm)	**(cm)**	**(ka)**		**(cm)**				**(%)**	**(%)**	**(%)**	**(%)**	**(% of shallow water material)**
2729-2735	2612-2618	844	Dark fine grained	6	Very dark brown, fine-medium sand; sharp base but top bioturbated.	6	**251**	**96**	4	0	0	0
2820-2831	2703-2714	899	Coarse grained	11	Erosional base; medium coarse sand at base; fines up to fine sand; dark coloured.	10	2,274	**69**	13	18	0	3
2857-2857	2740-2740	910	Dark fine grained	1	Very fine grained sand, not a full cm wide.	2	472	**100**	0	0	0	0
2892-2894	2775-2777	947	Dark fine grained	2	Dark brown; fine sand.	0	**0**	N/A	N/A	N/A	N/A	N/A
2945-2972	2828-2855	983	Coarse grained	27	Sharp, erosional base; medium coarse sand at base; fines up to fine sand at top; medium colour at base becomes darker brown at top.	11	968	**66**	7	27	0	1
2976-2977	2859-2860	985	Dark fine grained	1	Sharp base; dark brown colour.	1	**33**	**94**	0	6	0	0
3058-3063	2941-2946	1,014	Light fine grained	5	Mud/silt matrix pale coloured at base, dark by top; no sharp base; curved base of layer- pistonage?	5	1,507	**96**	2	1	0	0
3069-3072	2952-2955	1,016	Dark fine grained	3	Curved base of layer- pistonage?	4	421	**76**	18	6	0	0
3096-3097	2979-2980	1,025	Dark fine grained	1	Moderately sharp base, dark brown.	3	573	**98**	1	1	0	0
3145-3177	3028-3060	1,068	Coarse grained	32	Sharp base; medium coarse sand; fines up; dark coloured.	15	3,850	21	**45**	34	0	0
3194-3198	3077-3081	1,079	Dark fine grained	4	No sharp base, dark brown.	4	831	**93**	6	1	0	0
3227-3229	3110-3112	1,094	Dark fine grained	2	Moderately sharp base; fines up; lighter colour at base.	3	2,643	**93**	2	6	0	0

MD06-3019 Turbidite Layer Summary												
Raw layer depth down-core	**Corrected layer depth down-core**	**Age**	**Turbidite layer type**	**Turbidite layer width**	**Additional Notes**	**Number of layers point counted**	**Number of grains point counted**	**Planktic**	**Terrigenous**	**Shallow water carbonate**	**Miscellaneous**	**Coral abundance**
(cm)	**(cm)**	**(ka)**		**(cm)**				**(%)**	**(%)**	**(%)**	**(%)**	**(% of shallow water material)**
3295-3303	3178-2186	1,122	Coarse grained	8	Medium coarse sand; mid-fawn-brown coloured mud/silt matrix component.	6	2,164	**78**	5	16	0	3
3337-3351	3220-3234	1,142	Coarse grained	14	Medium coarse sand; fines up to fine sand at top, generally dark coloured mud/silt matrix component.	4	637	**76**	4	21	0	1
3357-3361	3240-3244	1,146	Coarse grained	4	Medium coarse sand; fines up to very fine sand at top.	2	574	**64**	9	27	0	5
3390-3392	3273-3275	1,159	Dark fine grained	2	Very fine grained; doesn't continue across the whole core diameter.	1	**119**	**99**	1	0	0	0
3437-3439	3320-3322	1,182	Dark fine grained	2	Very sharp base, dark grey-black colour.	1	**61**	**87**	3	10	0	0
3477-3488	3360-3371	1,207	Dark fine grained	11	Sharp base; fines up.	5	346	41	**43**	16	0	0
3496-3497	3379-3380	1,210	Dark fine grained	1		1	**181**	**87**	13	0	0	0
3503-3523	3386-3406	1,220	Coarse grained	20	Sharp erosional base; coarse shell material at base; fines up to fine sand at top; organics visible 3503-3507cm.	8	3,461	13	25	**61**	2	3
3563-3565	3446-3448	1,236	Dark fine grained	2	Relatively sharp base and top; contains some medium sized sand.	1	**192**	**61**	14	24	0	0
3607-3609	3490-3492	1,254	Dark fine grained	2	Completely fine grained.	3	1,665	**94**	1	6	0	3
3615-3616	3498-3499	1,257	Dark fine grained	1	Mid-brown fine sand, doesn’t continue across the whole core diameter.	1	735	**99**	0	1	0	0

Table A.2 Summary of the positions, ages, widths, type and composition (obtained by point counting) of turbidite layers present in core MD06-3019. For layers with fewer than 300 grains present in the >500µm fraction, which were excluded from the point counting analysis, the number of grains point counted is highlighted in red. The dominant component (planktic, terrigenous or shallow water carbonate material) of each layer is highlighted in bold.

A.6.2 MD06-3020 turbidite ages and descriptions

MD06-3020 Turbidite Layer Summary					
Raw layer depth (cm)	**Corrected layer depth (cm)**	**Age (ka)**	**Turbidite layer type**	**Turbidite layer width (cm)**	**Notes**
19-21	19-21	11	Coarse grained	2	
27-39	27-34	20	Coarse grained	7	Void in layer, sharp base
171-174	166-169	113	Dark fine grained	3	
180-182	175-177	119	Coarse grained	2	
186-187	181-182	122	Coarse grained	1	
204-207	199-202	133	Coarse grained	3	
210-214	205-209	134	Coarse grained	4	Fines up

Table A.3 Summary of the positions, ages, widths and type of turbidite layers present in core MD06-3020.